Physical properties and interactions in pressurised metered dose inhalers

Traini, Daniela

Award date:
2005

Awarding institution:
University of Bath

PHYSICAL PROPERTIES AND INTERACTIONS IN PRESSURISED METERED DOSE INHALERS

Submitted by:

Daniela Traini

for the degree of Doctor of Philosophy
of the University of Bath
June 2005

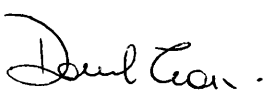

ProQuest LLC
789 East Eisenhower Parkway
P.O. Box 1346
Ann Arbor, MI 48106-1346

TABLE OF CONTENTS

ACKNOWLEDGEMENTS

Firstly I would like to thank Robert Price not only for sharing his scientific knowledge and being an excellent supervisor, but also for many friendly moments during all these years. Furthermore, I am indebted to my industrial supervisor Philippe Rogueda at AstraZeneca for his continuous support and the Colloid IMPACT Faraday Partnership together with AstraZeneca R&D for the financial support. I would like to thank my internal examiner Professor Mike Brown for his support and a dear friend, Dr. Michael J Tobyn for his encouragement.

In addition, thanks to my family, whose love and continued support made all this possible.

I would also like to express my gratitude to the past and present members of the pharmaceutical technology research group, including Matthew Jones without whom I would not have been able to submit this thesis. I would also like to thank Rod and Steve for their practical help and Paul Fritts for his friendly outlook on life and technical skill. Rhys – thanks for a perfect mix of friendship and software swapping.

To Rebecca Davies, my best friend throughout this period and through life in general, good luck for a bright future and thanks for everything!
And Cheryl Clinch that made me smile even in the darkest moments!

Last, but not least, I would like to thank PY, thanks for your love, support, professional collaboration, never-ending chat about science and the essence of life..... I owe you a big part of this thesis.

TABLE OF COMMONLY USED ABBREVIATIONS

A'	-	Cross-section area of capillary
a	-	Projected surface area of the sample probe
A	-	Hamaker constant
ACI	-	Andersen cascade impactor
AFM	-	Atomic force microscope
AN	-	Lewis acid-base acceptor number
B.E.T	-	Brunauer, Emmet and Teller equation
BUD	-	Budesonide
C	-	B.E.T. constant
c	-	Material constant
CA	-	Contact angle
CAB	-	Cohesive/adhesive balance
CFC	-	Chloro-fluorocarbons
CI	-	Capillary intrusion
D	-	Deflection
DLVO	-	Derjaguin-Landau-Verwey-Overbeek
DMT	-	Derjaguin, Müller and Toporov model
DN	-	Lewis acid-base donor number
DPI	-	Dry powder inhaler
DSC	-	Differential scanning calorimetry
DVS	-	Dynamic vapour sorption
ED	-	Emitted dose
F	-	Force

F_{ad} - Force of adhesion

F_{coh} - Force of adhesion

FFD - Formoterol fumarate dihydrate

FPF - Fine particle fraction

GC - Gas chromatography

HFA - Hydro-fluoroalkane

HPLC - High performance liquid chromatography

IGC - Inverse gas chromatography

JKR - Johnson, Kendall and Roberts model

K - Spring constant

K_a - Acceptor (acidic) component contribution to surface energy

K_d - Donor (basic) component contribution to surface energy

l - Distance between particles

L - Liquid

LW - Lifshitz van der Waal

M - Mass f adsorbed liquid

mHFA - Model hydro-fluoroalkane

MMAD - Mass media aerodynamic diameter

n - Pre-determined constant n=3/2 JKR and n=2 DMT

N - Avogadro's number

P - Partial pressure of adsorbate

pMDI - Pressurised metered dose inhaler

Po - Saturation point of the adsorbate

R - Gas constant

R^* - Harmonic mean of the particle radii, also called contact radii

RH - Relative humidity

R_{rms} - Root mean square roughness

RSD - Relative standard deviation

S - Solid

SAMP - Sample

SCA - Surface component approach

SD - Standard deviation

SEM - Scanning electron microscopy

SS - Salbutamol sulphate

STD - Standard

T - Temperature

t - Time

TSI - Twin stage impinger

UV - Ultraviolet

V_a - Volume of gas at adsorbed at a specific partial pressure

V_g Retention volume

V_g^{ref} - Surface retention volume of a correspondent reference alkane

V_m - Volume of adsorbed gas for monolayer coverage

V_N - Net volume of carrier gas

W_{AB} - Polar component of the thermodynamic work of adhesion

W_{adh} - Thermodynamic work of adhesion

W_{LW} - Dispersive component of the thermodynamic work of adhesion

W^{Tot} - Total component of the thermodynamic work of adhesion

XRPD - X-ray powder diffraction

ΔG_{131} - Free energy of interaction between solid 1 and liquid 3

ΔG_{132} - Free energy of interaction between solid 1 and 2 with liquid 3

ΔG^{AB} - Polar surface free energy

ΔG^{EL} - Electrostatic double layer surface free energy

ΔG^{LW} - Dispersive surface free energy

ΔG_{SLS} - Interfacial free energy between solid-liquid-solid

ΔG^{Tot} - Total surface free energy

ΔH^{AB} - Enthalpy of desorption

γ - Liquid surface tension

γ^- - Electron donor/Lewis base

γ^+ - Electron acceptor/Lewis acid

γ^{AB} - Polar component of the surface free energy

γ^{LW} - Dispersive component of the surface free energy

η - Viscosity

π - Pi

π_e - Equilibrium spreading pressure

θ - Contact angle

ρ - Density

σ - Specific surface area

ABSTRACT

An investigation has been conducted into factors influencing inter-particulate forces in pressurised metered dose inhalers (pMDI). Colloid probe atomic force microscopy (AFM) measurements of inter-particulate interactions were correlated with physico-chemical properties, theoretical surface energy calculations and the *in vitro* deposition characteristics of suspension based pMDI formulations.

Since pMDI formulations are rather complex, with various interactions being influenced by many variables, specific areas of pMDI formulation science were investigated. These included particle interactions in single formulations; particle interactions in combination drug systems; interaction of drug particulates with pMDI canister wall materials; and the influence of stabilizers on drug interactions.

The underpinning tools used to study such factors was AFM and surface energy measurements. AFM measurements were achieved by preparing colloid drug probes of micronised drug particulates of salbutamol sulphate (salbutamol) budesonide and formoterol fumarate dihydrate (formoterol) via a micromanipulation technique. Interactions between the AFM 'drug probes' and specific formulation surfaces (drug or canister material) were conducted *in situ* in a model propellant system.

A series of surface energy measurement techniques were utilised during the course of the study. Contact angle measurements were chosen to assess the dispersive (apolar), acid and basic (polar) components of the surface energy of the components used. The interfacial free energy of interactions for drug-drug and drug-device interactions were also theoretically predicted using the extended-DLVO theory and applied using the surface component approach (SCA).

The force of interaction between each drug probe and a series of canister materials was compared with the predicted work of adhesion (calculated from the SCA). The force of adhesion, measured by AFM, was shown to correlate well with the predicted work of adhesion using the SCA. Moreover, the linear relationship between the work of adhesion and AFM measured adhesion was shown to be highly dependent on the polar contributions of the surface free energies of the interacting materials.

The force of interaction between a series of drug probes of a material and atomically smooth surfaces of each drug material (produced using controlled crystallisation) were compared with the predicted work of adhesion or cohesion from the SCA. The use of atomically smooth drug substrates allowed direct comparison between the adhesion/cohesion of each drug probe as the contact geometry remained constant. In general, comparison of the predicted adhesion/cohesion ratio (calculated using SCA) correlated well with the AFM measurements. In particular, salbutamol had a high cohesion force when comparing interactions between budesonide and formoterol. In addition, a series of *in vitro* studies, comparing the aerosolisation efficiency of both single and combination formulations of each drug were in general agreement with predicted and fundamental measurements of the interfacial interactions.

To investigate the potential of reducing inter-particulate cohesion in salbutamol sulphate pMDI formulations, the use of solubilised stabilisers was investigated. It was found that an increase in chain length (MW 200-600) and concentration (0.05 - 0.5 $\%^{v}/_{w}$), of low molecular weight polymers (polyethyleneglycol), added to the model propellant resulted in a decrease in a significant decrease in particle adhesion by AFM measurements. Furthermore, the addition of polyvinylpyrrolidone, at low concentrations ($0.001\%^{v}/_{w}$) resulted in a significant decrease in adhesion, regardless of PEG concentration ($P<0.05$). These observations correlated well with theorised hypothesis regarding inter-particulate stabilisation using non-ionic polymers.

The AFM colloid probe technique, in combination with physico-chemical characterisation and theoretical calculation, has successfully been employed to predict particle-particle and particle-substrate interactions specific to pMDI based inhalation technology. Furthermore, the correlation between theoretical, fundamental and *in vitro* behaviour may provide a rapid screening of formulation components during formulation development and pMDI product design.

CHAPTER 1: INTRODUCTION

Localised delivery of pharmaceutical drug particulates to the respiratory tract has become an essential and effective therapeutic method for treating a variety of pulmonary disorders, including asthma, COPD (Chronic obstruction pulmonary disease) bronchitis and cystic fibrosis (British Thoracic Society et al., 1997). Such popularity can be related to the relative small dose required for effective therapy, reduced systemic exposure and minimised side effects. Furthermore, the large surface area for absorption at the terminal bronchioles and alveoli (~100 m^2) provides a portal entry for systemic drugs (Patton, 1996).

Drug distribution and deposition in the respiratory tract depends on many factors including: physico-chemical properties of a formulation (particle size, particle shape (Tang et al., 2004)), its delivery characteristics (aerodynamic diameter (Patton, 1996)), charge (Glover and Chan, 2004), density (William III et al., 1998; Steckel and Brandes, 2004) and hygroscopicity (Price et al., 2002), anatomy of the respiratory tract and the co-ordination and breathing manoeuvre of a patient (Hickey and Martonen, 1993; Timsina et al., 1994).

The pressurised metered dose inhaler (pMDI) remains the most common prescribed device for therapeutic aerosol delivery (Ross and Gabrio, 1999). However, following the Montreal protocol in 1987, which has resulted in the gradual phasing out of chlorofluorocarbon (CFC) propellants, several new and unexpected challenges in the reformulation of hydrofluoroalkane (HFA) propellant based pMDI formulations have arisen. Of these, dispersion stability and particle interactions have been of utmost importance (Ranucci et al., 1990; Fu and Riman, 1993; Ruckenstein, 1993). With the ultimate aim of delivering a reproducible dose of medication to a target site, an understanding of particulate interactions within propellant based systems and their influence on formulation stability is of critical importance.

1.1 STRUCTURE OF THE AIRWAY

The human respiratory tract consists of a series of bifurcating airways, starting at the oropharynx and finishing at the alveolar sacs. The airway anatomy consists of the oro, nasopharynx, larynx, trachea, two main bronchi, five lobar bronchi (three on the right, two on the left) and fifteen to twenty dichotomous branching of the bronchi and bronchioles down to the level of the terminal bronchioles and the alveoli. A schematic diagram of a human respiratory tract is given in Figure 1.

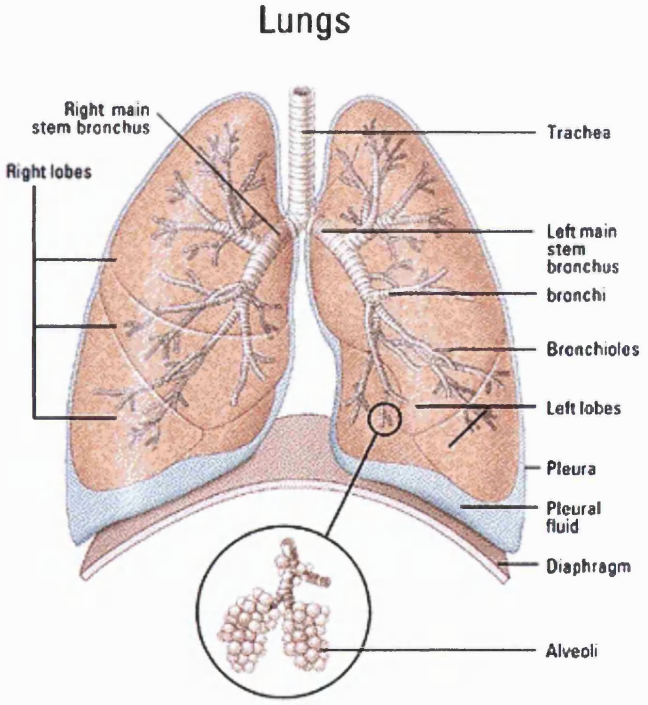

Figure 1 Diagrammatic representation of the structure of a human lung (Copyright © 1996 Johns Hopkins University)

The portion of the airways that participates in gas exchange with the pulmonary capillary blood is the respiratory bronchioles, and the alveoli themselves. The alveoli act as the primary gas exchange units of the lung, especially as the gas-blood barrier between the alveolar space and the pulmonary capillaries are extremely thin, allowing rapid gas exchange.

Oxygen can subsequently diffuse via the alveolar epithelium (a thin interstitial space) and the capillary endothelium.

The surface area provided by the respiratory bronchioles and alveoli for gas exchange is tremendous. It is estimated that the adult human lung has over 300 million alveoli with a total surface area of approximately 100 m^2 (Patton, 1996). In simple terms, this provides a high surface area, low surface fluid coverage, thin diffusion layer and sluggish cell surface clearance by macrophages. These properties provide an alternative delivery system to the more conventional gastrointestinal, nasal, buccal or transdermal delivery routes (Patton, 1996).

However, the delivery of medicaments to the respiratory tract is not a simple process. The entrainment and efficient delivery of particulates to the lung is regulated by three intrinsic physiological factors: inertial impaction, gravitational sedimentation and diffusion (via Brownian motion) (Hinds, 1999).

When designing and formulating a delivery system, consideration of the many factors which influence the deposition of drug particles needs to be understood. The main factors are the properties of the aerosol particles (aerodynamic diameter) and the mode of inspiration (flow rate, velocity profile) (Smyth, 2003). The optimum size range of particulates for inhalation therapy has been shown to be between 2.5 and 6 μm (Pritchard, 2001).

Asthma, together with Chronic Obstructive Airways Diseases is associated with approximately one-third of the common causes of death in the European Union (International Pharmaceutical Aerosol Consortium (IPAC), 1997). Clearly, the requirement for an effective treatment of such respiratory diseases remains in continuous demand.

1.2 CURRENT RESPIRATORY DELIVERY MECHANISMS

Current mechanisms of drug delivery to the respiratory tract can be classified via three approaches: dry powder inhalers (DPIs), nebulisers and pressurised metered dose inhalers.

Dry powder inhalers are the most recent development in the delivery of drug therapy to the lung. They rely on the energy supplied by the forced inhalation breath of patients to de-aggregate and deliver the active ingredient to the site of action. In general, the drug is in the form of micronised particles, either as agglomerates or in combination with a carrier substance (typically lactose). The main advantage of this delivery system is that it does not rely on patient compliance. However, the efficiency of a dry powder inhaler is often hindered by the energy required to overcome de-aggregation of the small drug particles (Ganderton and Jones, 1987) upon actuation.

Nebulisers can produce a constant stream of aerosol particles that can be inhaled via tidal breathing. The main advantage of such delivery systems is that they provide a potential means of administrating aqueous formulations. Furthermore, the aerosol droplets produced are smaller than DPIs and pMDIs, making them capable of easily penetrating the small airways (Gupta and Hickey, 1991). However, the system is usually cumbersome and can only be used at home or in a clinical setting. The most significant draw backs of this delivery system include: length of time needed for delivery of medication, the complexity of device assembly and the requirement on mains electrical supply for operation.

1.2.1 Pressurised metered dose inhalers

Pressurised metered dose inhalers (Figure 2) have been marketed to the public as a medicament since the mid 1950's. They were first introduced by Riker Laboratories in Santa Barbara, now 3M Healthcare (Clarke, 2002). Fundamentally, pMDIs rely on aerosol propellant technology, in which a high vapour pressure gas (typically a liquid propellant) is contained in a pressurised canister, under a super-cooled state. On release of a metered volume of the drug/propellant mixture, the volatile propellant rapidly expands through the metering stem and vaporises through an actuator orifice to deliver micrometer-sized drug aerosols (Dunbar et al., 1997).

In pMDI based systems, the drug can either be homogeneously suspended (colloidal system) or solubilised in a propellant (either with or without the addition of co-solvents). By metering the release of a given volume of propellant (typically 25 to 100 μl) within an integral metering valve, a reproducible dose of drug can be delivered. The high, internal energy produced upon evaporation of the propellant, provides the inertial driving force for the delivery of drug particles to the respiratory tract.

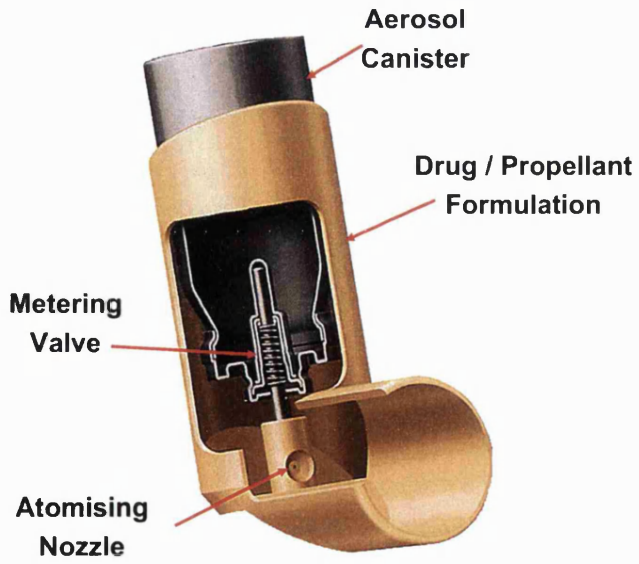

Figure 2 Basic pMDI design

Until 1995, all marketed pMDI products contained CFC as the delivery propellant. However, concerns over the possible detrimental ozone depleting effects of CFCs (Molina and Rowland, 1974) brought 150 nations to sign the Montreal protocol in 1987, which committed the signatory nations to cease CFC production by 1996 (United Nation Environment Programme, 1996). As a result, pharmaceutical companies have committed large resources to the research and development of CFC-free pMDI systems (Vervaet and Byron, 1999).

The candidates that emerged from this research as potentially suitable CFC replacements were short-chain hydrofluoroalkanes (HFAs) (Dalby et al., 1990): Specifically, 1,1,1,2,3,3,3 Heptafluoropropane (HFA-227) and 1,1,1,2 Tetrafluoroethane (HFA-134a). However, HFA and CFC propellants posses quite different physical and chemical proprieties, as shown in Table 1, producing a whole new series of challenges in the formulation of pMDIs.

Propellant	Liquid density (g/ml)	Liquid viscosity (mPas)	Boiling point (°C)	Vapour pressure (psig @ 20°C)	Ozone depletion potential	Global Warming potential*
CFC 11	1.49	0.43	23.7	-1.8	1	1
CFC 12	1.33	0.22	-29.8	67.6	1	3
CFC 114	1.47	0.36	3.6	11.9	0.7	3.9
HFA 134a	1.21	0.22	-26.5	68.4	0	0.3
HFA 227	1.41	0.26	-17.3	56.0	0	0.7

** Relative to CFC 11*

Table 1 Physico-chemical properties of pMDI propellants (adapted from McDonald and Martin, 2000)

As indicated in Table 1, the boiling points and vapour pressures of CFCs and HFAs vary significantly. Vapour pressure ultimately will relate to the speed of evaporation, and, consequently the aerosol droplet size and efficiency of deposition within the lung. A high vapour pressure propellant (as for HFA propellants) would produce rapid evaporation resulting in the formation of small droplets. Furthermore, the increased internal energy within the system upon evaporation of the propellant may lead to high plume velocities that may result in a large percentage of drug particles being impacted on the oro-pharynx (Polli et al., 1969). Similarly, propellant boiling points may have an impact on the filling method of pMDI canisters. For example, CFC filling can be achieved at ambient temperature (using a CFC mix) while HFA filling must occur under pressure at low temperature via the valve.
More importantly, however, is the solvency properties of HFAs differ from that of CFCs (Dickinson el al., 2000). Partial solubility of a suspended drug in the dispersant may result in Ostwald ripening, crystal growth, poor physico-chemical stability and out of specification performance as a function of storage.

Propellant driven suspension metered dose inhaler formulations consist of solid drug(s), typically micronised, dispersed in a propellant medium, which is liquefied under pressure. Given the relative poor solvency power of HFAs relative to CFCs propellant, suspensions containing micronised drug in liquefied HFA propellants have become widely used in pMDIs (Michael et al., 2001). Such formulation approaches are unique in pharmaceutical systems, and are only otherwise applied to non-aqueous dispersions in, for example, the oil and paint industries.

One area of concern however, in such systems, is suspension stability. Since the drug particles being delivered to the respiratory tract are of micron size, the suspended particles have a tendency to agglomerate together or adhere to internal components of the device. The reason for such adhesion is due to the high surface area to mass ratio of the micronised particles and the interaction forces dominating particulate interactions, which are the omni present van der Waals force, polar and electrostatic-double layer interactions.

Such interactions can be described using conventional physics, with the most relevant approaches being discussed below.

1.3 PARTICLE INTERACTION THEORY

Interactions between colloidal particles are usually described by the Derjaguin-Landau-Verwey-Overbeek (DLVO) theory (Derjaguin and Landau, 1941; Verwey and Overbeek, 1948). The DLVO theory considers two types of interactions: a dispersive attractive interaction of the Lifshitz van der Waals (LW) type, and a predominately repulsive electrostatic (EL) interaction due to the interpenetration of electrical double layers.

1.3.1 DLVO theory

The Lifshitz-van der Waals force (van der Waals, 1899), which is generally attractive in nature, is a short range force. This force can be further divided into three closely connected phenomena: Debye-Induction force (Debye, 1920), Keesom-orientation forces (Keesom, 1912) and London dispersion forces (London, 1930). However, the most ubiquitous of the van der Waals forces are the dispersive or London forces. Dispersive forces are finite between all atoms and are of predominant importance between macroscopic bodies (Overbeek, 1952).

From the interactions on a molecular basis, two different approaches have been developed to predict interactions on a macroscopic level.

Hamaker developed a theory to calculate the van der Waals forces conducting pair-wise summation of the dispersion (van der Waals-London) energies theoretically, based on microscopic interactions, for macroscopic bodies (of flat surfaces) interacting with each other, by assuming additive molecular forces throughout the material. He went on to show that the dispersive energy between two surfaces decayed proportionally with the square root of the separation distance (Hamaker, 1937) and that it was actually possible for the van der Waals-London interactions between two different materials immersed in a liquid to be repulsive.

In simple terms, for two materials 1 and 2 immersed in a medium 3, the combining rule is described by Equation 1and Equation 2.

Equation 1

$$A_{131} = A_{11} + A_{33} + 2A_{13}$$

where A is described as the Hamaker constant and A_{11} and A_{33} refer to the Hamaker constants of the solid/solids and the medium, respectively, in vacuo.

Equation 2

$$A_{132} = A_{12} + A_{33} - A_{13} - A_{23}$$

It is clear that A_{131} is always positive or zero, however A_{132} can assume negative values, when $A_{11} > A_{33} > A_{22}$ or $A_{11} < A_{33} < A_{22}$.

In contrast to Hamaker's approach, which started with single interatomic interactions, to arrive at the total interaction energy for macroscopic bodies by a process of summation, Lifshitz (Lifshitz, 1956) has constructed a more accurate approach through a purely macroscopic framework. The problems associated with the use of summation process have been completely eliminated in this macroscopic treatment of dispersion forces.
Lifshitz treated the interacting bodies as continuous media. The dispersion forces in this approach have been derived in terms of the macroscopic properties of interacting bodies, such as their dielectric constants or refractive indexes. In his macroscopic approach, Lifshitz eliminated the total additive molecular force in favour of a screening effect caused by the atoms present on the surface of the two contiguous bodies. (Israelachvili, 1992) used this theory to calculate the Hamaker constant and found the following relationship:

Equation 3

$$\gamma^{LW} \propto \frac{A}{l^2}$$

where *l* is the distance between the particles and γ^{LW} the apolar component of the surface free energy.

Surface free energy of a liquid or a solid is defined as half of the free energy charge ΔG^{LW} due to the cohesion of material *in vacuo* according to Equation 4.

Equation 4

$$\gamma^{LW} = -\frac{1}{2}\Delta G^{LW}$$

The application of the DLVO theory to the stabilisation of drug suspensions in non-aqueous pMDI media has not been fully validated. The possible limitation of the approach, which has been successfully employed to describe the behaviour of aqueous suspensions, is the absence of an ionic double layer (Kitahara, 1974; Pugh et al., 1983). However, a quick theoretical calculation of the repulsive electrostatic energy of interaction between 1 μm solid particles as a function of inter-particulate distances in liquefied propellants with varying dielectric constants (reciprocal thickness of the diffuse double layer set at $2x10^6$ cm^{-1}) show that the electrostatic repulsive forces acting between particles are small. This is attributed to the overlap of very diffusive electrical double layers due to a combination of low dielectric constants and low ionic strengths (Wyatt and Vincent, 1989). Thus, the attractive Lifshitz van der Waals forces are thought to predominate at all separation distances. As a result, DLVO theoretical descriptions of non-aqueous drug suspensions such as pMDI formulations are very limited, as they fail to predict the stability of these formulations observed in some cases.

1.3.2 Surface component approach

An alternative approach to the DLVO theory has been proposed by van Oss (van Oss, 1994). The van Oss approach decomposes the surface energetics (i.e. surface tension or contact angle values) into independent contributions, and in particular introduces a polar acid-base (AB, electron donor/electron acceptor) component (van Oss, 1994). These electron-acceptor (γ^+, Lewis acid type), electron-donor (γ^-, Lewis base type) interactions are essentially asymmetrical. The corresponding polar free energy of interaction, which can be repulsive or attractive (depending on the chemical structure, suspending medium properties and surface potential), can control the total energy of interaction at small separation distances.

In general, the polar component of the free energy of a material can be expressed as:

Equation 5

$$\gamma^{AB} = 2\sqrt{\gamma_1^+ \gamma_1^-}$$

Given that electron-acceptor and electron-donor parameters of most substances are not equal to each other and that material 1 will react with material 2 and *vice versa*, the acid-base free energy of adhesion can be described using the following relationship:

Equation 6

$$\Delta G_{12}^{AB} = -2\sqrt{\gamma_1^+ \gamma_2^-} - 2\sqrt{\gamma_1^- \gamma_2^+}$$

So adapting for polar interactions the acid-base free energy, γ_{12}^{AB}, can be expressed as:

Equation 7

$$\gamma_{12}^{AB} = 2\left(\sqrt{\gamma_1^+} - \sqrt{\gamma_2^+}\right)\left(\sqrt{\gamma_1^-} - \sqrt{\gamma_2^-}\right)$$

According to this surface component approach (SCA), the total surface free energy of a solid is determined by the Lifshitz van der Waals (γ^{LW}) dispersive component and the polar AB component (γ^{AB}), as given in Equation 8.

Equation 8

$$\gamma^{TOT} = \gamma^{LW} + \gamma^{AB}$$

The total free energy of interaction between two surfaces in a liquid medium is subsequently defined as the sum of the Lifshitz-van der Waals (LW) dispersive interactions, the polar component (AB), and electrostatic double layer (EL) interactions:

Equation 9

$$\Delta G^{TOT} = \left\{\Delta G^{LW} + \Delta G^{AB}\right\} + \Delta G^{EL}$$

In the absence of an electrostatic influence, the interaction energy between solid surfaces (S) immersed in a liquid (L) can be expressed by the interfacial free energy (ΔG_{SLS}), (see Equation 10). This in turn can be related to the solid-liquid interfacial tension.

Equation 10

$$\Delta G_{SLS} = \Delta G^{LW} + \Delta G^{AB} = -2\gamma_{SLS} = -2\left(\gamma_{SLS}^{LW} + \gamma_{SLS}^{AB}\right)$$

The interfacial energy parameters for the LW and AB contributions between similar solids (1) in a liquid (3) can be obtained from the surface free energy and surface tensions of the solid and liquid by using the Good-Girifalco-Fowkes approach (Fowkes, 1963; Good and Girifalco, 1960) (Equation 11).

Equation 11

$$\Delta G_{131} = -2\left(\left(\sqrt{\gamma_1^{LW}} - \sqrt{\gamma_3^{LW}}\right)^2 + 2\left(\sqrt{\gamma_1^+\gamma_1^-} + \sqrt{\gamma_3^+\gamma_3^-} - \sqrt{\gamma_1^+\gamma_3^-} - \sqrt{\gamma_1^-\gamma_3^+}\right)\right)$$

For liquids with very low polarity ($\gamma_3^+ = \gamma_3^- \sim 0$ mJ.m^{-2}), the free energy of interaction can be simplified to:

Equation 12

$$\Delta G_{131} = -2\left(\sqrt{\gamma_1^{LW}} - \sqrt{\gamma_3^{LW}}\right)^2 - 4\sqrt{\gamma_1^+\gamma_1^-}$$

Hence, knowledge of the surface energy of the solid (γ_1^{LW}, γ_1^+ and γ_1^-) and the surface tension of the liquid (γ_3^{LW}, γ_3^+ and γ_3^-) enables the determination of interaction energy between particles.

Similarly, the energy of interaction between dissimilar solid surfaces (1 and 2) in a liquid (3) can be calculated using the following expression:

Equation 13

$$\Delta G_{132} = 2\left[\begin{array}{l}\sqrt{\gamma_1^{LW}\gamma_3^{LW}} + \sqrt{\gamma_2^{LW}\gamma_3^{LW}} - \sqrt{\gamma_1^{LW}\gamma_2^{LW}} - \gamma_3^{LW} + \sqrt{\gamma_3^{+}}\left(\sqrt{\gamma_1^{-}} + \sqrt{\gamma_2^{-}} - \sqrt{\gamma_3^{-}}\right) + \\ \sqrt{\gamma_3^{-}}\left(\sqrt{\gamma_1^{+}} + \sqrt{\gamma_2^{+}} - \sqrt{\gamma_3^{+}}\right) - \sqrt{\gamma_1^{+}\gamma_2^{-}} - \sqrt{\gamma_1^{-}\gamma_2^{+}}\end{array}\right]$$

In an apolar medium (γ_3^+ and γ_3^- ~ 0 mJ.m^{-2}), the energy of interaction can be used in the simplified form (Equation 14).

Equation 14

$$\Delta G_{132} = 2\left[\begin{array}{l}\sqrt{\gamma_1^{LW}\gamma_3^{LW}} + \sqrt{\gamma_2^{LW}\gamma_3^{LW}} - \sqrt{\gamma_1^{LW}\gamma_2^{LW}} - \gamma_3^{LW} + \\ - \sqrt{\gamma_1^{+}\gamma_2^{-}} - \sqrt{\gamma_1^{-}\gamma_2^{+}}\end{array}\right]$$

1.3.3 Interparticulate adhesion (JKR & DMT)

The force of adhesion can then be derived from the thermodynamic work of adhesion ($W_{ad} = - \Delta G_{SLS}$) through the Hertz approximation for elastic bodies (Hertz, 1882). This takes into additional account the separation distance and the contact geometry of interacting surfaces. Two models can be used for this purpose: the Johnson, Kendall and Roberts (JKR) and the Derjaguin, Müller and Toporov (DMT) models (Derjaguin et al., 1975; Johnson et al., 1971). The general form of the force of adhesion with relationship to energy (derived for van der Waals interactions between two spherical particles) can be expressed via: (Hertz, 1882).

Equation 15

$$F_{ad} = n\pi R^{*} W_{ad}$$

Where R^{*} is the harmonic mean of the particle radii (also called contact radius) and n is a pre-determined constant depending on the selected model (n=3/2 for JKR and n=2 for the DMT).

Both models have shown their strengths and limitations. The JKR model is applicable only when compliant materials of high surface energy and a large radius come into contact, *i.e.* in the regimen where elastic deformation due to the adhesion force is large compared to its effective range of interaction. In comparison, DMT theory is applicable only to relatively stiff systems with a low adhesion force and a small sphere radius, *i.e.* the regimen in which elastic deformation due to surface forces is small compared to the interaction range.

Consequently it is instructive to notice how the choice of contact mechanics theory can produce inaccurate values, for example, the surface energy. Thus, the validity of contact mechanics models should be fully scrutinised when applied to experimentally derived force measurements.

Over the past few years, many techniques have been developed to characterise particle-particle interactions. These include techniques such as centrifugal detachment, that characterise adhesion by measuring the centrifugal forces required to detach particles (Booth and Newton, 1987; Clarke et al., 2002; Kulvanich and Stewart, 1988; Podczeck et al., 1996; Staniforth, 1980) and electric field detachment, that uses electric fields to remove particles from a surface (Eklund et al., 1994; Zhou et al., 2003).

An alternative approach to such methods of fundamental adhesion measurement is the atomic force microscope (AFM) (as used in this investigation). Both centrifugal detachment and electrical filed detachment monitor the adhesion of many particles, and the output of these measurements are a distribution of adhesion forces. In comparison the AFM is capable of accurately measuring the adhesion of single micron sized particles with a variety of surfaces with high precision and control. In addition, using the AFM it is possible to look at the force of attraction/repulsion between the particle and the surface prior to and post particle contact with the surface. Thus, allowing the elucidation of the relationship between the interactive forces described earlier and experimentally measured adhesion forces (Schaefer et al., 1994; Schaefer et al., 1995).

However, comparison of calculated theoretical force of adhesion with direct and quantitative experimental measurements of interactive forces for "model" spheres (e.g. colloidal polystyrene) on atomically flat surfaces (e.g. mica) by AFM have shown large discrepancies (Schaefer et al., 1995). It has been suggested that the main source of inconsistency may be due to the difference in contact areas at any particular time between a particle and substrate.

To further overcome such limitations of knowing the true area of contact between drug probes, the cohesive and adhesive force ratios may be analysed and compared using the recently developed cohesive/adhesive balance (CAB) analysis procedure developed by Begat et al. (Begat et al., 2004). This AFM based approach provides for the first time a means of quantifying the adhesive and cohesive force balance within a powder formulation. Furthermore, the use of the CAB approach using AFM measurements of inter-particulate forces may be directly correlated to the thermodynamic work of cohesion and adhesion of interacting surfaces via surface energy measurements (e.g. using contact angle (CA) and inverse gas chromatography (IGC)).

In general, for a drug particulate interacting with two atomically flat surfaces (one alike and one different) the cohesive/adhesive balance between the two materials can be expressed by:

Equation 16

$$\frac{F_{coh}}{F_{adh}} = \frac{R^*_{cohesion}\, n\pi W_{coh}}{R^*_{adhesion}\, n\pi W_{adh}}$$

Where F_{coh} and F_{adh} are the cohesive and adhesive forces measured by AFM, and W_{coh} and W_{adh} are the thermodynamic works of cohesion and adhesion, respectively. Assuming that the contact mechanics of the cohesive and adhesive interaction follow the same theoretical model, the ratio of the forces for a series of colloidal probes should be directly proportional to the thermodynamic ratio of the works of cohesion and adhesion of the interfacial interactions. Furthermore, determining the balance of forces for a series of colloidal probes via AFM measurements overcomes the need to determine variations in the spring constant (k) of each individual AFM cantilever.

1.4 IMPLICATIONS OF PHYSICAL-CHEMICAL FACTORS ON THE PERFORMANCE OF PMDI SUSPENSION FORMULATIONS

The culmination of physical-chemical factors that influence interparticle adhesion may result in quantifiable variations in pMDI aerosolisation performance.

Two of the major factors influencing such performance are canister adhesion and suspension behaviour. For example increased force of adhesion between drug particles and canister walls may result in a decrease in emitted dose (Michael et al., 2001; Young et al., 2003). When considering low dose medicaments (such as formoterol fumarate dihydrate: approx. 6-12 µg/dose) the possibility of drug loss to the canister wall becomes critical, since the internal surface area of the canister may approach the projected surface area of the total suspended drug.

When considering suspension behaviour, the interparticulate forces can be directly related to the adhesion, flocculation, caking and re-suspension behaviour of a formulation. Ideally, drug particles should form lose floccules when suspended in the propellant medium, allowing easy re-suspension upon shaking. In addition, it is essential that such lose flocs separate upon aerosolisation to result in discrete particulates for respiratory deposition. Variation in forces between particulates may result in alteration of the suspension behaviour inducing irreversible flocculation, sedimentation and caking/creaming.

Such factors become further complicated, when considering multicomponent systems. In the case of combination drug therapies, the variation in adhesive/cohesive between the formulation components may result in different aersolisation behaviour when compared to their single component therapies (Louey et al., 2003; Michael et al., 2001).

In general, many formulation strategies have been developed to overcome such issues. These include particle engineering (Shekunov and York, 2000; Steckel and Brandes, 2004; York, 1999), canister modification (Ashurst et al., 1996; Young et al., 2003), and the addition of formulation stabilisers (Ashayer et al., 2003; Brambilla et al., 1999; Clarke et al., 1993). The later two will be investigated in this thesis.

1.5 GENERAL DISCUSSION: AIMS AND SCOPE

As previously stated, understanding the interaction and behaviour of surfaces and drug particulates in pharmaceutical systems is of critical importance to enable us to model these systems accurately. The classical model of suspension stability, DLVO, has historically described these interactions. This model derives from an energy balance composed of attractive and repulsive interactions. The original model focused exclusively on attractive van der Waals and repulsive coloumbic interactions. In the last several years, this traditional model has been unable to describe correctly the behaviour of drug particulate in pharmaceutical environments. In 1986 van Oss introduced a new theory, in which he suggested the presence of other interactions that could play a role in suspension systems not commonly included by traditional particle stability models: e.g. Lewis acid/base interactions and steric interactions. Significant work has been focused on extending the principle of the traditional DLVO model to accommodate these non-DLVO forces (energies) for pharmaceutical suspension systems, using the SCA model (Traini et al, 2005).

Therefore, the purpose of this investigation was to investigate such factors in relation to HFA based pMDI systems using a combination of conventional and novel techniques.

As previously stated, there are many formulation variables in pMDI systems. Here, the author has focussed on three major areas; drug-canister interactions, drug-drug interactions in single and combination formulations and the influence of stabilisers. Since such systems are complex, the focus on discrete areas allowed in depth investigation, while keeping other possible variables constant.

The interactions in such systems were characterised using both theoretical and experimental approaches, in order to understand and predict formulation aersolisation performance.

CHAPTER 2: GENERAL MATERIALS AND METHODS

In order to fully understand particle-particle and particle-substrate interactions in pressurised metered dose inhalers the materials were first characterised in terms of sample morphology, particle size, surface energy, surface area, density and solubility. Furthermore, the preparation of materials used throughout the study is described.

2.1 MATERIALS

Drugs, propellants and pressurised metered can materials used throughout the investigation are given in Table 1. All organic solvents used in the study were supplied by BDH (Poole, Dorset, UK) and were of at least analytical grade. Water was prepared by reverse osmosis (MilliQ, Molsheim, France).

Material	Supplier
Salbutamol sulphate	AstraZeneca, R&D Charnwood, UK
Budesonide	AstraZeneca, R&D Charnwood, UK
Formoterol fumarate dihydrate	AstraZeneca, R&D Charnwood, UK
Polyethyleneglycol (200, 400, 600 M.W)	Acros Organics, New Jersey, USA
Polyvinylpyrrolidone (Povidone K25)	AstraZeneca, R&D Charnwood, UK
2H, 3H, decafluoropentane model propellant	Apollo Scientific, Derbyshire, UK
HFA 134a, hydrofluoroalkane propellant (Zephex 134a)	IneosFluor, Cheshire, UK
Inverted metering valves BK 357 (50 µl)	Bespack Europe Limited, Norfolk, UK
Inverted continuous valves BK 357 (cont)	Bespack Europe Limited, Norfolk, UK
Cut edge aluminium cans (18 ml brim capacity)	Presspart, Lancashire, UK
Cut edge anodised aluminium cans (18 ml brim capacity)	Presspart, Lancashire, UK
Cut edge perfluoroalkoxy cans (18 ml brim capacity)	Intrapacgroup, Harrisonburg, VA, Canada
Cut edge fluorinated ethylene propylene – polyether sulphone (18 ml brim capacity)	Intrapacgroup, Harrisonburg, VA, Canada
Cut edge polytetrafluoroethylene	3M United Kingdom PLC-Bracknell, UK
Actuators (0.3 mm orifice diameter)	Bespack Europe Limited, Norfolk, UK
Glass containers	Saint Gobain plc, London, UK

Table 2 Drugs, propellants, formulation components and pressurised metered can materials used throughout the investigation

2.1.1 Note on the drug materials used for investigation

The chemical structures of salbutamol sulphate budesonide and formoterol fumarate dihydrate are shown in Figure 3 a, b and c, respectively.

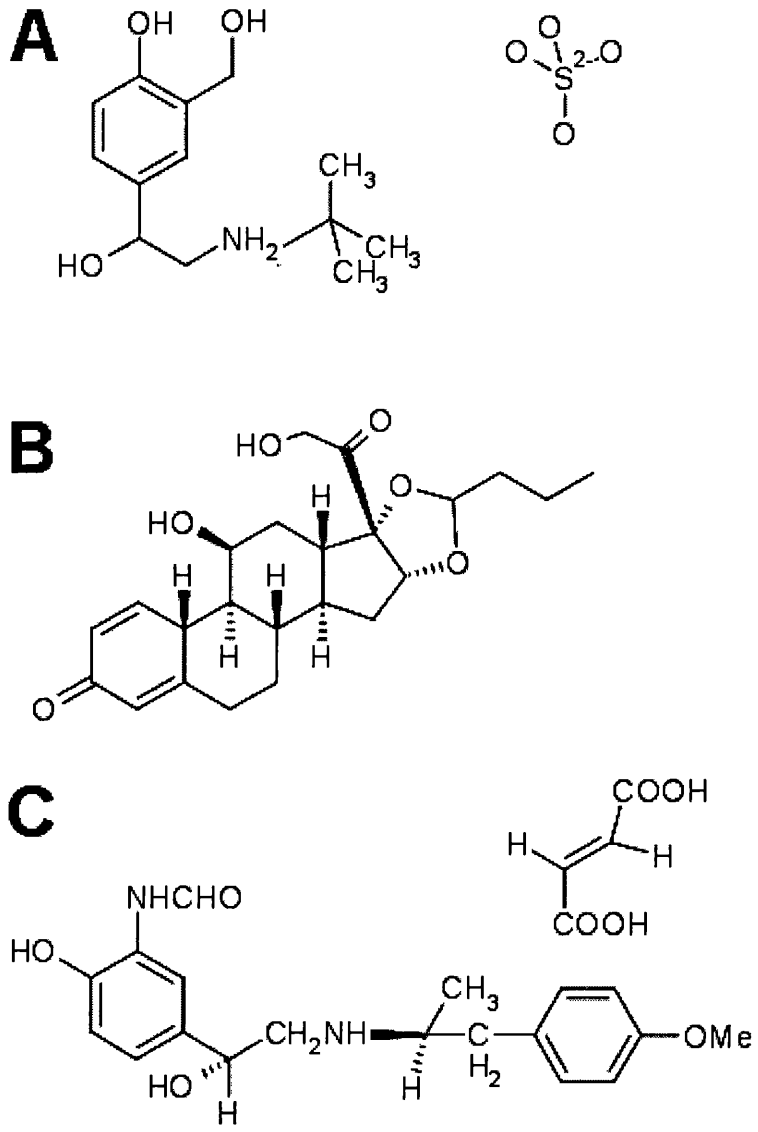

Figure 3 Chemical structures for (a) salbutamol sulphate, (b) budesonide and (c) formoterol fumarate dihydrate

Salbutamol sulphate is a β_2 bronchodilators agonist prescribed for chronic and sever asthma.

Likewise the structure for budesonide (corticosteroid used in prophylaxis of asthma) is generally considered relatively normal and can be compared to other commonly used steroids such as beclometasone dipropionate (Florey, 1972).

The crystallographic asymmetric unit of formoterol fumarate dihydrate (potent β_2 adrenoreceptor agonist used as long acting bronchodilator in asthma therapy) contains one molecule of formoterol, a half molecule of fumarate and one molecule of water. The crystal water and fumarate anion are both involved in intricate hydrogen bonding, both as donor and acceptor (Ertan et al., 1997).

2.1.1a Important note relating to drug names

Unless otherwise stated in the text, salbutamol sulphate shall be referred as salbutamol and formoterol fumarate dihydrate shall be referred to as formoterol.

2.2 SCANNING ELECTRON MICROSCOPY

The morphology of the drug particle surfaces used throughout the investigation was investigated by scanning electron microscopy (SEM). Scanning electron microscopy involves generating a high-resolution image of a conducting sample, by collecting and analysing the secondary electrons (weakly bound conduction-band electrons) emitted as a result of high-energy electron beam collisions.

2.2.1 Materials and methods

The morphology of each micronised drug powder was investigated using a JOEL 6310 SEM (JEOL, Japan) at 10 KeV. All samples were mounted on adhesive black carbon tabs, (pre-mounted on aluminium stubs), and coated with gold (using a sputter coater S150B, Edwards High Vacuum, Sussex, UK) prior to analysis.

2.2.2 Results and discussion

Representative scanning electron micrographs of the micronised salbutamol, budesonide and formoterol samples are shown in Figure 4, Figure 5 and Figure 6, respectively.

In general, representative photomicrographs of the 'as supplied' salbutamol suggest the crystals have a columnar shape. In comparison, analysis of the budesonide and formoterol images suggests the crystal form to have both columnar and irregular plate-like crystal shapes.

In addition, it is important to note, large variations in crystal size were observed for all three drugs. Such observations may be attributed to the limitations of high-energy milling processes (Buckton, 1997; Larhirib et al., 2003).

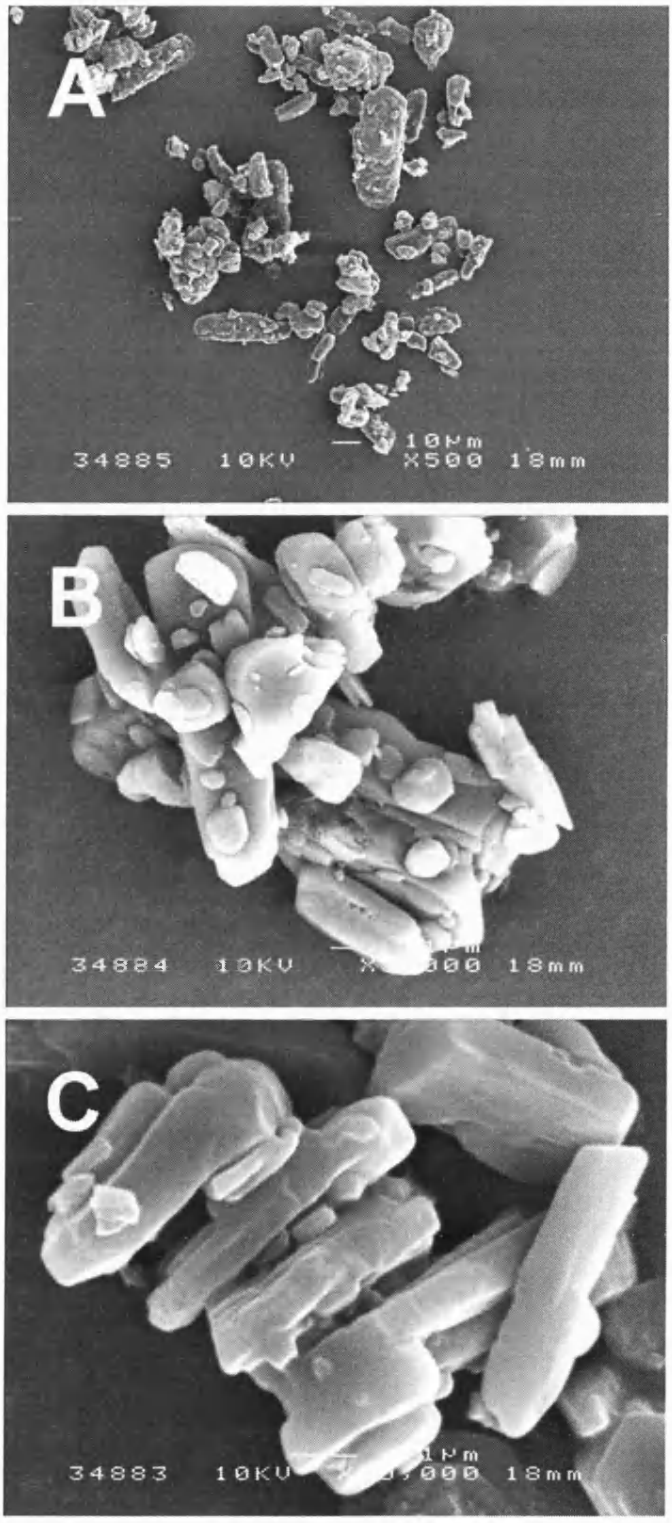

Figure 4 Representative scanning electron micrographs of micronised salbutamol taken at (A) X 500, (B) X 5,000 and (C) X 10,000 magnifications

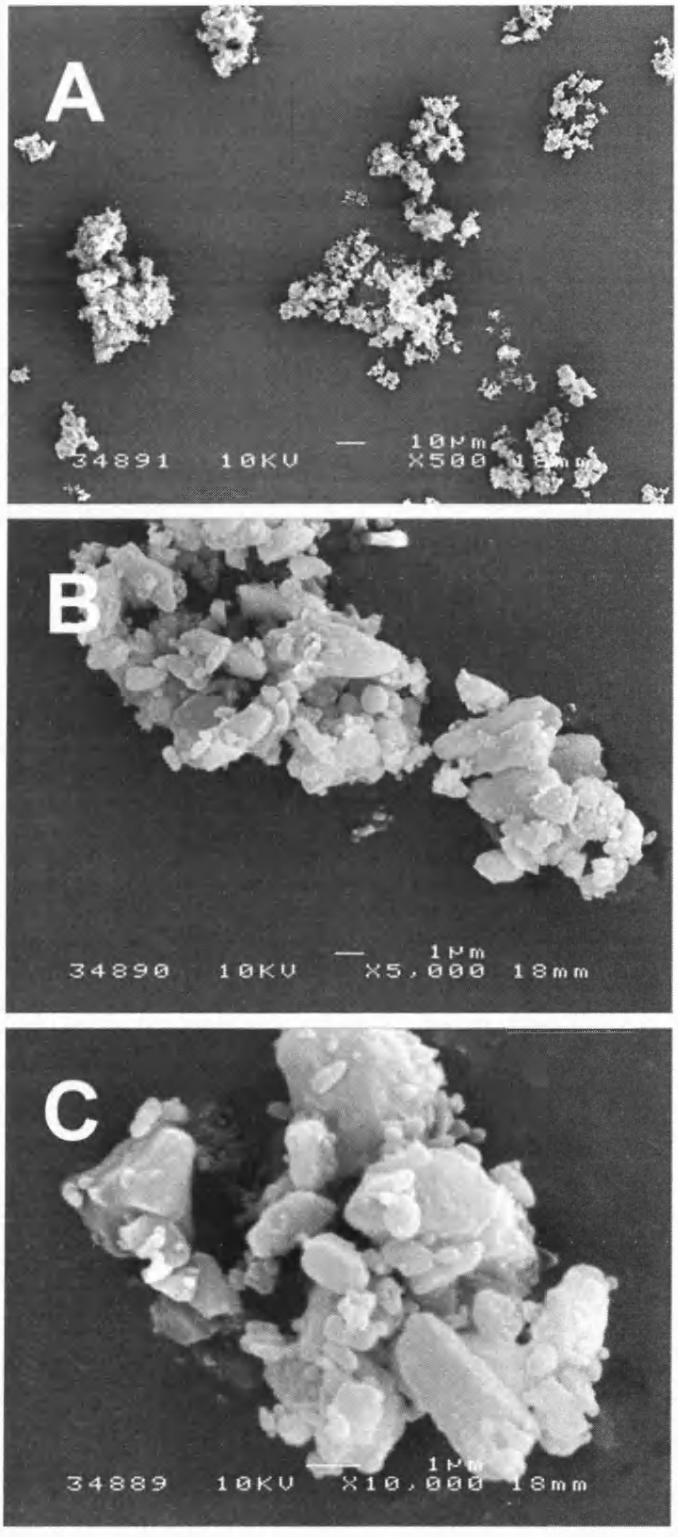

Figure 5 Representative scanning electron micrographs of micronised budesonide taken at (A) X 500, (B) X 5,000 and (C) X 10,000 magnifications

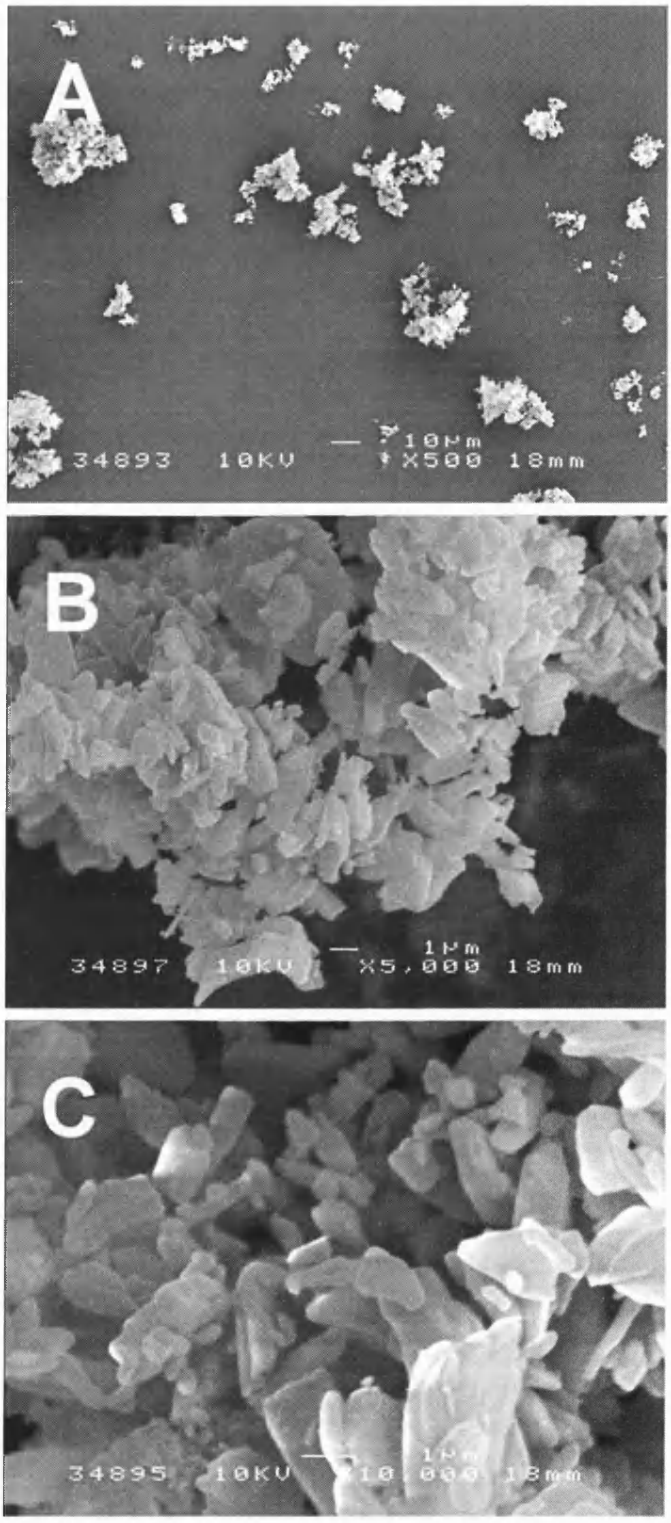

Figure 6 Representative scanning electron micrographs of micronised formoterol taken at (A) X 500, (B) X 5,000 and (C) X 10,000 magnifications

2.3 PARTICLE SIZE ANALYSIS

The particle size distribution of each drug material was investigated using laser light scattering. In simple terms, particle size measurement using laser light scattering involves measuring the intensity and pattern of scattered light from a laser passing through a particulate sample. However, when investigating particles of a diameter of less than 10 μm the optical properties of the material are considered (Mie theory). The final particle size distribution is calculated by matching the experimental diffraction pattern to theoretical patterns (British Standard, 1999).

2.3.1 Materials and methods

Particle sizing of each drug sample were performed using a Malvern Mastersizer X (Malvern Instruments Ltd, Malvern, UK). The instrument was equipped with a small volume circulating cell and a 100 mm lens. Approximately 1 mg of drug material was suspended in a 0.1% lecithin / cyclohexane solution dispersant. Each sample was subsequently sonicated for 10 minutes at 25°C prior to analysis (determined sufficient to fully de-aggregate the powder sample) (Chawa et al., 1994; Franco et al., 2004). Each sample was conducted in triplicate and represented as a volume distribution.

2.3.2 Results and discussion

The 10%, 50% (median) and 90% cumulative percentile volumetric diameters for the micronised drugs are given in Table 3, while full distributions are shown in Figure 7.

Micronised salbutamol was found to have a median diameter of 3.33 μm (with over 74% of particles below 5 μm), budesonide a median diameter of 3.24 μm (with over 82% of particles below 5 μm) and formoterol a median diameter of 2.69 mm (with 93% of particles below 5 μm).

Drug Sample	$D_{0.1}$ μm	$D_{0.5}$ μm	$D_{0.9}$ μm
Micronised salbutamol	1.60 ± 0.01	3.33 ± 0.03	6.92 ± 0.06
Micronised budesonide	1.80 ± 0.00	3.24 ± 0.01	5.93 ± 0.03
Micronised formoterol	1.54 ± 0.01	2.69 ± 0.01	4.63 ± 0.02

Table 3 Basic size distribution percentiles for the micronised drug materials (n=3, ± Standard deviation)

In general, the particle sizing data agreed well with SEM observations, with drug samples falling within the optimum size range required for pulmonary delivery (Pritchard, 2001).

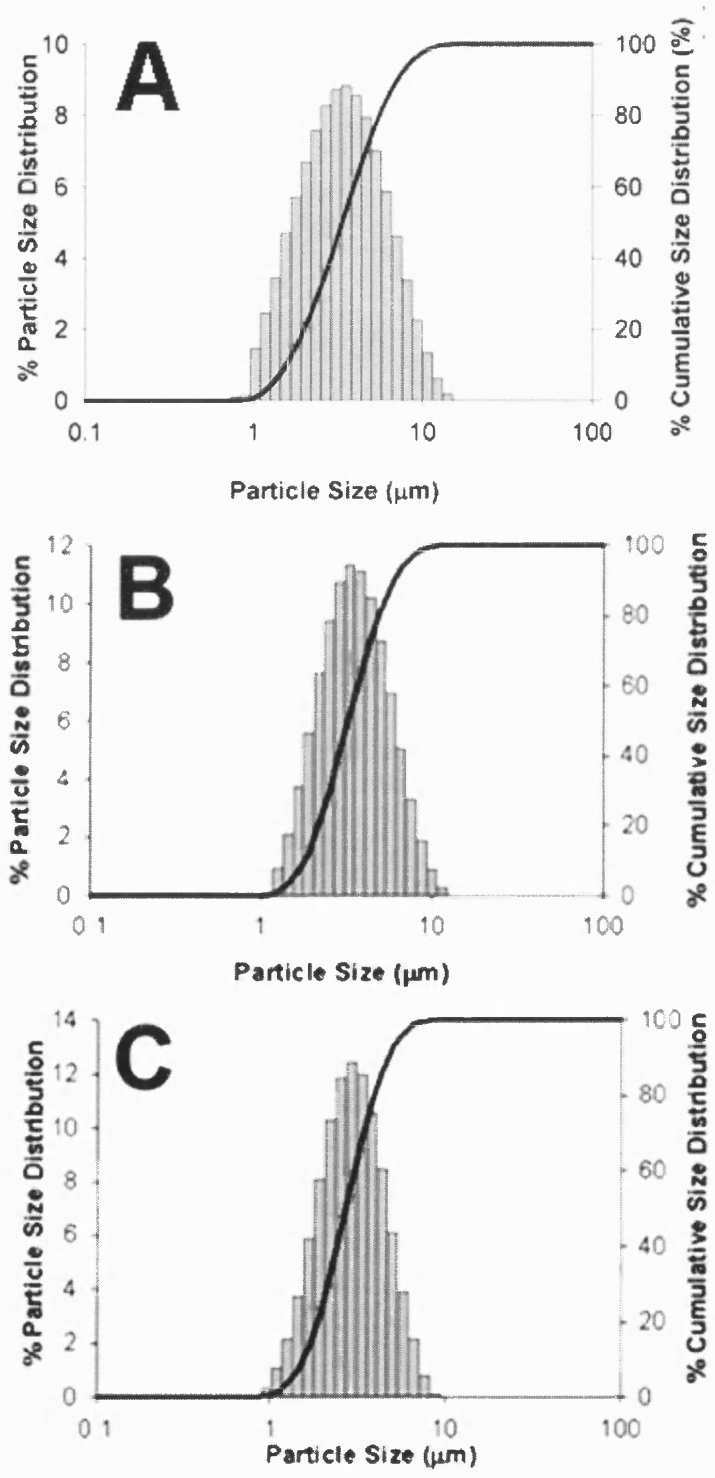

Figure 7 Particle size distributions for micronised (A) salbutamol, (B) budesonide and (C) formoterol

2.4 X-RAY POWDER DIFFRACTION

X-ray powder diffraction (XRPD) involves the measurement of diffracted monochromatic X-rays as they pass through the atomic spacing that exists between the atoms in a crystalline material. In simple terms, the rotation of a crystalline sample, in relation to the X-ray beam, allows calculation of the three-dimensional structure from the diffracted X-rays that pass between the crystal planes. In comparison to single crystals, a powder sample will have a random orientation of crystallites. Thus, for a powder sample, a diffraction cone of semi apex angle 2-Theta is produced. The subsequent diffraction pattern will be particular to the material under investigation (Guinier, 1994).

2.4.1 Materials and methods

X-ray diffraction spectra of the micronised drugs samples were obtained using a Phillips X-ray powder diffraction system (Phillips X-Ray Analytical, Cambridge, UK) fitted with a 4-kW X-ray generator (PW 1730/00). Scanning was performed in steps of 2-Theta over the range of 2θ, 5–60° to produce each spectrum.

2.4.2 Results and discussion

Powder X-ray diffractograms of micronised salbutamol, budesonide and formoterol are shown in Figure 8 A, B and C, respectively.

Analysis of the X-ray powder diffractograms for the micronised drugs suggest a predominantly crystal structure. In addition, the diffractograms suggest good correlation with studies reported previously (Columbano et al., 2002; Ertan et al., 1997; Steckel et al., 2004; Ticehurst et al., 1994).

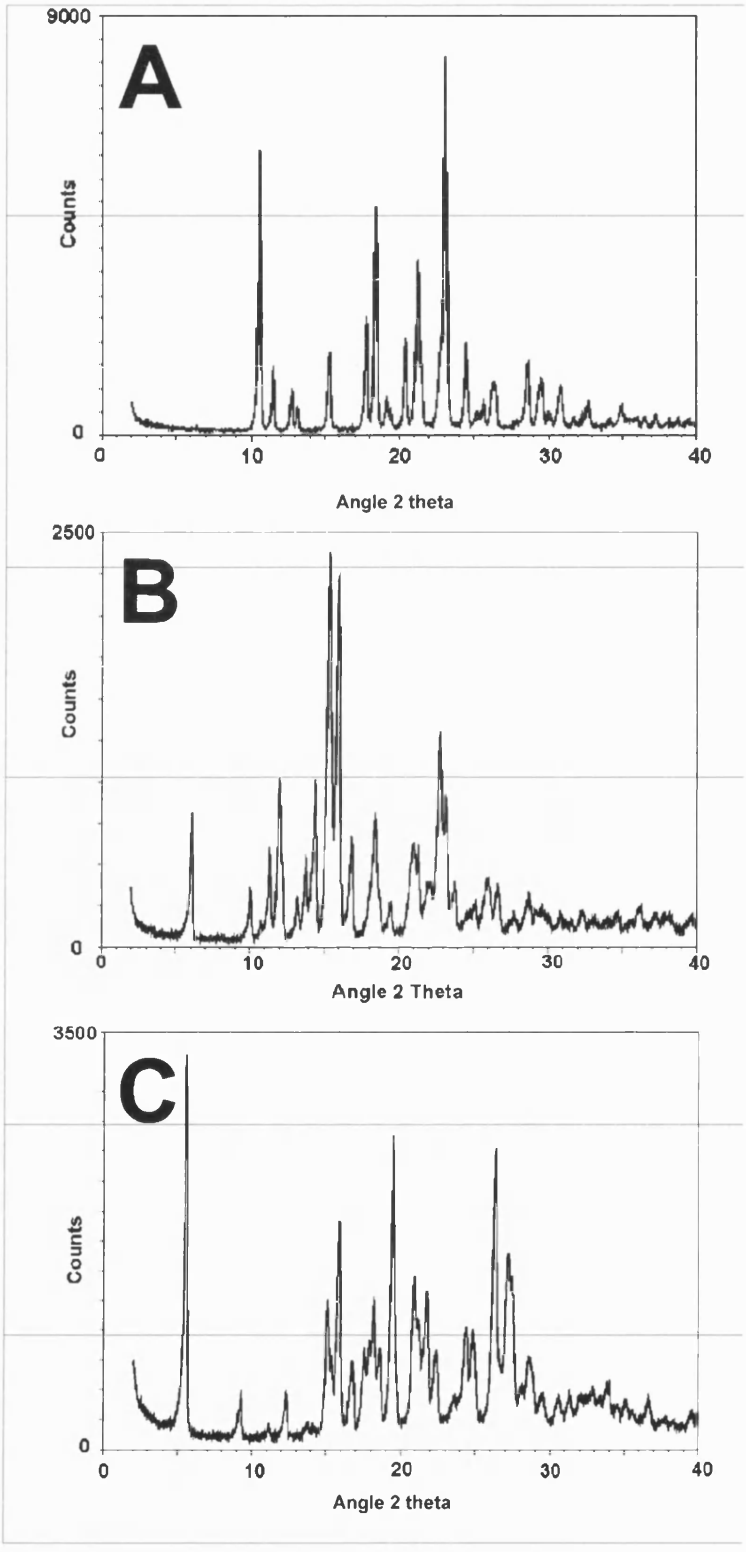

Figure 8 XRPD diffractographs for micronised (A) salbutamol, (B) budesonide and (C) formoterol

2.5 TRUE DENSITY

For pMDI suspension systems, the density of drug particulates will play an important role on the physical behaviour of the system. True density of powder samples are generally measured using helium pycnometry. Helium pycnometry measures the true density by calculating the pressure change of helium in a calibrated volume in relation to an unknown mass with an unknown volume (Webb and Orr, 1997).

2.5.1 Materials and methods

True density measurements were determined using helium pycnometry (Accupyc 1330 Gas Pycnometer, Micromeritics, Norcross, GA). Samples were prepared by storing in open pans at 40 °C for 48 hours prior to analysis. The temperature was maintained at 27°C during out-gassing and analysis.

2.5.2 Results and discussion

True density measurements are given in Table 4.

Drug Sample	Sample density (g.cm^3)
Micronised salbutamol	1.306 ± 0.001
Micronised budesonide	1.240 ± 0.007
Micronised formoterol	1.295 ± 0.007

Table 4 Density measurements for the micronised salbutamol, budesonide and formoterol. (n=10, ± Standard deviation)

2.6 SURFACE AREA

Specific surface areas of the three micronised drugs were determined by nitrogen adsorption. Briefly, the principle involves measuring the difference in pressure between a sample and reference blank, under isothermal conditions, after addition of finite quantities of adsorption gas. By applying the B.E.T equation (Brunauer et al., 1938), describing monolayer-multilayer surface adsorption it is possible to calculate the point of monolayer coverage and thus surface area (Webb and Orr 1997). The linear form of the B.E.T equation is given by:

Equation 17

$$\frac{P}{V_a(P_0 - P)} = \frac{1}{V_m C} + \frac{(C-1)}{V_m C}\frac{P}{P_0}$$

Where P is the partial pressure of adsorbate, V_a is the volume of gas adsorbed at the specific pressure, V_m is the volume of adsorbed gas in a monolayer, P_o is the saturation point of the adsorbate and C is the B.E.T constant. Subsequently, by plotting the transform of the equation the monolayer coverage can be calculated from the slope and intercept.

Equation 18

$$\frac{P}{V_a(P_0 - P)} \quad vs \quad \frac{P}{P_0}$$

2.6.1 Materials and methods

Specific surface area was measured by 5-point B.E.T nitrogen adsorption (Gemini 2360, Micromeritics, Dunstable, UK) at 77 K in triplicate. Samples were accurately weighed into standard glass bulbs and dried under nitrogen at 40°C for 24 hours prior to analysis (FlowPrep 060 Micromeritics, Dunstable, UK).

2.6.2 Results and discussion

Specific surface areas for salbutamol, budesonide and formoterol are given in Table 5.

Drug sample	Surface area (m^2g^{-1})
Micronised salbutamol	3.11 ± 0.01
Micronised budesonide	5.90 ± 0.06
Micronised formoterol	5.63 ± 0.04

Table 5 Specific surface areas of the micronised drug samples measured by multipoint B.E.T nitrogen adsorption. (n=3, ± Standard deviation)

It is interesting to note that while budesonide and formoterol have comparable surface area, the surface area of salbutamol is relatively smaller. This is in agreement with particle size values for the same drugs where salbutamol had the largest mean values and consequently smaller surface area.

2.7 DIFFERENTIAL SCANNING CALORIMETRY

The influence of heating on the thermal properties of the micronised drugs was investigated using differential scanning calorimetery (DSC). In principle, DSC operates by measuring the heat flow associated with chemical changes in a material (i.e. crystallisation or melting) in relation to change in temperature. This is achieved by measuring the current required to maintain an equal heat flow to both a sample and reference during heating or cooling (Charsley and Warrington, 1992).

2.7.1 Materials and methods

Thermal properties of the micronised drugs were investigated using a differential scanning calorimeter (DSC 2920, TA instruments, Surrey, UK). Approximately 5-10 mg of micronised drug was accurately weighed into a DSC sample pan and crimped with a lid to form a hermetic seal. The sample and reference (empty hermetically sealed pan) were heated using a $10^{o}C.min^{-1}$ ramp rate. Calibration of the DSC was checked by measurement of an indium standard (melting point, 156.6°C).

2.7.2 Results and discussion

Representative thermograms of salbutamol, budesonide and formoterol are shown in Figure 9 A, B and C, respectively.

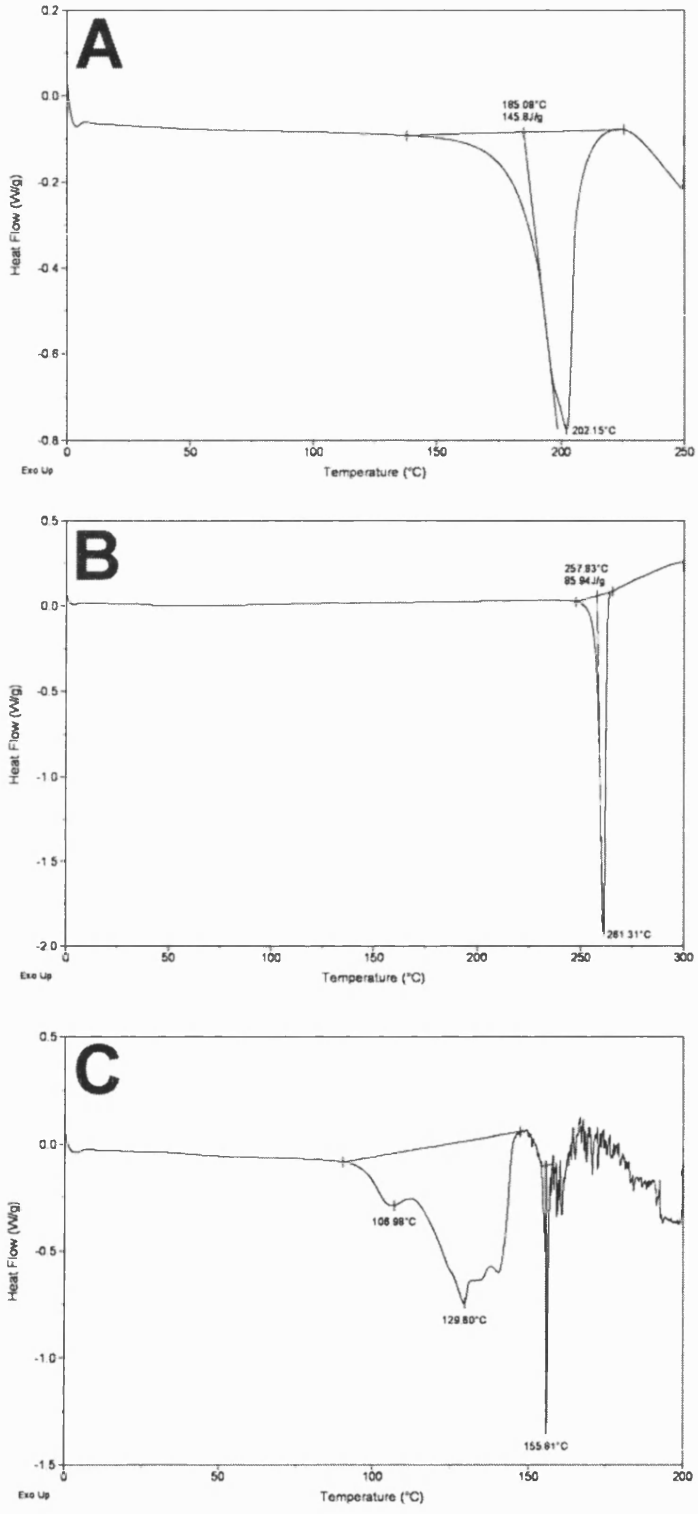

Figure 9 Differential scanning calorimeter thermographs of (A) salbutamol, (B) budesonide and (C) formoterol

The DSC thermograph for salbutamol (Figure 9 A) suggested an isothermal response with respect to heat flow, until an endothermic response was observed with a peak at approximately 202°C (suggesting a melt with decomposition). In general, such observations were in good correlation with previously published data (Ticehurst et al., 1994; Ward and Schultz, 1995).

Analysis of the DSC thermographs for budesonide (Figure 9 B) suggested an isothermal response with respect to heat flow until an endothermic response was observed with a peak at approximately 261°C (suggesting a melt with decomposition) (Martin et al., 2002).

In contrast, the thermal response for formoterol (Figure 9 C) produced a wide endothermic response from approximately 100°C to 160°C, indicative of water loss and melting of a hydrated organic material which demonstrated formoterol to undergo a complex phase transition when heated.

2.8 KARL FISHER WATER DETERMINATION

The water content of the micronised salbutamol budesonide, and formoterol, were determined by coulometric Karl Fisher water titration.

In the Karl Fisher moisture content measurement, water reacts with iodine and sulphur dioxide in the presence of an alcohol and base.

$$SO_2 + CH_2OH + RN \leftrightarrow CH3SO_3^- + RNH^-$$
$$CH_3SO_3^- + H_2O + I_2 + 2RN \leftrightarrow CH_3SO_4 + 2RNH^+ + 2I^-$$

In a coulometric Karl Fisher titration, the iodine is electronically generated from the anolyte and monitored by a platinum electrode.

As long as water is present in the reaction cell, a proportional current will be generated to produce iodine. This iodine is detected by the platinum electrode and the iodine production is stopped when the water has been converted. The reaction between one mole of water and iodine is equivalent to a charge of 10.72 $C.mg^{-1}$, therefore allowing total water content to be measured as a function of electrical input (Connors, 1988).

2.8.1 Material and methods

Each drug was accurately weighted (~ 10 mg for all three drugs) and placed directly into the titration cell before being analysed for total water content (n=3) by coulometric Karl Fischer Titration (MKC-510E, Kyoto Electronics, Tokyo)

2.8.2 Results and discussion

The ubiquitous presence of water in the atmosphere enables it to be readily sorbed by solid pharmaceutical materials during processing and storage. The amount of water that is sorbed is dependent on the chemical identity and polarity of the compound, as well as the relative humidity and temperature (Dalton and Hancock, 1997). The water content for the drugs is showed in Table 6.

Drug sample	% Moisture Content
Micronised Salbutamol	0.2 ± 0.01
Micronised Budesonide	0.6 ± 0.03
Micronised Formoterol	4.9 ± 0.20

** Analysis performed in triplicate at 21°C and 55% RH*

Table 6 Karl Fisher water contents for the micronised drugs. (n=3, ± Standard deviation)

In accordance with other investigations (Young, 2002; Ticehurst et al., 1994) salbutamol indicated low water content along with the steroid budesonide (although the previous study used a similar steroid, triacinolone acetonide). In comparison formoterol, being a dihydrate, showed the highest water content.

Unfortunately, Karl Fisher water determination revealed little information about the water sorption capacity of the micronised drugs, since measurements were conducted from an ambient environment.

Thus, to further understand such relationships, dynamic vapour sorption was applied.

2.9 DYNAMIC VAPOUR SORPTION

The influence of humidity on water sorption and de-sorption for salbutamol, budesonide and formoterol was investigated gravimetrically using dynamic vapour sorption (DVS). A schematic representation of the DVS is presented in Figure 10.

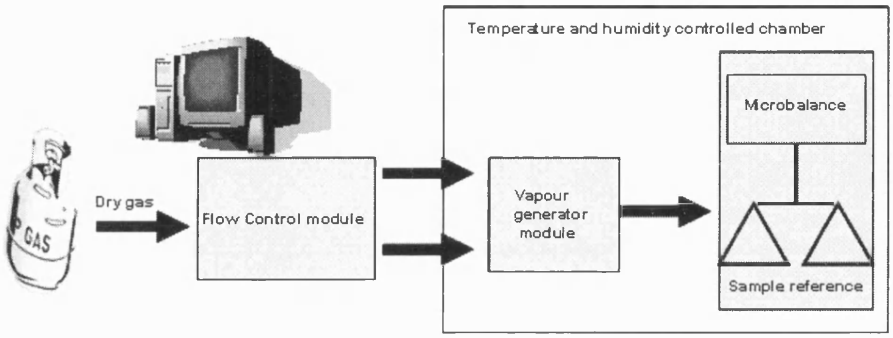

Figure 10 Schematic representation of a DVS

In simple terms the DVS is an ultra-sensitive microbalance with a resolution of 1 part in 10 million (Cahn microbalance). The main instrument is housed in a temperature controlled chamber (5-85°C) and required humidities are generated by mixing dry and saturated vapour gases using a mass flow controller before passing over the sample and reference holders (Buckton and Darcy, 1995).

2.9.1 Materials and methods

Moisture sorption for salbutamol, budesonide and formoterol, were determined using a DVS (DVS-1, Surface Measurement Systems Ld, London UK). Approximately 10 mg of sample was weighted into the sample cell and subjected to two 0-90% RH cycles, over 10% RH increments. Equilibration moisture content at each humidity was determined by a change in mass to time ratio of 0.002 dm/dt (%).

2.9.2 Results and discussion

Graphical representation of time versus equilibrium moisture content and DVS moisture sorption isotherms (calculated as a percentage of dry mass) for salbutamol, budesonide and formoterol, are shown in Figure 11, Figure 12 and Figure 13, respectively.

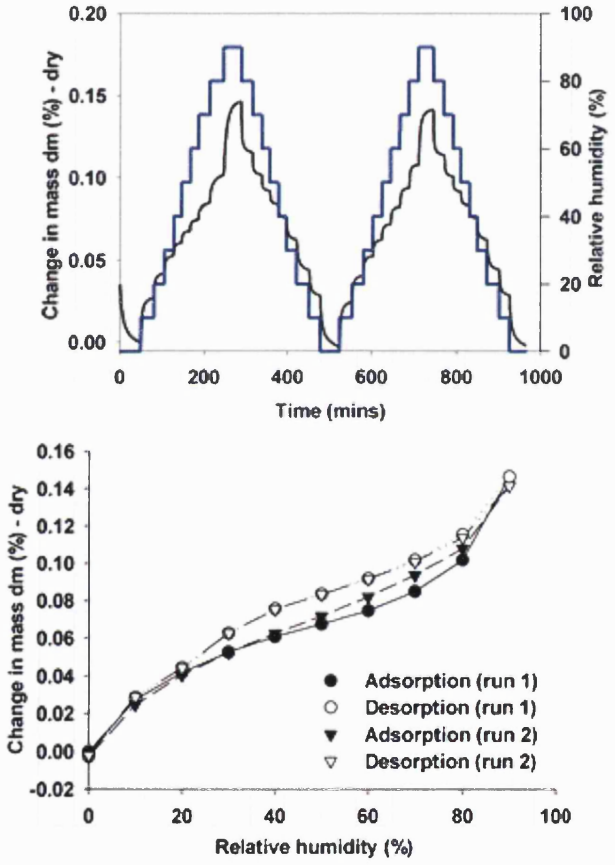

Figure 11 Moisture sorption profile (A) and moisture sorption isotherms for salbutamol

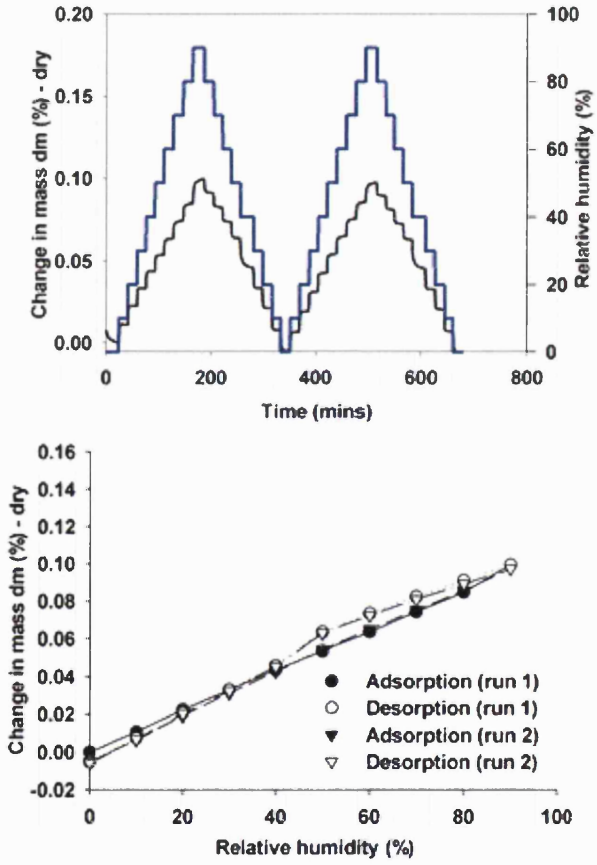

Figure 12 Moisture sorption profile (A) and moisture sorption isotherms for budesonide

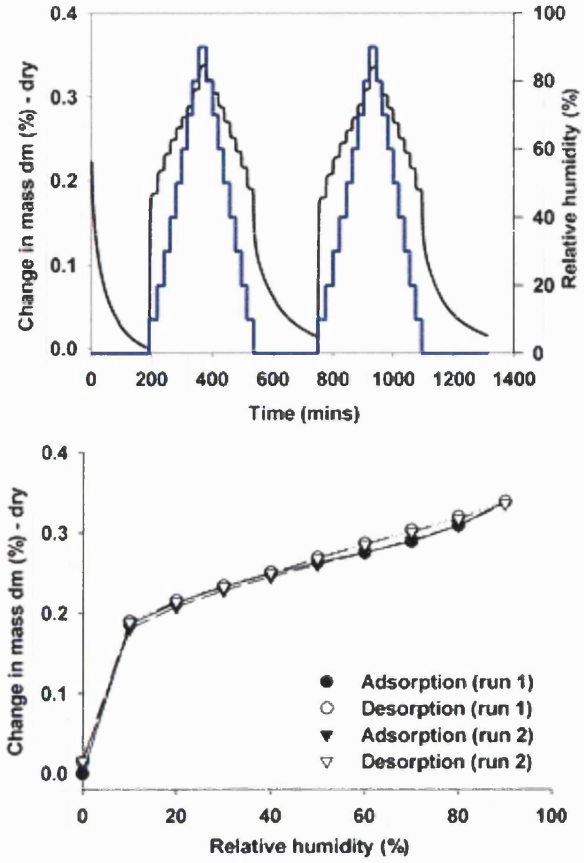

Figure 13 Moisture sorption profile (A) and moisture sorption isotherms for formoterol

Analysis of water sorption isotherms for salbutamol indicated an "L -3 type curve", typically representative of multilayer water molecules absorbing flat on the surface, or, sometimes, vertically oriented with particularly strong intermolecular interaction (Giles et al., 1960).

In comparison, analysis of the moisture sorption curves for budesonie suggested a "C, constant partition" isotherm. In general, "C-1 curves" result when the availability of sites for solute molecules remains constant at all concentrations up to saturation (Giles et al., 1960). Such curves are commonly observed in materials that have high affinity for the adsorbate or are porous. Previous investigations, studying the steroid, triacinolone acetonide (Young, 2002) suggested similar isothermic curves.

Water sorption isotherms for formoterol is indicative of a "C -2 type curve", characterised by the constant partition of solute between solution and substrate, right up to the maximum possible adsorption, where an abrupt change to a horizontal plateau occurs. Fundamentally, the linearity shows that the number of sites of adsorption remains constant; such situations could arise where the solute has a higher attraction for the substrate molecules than the solvent itself has (Giles et al., 1960).

In addition analysis of the formoterol data, suggested a linear relationship between humidity and mass, after the initial 0-10% RH increment. It is suggested that the relatively large increase in mass between 0% and 10% RH is due to interconversion between an anhydrous/partial hydrate to dehydrate form. The relative percent moisture sorption for formoterol was approximately double than that of salbutamol. Since the surface areas were of similar order of magnitude (3.11 and 5.63 $m^2.g^{-1}$ for salbutamol and formoterol, respectively) these data suggested that formoterol had a higher affinity for water.

In general, moisture sorption of powders in pMDI systems may result in variation of drug solubility and stability. However, in the case of the three drugs under investigation, moisture sorption values were relatively low (when compared to pMDI drug formulations such as disodium cromoglycate, which has the potential of adsorbing 9 molecules of water per unit cell (Young, 2002).

More importantly, is the relevant sorption and solubility properties of the drugs in the propellant based systems (as investigated in Chapter 2.10 and 2.11).

2.10 SOLUBILITY

The *in situ* determination of drug solubility in suspension or solution-based pMDI systems is clearly of importance. For example, the potential solubilisation of suspended drug particles may result in chemical degradation of the dissolved molecules. Furthermore, the potential for dissolution of smaller particulates (through the Kelvin effect) and potential crystal growth of large particulates (Oswald ripening) may result in particles outside the size range for inhalation therapy. (Johnson, 1996)

Previously, Dalby et al. (1991) described an apparatus for the determination of salicylic acid solubility in mixtures chlorofluorocarbons, and demonstrated how a limited solubility of the drug can result in Oswald ripening. More recently, Williams et al. (1999) modified the apparatus for the measurement of steroid solubility in hydrofluorocarbon based systems. A schematic of the original apparatus described by Dalby et al. (1991) is shown in Figure 14.

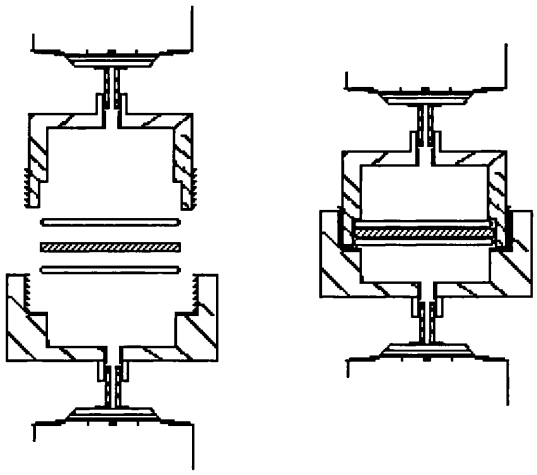

Figure 14 Solubility filter as described by Dalby el al., 1991

Although the technique described was a powerful tool for determining solubility in pMDI systems, limitations in the experimental apparatus existed. For example the seal between the two connecting pMDI canisters and filter needed to be firmly secure. In addition, the experimental apparatus required crimp assembly and disassembly (through can cutting) for each solubility study.

Therefore, for this study, a re-usable pMDI solubility apparatus that contained an integral filter holder was developed. The device was designed to be used in conjunction with a pressurised, reusable, reciprocal continuous/metering valve (similar to the method described previously (Dalby et al., 1991; Williams et al., 1999)) and/or in conjunction with a dose uniformity or impinger apparatus (as conducted here). Furthermore a high performance liquid chromatography (HPLC) assay was used. In previous investigations, using ultraviolet light detector (UV) to determine solubility, experiments suggested pMDI valve component extractables influenced the measured drug absorbance (Dalby et al., 1991).

2.10.1 Materials and methods

A schematic diagram of the solubility apparatus is shown in Figure 15. The apparatus consists of a primary and secondary stainless steel casing that sandwiched a steel frit and stainless steel filter (0.1 μm) between two slit O-rings. Micronised drugs: salbutamol, budesonide and formoterol, were investigated. Excess drug was accurately weighed into the secondary casing which was then assembled as shown in Figure 15 B.

A standard continuous pMDI valve was crimped to the primary casing and the apparatus accurately filled with approximately 7 g of HFA134a using a manual fill Pamasol device (Pamasol Willi Mäder AG, Pfäffikon, Switzerland). Samples were agitated in a gyratory water bath shaker (Gallenkemp BKS-350, Loughborough, UK) at 25°C for 48 hours prior to analysis. Drug solubility was determined using the twin stage impinger (TSI) sampling apparatus (Copley Instruments Ltd, Nottingham, UK). The TSI was used as a simple dose collection device and contained 7 ml of mobile phase in stage one and 30 ml of mobile phase in stage two. The equilibrated solubility apparatus was connected to a standard actuator (fitted with a 0.30 mm diameter orifice), which was fired to exhaustion in the TSI apparatus at 60 $L.min^{-1}$. Mass of the solubility apparatus was recorded prior to and post firing.

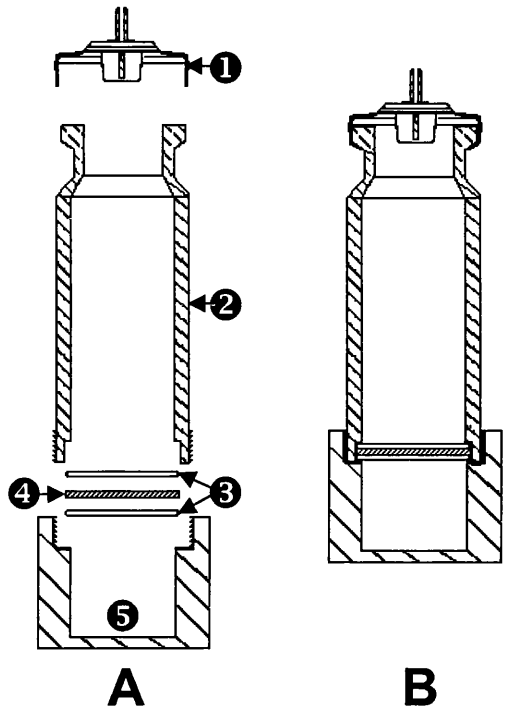

Figure 15 (A) Solubility apparatus components. Where 1, standard pMDI continuous valve; 2, primary casing for solubilised drug; 3, o-ring supports; 4, filter; 5, secondary casing (drug under investigation is weighed into this compartment). (B) Assembled solubility apparatus

The TSI components, actuator and upper/lower casings of the solubility device were rinsed into separate volumetrics with appropriate mobile phase and made to volume. Methods for HPLC drug analysis are given in Table 7 using HPLC apparatus described in more detail in Chapter 8. Samples were sequentially diluted as to fit within the linearity region of the HPLC analysis (0.5 $\mu g.ml^{-1}$ – 10 $\mu g.ml^{-1}$).

Solubility of each drug in HFA134a was determined by dividing the total drug mass recovery from the upper casing and all TSI-actuator components by the initial HFA 134a mass added. In addition the total recovered drug was compared to the initial weighed drug for mass balance. Each solubility study was conducted in triplicate.

Drug	HPLC column	Mobile Phase	Flow Rate	UV Absorbance Wavelength	Retention Time
Salbutamol	Sphereclone™ ODS, 5 μm packing, 25 cm x 0.32 mm id.	8/92 CH_3CN/H_2O (0.5 M orthophosphoric acid buffer)	0.75 $ml.min^{-1}$	223 nm	~ 8 mins
Budesonide	Supercosil™ LC-SI, 5 μm packing, 5 cm x 4.6 mm id.	40/60 CH_3CN/H_2O	1.5 $ml.min^{-1}$	248 nm	~ 6 mins
Formoterol	Supercosil™ LC-SI, 5 μm packing, 5 cm x 4.6 mm id.	40/60 CH_3CN/H_2O (2.3 mM orthophosphoric acid buffer)	1.5 $ml.min^{-1}$	218 nm	~ 8 mins

Table 7 HPLC conditions for the drug materials under analysis. Where column temperature = 25°C and injection volume = 100 μl

2.10.2 Results and discussion

Solubility values for the micronised salbutamol, budesonide and formoterol are shown in Table 8.

Drug sample	Solubility of drug in propellant (ug.g^{-1})	Mass balance %
Micronised salbutamol	0.000 ± 0.000	99 % ± 2.3
Micronised budesonide	23.136 ± 2.951	101 % ± 1.7
Micronised formoterol	7.761 ± 1.023	95 % ± 2.0

Table 8 Summary table of solubility values for salbutamol, budesonide and formoterol with relative mass balance (n=3, ± Standard deviation)

Significant differences (ANOVA $p<0.05$) in the solubility of each drug was observed, however the processing method did not effect the solubility in HFA 134a. In general the solubility of budesonide (23 ug.g^{-1}) using the new apparatus suggested similar values to previous studies using steroids (Williams et al., 1999, from graphical data: approximated as 20-45 ug.g^{-1}). Furthermore solubility of salbutamol (0.00 µg.g^{-1}) using the new apparatus suggested similar values to previous studies of β_2 agonists (Dickinson et al., 2000, described as < 0.004 mg.g^{-1}).

Recovery efficiency was greater than 95 %, for all drugs examined. Furthermore, it is interesting to note that multiple peaks were observed during HPLC analysis which did not correlate to the drug standard peak. It is speculated that such peaks are related to valve extractables and without resolution would clearly contribute to the measurement errors observed by Dalby et al., (1991).

2.11 SOLUBILITY IN MHFA

The molecular parameters affecting the solubility of a compound in a variety of solvents have been well documented (Barton, 1974; Barton, 1983; James, 1986). The predictive nature of this characteristic, however, tends to be dependent on the system (i.e. solvent) (Ruoff, et al., 1994)

Due to the fact that "real" propellants are not liquid at atmospheric pressure/temperature and taking into consideration that a great part of this study was undertaken using model propellant conditions (liquid at room temperature and atmospheric pressure), accurate solubility values for salbutamol, budesonide and formoterol were determined in order to understand the affinity and interactions of the drugs in a model propellant (mHFA, 2H, 3H-decafluoropentane).

2.11.1 Materials and methods

To insure the absence of any water residue or impurity in the system, mHFA was stored with molecular sieves (3A, 3.2 mm pellets, Aldrich Chemical Company, Inc., USA) purified with acid and basic alumina (aluminium oxide, type 5016 A basic and 504 C acidic, Fluka, GmbH) and filtered trough a 0.1 μm PTFE filter before use (according method devised by Goebel and Lunkenheimeir, 1997). A supersaturated solution of drug in mHFA was prepared by addition of approximatly 25 mg of drug in 50 ml of mHFA. Samples were agitated in a gyratory water bath shaker (Gallenkemp BKS-350, Loughborough, UK) at 25°C for 48 hours prior to analysis. Each sample was filtered through a 0.1 μm pore size PTFE filter (13 mm diameter, Whatman USA). The recovered solution was weighed and dried in an oven at 50°C for 24 hours. The recovered dry mass was then reweighed and solubility calculated by HPLC (as described previously). Samples were analysed in triplicate.

2.11.2 Results and discussion

Solubility for the three drugs in mHFA is given in Table 9.

Drug sample	Solubility of drug in model propellant ($ug.ml^{-1}$)
Micronised salbutamol	0.000 ± 0.000
Micronised budesonide	81.970 ± 1.185
Micronised formoterol	0.553 ± 0.048

Table 9 Solubility values for salbutamol, budesonide and formoterol in mHFA at 25 °C (n = 3, ± Standard deviation)

Significant differences (ANOVA $p<0.05$) in the solubility of each drug was observed.

Previous data by Dickson et al., 2000, shown salbutamol to have a solubility of < 0.007 $mg.g^{-1}$ in perfluorohexane and 0.12 ± 0.02 $mg.g^{-1}$ in 1H-fluorohexane. As expected, the introduction of a hydrogen substitute in the model propellant produced an increase of the solubility of the solute in the solvent. Conversely, the mHFA propellant (2H-3H decafluoropentane), used in this investigation, has two hydrogen atoms that substitute the fluorine atoms (increasing the polarity and solubility of the solutes), a longer carbon chain, and different dielectric constant. Consequently a direct comparison with previous findings can not be established.

However, as expected a similar rank order in solubility between HFA134a and mHFA was observed. Clearly such issues should be considered when developing an experimental protocol for AFM based measurements. These factors are investigated further in Chapters 4-7.

2.12 GENERAL DISCUSSION

From preliminary investigations into the physical properties of micronised salbutamol, budesonide and formoterol, it becomes apparent that all three drugs differ, for instance, in particle size, morphology, water sorption and solubility.

As such materials are chemically and physically very dissimilar, such differences were expected. This will have a significant effect on the specific physical –chemical and mechanical characteristics, influencing all aspects of formulation development, performance and storage.

For instance, characteristics such as surface area, density and particle size will directly influence inter-particulate adhesion forces (Hinds, 1999). Additionally, solubility and differential vapour sorption calculations indicate that the three materials have varing degrees of water affinity, suggesting a potential for Ostwald ripening, crystal growth, surface dissolution, crystal bridging and potentially poor physico-chemical stability.

Consequently, a series of investigations were undertaken to examine the cohesive and adhesive interactions of individual drug particles with neighbouring drug particles and model surfaces in the present of a model hydrofluoroalkane propellant, with the final aim of characterising pressurised metered dose inhaler performance.

CHAPTER 3: SURFACE ENERGY MEASUREMENTS

3.1 GENERAL INTRODUCTION

The majority of pharmaceutical processes require interfacial contact between particulates. It is not surprising, therefore, that surface energetics play an important role in determining the outcome of all particulate interactions. For a pressurised metered dose inhaler system, the interfacial energy may relate to drug–drug interactions (cohesion/adhesion), drug–carrier or drug–device interactions (adhesion) and de-aggregation phenomena during use.

Since all adhesive and cohesive interactions are interfacial phenomena, it is logical to accept that the basis of interactions within pressurised metered dose inhalers is via interfacial forces. As previously discussed (Chapter 1), these can be divided into apolar (Lifshitz–van der Waals), polar (electron donor–electron acceptor) and electrostatic (electrostatic double layer) components.

Consequently, changes in the nature of any surface within the product (the drug, the carrier or the container) can be expected to result in changes in the relative surface interactions. Hence, measurement of these surfaces energetic becomes of paramount importance.

Given the importance of surface energy terms as a means of predicting the interactions between different formulation components, it is desirable to gain clear insights into the relative merits of different surface energy measurement techniques. In this study, a comparison is made between contact angle (CA), inverse gas chromatography (IGC), organic differential vapour sorption (DVS) and capillary intrusion (CI) techniques.

While the contact angle method, even with its limitations (Buckton, 1995), is an established technique, the use of IGC, organic DVS and CI have only relatively recently been applied to pharmaceutical systems (Ahfat et al., 2000; Buckton and Darcy, 1995; Dove et al., 1996; Feeley et al., 1998; Kiesvaara et al., 1993; Prestidge and Tsatouhas, 2000; Sunkersetta et al., 2001; Ticehurst et al., 1994). Clearly, it would be interesting to compare the data yielded from such different approaches when applied to pMDI based systems.

Here, each technique is described in detail and investigated for its potential in examining interactions in pMDI based formulations.

3.2 CONTACT ANGLE MEASUREMENT

3.2.1 Introduction

Measuring the contact angle (θ) of powders is a useful indicator of wettability, giving information on surface energetics.

Interfacial tension is a phenomenon between two immiscible phases due to molecular attractions. In simple terms, molecules at the interfacial region between two contiguous bodies are subject to attractive forces from neighbouring molecules in both phases.

In a paper presented at the Royal Society in 1804, Thomas Young correlated the work of adhesion between the surface tension of a solid (γ_s) and a liquid (γ_l), the interfacial tension between the solid and the liquid (γ_{ls}) and the contact angle θ made by a drop of liquid (L), deposited on a horizontal flat solid surface (S). Dupré (1869) developed the equation that is now universally used and that express the relationship between work of adhesion between solid and liquid (Young-Dupré: Equation 19).

Equation 19

$$-\Delta G_{SL}^{LW} - \Delta G_{SL}^{AB} = \gamma_L(1+\cos\theta)$$

where ΔG_{SL}^{LW} and ΔG_{SL}^{AB} are the dispersive and acide/base surface free enenergy contribution for the solid and the liquid, respectively. The negative sign is made imperative by the thermodynamic convention that a negative sign for ΔG signifies an attraction.

Since the free energy of adhesion is contributed by a number of more or less independent forces, Fowkes (1962) proposed that the surface tension can also be broken down into separate components. Van Oss (van Oss et al., 1988a) developed such theory further to suggest that electron-acceptor-electron-donor interactions are essentially asymmetrical and additive.

According to Fowkes (1962, 1963) and van Oss et al., (1988a) (and their theory that most solids have Lewis acid and basic sites on their surfaces that are capable of forming complexes with a second phase), the total surface energy (calculated from the interaction between a liquid with known physical properties and solid surface) can be defined from the following equation:

Equation 20

$$W_{SL}^{Total} = \gamma_l^{Total}(1+\cos\theta) = 2\sqrt{\gamma_s^{lw}\gamma_l^{lw}} + \sqrt{\gamma_s^{+}\gamma_l^{-}} + \sqrt{\gamma_s^{-}\gamma_l^{+}}$$

The parameters in question, namely, γ_s^{LW}, γ_s^{+} and γ_l^{-}, can be evaluated by a three liquid method. In this method, an apolar and two polar liquids of know surface energy parameters are used. Solving Equation 20 using an apolar liquid Equation 21 can be derived, since γ_s^{+} and γ_l^{-} are zero, and γ_s^{LW} can be evaluated.

Equation 21

$$W_{sl}^{lw} = 2\sqrt{\gamma_s^{lw}}\gamma_l^{lw} = (1+\cos\theta)\gamma_l^{lw}$$

Because two unknown remain (γ_s^{+}, γ_l^{-}), Equation 20 is with two known polar liquids which can be solved simultaneously. From this discussion it is evident that to be able to compute the interfacial free energy of a given solid-liquid systems, the contact angle between the two needs to be determined (Figure 16).

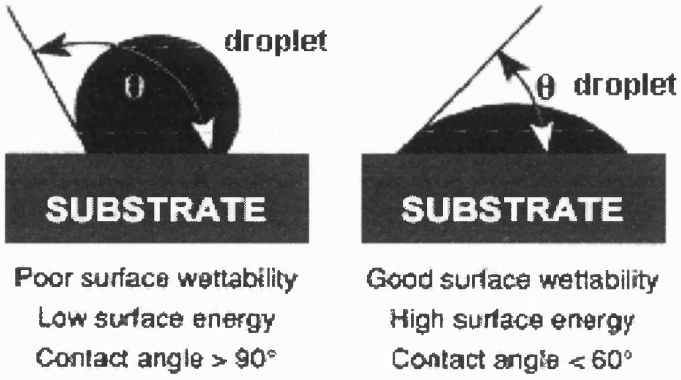

Figure 16 Diagram indicating the measurement of contact angle (θ) between a liquid and solid surface

Unfortunately, data for liquids are still scarce but they may be obtained from contact angle measurements in appropriate liquid/solid systems or from interfacial tension measurements. Moreover, the values of the surface tension components are relative to the reference value assumed for water as $\gamma^+ = \gamma^- = 25.5\ mJ.m^{-2}$

3.2.2 Materials and methods

Contact angle measurements were obtained using the sessile drop method on model compacts of the micronised drug. Compacts were prepared by direct compression using a servo hydraulic press (Model 25010, Specac Ltd., Kent, UK). Approximately 250 mg of the micronised material was weighed into a 10 mm stainless steel die, spread evenly in the die and compacted with a compression force of 10 kN. Compacts were stored in sealed containers in a controlled environment (44 %RH, 25 °C) for at least 24 hours prior to use.

The contact angle of the powder compact surfaces were measured using the sessile drop method (Good, 1992; Good and Girifalco, 1960; van Oss, 1994; van Oss et al., 1988b) with a NRL goniometer (Ramé-Hart, Inc., New Jersey, USA) equipped with a 2.3x objective lens and an 10x Ramsden type eyepiece. A liquid drop was introduced onto the substrate surface via a microsyringe. The advancing contact angles (i.e. the angle the drop makes when it has ceased advancing) were measured for three different liquids (water, diiodomethane and ethylene glycol) at room temperature (20°C). A summary of the surface tension components of the liquids used in the direct contact angle determination (van Oss, 1994) is presented in Table 10.

	Surface tension components and parameters ($mJ.m^{-2}$)			
	γ^{LW}	γ^{+}	γ^{-}	γ^{AB}
Diiodomethane	50.8	~0	0	0
Water	21.8	25.5	25.5	51.0
Ethylene glycol	29.0	1.92	47.0	19.0

Table 10 Surface tension components and parameters of liquids used in CA measurements at 20 °C (van Oss, 1994)

3.2.3 Results and discussion

The surface energy components obtained by CA measurements are presented in Table 11.

	Surface energy components from CA ($mJ.m^{-2}$)			
	γ^{LW}	γ^{+}	γ^{-}	γ^{AB}
Salbutamol	46.5 ± 0.7	8.3 ± 1.5	18.5 ± 1.2	24.6 ± 2.5
Budesonide	49.1 ± 0.4	0.34 ± 0.43	22.5 ± 3.8	4.6 ± 2.9
Formoterol	48.5 ± 0.4	0.11 ± 0.15	35.0 ± 3.2	3.2 ± 3.0

Table 11 Surface free energy components obtained using CA measurement. (n=3, ± Standard deviation)

The highest dispersive value was measured for budesonide followed by formoterol and salbutamol, respectively.

Interestingly, there are clear statistical differences in the electron donor and electron acceptor components of the surface free energies. These variations are most likely due to the chemical nature of the drug and the surface functional groups on the faces of the micronised crystalline (Chapter 2) material. However, since such these materials are micronised, it becomes difficult to associate each component with specific surface chemistry.

The contribution of the polar and dispersive components is however discussed in more detail in subsequent Chapters.

3.3 INVERSE GAS CHROMATOGRAPHY

3.3.1 Introduction

Inverse gas chromatography (IGC) is an extension of conventional gas chromatography (GC) in which the non-volatile material to be investigated is packed as the stationary phase within a GC column. Inverse gas chromatography is able to generate adsorption isotherms of known analytes with the packed "unknown" stationary phase. Thus allowing evaluation of dispersive and acid/base interactions for specified adsorbate-adsorbent pairs.

IGC has become a widely used technique to characterise the surface properties of organic and inorganic materials. More specifically, the physical properties of pharmaceutical solids have been investigated (Planinsek et al., 2001; Planinsek and Buckton, 2003; Ticerhurst et al., 1994). In simple terms, the technique consists of measuring the chromatographic retention times of vapour-phase probes of known properties on a column packed with the material of interest (Figure 17). Acid-base probes are used to measure the acid-base characteristics of the solid surface, and saturated n-alkenes are used to measure the dispersive components of the surface energy of interaction.

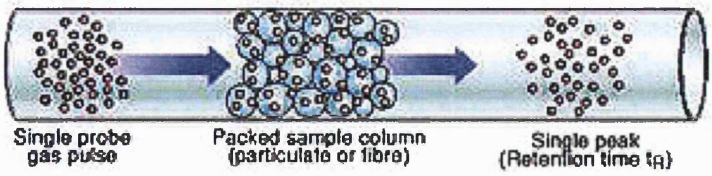

Figure 17 Inverse gas chromatography (Modified from Surface Measuremet Systems website: www.smsuk.co.uk)

In the present study, retention times of saturated n-alkanes and acid-base probes, injected at infinite dilution, were used to calculate the dispersive component (γ^{LW}) of the surface energy, the free energy of adsorption (ΔG^{AB}), and the enthalpy of desorption (ΔH^{AB}) corresponding to acid-base surface interactions.

Papirer's approach (Gutmann, 1978; Lavielle and Schultz, 1991; Papirer et al., 1999) as described by Schultz and colleagues may be used to estimate the acceptor (K_a) and donor (K_d) parameters of the test substrate.

The fundamental parameter in the IGC measurements is the specific retention volume, V_N, defined as the volume of carrier gas required to elute a probe from a column containing the test substrate material.

The interaction of neutral probes, such as saturated n-alkanes, with the substrate material is predominated by the van der Waals dispersive forces of interaction. Furthermore, it has been shown that under conditions of infinite probe dilution, the dispersive component γ^{LW}_s of the total surface energy of the substrate is related to V_N by:

Equation 22

$$RT \ln V_N = 2N(\gamma_s^{LW})^{0.5} a(\gamma_l^{LW})^{0.5} + C$$

Where R is the gas constant, T the temperature, N Avogadro's number, *a* the projected surface area of the sample probe, γ_l^{LW} the dispersive component of the probe and V_N the net volume of carrier gas required to elute the probe molecules from the column (corrected for column dead time and compression factors). A plot of $RT \ln V_N$ *versus* $a(\gamma_l^{LW})^{0.5}$ should provide a linear profile and the slope = $(\gamma_s^{LW})^{0.5}$.

The interaction of polar probes with the substrate involves both dispersive and acid-base interactions. The free energy of resorption, ΔG^{AB}, corresponding to acid-base surface interactions, may be related to Vg by:

Equation 23

$$RT= ln(V_N/V_N{}^{ref}) = \Delta G_{AB}$$

where V_N *is* the specific retention volume of a polar probe and $V_N{}^{ref}$ is the specific retention volume of a corresponding reference *n* -alkane. The equation suggests that values of $RT \ln V_g$ plotted versus $a(\gamma_l^{LW})^{0.5}$ for polar probes should fall above the straight line obtained by plotting $RT \ln V$ versus $a(\gamma_l^{LW})^{0.5}$ for the reference *n*-alkane probes. The difference in the ordinates between the point corresponding to the specific polar probe and the reference line gives an estimate of the value of the free energy of resorption corresponding to the specific acid–base interactions. The free energy of adsorption corresponding to the specific acid-base interactions may be related to the enthalpy of resorption, ΔH^{AB} by:

Equation 24

$$\Delta G^{AB}= \Delta H^{AB}- T\Delta S^{AB}$$

where ΔG^{AB} is the entropy of resorption corresponding to the specific acid-base interactions.

A plot of $\Delta G^{AB}/T$ versus 1/T should yield a straight line with slope, ΔH^{AB}. The enthalpy of resorption corresponding to the specific acid base interaction is related to the acceptor and donor parameters, K_A and K_D, of the substrates by:

Equation 25

$$\Delta H_{AB} = K_A DN + K_D AN^*$$

Where *DN* and *AN* are the donor and acceptor numbers, respectively, of the acid-base probe as defined by Gutmann (Gutmann, 1978). Riddle and Fowkes (1990) determined that part of the electron acceptor value, *AN*, was due to dispersive forces; therefore, *AN** was developed, being solely due to polar interaction forces. A plot of $\Delta H^{AB}/AN$ versus *DN/AN* should yield a straight line with slope K_A and intercept K_D.

3.3.2 Materials and methods

The surface free energy components of micronised salbutamol, budesonide and formoterol were determined using a commercially available IGC (SMS IGC 2000, Surface Measurement Systems Ltd, London, UK). Approximately 1 g of drug powder was weighed into standard glass IGC columns and plugged with glass wool. Each column was tapped for five minutes, using the minimum setting on a jolting voltameter (Surface Measurement Systems Ltd, London, UK) to a produce 'uniform' powder bed. Each column was equilibrated in the IGC at 0% RH, at 318.05 K, under dry nitrogen for 3 hours prior to analysis. The retention time of a series of n-alkanes (hexane to decane) and polar probes (ethanol, ethyl acetate, acetone and chloroform) were analysed at infinite dilution by flame emission detector. Column settings and run times for all three drugs were optimised at 318.05 K. Three columns for each drug were analysed.

3.3.3 Results and discussion

Micronised salbutamol, budesonide and formoterol were analysed by IGC using both apolar and polar probes. An example of the apolar linear response and polar probe retention times for micronised salbutamol is shown in Figure 18. An example of the acid base plot for micronised salbutamol is shown in Figure 19.

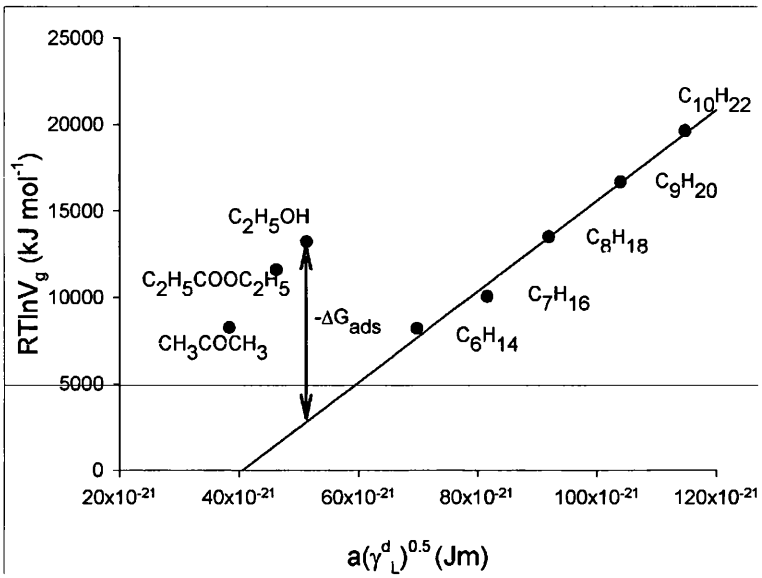

Figure 18 Micronised salbutamol surface energy plot. Where R^2 = 0.999 for apolar probes

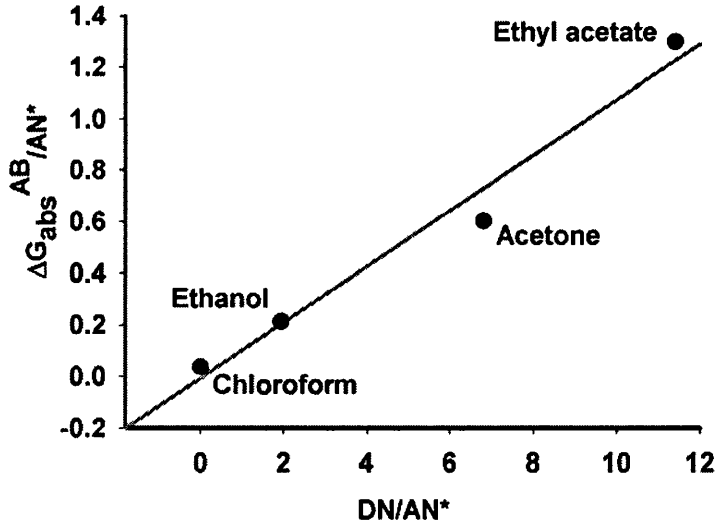

Figure 19 Micronised salbutamol acid-base component plot. Where R^2 = 0.976

The specific surface free energy components (calculated from the probe retention time) are shown in Table 12. Corrected donor DN numbers (Gutmann, 1978) and acceptor numbers AN* (Riddle and Fowkes, 1990), used for the estimation of the acidic and basic components of the surface

free energy, were as follows (AN*:DN, in Kcal/mol) ethanol 10.3:20, acetone 2.5:17, ethyl acetate 1.5:17.1, chloroform 5.4:0.

	Surface energy components from IGC		
	γ^{LW} (mJ.m^{-2})	K_A	K_D
Salbutamol	39.1 ± 1.3	0.085 ± 0.002	0.029 ± 0.001
Budesonide	62.9 ± 1.7	0.113 ± 0.002	0.013 ± 0.001
Formoterol	51.2 ± 0.7	0.093 ± 0.002	0.026 ± 0.001

Table 12 Surface free energy components obtained using IGC measurement. (n=3, ± Standard deviation)

The higher dispersive value was measured for budesonide, followed by formoterol and salbutamol, respectively. The surface energy components obtained by CA and IGC measurements follow a similar trend. The highest dispersive values were measured for budesonide by both techniques, followed by formoterol and then salbutamol. These observations are in general agreement with related studies of the ranking of the dispersive parameters of pharmaceutical powders (Ahfat et al., 1997; Ahfat et al., 2000; Planinsek et al., 2001).

A direct comparison of the data between the two techniques is difficult due to the variations in experimental and theoretical approaches (Ticehurst et al., 1994). The acid and basic components of the powder samples from IGC measurements are not consistent with the results obtained from CA measurements. This is because determination of the polar components from IGC would require specific knowledge of the surface contact area of the solvent probes with the solid. This limitation currently precludes the use of the surface component approach (SCA) in determining the polar free energy of interaction from IGC measurements.

3.4 ORGANIC DVS

3.4.1 Introduction

Organic DVS is a relatively novel method for determining the surface energy of powders by measuring the adsorption isotherm of organic vapours using an automated gravimetric vapour sorption analyser. In general, the organic DVS works using the same principle as standard water moisture sorption described in Chapter 2.9.

Using organic probes with known physical properties, and assuming Langmuir type adsorption (B.E.T type adsorption described in Chapter 2.6), it is possible to calculate the monolayer coverage for each probe, and thus relative spreading pressure. From this specific surface energy components may be calculated (Levoguer and Williams, 1999)

3.4.2 Materials and methods

All vapour sorption experiments were carried out on a modified DVS-1 automated gravimetric vapour sorption analyser (Surface Measurement Systems Ltd., London) according to the method previously described in Chapter 2. The humidity probes in the instrument were removed and replaced with sealing blanks to protect them from irreversible damage due to the organic vapours, and the vapour outlet was exhausted to a fume extractor due to safety considerations. The substrate was initially dried by flowing under dry nitrogen, and the relative partial pressures of an organic liquid probe were generated by mixing dry and saturated vapour gas flows in a similar manner to the water vapour sorption experiments described in Chapter 2.

Isotherms were measured on micronised samples of salbutamol, budesonide and formoterol in the partial pressure P/P_0 range 0-1.0 using both analytical grade n-octane and isopropyl alcohol (IPA) vapours at 25.0°C. Typical powder sample sizes were approximately 50 mg, with baseline instrument performances better than 2 μg drift per day during instrument operation.

Table 13 includes data recently obtained for the components of the surface energy of IPA and octane. Data is based on Wilhelmy wetting experiments performed using a PTFE substrate of known surface energy (Booth and Williams, 1998). This data is necessary so that a full analysis of the surface energy may be undertaken.

Solute	γ_l^{LW} (mN m^{-1})	γ_l^{AB} (mN m^{-1})	γ_l^{Tot} (mN m^{-1})
Octane	21.8	0	21.8
IPA	19.3	2.4	21.7

Table 13 Literature values for γ^{LW}, γ^{AB} and γ^{Tot} for octane and isopropyl alcohol

In the case of a non polar wetting agent (i.e. octane), the work of adhesion W_{adh} is a function of the dispersive interactions only, whereas for polar wetting agents (i.e. isopropanol), it may be expressed as the sum of dispersive and polar components of the wetting interaction. Therefore, measuring W_{sl} for both non polar and polar interactions, allows the polar and dispersive components of the surface energy to be calculated for a particular unknown material using an extension of the Fowkes equation (Equation 26).

Equation 26

$$W_{sl} = 2\sqrt{\gamma_l^{LW}\gamma_s^{LW}} + 2\sqrt{\gamma_l^{AB}\gamma_s^{AB}}$$

Where W_{sl} is the work of adhesion between the solid and the liquid surfaces, γ_s^{LW} and γ_l^{LW} are the dispersive component of the surface energy of the solid and liquid, respectively; and γ_s^{AB} and γ_l^{AB} are the polar component of the surface energy of the solid and liquid, respectively.

3.4.3 Results and discussion

As an example, Figure 20 shows typical gravimetric data for two complete cycles of sorption and desorption and respective isotherms of octane vapour on salbutamol.

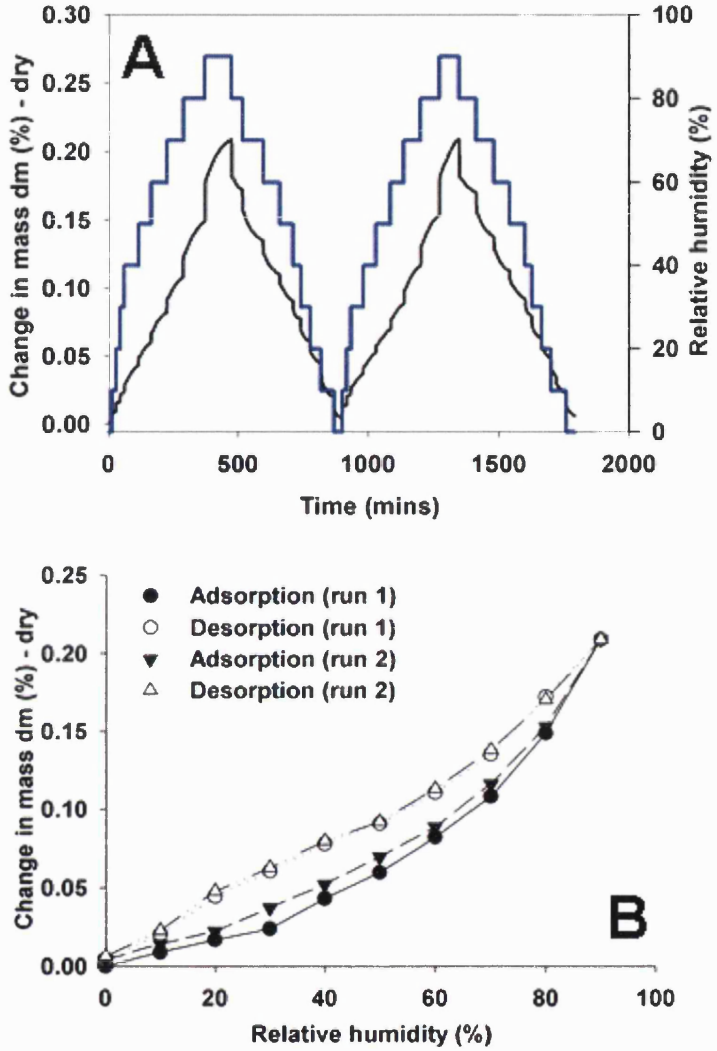

Figure 20 Moisture sorption profile (A) and moisture sorption isotherms (B) of octane vapour for salbutamol

Table 14 summarises the surface energy values obtained by the above methodology for samples of micronised salbutamol, budesonide and formoterol.

Sample	Vapour	W_{SL} (mN m^{-1})
Salbutamol	**Octane**	69.06
	IPA	84.94
Budesonide	**Octane**	71.95
	IPA	81.83
Formoterol	**Octane**	64.02
	IPA	79.52

Table 14 Experimentally determined W_{SL} data

Solute	γ_s^{LW} (mN m^{-1})	γ_s^{AB} (mN m^{-1})	γ_s^{Tot} (mN m^{-1})
Salbutamol	54.69	41.50	96.20
Budesonide	59.37	20.80	80.17
Formoterol	47.00	38.73	85.73

Table 15 Experimental values for γ_s^{LW} γ_s^{AB} and γ_s^{Tot} for salbutamol, budesonide and formoterol via organic DVS measurements

The γ_s^{LW} values for both salbutamol and budesonide calculated by organic DVS, although in the same order of magnitude, are slightly higher than that obtained by IGC and CA. In comparison, formoterol γ_s^{LW} values calculated by organic DVS were slightly lower than that obtained by IGC and CA. Budesonde appeared to have the higher dispersive surface energy value in all three surface energy applied techniques. All the γ_s^{AB} values calculated by organic DVS are higher than via the other surface energy technique.

These observations are consistent with the notion that IGC experiments are conducted at infinite probe dilution involve probing only higher energy surface sites at less than 0.1% surface coverage. The vapour adsorption method obtains average information based on complete surface coverage. Thus, the vapour adsorption method is similar to traditional wetting experiments in which the solid surface is covered completely by either vapour or liquid species.

Unfortunately, as for the IGC method employed in the Chapter 3.3, the organic DVS technique does not allow, at the present, the calculation of the specific polar contributions of the acid and basic components of the surface energy. Although empirical information may be obtained from both IGC and organic DVS (relating to polar components), the use of these techniques with the use of the surface component approach (Chapter 1) is presently not possible. Such limitations will be discussed in more detail when applied to fundamental measurements later in Chapter 4-7.

In summary, the gravimetric flow gas techniques have been shown to be a highly sensitive method for obtaining adsorption/desorption isotherms for organic vapours on particulate pharmaceutical materials. These adsorption isotherms may be analysed to obtain the equilibrium spreading pressure and this has been successfully undertaken for octane and isopropanol on all three micronised drug samples. From this data the dispersive, polar and surface energies of these powders have been accurately estimated using the classical semi-empirical model of Fowkes. This recently developed technique does not suffer from any of the problems often associated with liquid wetting based approaches and has the significant benefit of being able to monitor some aspects of the morphological stability of the powder during the experiment.

3.5 CAPILLARY INTRUSION TECHNIQUE

3.5.1 Introduction

An alternative practical technique to obtain the solid surface tension of rough and porous solids is capillary intrusion (CI). In this system a powder column is analogous to a packet column of capillaries (Buckton, 1993). The spontaneous filling of a void by a liquid is due to the capillary force and consequently, in a powder sample, contact angle may be determined via the liquid rate uptake through capillary action.

Washburn (Washburn, 1921) introduced the basic theory for determining the contact angle of a solid-liquid particle system by liquid intrusion method. Grundke (Grundke et al., 1996) modified the Washburn equation and proposed an alternative method to obtain the surface energy of rough and porous solid by capillary intrusion technique. The modified Washburn equation was used to relate the measurements of liquid uptake rate to contact angle for the spontaneous uptake of liquid due to capillary action (Equation 27).

Equation 27

$$t = A'm^2$$

Where t is time, m is the mass of adsorbed liquid and A' is a constant determining the cross-sectional area of capillary (Equation 28).

Equation 28

$$A' = \frac{\eta}{c\rho^2\gamma\cos\theta}$$

Where η is the viscosity of the liquid, c is the material constant, ρ is the density of the liquid, γ is the surface tension and θ is the contact angle.

The material constant is dependent on the porosity of the sample. The two equations (Equation 27 and Equation 28) can be combined and rearranged to give:

Equation 29

$$\cos\theta = \frac{m^2}{t}\frac{\eta}{\rho^2 \gamma c}$$

Consequently, if m^2/t is monitored experimentally, the contact angle can be measured. The c value still remain an unknown but may be determined for a reproducible sample using a liquid with a 0° contact angle ($\cos\theta = 1$).
For many materials, such as the micronised drugs in this study, n-hexane may be used to determine the value of c (Roulison, 1996). Careful attention must be taken to obtain a uniform and homogeneous powder packed column. This may be achieved by control tapping providing the initial powder loading is carried out in a reproducible manner (Desai et al., 2001).

3.5.2 Materials and methods

All drug materials were used as supplied. Diiodomethane, glycerol, n-hexane and ethanol where supplied by Aldrich (Gillingham, UK), were of analytical grade, and used as supplied. The rate of uptake of liquid by the powder column was determined gravimetrically. Experiments were performed at 25 °C in an air-conditioned room. Custom built borosilicate capillary tubes, fitted with a porous frit, where reproducibly filled with 1000 ± 10 mg of powder. Tubes were tapped 50 times using a jolting voltameter (J. Engelslsmann, Ludwigshaven, Germany). The tube was then suspended under a modified analytical balance and over a large 10 cm diameter bath containing the solvent in use. Using such a large bath is preferred because the liquid level

will not be significantly affected by the liquid uptake of the powder column. The bath was then raised manually toward the hanging borosilicate tube until just in contact with the liquid surface and the capillary rise could be seen to have begun, affecting the reading in the balance. Mass vs. time data were collected automatically at a rate of one point per second over no more than 400 seconds of the intrusion. The n-hexane was initially run as a blank (n = 3) using 3 intrusion tubes in order to determine the contribution of the solvent adsorbed in the frit. This value, which should remain constant throughout the experiment, was subtracted from the raw data prior to plotting the m^2 against the time curve. A schematic of the capillary intrusion apparatus is presented in Figure 21.

Physical data and surface tension parameters for the four liquids used for the capillary intrusion analysis are listed in Table 16.

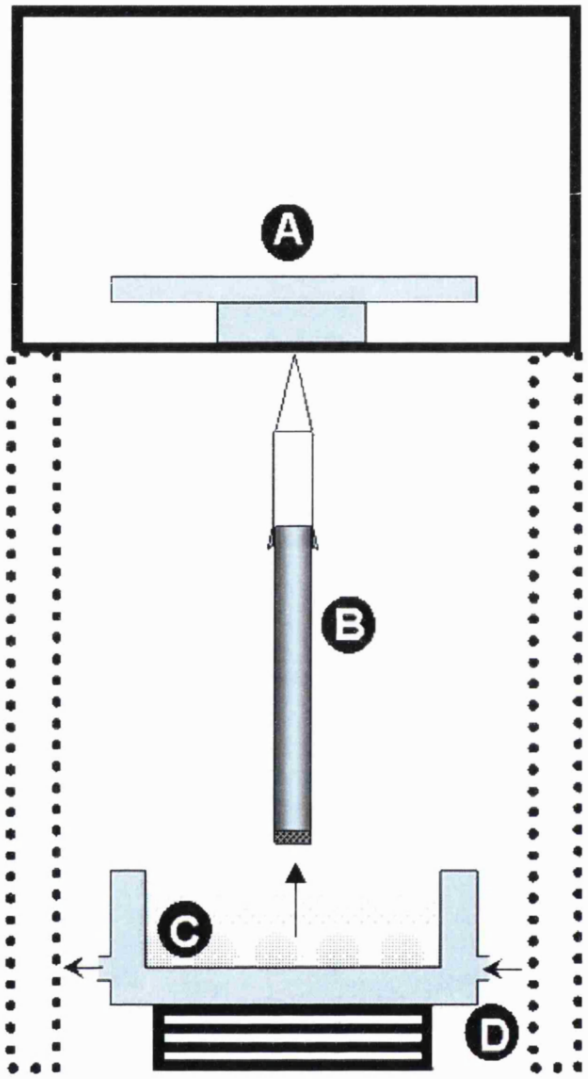

Figure 21 Capillary Intrusion Apparatus A) Balance, B) borosilicate tube, C) solvent bath, D) laboratory jack

Each micronised drug sample was analysed to determine the "c" constant. Least square linear regression analysis was used to obtain the slope over the straight part of the m^2 against time curve. It was noted that slight variations in the diameter of the tubes were shown to affect the "c" value, consequently each drug was analysed using the same three tubes.

Liquid	Density (kgm^{-3})	Viscosity (mPas)	γ_L ($mJ.m^{-2}$)	γ_L^{LW} ($mJ.m^{-2}$)	γ_L^{+} ($mJ.m^{-2}$)	γ_L^{-} ($mJ.m^{-2}$)	γ_L^{AB} ($mJ.m^{-2}$)
n-hexane	659	0.31	18.1	18.4	0	0	0
glycerol	1261	945	64.0	34.0	3.92	57.4	30
diiodomethane	3325	2.6	50.8	50.8	0	0	0
MilliQ water	1000	1.00	72.3	21.8	25.5	25.5	51.0
ethanol	789	1.20	21.4	18.8	0.019	68	2.6

Table 16 Summary of physical and surface tension parameters for the five liquids at 20°C. (van Oss, 1994.). Due to the solubility of salbutamol in water, ethanol was used as a substitute for the correspondent analysis

3.5.3 Results and discussion

The main factors affecting capillary intrusion are both the properties of the wetting liquid and the drug particulate characteristics. Of this, particle size is of great importance. Samples analysed in this case had particle size distributions smaller than powder samples reported in the literature (Prestidge and Tsatouhas, 2000) with consequent larger surface areas and greater heterogeneity. Clearly, such conditions are undesirable due to the negative effect relating to the variation in the effective capillary radii of the particle bed (Diggings et al., 1990).

The material "c" constant and its relative standard deviation was calculated and presented in Table 17.

Drug sample	C constant ($\times 10^{-10}$ m^5)	Stdev
Micronised salbutamol	1.9656	± 1.1852
Micronised budesonide	6.2330	± 3.7871
Micronised formoterol	22.7467	± 1.3663

Table 17 Material constant determination for micronised salbutamol, budesonide and formoterol (n = 3, ± Standard deviation)

Using the relative c values, the contact angle data for the three micronised drug samples via CI measurements were calculated and summarised in Table 18.

Drug	Diodomethane		Glycerol		Water		Ethanol	
	Angle (°)	Std	Angle (°)	Std	Angle (°)	Std	Angle (°)	Std
Salbutamol	70.19	1.43	*	*	N/A	N/A	54.50	14.51
Budesonide	80.19	8.58	*	*	84.52	6.39	N/A	N/A
Formoterol	89.84	0.05	*	*	89.98	0.01	N/A	N/A

*Table 18 Contact angle (θ°) data for the three micronised drug samples investigated using CI method. * Glycerol produced a values for cos θ bigger then one, consequently no angle value could be extrapolated. N/A is due to solubility of the drug in the respective solvent*

As previously discussed, the determination of contact angle using the CI method is dependent on a reproducible determination of the material constant "c".

As results of small particle size for the three drug samples, the experiments produced very poor reproducibility of the material constant with consequent inconsistent final results. This is in agreement with previously published data (Kiesvaara et al., 1993; Kiesvaara and Yliruusi, 1993), where particle size has an effect on the liquid penetration. In addition, due to differences in solubility for the three drug samples, one of the solvents could not be used throughout all the experiments. Further, the use of glycerol as polar liquid produced inconsistent results in all cases. In conclusion, without one set of the results obtained using this polar liquid, calculation of the surface energy was limited in all cases.

3.6 GENERAL DISCUSSION

The techniques investigated in Chapter 3, for determining surface properties are based on essentially different theoretical approaches. Clearly such different approaches make comparing results a difficult task.
Indeed, others have reported such difficulty when attempting the measurement of particulate surface energies (Buckton, 1993).

Contact angle methods are not well suited to powdered samples and the presence of liquid probes may result in a potential change in the physical form (e.g. dissolution and/or crystallisation of amorphous regions). Furthermore, to obtain contact angle of a pharmaceutical powder it is necessary to first compress the particle to obtain a flat surface. This compression may cause changes in surface properties, and the rough micro-surface produced often leads to contact angle hysteresis, reducing the accuracy of the results (Buckton and Newton, 1986).

One possible method of overcoming such issues in CA is capillary intrusion. In the case of CI, powder compaction is not required, since analysis relies on capillary intrusion through a powder bed. However, again, CI has potential drawbacks due to powder column repeatability, possible phisco-chemical change in presence of probes and relative solubilities of different powders in the organic probes.

Recently it has been argued that vapour sorption methods are the preferred approach to the study of powder surface energetics. Vapour sorption methods include gravimetry (Buckton and Darcy, 1995), isothermal microcalorimetry (Buckton and Darcy, 1995) and inverse gas chromatography.

The merits of each of the techniques investigated in Chapter 3 are discussed below, and related to the proposed fundamental adhesion measurements in Chapter 4-7. For completion, direct comparison of the results obtained from the four techniques is presented in Table 19.

	Surface energy components from CA ($mJ.m^{-2}$)				Surface energy components from IGC ($mJ.m^{-2}$)			Surface energy components from organic DVS ($mJ.m^{-2}$)	
	γ^{LW}	γ^{+}	γ^{-}	γ^{AB}	γ^{LW}	K_a	K_b	γ^{LW}	γ^{AB}
Salbutamol	46.5 ± 0.7	8.3 ± 1.5	18.5 ± 1.2	24.6 ± 2.5	39.1 ± 1.3	0.085 ± 0.002	0.029 ± 0.001	54.7	41.5
Budesonide	49.1 ± 0.4	0.34 ± 0.43	22.5 ± 3.8	4.6 ± 2.9	62.9 ± 1.7	0.113 ± 0.002	0.013 ± 0.001	59.4	20.8
Formoterol	48.5 ± 0.4	0.11 ± 0.15	35.0 ± 3.2	3.20 ± 3.0	51.2 ± 0.7	0.093 ± 0.002	0.026 ± 0.001	47.0	38.7

*Note: no values from CI are given due to experimental limitations discussed previously

Table 19 Surface free energy components obtained using CA, IGC and organic DVS measurement. (n=3 ± Standard deviation)

In general, CA, IGC and organic DVS values follow a similar trend. The highest dispersive values were measured for budesonide for all three techniques. These observations are in general agreement with related studies of the ranking of the dispersive parameters of pharmaceutical powders (Ahfat et al., 1997; Planinsek et al., 2001). Dispersive values of formoterol and salbutamol follow the same ranking for both CA and IGC techniques (with formoterol higher then salbutamol), but the order changes when the same drugs are analysed by organic DVS (salbutamol higher then formoterol). Furthermore, the same ranking pattern is present if the total polar component is considered only between CA and organic DVS. Unfortunately in this respect IGC data cannot be included since Ka and Kb are dimensionless numbers.

As previously stated, similar correlations using CI could not be made due to logistics of the experimental analysis.

In summary, direct comparison of the data between the three techniques is difficult due to the variations in the experimental and theoretical approaches (Ticehurst et al., 1994).

Furthermore, since individual polar components of the surface free energy are not obtainable using either organic DVS, IGC or CI, it therefore remains, that direct CA measurement may be the most useful technique when considering the SCA model for predicting particle interactions.

Therefore, CA measurements were specifically utilised for comparison when conducting fundamental particle interaction measurements in Chapter 4-7.

CHAPTER 4: INTERPARTICULATE INTERACTIONS MEASURED BY AFM - GENERAL METHODOLOGY

4.1 GENERAL INTRODUCTION

As previously stated, a common approach to formulating pMDI is to prepare suspensions (Chapter 1). However, few works have been published addressing the nature and range of the particle interactions involved in such a system (Michael et al., 2000; Young et al., 2003).

High resolution topographical analysis of material surfaces has been revolutionised with the invention of the Atomic Force Microscopy (AFM) in 1986 (Binnig et al., 1986). The nature of the technique allowed rapid development of other AFM based techniques including the capability for measurement of interactive forces acting between a tip and substrate under specific media (Ducker et al., 1992). With the capability of measuring a range of physical and/or chemical properties on the sub-nanometer scale coupled with high-resolution imaging and versatility, the AFM briskly found application across a vast range of scientific disciplines (Wickramasinghe, 2000). More recently the AFM has also been applied to a number of pharmaceutical problems (Ibrahim et al., 2000; Louey et al., 2001; Sindel and Zimmermann 2001; Young et al., 2003). The AFM has been particularly useful for characterising the surface morphology of materials at very high resolution and measuring fundamental interactive forces between contiguous surfaces. For pharmaceutical analysis, the AFM colloid probe approach has successfully been developed to allow the measurement of micronised particle interactions specific to inhalation technology (Eve et at., 2002; Young et al., 2003) under controlled environmental conditions.

The AFM operates by measuring the deflection of a microfabricated cantilever (usually by laser reflection) as it interacts with a surface. In simple terms, the AFM consists of four major components: (1) a micro-fabricated cantilever probe, (2) a detection system, (3) a piezoelectric scanner and (4) a computer controlled feedback system. These components are discussed in more detail below and shown graphically in Figure 22.

(1) Cantilever probe.

Cantilevers are critical components of an atomic force microscope system since they determine the force applied to the sample and directly relate to the ultimate lateral resolution of the AFM system. The cantilever consists of a spring-like probe generally with an integrated tip. Cantilever assemblies are fabricated from silicon or silicon nitride using photolithographic techniques. For topographical imaging, sharp proximal tips are produced with high aspect ratio probes. However, tipless cantilevers can also be utilised for allowing the preparation of colloidal drug probes for measurement of particle interactions. Atomic force microscope cantilevers are produced with spring constants lower than the effective spring constant between atoms in a solid, which are of the order of 10 $N.m^{-1}$. The spring constant of the cantilever depends on its shape, dimension (particularly the thickness), and the material from which it is fabricated. Since the cantilever obeys Hooke's Law (Equation 30), for small displacements the interaction force between a probe and an interacting surface sample can be measured:

Equation 30

$$F = -k.\Delta D$$

Where F is the Force (N), k is the cantilever spring constant ($N.m^{-1}$) and ΔD is the recorded deflection.

(2) Photodiode detector.

A quadrant photodiode detector is used to measure the position of a laser that is reflected from the tip of the cantilever probe. As the cantilever flexes, the light from the laser is reflected onto the split photo-diode. By measuring the difference between the two photodiode signals, the angular deflection of the cantilever can be calculated.

(3) Piezoelectric scanner.

The movement of the sample (or tip depending on AFM system) is performed by an extremely precise positioning device made from a piezoelectric ceramic (typically constructed of lead zirconium titanate, with various dopants). The scanner is capable of sub-Ångstrom resolution through x, y and z dimensions. The z-axis is conventionally perpendicular to the sample. Four electrodes cover the outer surface of the tube, while a single electrode covers the inner surface. Application of voltage to one or more of the electrodes causes the tube to bend or stretch through the chosen axis. The maximum scan size that can be achieved with a particular piezoelectric scanner depends upon the length of the scanner tube, the diameter of the tube, its wall thickness and the strain coefficients of the particular piezoelectric ceramic from which it is fabricated (typically this ranges laterally from tens of Ångstroms to over 100 microns and vertically from the sub-Ångstrom range to about 10 microns).

(4) Feedback loop controller.

Maintaining the optimal pre-set parameters (cantilever deflection, amplitude etc) a digital feedback loop adjusts the tip-sample separation via the displacement of the piezo in maintaining a constant amplitude or constant force between the tip and the sample.

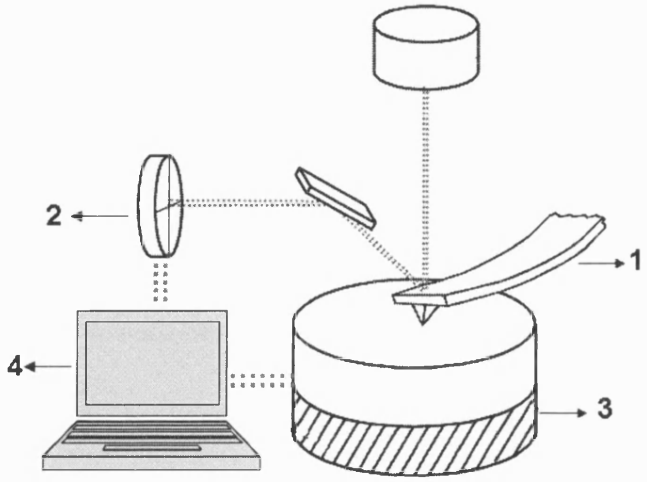

Figure 22 Schematic representation of the AFM components. where (1) cantilever probe, (2) photodiode detector, (3) piezoelectric scanner and (4 feedback loop controller

During this investigation, the AFM was used in two distinct modes of operation: its conventional topographical imaging mode and in the force measurement mode. Each method of operation is described in more detail below.

4.1.1 High resolution topographical imaging using AFM

The atomic force microscope was originally developed as an imaging tool for conducting materials (Binning and Quate, 1986). The rapid development of this technique has allowed the routine imaging of a variety of non-conducting materials in various media and between various surfaces (Atkins and Pashley, 1993; Li et al., 1993; Weisenhorn et al., 1992)

Imaging modes can be classified as "contact" or "tapping" depending on the net forces between the probe and sample.

In simple terms the contact mode operates by maintaining a pre-defined deflection (constant force) between the tip-cantilever assembly and sample surface (via a feedback loop), as the probe is rastered across a surface. The degree to which the sample is moved through the z axis to maintain constant force between the tip and sample surface is recorded and when combined with the x, y raster scan data produces a 3 dimensional topographic image of the surface.

Contact mode is the most common method of operation for imaging in liquids. However, since the tip is 'dragged' across the surface, for very soft samples, there is the potential for sample damage due to frictional forces.

In air, tapping mode AFM imaging is often employed. Tapping mode imaging is similar to contact mode, however the image is produced by oscillating a "stiff" cantilever at a specific resonant frequency. As the tip is brought close to the sample it encounters a dampening force, reducing the oscillation amplitude. A constant amplitude (set point) is maintained by moving the sample z axis, as the tip is rastered across the surface. The feed back controlled movement is recorded and used to produce a 3 dimensional topographic image of the surface. By maintaining a low set point, tapping mode is capable of imaging delicate samples, or regions containing low yield stress without causing sample damage (Höper et al., 1995; Price and Young, 2004).

A schematic of both (A) contact mode and (B) tapping mode imaging methods are shown in Figure 23.

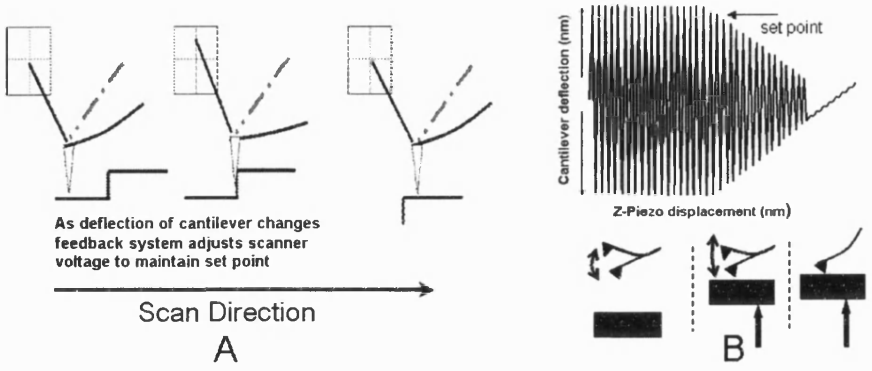

Figure 23 Schematic of (A) contact mode and (B) tapping mode imaging techniques

4.1.2 Force-distance measurements

Force measurements are recorded as an AFM probe is brought into (approach curve) and out of contact (retraction curve) with a sample surface. The raw output data obtained by cycling a probe towards, in-contact and away from a sample is referred to as a force-distance curve. A force-distance curve provides a large amount of information to be extracted about the interactive and adhesive forces acting between two surfaces. As previously discussed, by mounting an individual drug particle to the apex of a tipless cantilever, it becomes possible to investigate drug-sample interactions.

A typical force-distance curve with schematic of particle-substrate interaction during the approach and retraction cycle is shown in Figure 24.

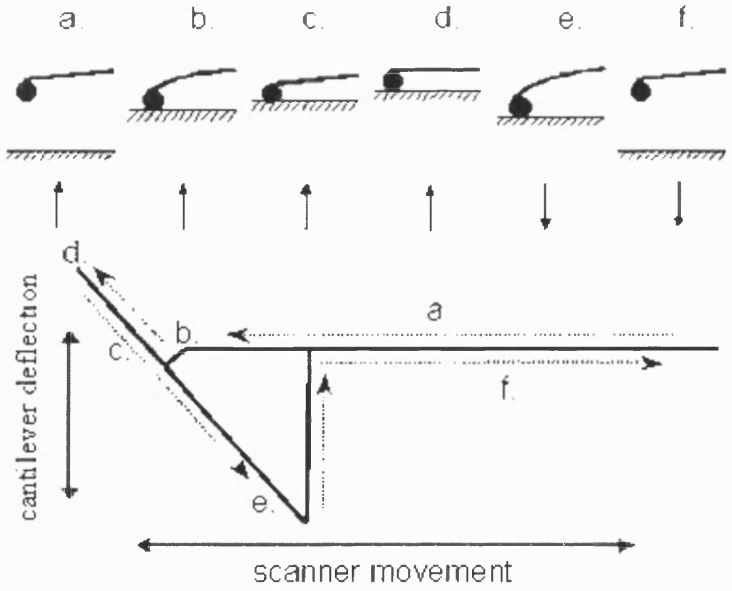

Figure 24 Typical schematic particle-substrate interaction (top) and the corresponding force-distance curves (bottom)

A detailed explanation of the measurement of a force-distance curve is described below:

The cantilever starts far above the surface at point ***a*** where no distance dependent forces act on the probe. This leads to no deflection of the cantilever. When the piezo has moved the sample to position ***b*** an attractive force deflects the cantilever-probe assembly downwards. When the gradient of the tip-sample force becomes larger than the elastic constant of the cantilever, equilibrium can no longer be maintained and the cantilever jumps into contact with the surface at point ***c***. The contact region ***cd*** is called the constant compliance region and reflects the combined deformation of probe, cantilever and sample. Continued vertical movement of the surface is met by a linear response in cantilever deflection as a predetermined cantilever load is applied and removed; lack of linearity within this region indicates tip and/or surface deformation. The piezo motion is reversed at ***d*** and the retraction continues back to the starting position to complete the cycle. At point ***e*** the force acting on the cantilever becomes greater than the adhesive force and the cantilever jumps to point ***f***. The distance ***e-f*** will always be larger than the jump-in to contact due to the presence of the adhesion forces (i.e. van der Waals). Utilising Hooke's law, relating cantilever deflection and the spring constant of the cantilever to interactive forces, the adhesive/cohesive force can be determined. Furthermore, by integrating the area under the adhesion part of the curve the energy of separation may be measured.

4.1.3 Force volume imaging

The measurement of individual force curves between an individual drug probe and given substrate can yield limited data, since the contact geometry (and thus adhesion) may vary with lateral resolution. To overcome such issues, force-distance measurements can be conducted using force volume imaging. Force volume imaging mode conducts multiple (up to 4096) individual force curves over a specific area. The result is: (1) a large quantity of data points that can be statistically analysed, (2) a low resolution height imaged produced from the constant compliance value and (3) a map of the forces across the area under investigation. Since the data collection rate for force volume imaging is high, an in-house computer program was developed to analyses the data.

4.1.4 *In situ* atomic force microscopy

One of the key advantageous of the AFM technique is the relative ease of sample preparation. For example, samples can be investigated in their native environments, such as air or liquid with little more than simple mounting on a substrate. Although, some basic sample topography (tapping mode) in this study was conducted in air, the majority of measurements were conducted in an *in situ* cell containing model propellant. The *in situ* cell allows sample measurements to be conducted in liquids under static or constant flow regimens. Furthermore, when investigating soluble excipients, samples could be changed without disturbing the probe/substrate set-up. A schematic of the *in situ* AFM cell is given in Figure 25.

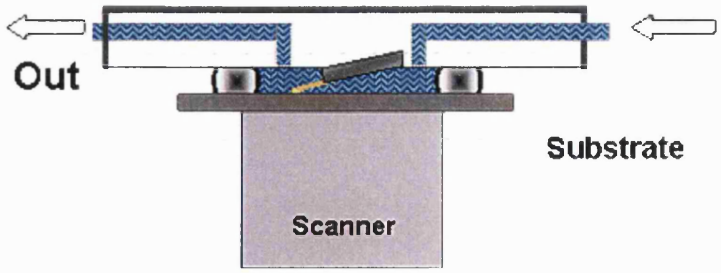

Figure 25 Schematic of the AFM in situ liquid cell

During the course of these investigations, only mHFA propellant was used since, to date, AFM measurements cannot be performed under pressure. Future innovations, including the development of a pressurised AFM cell, may allow a better insight into the interactions of such a complex system.

The aim of this investigation was to utilise the *in situ* AFM colloid probe technique as a tool to quantitatively measure the influence of adhesive and cohesive interactions between three drugs (salbutamol, budesonide and formoterol) within combination formulations and with ternary excipients and pMDI can materials.

4.2 PREPARATION AND ANALYSIS OF CRYSTAL SUBSTRATES

In order to investigate the influence of the adhesive and cohesive properties of micronised drugs using the colloid probe technique, the preparation of single crystal drug substrates was required. One of the limitations of the colloidal probe AFM approach has been associated with dramatic inter and intra variations in cohesion and adhesion measurements related to differences in contact geometry between interacting surfaces. In this study, direct comparisons of the force of interaction between specific colloid probes and an array of substrate materials was possible by crystallising molecularly smooth single crystals directly from solution.

4.2.1 Materials and methods

4.2.1a Crystallisation of drug substrates

Single crystals of salbutamol, budesonide and formoterol were heterogeneously nucleated and grown on borosilicate glass substrates using a sitting drop technique (Rhodes, 1993). Briefly, a saturated solution (25°C) of each drug was produced using an appropriate solvent: an aqueous solution of salbutamol, ethanol for budesonide and methanol for formoterol.

Each saturated solution was filtrated through a 0.1 μm PTFE filter and deposited as a droplet onto a 15 mm circular borosilicate microscope cover-slip. The subsequent saturated solutions were crystallised via primary nucleation, using an appropriate anti-solvent (ethanol for salbutamol, water for budesonide and acetone/methanol (50:50 % v/v) for formoterol). Crystallisation was achieved over a period of 48 hours in an enclosed chamber surrounded by the respective anti-solvent vapour. A schematic of the sitting drop crystallising technique is presented in Figure 26.

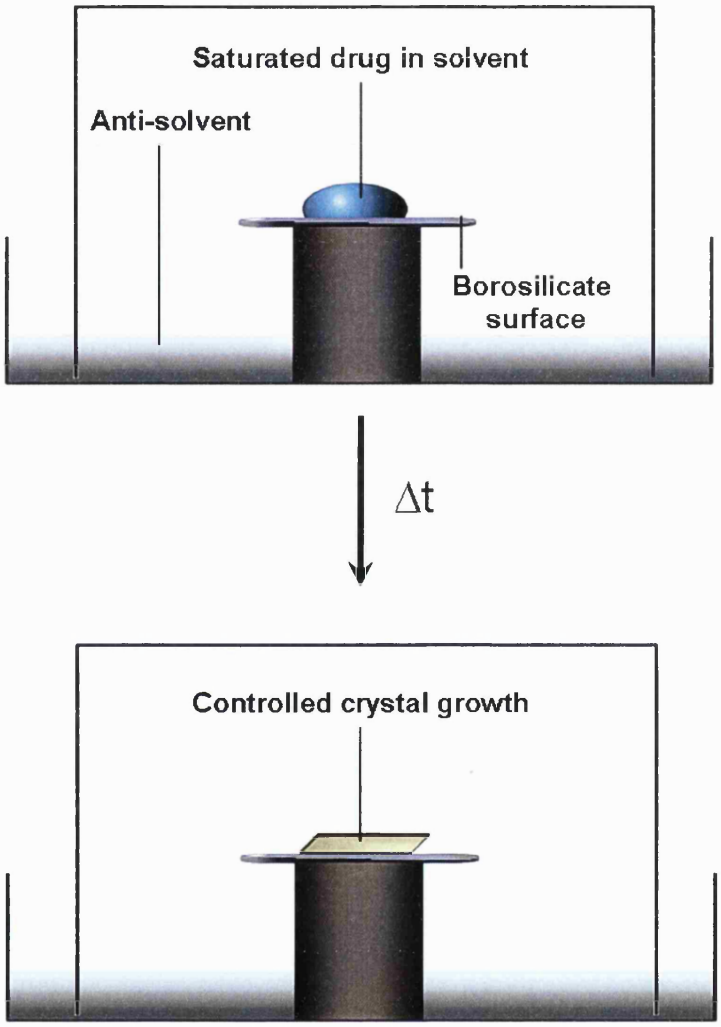

Figure 26 Schematic representation of the sitting drop crystallising technique

This process produced crystals with large areas (≥ 100 μm diameter). All crystal samples were subsequently stored in hermetically sealed containers prior to analysis.

4.2.1b General analysis of drug crystal morphology

The general morphology of the drug crystals was investigated using optical microscopy, AFM tapping mode (air) and computationally via the use of a crystal shape prediction software.

Optical photographs of each crystal were taken using a 200x long working distance microscope (Digital Instruments, Cambridge, UK) connected to CCD camera and associated software. The scale was determined by overlaying the image with a calibration grid (Digital Instruments, Cambridge, UK).

Predictive crystal morphology was conducted by inputting the crystal structure data for salbutamol (Crystal system: monoclinic; Space group: *Cc; Z=8: a=28.069 (5), b=6.183 (1), c=16.914 (2)* Å), budesonide (Crystal system: orthorhombic; Space group: $P2_12_12_1$; Z=4: a=8.550 (1), b=9.406 (1), c=28.401 (3) Å) and formoterol (Crystal system: triclinic; Space group: $P\bar{1}$; Z=2: a=6.737(1), b=10.384 (1), c=16.571(1) Å), (obtained by Albertsson et al., 1978; Ertan et al., 1997; and Leger et al., 1978, respectively) into SHAPE V 7.0 crystal computational software (Kingsport, USA).

Topographical data was produced using Tapping Mode™ with a high-aspect-ratio silicon probe (OTESP, Digital Instruments, UK), at a scan rate of 0.7 Hz. All AFM studies were performed using a commercially available Multi Mode AFM with a Nanoscope III controller (Digital Instruments, Cambridge, UK). The root mean squared surface roughness (R_{rms}) of each sample was calculated from the AFM height data over a 5 µm x 5 µm area as follows (Equation 31).

Equation 31

$$R_{rms} = \sqrt{\frac{1}{n}\sum_{i=1}^{n} y_i^{\,2}}$$

Where n is the number of points in topography profile and y_i is the distance of asperities (i) from the centre line.

4.2.1c In situ analysis of drug crystal morphology

To investigate the stability of active particles in a model pMDI system, *in situ* contact mode imaging of the surface topography of the dominant crystal growth faces of salbutamol, budesonide and formoterol were recorded in model propellant.

In situ AFM Imaging of the bespoke crystals was performed in contact mode with standard SiN_4 contact mode probes, (Digital Instruments, UK) over 50 µm x 50 µm areas at a scan rate of 0.7 Hz. To further investigate potential dissolution of the crystal substrates during AFM investigation, experiments were conducted in both pure mHFA and saturated mHFA solutions of the respective drug. Saturated solutions were prepared as described in Chapter 2. Measurements were conducted at 30 minute time intervals for both saturated and unsaturated mHFA on all three drug crystals.

4.2.2 Results and discussion

As previously discussed, with the aim of significantly reducing the influence of substrate roughness on drug probe interactions, a series of 'mesoscopically smooth' surfaces were produced by controlled crystallisation using the sitting drop technique.

4.2.2a General analysis of drug crystal morphology

The dominant crystal face predicted for each of the three drugs was used throughout this investigation. The Miller indicies of these faces were the {111} for salbutamol, {002} for budesonide and the {100} for formoterol.

Representative SEM micrographs of the re-crystallised salbutamol, budesonide and formoterol and predicted crystal morphology derived from SHAPE V 7.0 crystal computational software (Kingsport, USA) are shown in Figure 27 (A, B and C, respectively).

In general, good correlation between the SEM micrographs and predicted crystal morphology was observed for all drug materials.

Specific analysis of the topographical data produced by tapping mode AFM is discussed later in the text, since fresh batches of drug crystals were prepared for each colloidal probe study. However, for the purpose of this section analysis of topographical data indicated R_{rms} values of 1.33 nm ± 0.04 nm for salbutamol, 0.68 nm ± 0.01 nm for budesonide and 1.52 nm ± 0.01 nm for formoterol (n = 25).

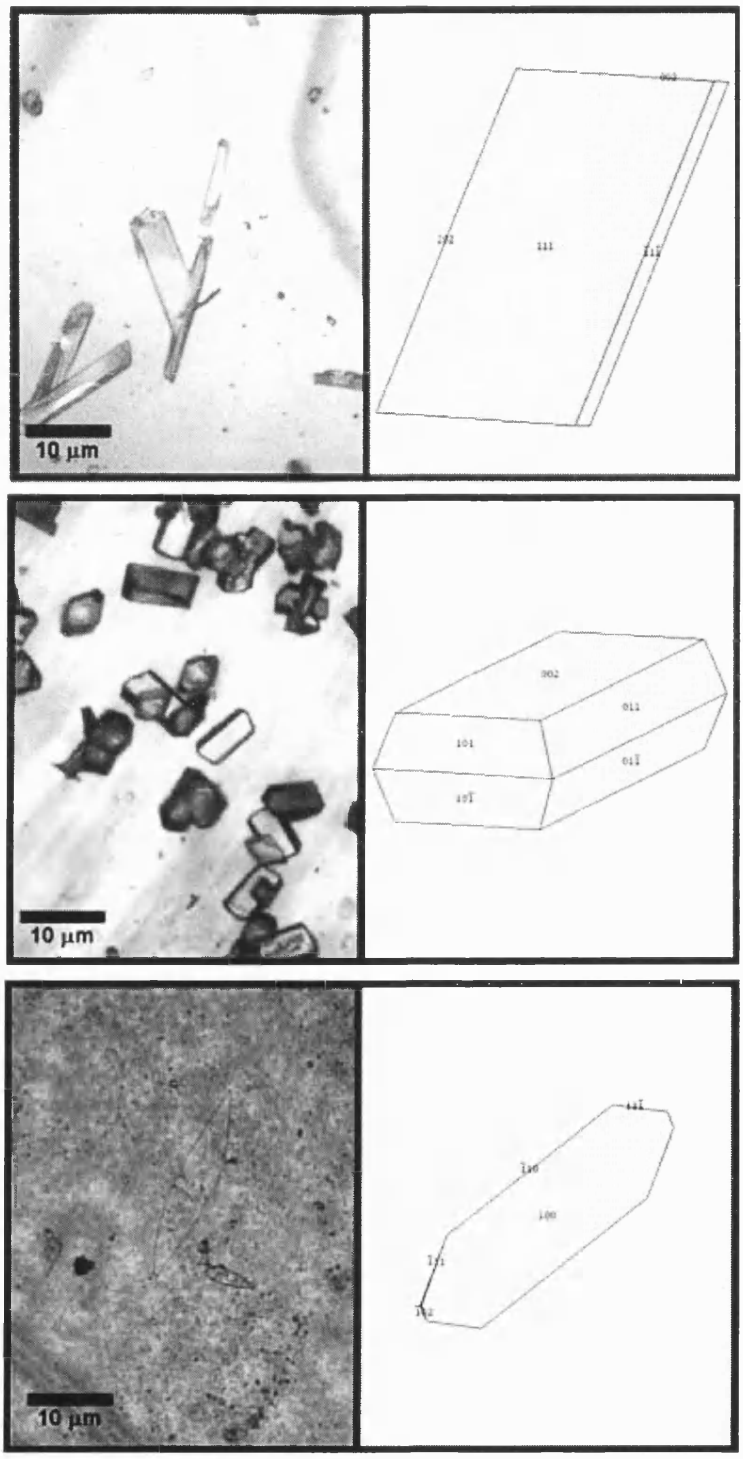

Figure 27 Salbutamol, budesonide and formoterol crystals SEM microphotographs and respective crystal morphology predictions.

4.2.2b In situ surface stability of crystal surfaces

The stability of the surface topography of individual salbutamol, budesonide and formoterol crystal faces in unsaturated model propellants are shown in Figure 28, Figure 29 and Figure 30, respectively.

In the presence of pure mHFA, real-time changes in the surface topography of budesonide crystal faces were observed over 30 minute periods. In comparison, no etching of the salbutamol or formoterol crystals was observed over the same time scale. Such observations were in good correlation with the solubility measurements conducted in Chapter 2, which indicated that budesonide was substantially more soluble than formoterol and salbutamol in mHFA.

It is interesting to note, budesonide crystals etched inward forming a pit starting from previous structural defects present on the dominant crystal plane, which formed larger and concomitantly rougher etch pits. Although not in the scope of this research, these preliminary observations suggest that surface dissolution may have a major implication on the stability issues and formulation properties of suspension based budesonide particles. Predicting how and at what rate a solid dissolves under certain conditions is paramount to the long term stability of a suspension based pMDI formulation and may limit the effects of Ostwald ripening on particle size characteristics (Blondino and Byron, 1998).

Studies using the saturated solutions of drug in mHFA (not shown here) suggested no change in crystal morphology for all drugs (images were conducted over a 6 hour period).

Consequently, unless otherwise stated, all particle interaction AFM investigations were conducted using saturated mHFA solutions of the respective drugs. All solutions were filtered using a PTFE 0.1 μm filter prior to each investigation.

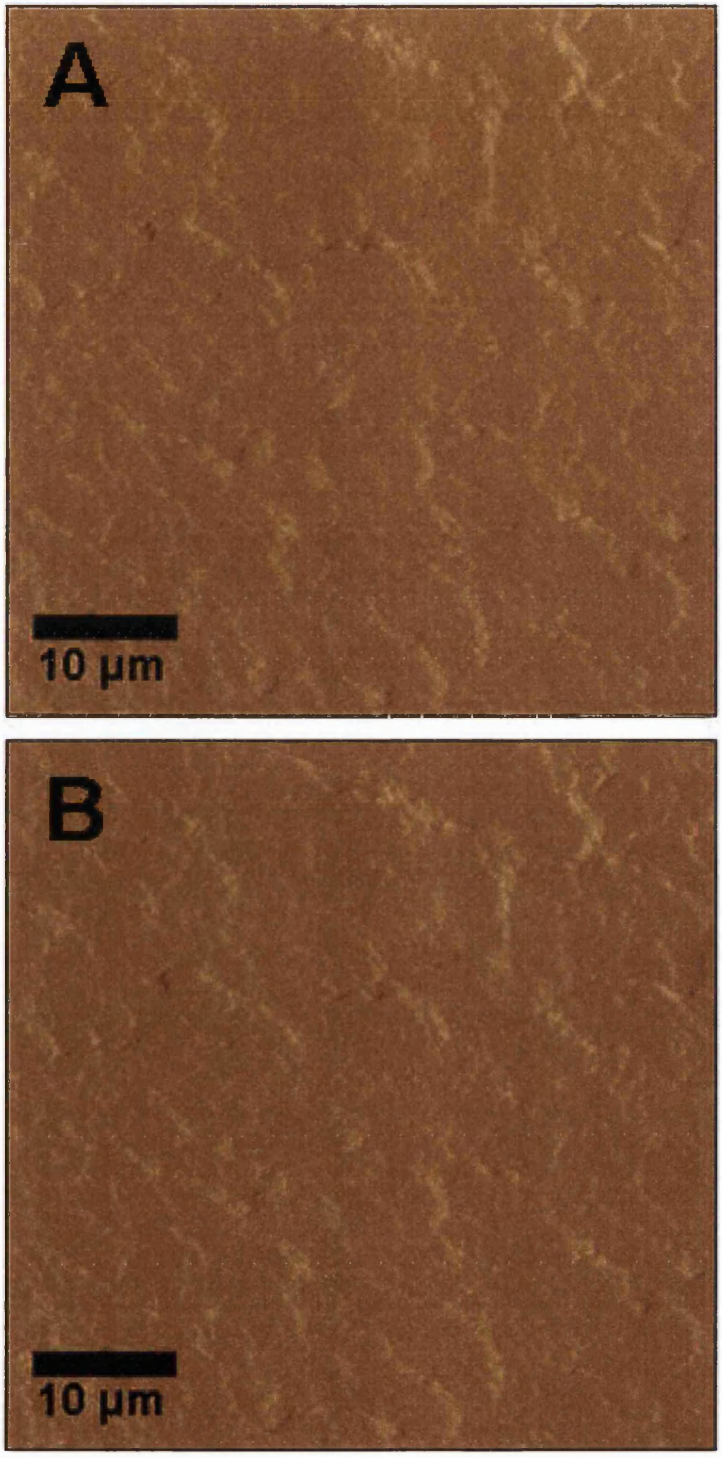

Figure 28 AFM in situ visualisation of salbutamol exposed to unsaturated solution of mHFA. A, t = 0 and B, t = 30 minutes

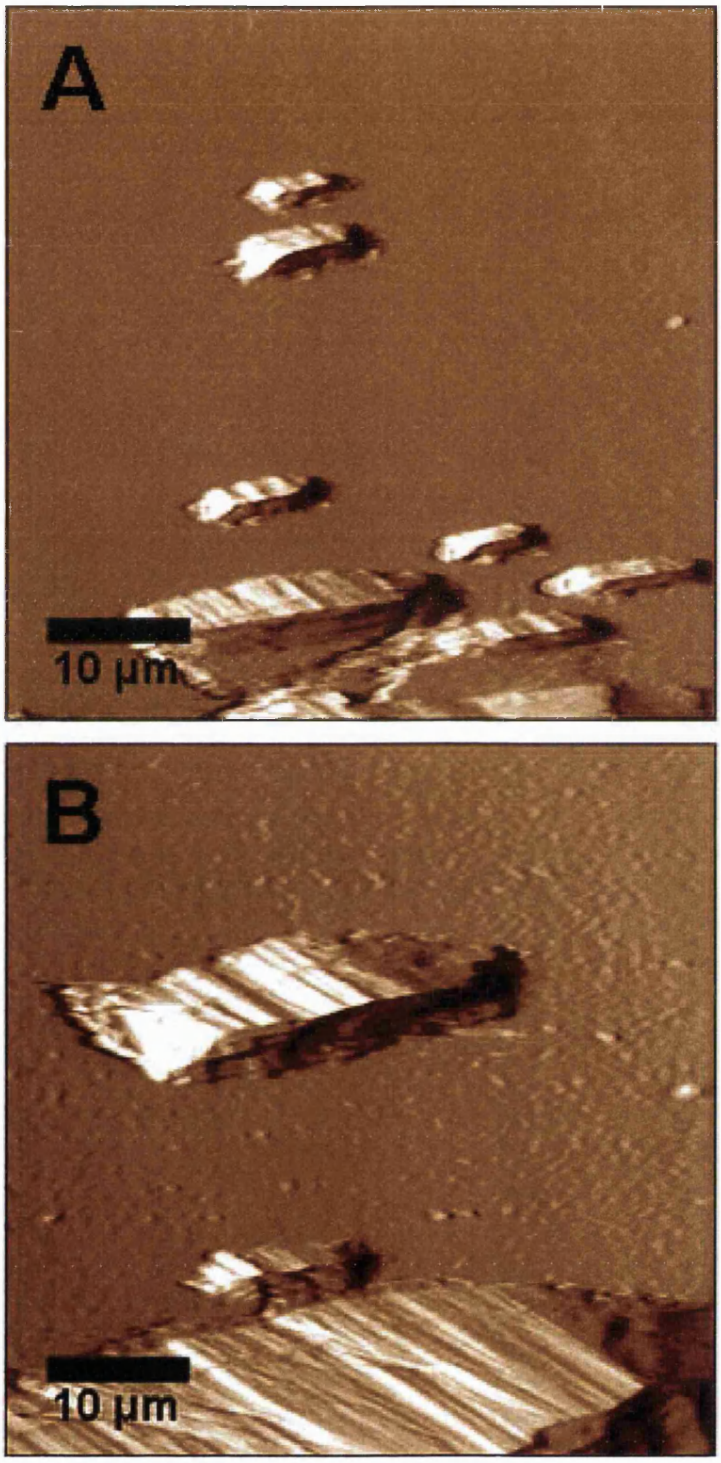

Figure 29 AFM in situ visualisation of budesonide exposed to unsaturated solution of mHFA. A, t = 0 and B, t = 30 minutes

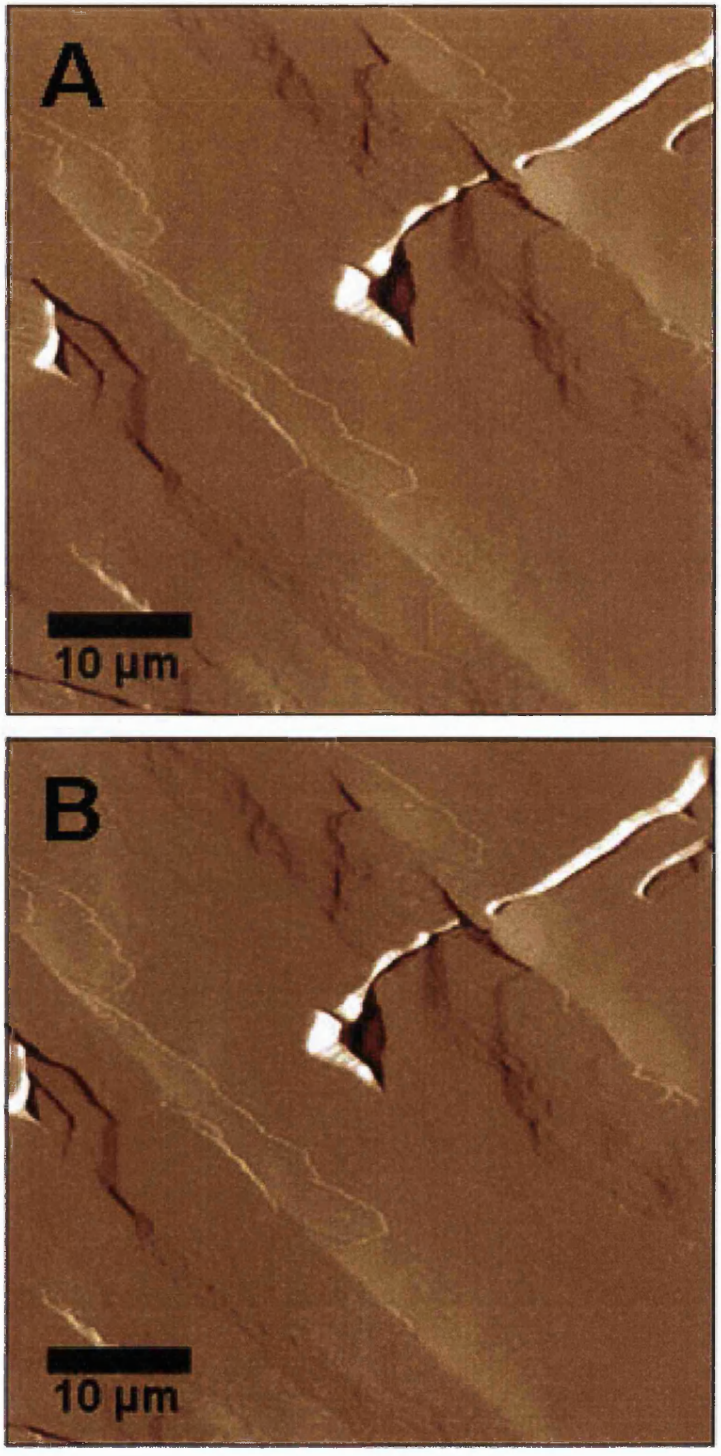

Figure 30 AFM in situ visualisation of formoterol exposed to unsaturated solution of mHFA. A, t = 0 and B, t = 30 minutes

4.3 MICROMANIPULATION OF DRUG PARTICLES ONTO TIPLESS CANTILEVERS

4.3.1 Materials and methods

Micron sized particles where attached to tipless AFM cantilevers using multi-stage micromanipulation. This technique has been adapted from the method described by Preuss and Butt (1998).

A glass cover slip, previously cleaned with methanol, was attached to a custom build microscope slide holder. At the centre of the glass cover slip, a micro droplet of epoxy resin (Ducker et al., 1991) was placed. This assembly was then fixed to a 160 X bifocal transmission microscope lens (Ziess, Germany) and focus adjusted on the glue.

A tippless 'v-shaped' cantilever (DNP20 Digital Instruments, Cambridge, UK), with a nominal 0.38 $N.m^{-1}$ spring constant, was mounted onto a custom built tip holder and attached to a X,Y,Z transition stage (Figure 31)

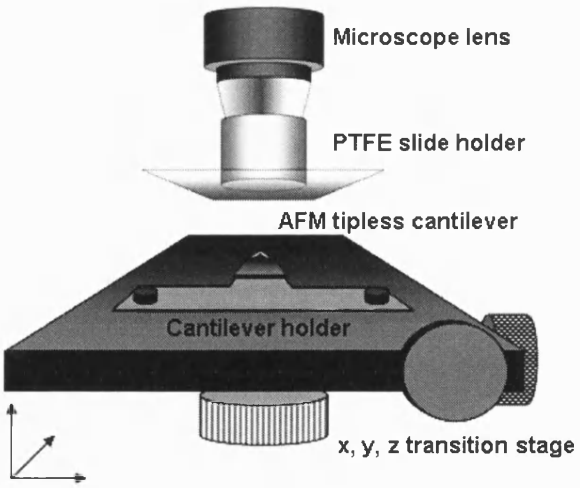

Figure 31 Graphical representation of the micromanipulation apparatus

The tip was placed in the holder at a 4° angle to allow just the end protrusion of the tip to touch the glue. The tip was then moved and placed at the edge of the glue droplet and adjusted to remove a small quantity of the glue from the protrusion (Figure 32 A).

After lowering the tip assembly, the glue coated cover slip was removed and replaced with another glass cover slip assembly. The second cover slip was sprinkled with a sample of the micronised drug particles under investigation. After re-lifting the tipless cantilever (now equipped with a micronsized drop of glue) close to the glass slide sample holder, the tip was adjusted to remove a representative single micron size particle from the glass slide surface (Figure 32 B).

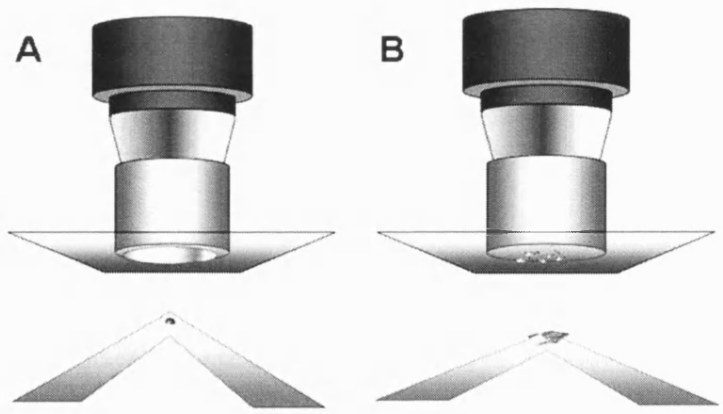

Figure 32 Graphical representation of the micromanipulation technique

A CCD video, reflection microscope (Digital Instruments, Cambridge, UK) with a 500 X long working distance lens was used throughout the micromanipulation process to evaluate tip quality, quantity of glue, and tip particle integrity prior to and post curing. Prepared drug probe tips were stored in tightly sealed containers for 24 hours prior to use.

Furthermore, at the end of each study the colloid probes were investigated using scanning electron microscopy, using the method described in Chapter 2. Samples were analysed at the end of each study (i.e. on completion of the required measurements), since the gold sputtering process would effectively render the tip redundant. If there was an issue with tip integrity, upon post observation by SEM, the colloid probe data would be discarded.

A sample tip with micronised budesonide particle mounted is presented in Figure 33.

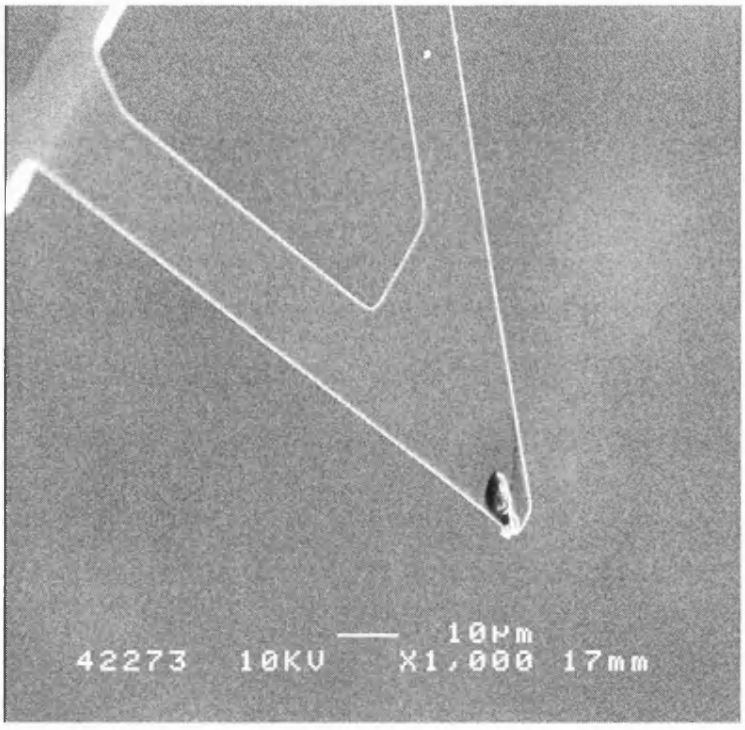

Figure 33 A scanning electronmicrograph of a micronised budesonide particle attached to a tipless AFM cantilever

4.4 COLLOID PROBE MEASUREMENTS

As previously mentioned, the interactions between individual particles and their respective surfaces were carried out in saturated drug solutions of mHFA with an *in situ* liquid AFM cell (Ashayer et al., 2003; Young et al., 2003). It is important to note that conventional AFM systems are currently limited to studies in air and/or low vapour pressure liquid environments. Thus, mHFA was chosen for its similarities to the physico-chemical properties of HFA227, used in pMDIs (Rogueda, 2003).

4.4.1 Materials and methods

Multiple force distance curves (n = 512) were determined between each drug probe and substrate over 5 μm x 5 μm areas with the following settings: approach-retraction cycle 0.5 μm, cycle rate 4.07 Hz, and a loading force of 20 nN. All studies were performed with a minimum of three probes of each drug.

To avoid significant variations in contact area between an individual probe and the respective substrate surfaces, a great deal of care and attention were taken to maintain the integrity of the colloid probe throughout the study.

After considering the complexity of pMDI systems, three key areas were chosen for investigation by AFM:

Chapter 5 ***Drugs-canister surface energy interactions;***
Chapter 6 ***Drug-drug interactions;***
Chapter 7 ***Effects of surfactant and stabilisers on drug-drug interactions;***

Where possible, AFM measurements obtained for each of the systems was discussed in relation to the physico-chemical properties, morphology and surface energy.

CHAPTER 5: DRUG-CANISTER SURFACE ENERGY INTERACTIONS VIA ATOMIC FORCE MICROSCOPY

5.1 INTRODUCTION

As previously stated, many pMDI formulations rely on the suspension of micronised drug particulates in propellant with or without stabilising excipients. Historically, the materials used within the device construction have sometimes been found to cause suboptimal performance of the formulation. Reasons for reduction in formulation performance include: elastomer swelling, extraction of low molecular weight polymers into the propellant, poor lubrication and adsorption of the formulation to canister walls (Tiwari et al., 1998).

During upright storage and use, the drug particulates will come into contact with the can wall resulting in a potential for non-reversible adhesion. This can be exemplified in a recent patent (Ashurst et al., 1996 - US Pat.No: 6,143,277) that describes coating the inside of aerosol containers with fluorocarbon and non fluorocarbon polymers to specifically reduce particle adhesion.

As previously stated, in any such system there is the potential for the adhesion of suspended micronised drug particulates to the pMDI canister walls (resulting in a deviation from delivered dose label claim). However, such interactions become particularly important for higher potency, low-dose formulations, as the total drug surface area will be less than that of the canister wall (Young et al., 2003).

Few works published to date have focused on the nature and range of the interactions (present in aqueous and non-aqueous systems), between drug particles in suspension and canister walls. Furthermore, such observations have generally been empirical and have studied the subject in a semi-quantitative manner (Chibowski et al., 1992; Parson et al., 1992; Podczeck et al., 1996; Young et al., 2003; Young and Buckton, 1990). Consequently, a more rational approach into the understanding of these interactions would be beneficial when considering the formulation of pMDI suspensions.

The primary objective for investigating such phenomena in this study was to quantitatively investigate the influence of canister wall material on the adhesion of micronised drug particulates, and to correlate the adhesion to the various surface free energy components and theoretical thermodynamic work of adhesion.

More specifically, the study involved an attempt to correlate the interfacial free energy of interaction (thermodynamic work of adhesion), modelled using the van Oss theory for interfacial forces in non-aqueous media (as described in Chapter 1), and the surface energy of different polymer coated and non-coated aluminium canister walls (measured using conventional contact angle methods) with direct adhesion measurements of micronised drug probes on respective surfaces (using AFM).

5.2 MATERIALS AND METHODS

Aluminium (ALU), anodised aluminium (AN-ALU) and polymer coated pMDIs: (perfluoroalkoxy (PFA), fluorinated ethylene propylene – polyether sulphone (FEP–PES) and polytetrafluoroethylene (PTFE)) were used for the study. For AFM and surface energy measurements, the materials were cut using metal snips, to produce ~1 cm^2 substrates suitable for analysis. The canister materials were washed with methanol and dried using filtered nitrogen prior to study.

5.2.1 Surface morphology of the canister materials

The morphology of each canister material was studied using both SEM and conventional tapping mode AFM. The methods for preparation and analysis follow those described in Chapter 2 and 4, respectively.

5.2.2 Surface free energy measurement of drug and can materials

The surface free energy of the canister and drug materials were investigated using the sessile drop method (CA) as described in Chapter 3 (Buckton, 1995; Good, 1992; Good and Girifalco, 1960; Good and Stromberg, 1979; van Oss et al., 1988b). As previously stated small 1 cm^2 areas of the canister materials were used, while the drug materials were formed into model compacts using the method described in Chapter 3.

5.2.3 *In vitro* AFM measurements of micronised drug probes on respective canister surfaces

The interaction of drug particles with canister surfaces, in a mHFA system (Rogueda, 2003) filled with saturated mHFA solution of the respective drugs under investigation was conducted using the atomic force microscope equipped with an *in situ* cell (Chapter 4). Force volume settings were as follows: scan size 10 µm x 10 µm, approach retraction cycle 500 nm, cycle rate 4.07 Hz and a constant compliance of 60 nm.

A drawback in the use of the colloid probe technique in adhesion studies is the fact that the actual size and geometry of the AFM probe is unknown and, therefore cannot be normalised. Consequently, variability in probe contact radius geometry was expected. Accordingly, to avoid significant variations in contact area between each probe and the model canister material surface, the same drug probes (3 for each drug) were used for all the measurements.

Data was processed to produce separation energy values between each drug probe and canister surface. The adhesion between each canister material and drug was repeated in triplicate (3 drug probes) for each material and micronised drug.

5.3 RESULTS AND DISCUSSION

5.3.1 Surface morphology of the canister materials

Previous investigations have suggested that canister morphology will significantly influence the drug-surface adhesion (Young et al., 2003). Therefore, to fully understand the relationship between surface fee energy, total work of adhesion and drug surface interactions in a mHFA system the canister surfaces were first investigated using tapping mode AFM and SEM. Tapping mode height images and SEM microphotographs of ALU, AN-ALU, PFA, FEP-PES and PTFE canister surfaces are represented in Figure 34.

In general, SEM inspection of the canisters surface morphology suggested ALU and AN-ALU to have relatively planar surfaces containing linear striations similar to that reported previously (Young et al., 2003). PTFE appeared to have the smoother surface, while both PFA and FEP-PES presented creased, crumpled surfaces, probably due to the non uniformity of the coating materials during manufacture. In addition, the height data obtained by AFM was processed to produce root mean squared roughness values. Analysis of the R_{RMS} values over multiple 5 μm x 5 μm areas of each surface suggested statistical differences (ANOVA $p<0.05$) (n=25). Results are shown in Table 1. Roughness rank order for the canister materials under investigation was found to be PFA>PTFE>ALU>AN-ALU>FEP-PES, respectively.

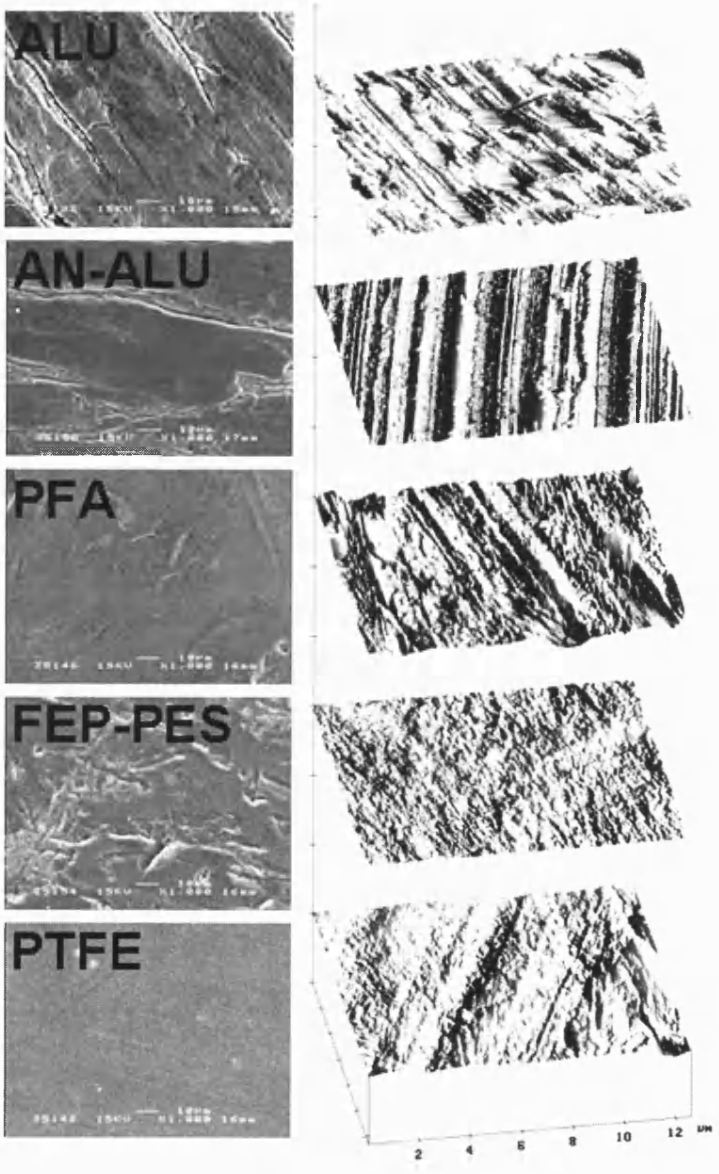

Figure 34 Taping mode height images (left) and SEM microphotographs (right) of ALU, AN-ALU, PFA, FEP-PES and PTFE canister surfaces

Materials	R_{RMS} (nm) 5 µm x 5 µm
ALU	37.36 ± 8.66
AN-ALU	20.93 ± 4.43
PFA	53.01 ± 16.23
FEP-PES	20.48 ± 7.24
PTFE	44.93 ± 16.05

Table 20 Analysis of root mean squared surface roughness values (Rrms) of the canister surface materials investigated (n =25 ± Standard deviation)

5.3.2 Surface free energy measurement of drug and can materials

The surface energy components (Lifshitz-van der Waals, electron donator/acceptor) and total surface free energy of the canister materials and drugs were determined using the contact angle method, and are shown in Table 21. Although the surface energy values for the micronised drugs have been reported previously, in Chapter 3, they are repeated in this section for convenience.

When comparing the canister materials, significant differences in the dispersive γ^{LW} surface energy was observed. Analysis of the data indicated a rank order for dispersive γ^{LW} surface energy parameter of AN-ALU>ALU>FEP-PES>PTFE>PFA, respectively. In addition, ALU and AN-ALU had γ^{LW} values approximately double that for the polymer coated canisters. A reasonable explanation for such difference in surface energy values may be related to the chemical nature of the coating material used. It is generally agreed that material surface free energy decreases with increased fluorine content (Zisman, 1963).

Analysis of the polar components of the surface free energy indicated a difference in rank order for γ^{+} PTFE>ALU>AN-ALU>PFA>FEP-PES and γ^{-} AN-ALU> ALU>PFA>FEP-PES>PTFE, respectively.

	Surface energy by CA ($mJ.m^{-2}$)				
	γ^{LW}	γ^{+}	γ^{-}	γ^{AB}	γ^{TOT}
AN-ALU	43.36 ± 0.76	0.54 ± 0.24	24.68 ± 2.23	7.14 ± 1.32	50.51 ± 0.52
ALU	40.44 ± 0.24	0.79 ± 0.24	16.05 ± 1.72	7.03 ± 1.23	47.67 ± 1.23
PFA	17.33 ± 0.78	0.42 ± 0.11	10.36 ± 0.91	4.17 ± 0.69	21.49 ± 0.16
FEP-PES	24.19 ± 0.87	0.02 ± 0.02	6.64 ± 0.23	0.49 ± 0.49	24.68 ± 0.47
PTFE	18.88 ± 0.80	3.14 ± 0.57	2.04 ± 0.27	5.01 ± 0.22	23.9 ± 0.59
SS	46.49 ± 0.69	8.25 ± 1.46	18.48 ± 1.16	24.64 ± 2.50	71.12 ± 2.97
BUD	49.07 ± 0.39	0.34 ± 0.43	22.47 ± 3.78	4.59 ± 2.85	53.66 ± 2.75
FFD	48.51 ± 0.40	0.11 ± 0.15	35.04 ± 3.18	3.18 ± 3.02	51.69 ± 3.24

Table 21 Surface energy values for canister surface material and drug calculated by contact angle ($mJ.m^{-2}$) (n = 3, ± Standard deviation)

5.3.3 Determination of the theoretical work of adhesion of different polymer coated and non-coated aluminium canister walls

The energy of interaction between salbutamol, budesonide and formoterol surfaces, were modelled against ALU, AN-ALU, PFA, FEP-PES and PTFE, respectively, using the surface component approach for interfacial forces in non aqueous media (SCA model described in Chapter 1). The dispersive component of the surface energy of the three drug particulates against the respective canister surfaces together with the acid/base, total and adhesive ratios are presented in Table 22.

Comparison of the LW and AB work of adhesion, for each drug with canister materials, suggested adhesive forces are controlled by the combination of dispersive and polar interactions. This is exemplified when comparing the rank order in predicted adhesion using dispersive or polar and dispersive calculations. For example, calculation of the work of adhesion for salbutamol with can materials shows a rank order of:
AN-ALU>ALU>FEP-ES>PTFE>PFA when considering dispersive forces only.

However, with the introduction of the acid-base component, the rank order alters with: AN-ALU> ALU>PTFE>PFA>FEP-PES.

Clearly, such a change in interaction if influential will directly affect particle adhesion and subsequent formulation performance.
Analysis of budesonide and formoterol theoretical work of adhesion, suggested a similar change in rank order, when combining dispersive and polar components.

With the aim of quantifying the contribution of the various surface free energy components (of the materials and drugs), to the thermodynamic work of adhesion, the theoretical values were compared with direct force measurements using AFM.

Theoretical thermodynamic work of adhesion ($mJ.m^{-2}$)									
Material	Salbutamol			Budesonide			Formoterol		
	γ^{LW}	γ^{AB}	γ^{TOT}	γ^{LW}	γ^{AB}	γ^{TOT}	γ^{LW}	γ^{AB}	γ^{TOT}
AN-ALU	18.16	34.85	53.00	19.24	12.78	32.02	19.01	11.94	30.95
ALU	16.74	30.66	47.40	17.74	13.13	30.87	17.52	13.06	30.68
PFA	2.98	24.08	27.06	3.16	9.94	13.10	3.12	9.79	12.92
FEP-PES	7.72	15.88	23.59	8.18	4.22	12.38	8.08	3.18	11.26
PTFE	4.14	23.42	27.55	4.38	18.46	22.84	4.32	21.89	26.22

Table 22 Theoretical thermodynamic work of adhesion between the drug materials and canister surfaces calculated using SCA model ($mJ.m^{-2}$)

5.3.4 *In situ* atomic force adhesion measurements of polymer coated and non-coated aluminium canister walls

Measurement of adhesive forces between individual particles and substrate surfaces by *in situ* AFM have been reported previously (Ashayer et al., 2003; Hooton et al., 2004; Young et al., 2003; Young et al., 2004;). However, a direct link between the macroscopic measurements of surface energy, theoretical predictions of the thermodynamic interfacial interactions and particle adhesion have not been undertaken.

The integrity of all three drug probes were investigated prior to and post measurement using a high-magnification 500 X long-working-distance reflective microscope. Drug probes appeared visibly proud of the cantilever surface, with no observable differences between the start and end of the experimental procedure (indicating no macroscopic change in drug probe morphology). As expected, comparison between drug probes (1-3) on the correspondent canister material indicated large variation in the adhesive force. A possible explanation is due to the difference in particle size and differences in contact area due to the irregularity of the drug-probes. Although attempts have been made to calculate the true contact area (Hooton et al., 2004), until now inter-probe variations cannot be quantified with accuracy. However by using one probe on a series of substrates, trends may be ranked (Appendix A1).

An obvious issue to consider when comparing the adhesion of a drug particle on a series of can substrates is the variation in roughness. Previous studies, have suggested similar roughness values to produce wide log-normal adhesion distributions when compared to measurements on atomically flat substrates (Young et al., 2004; Price et al., 2002). In such cases, a useful approach is to represent the data via its median (50^{th} percentile) value. Such an approach reduces the positive skew in mean values induced by the log-normal distribution, and also takes into account the elastic responses of the materials under investigation (Appendix A2).

Liner regression analysis for the separation energy between drugs and canister surface materials indicated a log-normal distribution for all substrates. Median separation energy values ($e_{0.5}$) were calculated for each individual specific distribution with 95% confidence limits. A summary table of median values for salbutamol, budesonide and formoterol (with respective high and low confidence intervals) are presented in Table 23, Table 24 and Table 25, respectively.

The AFM data for salbutamol drug probes suggested that the force of adhesion followed the following decreasing rank order of AN-ALU>ALU>PTFE>FEP-PES>PFA for all three probes. For the budesonide drug probe, rank order was AN-ALU>ALU>PTFE> PFA> FEP-PES. Finally, for the formoterol drug probe, rank order was AN-ALU> PTFE> ALU> PFA> FEP-PES.

Salbutamol	Separation energy Tip 1 (nJ)	Low (nJ)	High (nJ)	Separation energy Tip 2 (nJ)	Low (nJ)	High (nJ)	Separation energy Tip 3 (nJ)	Low (nJ)	High (nJ)
AN-ALU	86.40	82.84	90.12	43.17	41.46	44.94	80.07	77.30	82.93
ALU	79.14	76.57	81.80	28.60	27.55	29.69	52.75	51.02	54.55
PFA	2.84	2.74	2.94	9.11	8.70	9.54	6.41	6.09	6.75
FEP-PES	1.63	1.59	1.67	7.46	7.06	7.88	5.38	5.12	5.65
PTFE	4.15	3.96	4.34	13.11	12.52	13.73	12.80	12.11	13.54

Table 23 AFM median separation energy values with relative confidence intervals for salbutamol drug probes

Budesonide	Separation energy Tip 1 (nJ)	Low (nJ)	High (nJ)	Separation energy Tip 2 (nJ)	Low (nJ)	High (nJ)	Separation energy Tip 3 (nJ)	Low (nJ)	High (nJ)
AN-ALU	253.81	225.01	257.12	284.70	273.12	296.70	56.11	21.78	23.30
ALU	139.32	137.51	141.16	52.82	51.07	54.63	22.53	5.37	5.87
PFA	11.84	11.10	12.63	7.58	7.25	7.92	2.77	2.63	2.91
FEP-PES	4.60	4.41	4.79	5.85	5.56	6.16	0.58	0.56	0.60
PTFE	13.86	13.16	14.59	13.84	12.89	14.87	4.53	4.29	4.80

Table 24 AFM median separation energy values with relative confidence intervals for budesonide drug probes

Formoterol	Separation energy Tip 1 (nJ)	Low (nJ)	High (nJ)	Separation energy Tip 2 (nJ)	Low (nJ)	High (nJ)	Separation energy Tip 3 (nJ)	Low (nJ)	High (nJ)
AN-ALU	39.70	37.30	42.30	26.10	25.10	27.10	48.00	46.10	50.00
ALU	1.66	1.45	1.90	12.00	11.30	12.80	18.00	17.00	19.00
PFA	0.76	0.70	0.83	10.30	9.86	10.70	3.58	3.41	3.77
FEP-PES	0.59	0.57	0.61	7.29	6.88	7.73	1.93	1.79	2.08
PTFE	2.07	1.91	2.24	22.80	21.60	24.00	31.60	30.80	32.60

Table 25 AFM median separation energy values with relative confidence intervals for formoterol drug probes

5.3.5 Comparisons between thermodynamic work of adhesion and AFM measurements

From the equations discussed in Chapter 1, it is intuitive to derive that the thermodynamic work of adhesion is directly proportional to the force of adhesion. Thus by plotting the measured force of adhesion against the theoretical surface energy/work of adhesion, it may become possible to correlate theoretical and experimental measurements.

For comparison, the relationship between the surface free energy calculated by CA (LW-CA), the SCA theoretical work of adhesion (using the dispersive surface free energy only) and the total SCA theoretical work of adhesion with respect to the AFM separation energy measurements were plotted. Plots for salbutamol, budesonide and formoterol are shown in Figure 35, Figure 36 and Figure 37, respectively.

Comparison of the AFM adhesion measurements with theoretical values for salbutamol, indicated a direct relationship with surface free energy measured using the CA method (mean R^2 = 0.7952). However, when considering the theoretical work of adhesion dispersive components (calculated using the SCA method), data resulted in a less significant relationship (R^2 = 0.7020). In comparison, when assessing the relationship between adhesion measurement and the total theoretical adhesion values a more positive relationship was observed (R^2= 0.9260). Such observations suggest the SCA results in an improved relationship when considering interactions between drug particles and different canister materials.

Similar observations were also observed when considering budesonide and formoterol interactions with canister materials. In general, an increase in the linear relationship between theoretical and measured adhesion was observed when comparing theoretical surface free energy and total SCA values. In general, an increase in R^2 from 0.6947 to 0.7133 for budesonide and 0.6768 to 0.8012 for formoterol was observed when comparing AFM measurements with CA and SCA values, respectively).

Again, clearly, such measurements indicate the need to assess the polar contributions present in non aqueous media of model systems. Furthermore, the importance of incorporating these measurements is required when investigating particle-device component interactions using such theoretical approaches.

It is interesting to note, however, that the relative increase in R^2, when comparing the fundamental surface energy values with the SCA, was relatively small in comparison to results obtained in Chapter 5. This is most likely due to both the large differences in surface energy values between the polymer and aluminium substrates and variations in surface roughness.

One of the advantages of using the SCA model instead of direct surface energies, derived by CA, can be observed when comparing energetically similar polymers. For example, the surface energy rank order for the polymers is PFA<PTFE<FEP-PES. It would be therefore logical to conclude that, PFA would result in the lowest adhesion force when considering drug-substrate interactions. However, direct adhesion measurements between the drug particles and polymer substrates suggested a different rank order, where FEP-PES<PFA<PTFE. Subsequently, when comparing these results with the total theoretical SCA work of adhesion (in mHFA), a similar rank order to that of AFM was observed. Such observations highlight the importance of including the dispersive and AB components of the drug polymer and media when considering formulation development.

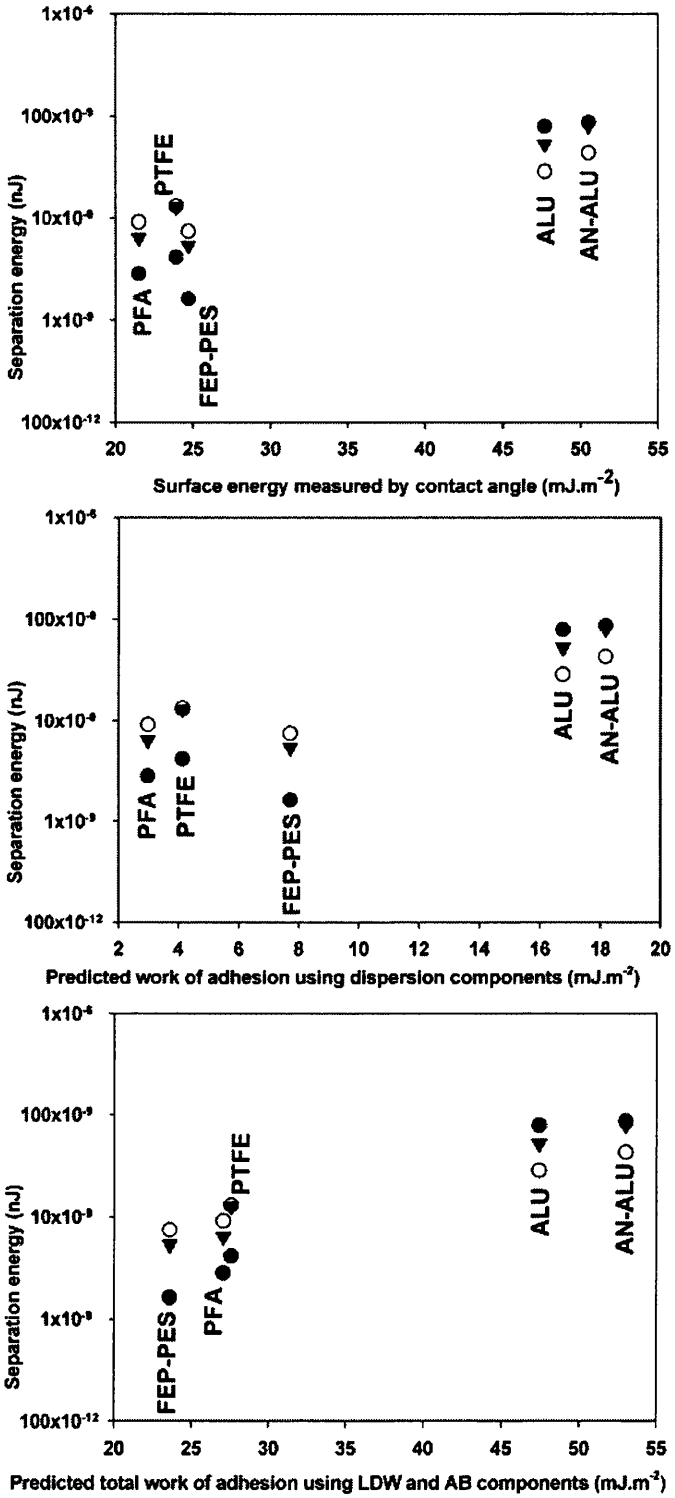

Figure 35 Plot of salbutamol AFM separation energy measurements against CA-surface energy and W-Dispersive and W-Total for the 5 canister materials. (n=3 drug probes)

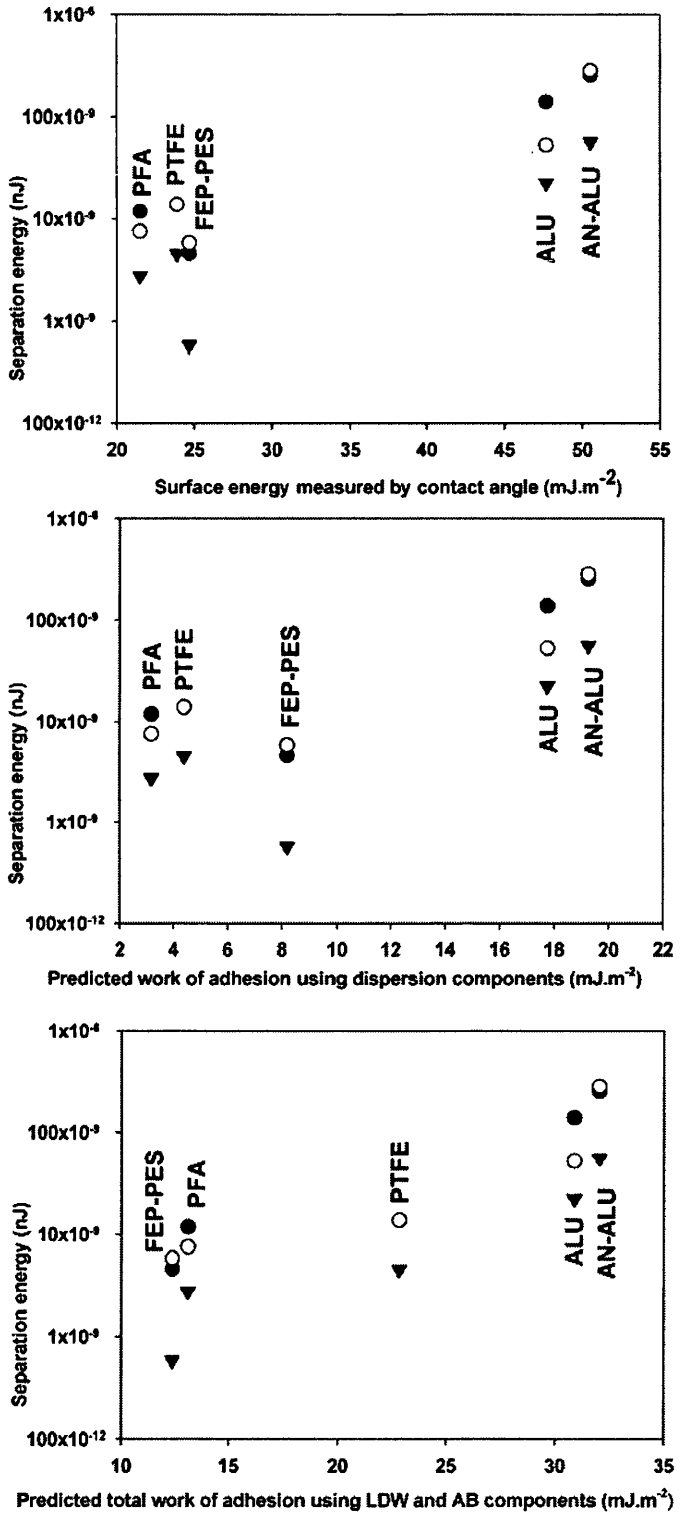

Figure 36 Plot of budesonide AFM separation energy measurements against CA-surface energy and W-Dispersive and W-Total for the 5 canister materials. (n=3 drug probes)

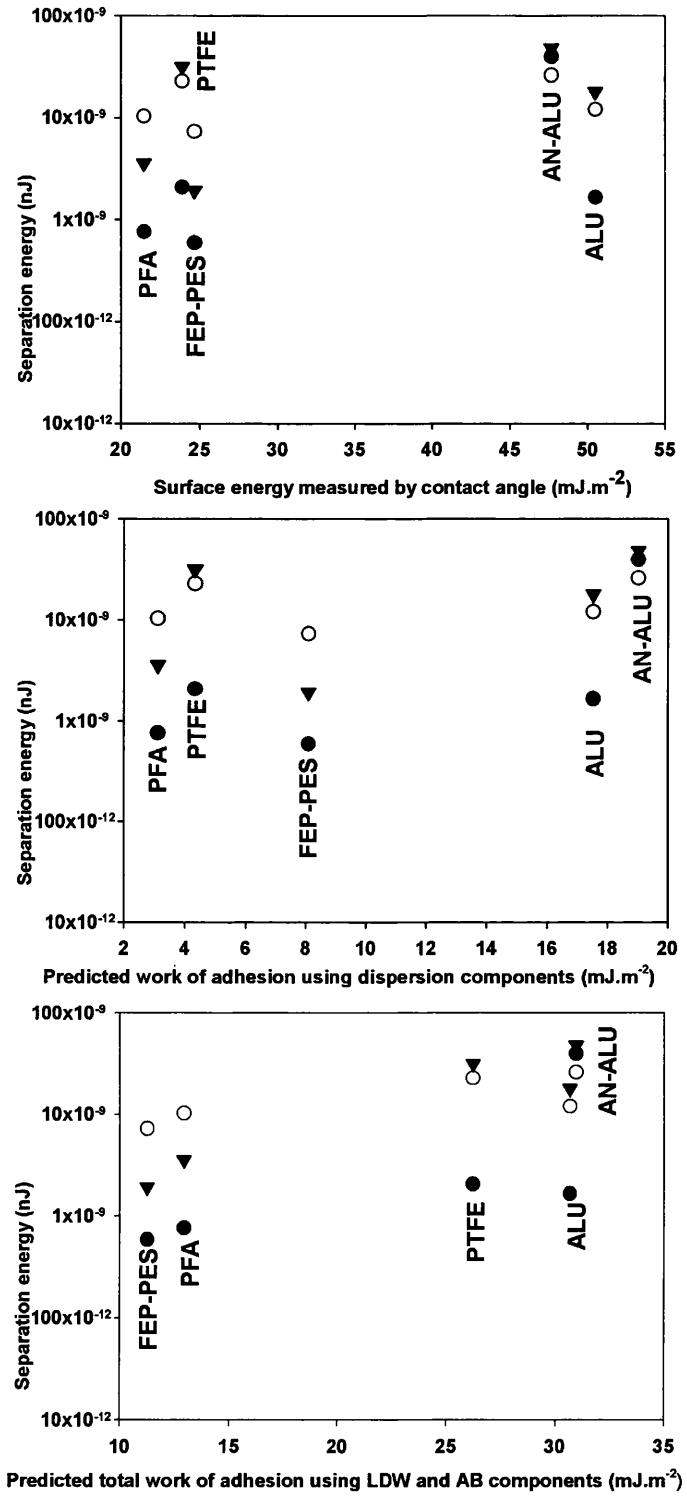

Figure 37 Plot of formoterol AFM separation energy measurements against CA-surface energy and W-Dispersive and W-Total for the 5 canister materials. (n=3 drug probes)

5.4 GENERAL DISCUSSION

As previously discussed, the primary objective of this quantitative study of drug particulate adhesion to pMDI canister materials *in situ* was to assess the contribution of all the relative forces of interactions using theoretical values and AFM force measurements. Furthermore, a correlation has been suggested.

In general, analysis of experimental adhesion data in combination with the thermodynamic work of adhesion, calculated using the SCA, provides evidence for the existence of non-DLVO type interactions in pMDI suspension based colloidal systems. Whilst classical DLVO theory could not satisfactorily illustrate the above phenomena, inclusion of Lewis AB type forces, in an extended DLVO (SCA) approach correlated well with the observed behaviour of the experimental measurements of particle adhesion on different substrates (shown by a relative increase in R^2 values).

CHAPTER 6: SURFACE ENERGY AND AFM MEASUREMENTS TO INVESTIGATE DRUG-DRUG INTERACTIONS

6.1 INTRODUCTION

The primary aim of this work was to combine direct force measurement, (obtained using the AFM colloid probe technique) with conventional surface energy measurements to gain a greater understanding of the thermodynamic and surface properties which control particle-particle interactions in pMDI model systems.

This quantitative study of adhesion/cohesion interactions in a model pMDI was carried out by colloid probe AFM, while the surface thermodynamic properties of the active ingredients were measured using contact angle measurements. As in the previous study, the relationship between AFM measurements and the interfacial behaviour of the colloid particles was modelled using a surface component theory derived from Fowkes, Good-Girifalco and van Oss (Good and Girifalco, 1960; Fowkes, 1962; van Oss, 1994).

6.2 MATERIALS AND METHODS

6.2.1 Preparation and characterisation of drug crystals

As previously discussed, one of the limitations of the colloidal probe technique has been associated with dramatic inter and intra variations in cohesion and adhesion measurements related to slight differences in contact geometry between interacting surfaces. In this study, direct comparisons of the force of interaction between specific colloid probes and an array of substrate materials was possible by crystallising molecularly smooth crystals directly from solution. Single crystals of salbutamol, budesonide and formoterol were heterogeneously nucleated and grown on a borosilicate glass substrate using the sitting drop technique described in earlier in

Chapter 4. This process produced planar crystals with large areas of sub-nanometre smooth surfaces.

Prior to force measurement the topography of the specific crystals used in each experiment was investigated using tapping mode AFM (in air) as described earlier in Chapter 4.

6.2.2 Surface energy measurements of the drug materials

Surface energy values, used to calculate the theoretical work of adhesion were calculated according to the methodology and results presented in Chapter 3.

6.2.3 AFM colloid probe measurements of specific drug crystals

Each study was performed with three probes of each drug. Data was processed to produce force of cohesion or adhesion values. To further overcome the limitation of not knowing the true area of contact between drug probes, the cohesive and adhesive forces ratios were analysed and compared using the recently developed cohesive/adhesive balance (CAB) analysis procedure as described in Chapter 1.

The AFM settings were as follows: Force volume scan size 5 µm x 5 µm, approach retraction cycle 500 nm, cycle rate 4.07 Hz and constant compliance region 60 nm.

6.3 RESULTS AND DISSCUSSION

6.3.1 Characterisation of the drug crystals

Prior to adhesion studies, the surface roughness on the dominant crystal face of each drug substrate was investigated. Root mean squared surface roughness (R_{rms}) analysis was conducted over 5 μm x 5 μm areas of each substrate (n = 25). Data were processed to produce R_{rms} values for each substrate and are presented in Table 26.

Drug crystal	R_{rms} (nm) 5 μm x 5 μm
Salbutamol	1.33 ± 0.04
Budesonide	0.68 ± 0.01
Formoterol	1.52 ± 0.01

Table 26 R_{rms} analysis of the drug crystal substrates used in AFM force measurements (n = 25, ± Standard deviation)

The data suggested that the surfaces of the crystals were extremely smooth, with all surfaces exhibiting a root-mean-squared roughness well below 2 nm over 5 μm x 5 μm areas. Although different degrees of roughness did exist between drugs (most likely related to differing crystal growth processes and kinetics during crystallisation), the uniform and smooth topography made them highly suitable for quantitative AFM analysis with micron sized drug probes. The critical size of rugosity is still an issue of debate, and it is probably dependent on both the material and the shape of the surface asperities, but the figure of 100 nm, proposed by Neumann et al., 1971, is still widely accepted to be a reasonable indication of the size below which roughness will not have a significant influence (Buckton, 1995). Only the dominant crystal faces of each crystal were studied in this investigation.

6.3.2 Surface energy components and potential interactions

In the previous AFM study (Chapter 5) the canisters surface energy values, used to compare with AFM based measurements, were obtained from contact angle measurements (since the logistics of conducting IGC, CI or DVS on the canisters samples was not feasible).

When investigating drug-drug interactions, it becomes possible to use the values obtained from the other surface energy measurements. However, for the purpose of this study, only contact angle and IGC values were utilised (since DVS is an adsorption based technique similar to IGC and use of capillary intrusion was not possible due to reasons discussed in Chapter 3). Although the surface free energy data is discussed in Chapter 3, it is presented here, in Table 27, for ease of comparison.

As previously discussed, both the CA and IGC values followed a similar trend with the highest dispersive values being measured for budesonide by both techniques, followed by formoterol and then salbutamol.

	Surface energy components from CA ($mJ.m^{-2}$)			
	γ^{LW}	γ^{+}	γ^{-}	γ^{AB}
Salbutamol	46.5 ± 0.7	8.3 ± 1.5	18.5 ± 1.2	24.6 ± 2.5
Budesonide	49.1 ± 0.4	0.34 ± 0.43	22.5 ± 3.8	4.6 ± 2.9
Formoterol	48.5 ± 0.4	0.11 ± 0.15	32.0 ± 3.0	3.2 ± 3.2
	Surface energy components from IGC ($mJ.m^{-2}$)			
	γ^{LW}	K_a	K_b	
Salbutamol	39.1 ± 1.3	0.085 ± 0.002	0.029 ± 0.001	
Budesonide	62.9 ± 1.7	0.113 ± 0.002	0.013 ± 0.001	
Formoterol	51.2 ± 0.7	0.093 ± 0.002	0.026 ± 0.001	

Table 27 Surface free energy components obtained using CA measurement and IGC. (n = 3, ± Standard deviation)

Using the dispersive and polar components of the surface free energy, the work of cohesion and adhesion for all drug particulate combinations were calculated using the surface component approach (Chapter 1).
Specific values for the W_{LW}, W_{AB} and W_{TOT} were calculated for each drug combination and are given in Table 28.

However, it is important to note, that at present it is not possible to calculate the polar components (and therefore total contribution) of the thermodynamic work of adhesion for IGC (as for DVS), since specific knowledge of the projected contact area of the solvent probes with the solid is required. Furthermore, current theoretical calculation of AN and DN from IGC results yield dimensionless numbers and not surface energetic measurements.

In general, comparison of the LW and AB works of cohesion/adhesion for salbutamol suggests that both the cohesive and adhesive interactions are dominated by polar interactions. When considering the dispersive components (salbutamol interactions), the theoretical interaction is greatest for the salbutamol-budesonide combination, and smallest for salbutamol-salbutamol. This is true for both CA and IGC measurements.
However, when considering the total energy of interaction for salbutamol based systems (i.e. when both LW and AB components are taken into consideration), the cohesion energies are greater followed by the adhesion energies of salbutamol-formoterol and salbutamol-budesonide.

For budesonide, the LW components dominate the AB interactions for cohesive and adhesive (budesonide-formoterol) energies. However, the polar contributions are higher for the budesonide-salbutamol adhesive energy. Interestingly the total theoretical energy of interaction is greater for budesonide-salbutamol, with a strong polar component.

For formoterol, the dispersive energy component is greater for the budesonide-formoterol adhesion. The polar energy component is greater for the formoterol-salbutamol adhesion, and the total energy is greatest for this system (thus, highlighting yet again the importance of polar energetic components).

In summary, this brief theoretical treatment of particle interactions derived from surface energetic components highlights the possibility of significant variations between interfacial interactions depending on whether they are calculated from dispersive components only or a combination of polar and dispersive contributions. The fact that polar components of the solids should be taken into account in non-polar liquids is counter-intuitive, although it cannot be overlooked.

Interaction	W_{LW} IGC	W_{LW} CA	W_{AB} CA	W_{TOT} CA
		Cohesive energies ($mJ.m^{-2}$)		
Salbutamol –Salbutamol	13.15	19.62	49.40	69.00
Formoterol-Formoterol	24.08	21.50	7.74	29.24
Budesonide-Budesonide	36.04	22.04	11.12	33.14
		Adhesive energies ($mJ.m^{-2}$)		
Salbutamol-Formoterol	17.79	20.54	36.82	57.34
Salbutamol-Budesonide	21.77	20.80	32.26	53.06
Budesonide-Formoterol	29.46	21.76	10.04	31.8

Table 28 Theoretical values drug-drug interaction energies in mHFA calculated with Equation 14

6.3.3 Direct adhesion/cohesion measurements by AFM

The *in situ* AFM probe technique allowed direct measurements of the cohesion and adhesion between single drug particulates and the dominant crystal faces of each drug material. As in the previous study, the integrity of all drug probes was investigated prior to and post measurement using a high-magnification 500x long-working distance optical microscope. In all cases, the drug probes appeared proud of the cantilever surface, with no visible differences between the start and end of the experimental procedure (indicating no macro/microscopic change in drug probe morphology).

In comparison to Chapter 5, the number distribution of each data set indicated a normal distribution with low variability. This is to be expected since the substrate surfaces were smooth and planar. Subsequently, the specific mean values and standard deviations for the interaction for each drug probe and drug substrate were calculated and are given in Table 29.

As expected, comparisons between probes of the same drug (probes 1-3) indicate large variations in adhesion force. This may be explained by the difference in particle size and variations in contact geometry due to the irregular probe shape. The interaction between a probe and the respective substrates were compared using one-way ANOVA. The results were found to be significantly different based upon 95% probability values ($p < 0.05$). Trends can be discerned for each drug probe and forces of interactions measured can be ranked.

	Probe								
	Salbutamol			Budesonide			Formoterol		
Substrate	**Tip 1**	**Tip 2**	**Tip 3**	**Tip 1**	**Tip 2**	**Tip 3**	**Tip 1**	**Tip 2**	**Tip 3**
Salbutamol	29.5 ± 1.5	41.5 ± 1.7	63.9 ± 2.3	10.9 ± 1.1	48.2 ± 2.9	71.9 ± 2.2	58.2 ± 2.1	15.3 ± 1.9	11.2 ± 2.4
Budesonide	12.5 ± 0.9	14.8 ± 1.0	25.8 ± 1.3	0.9 ± 0.2	5.0 ± 2.2	7.9 ± 4.0	13.7 ± 0.3	6.7 ± 1.9	3.7 ± 0.2
Formoterol	18.4 ± 1.9	32. 1 ± 0.8	45. 0 ± 3.7	1.2 ±1.1	3.7 ± 0.7	6.7 ± 1.4	13.1 ± 0.7	6.2 ± 0.9	4.1 ± 1.3

Table 29 AFM separation force measurements for micronised salbutamol, budesonide and formoterol (n = 3 probes, ± Standard deviation). All forces in nN

Statistical analysis of each drug probe with different drug substrates suggested the cohesive force between salbutamol-salbutamol to be stronger than the adhesion between salbutamol-formoterol, which in turn was higher than salbutamol-budesonide. The AFM data suggested that the salbutamol-formoterol interaction was approximately twice that of the salbutamol-budesonide adhesion.

For the budesonide probes, the rank order was budesonide-salbutamol, budesonide-budesonide and budesonide-formoterol. The quantitative AFM data suggests that the adhesive (budesonide-salbutamol) interaction is 9 times greater than the cohesive one.

Finally, for formoterol the order is formoterol-salbutamol, formoterol-formoterol and formoterol-budesonide. AFM data suggested that the formoterol-salbutamol interaction was approximately five times greater than the force of cohesion.

6.3.4 Comparisons between thermodynamic work of adhesion and AFM measurements

As previously discussed, the thermodynamic work of adhesion is directly proportional to the force of adhesion. To highlight this relationship and the specific role of the dispersive (LW) and total (LW + AB) interactions, representative plots of the theoretical work of adhesion of the Lifshitz- van der Waals (W_{ad}^{LW}) interactions and the influence of acid-base interactions ($W_{ad}^{Tot} = W_{ad}^{LW} + W_{ad}^{AB}$) versus the force measurements are shown in Figure 38 (for the case of salbutamol drug probe). It is anticipated that the work of adhesion/cohesion should increase with an increasing force of adhesion/cohesion.

In general, the plots suggested no direct relationship between the separation force measurements and the dispersive component of the work of adhesion (W_{ad}^{LW}) calculated from either IGC or CA measurements (Figure 38). However, a positive relationship is observed between the force measurements and the total work of adhesion (W_{ad}^{Tot}) when taking into account both the non-polar and polar contributions.

Similarly, analysis of the budesonide and formoterol interactions indicate no correlation between the LW work of adhesion (from IGC and CA) and AFM measurements, while the total theoretical works correlate well with experimental AFM data. Such observations suggested that polar interactions between contiguous surfaces play a significant role in particle adhesion/cohesion in non-aqueous media, and cannot be neglected in predictive theoretical studies.

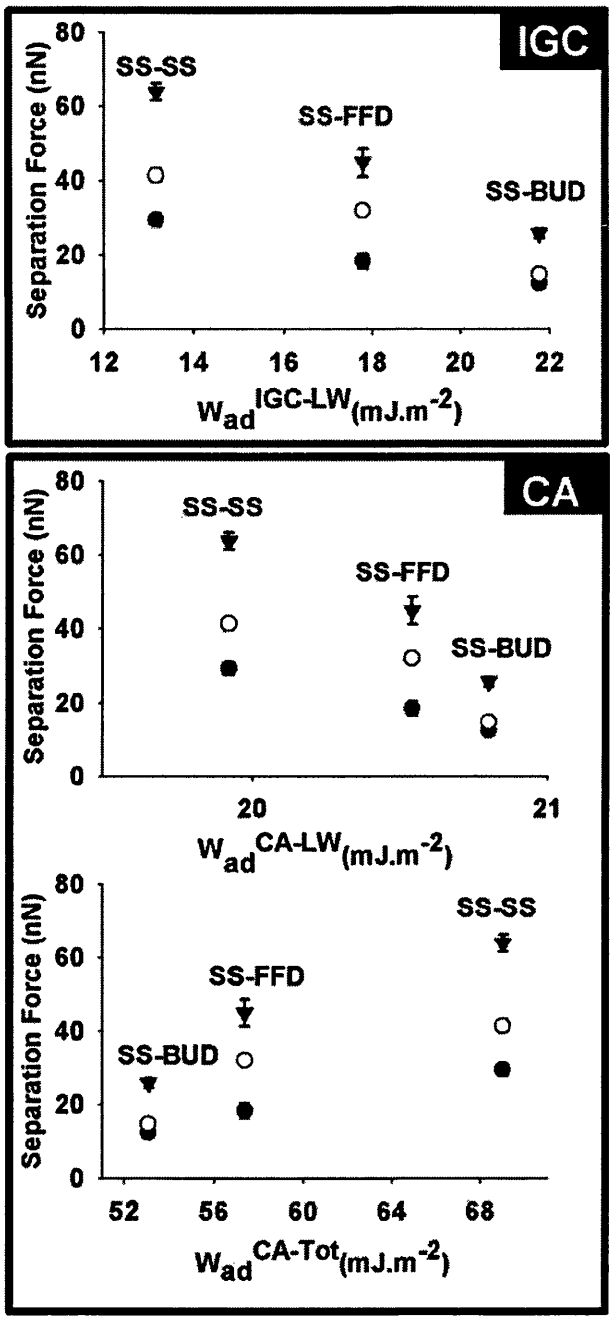

Figure 38 Plot of the theoretical thermodynamic work of adhesion vs. AFM force measurements for salbutamol drug probes (n=3 probes, ● = 1; ○ = 2; ▼= 3). Energies were calculated from IGC and CA measurements. Top 2 graphs take into account the dispersive contribution only. Bottom graph includes the polar as well as dispersive contributions. Key to the abbreviations: salbutamol (SS), formoterol (FFD) and budesonide (BUD)

6.3.5 Relationship between CAB plots and theoretical cohesion/adhesion ratios

An estimation of the separation force from theoretical treatment of the interfacial interactions via surface energy measurements would require knowledge of the effective contact area of each probe, as indicated by Equation 15 in Chapter 1. This limitation has precluded direct correlation of individual AFM force measurements for each probe with theoretical measurements. However, the determination of the force balance for a series of colloid probes utilising the cohesive/adhesive balance (CAB) analysis procedure does allow quantification of the relationship between the theoretical works of cohesion and adhesion and corresponding AFM measurements without prior knowledge of the contact area between an irregular probe and model substrate surfaces.

As previously discussed, from theory, the cohesion between material 1 and adhesion between materials (1) and (2) in a liquid media (3) can be expressed Equation 16 (repeated here for convenience):

Equation 16 (from Chapter 1):

$$\frac{F_{131}}{F_{132}} = \frac{n\pi R^{*}_{131} W_{131}}{n\pi R^{*}_{132} W_{132}}$$

Where F_{131} and F_{132} are the cohesive and adhesive forces, respectively. Assuming that the tailoring of the substrate surfaces enables equivalence of the contact radii R^{*}_{131} and R^{*}_{132}, the relationship between the theoretical measurement of the thermodynamic work of cohesion and adhesion and experimental measurements can be discerned. From Equation 16, the slope of a plot of the force of cohesion versus the force of adhesion for a series of probes would yield an experimental measurement of the ratio of the thermodynamic work of cohesion over the work of adhesion. In the theoretical CAB graph, the measurements of the adhesive force for a number of colloidal probes on the respective sample surfaces of the interactive

materials ($F_{adhesion}$) are plotted on the x axis; the correspondent force of cohesion of the same probes ($F_{cohesion}$) is plotted on the y axes. Considering the contact radius of the probes involved as being equivalents, the data obtained from the force measurements of several probes on the specific sample surfaces should follow a linear fit. The bisecting line (solid) corresponds to the $F_{adhesion}$, $F_{cohesion}$ equilibrium ($F_{coh} = F_{adh}$, or $W_{adh} = W_{coh}$). The relative position of the aligned experimental plots with respect of the bisector line is a direct indication of the adhesive/cohesive characteristic of the interactive material in the binary system. This line defines two distinctive regions on the CAB graph: plots on the lower sector of the graph indicate an affinity for the probe material to present adhesive interactions ($F_{adh} > F_{coh}$), conversely, plots above the bisector denote dominant cohesive properties. From the relative slope of the linear regression calculations, information on the quantitative relative strength of the adhesive and cohesive interactions can be directly calculated.

The CAB plots for the salbutamol, budesonide and formoterol drug probes are shown in Figure 39, Figure 40 and Figure 41, respectively. The dotted lines represent theoretical adhesion/cohesion ratios calculated from surface energy measurements while the data points represent experimentally determined forces.

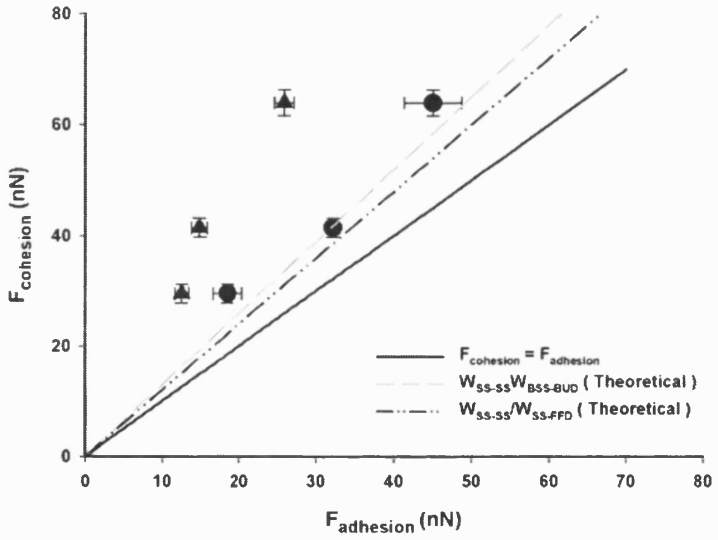

Figure 39 CAB plot. Relationship between AFM cohesion and adhesion measurements for salbutamol probes (SS, n=3). Solid line indicates line of cohesion/adhesion equilibrium ($F_{adhesion} = F_{cohesion}$). Dotted lines are theoretical ratios calculated from surface component approach with polar and dispersive contributions. ▲ = budesonide (BUD) substrate; ● = formoterol (FFD) substrate

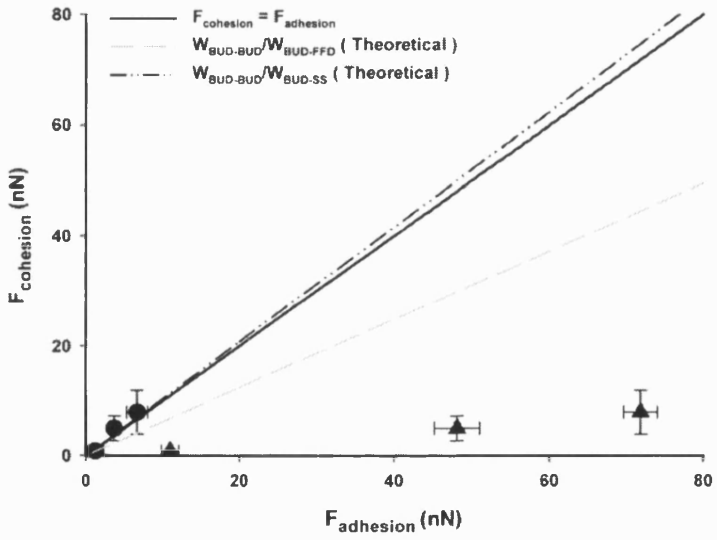

Figure 40 CAB plot. Relationship between AFM cohesion and adhesion measurements for budesonide probes (BUD, n=3). Solid line indicates line of cohesion/adhesion equilibrium ($F_{adhesion} = F_{cohesion}$). Dotted lines are theoretical ratios calculated from surface component approach with polar and dispersive contributions. ▲= formoterol (FFD) substrate; ● = salbutamol (SS) substrate

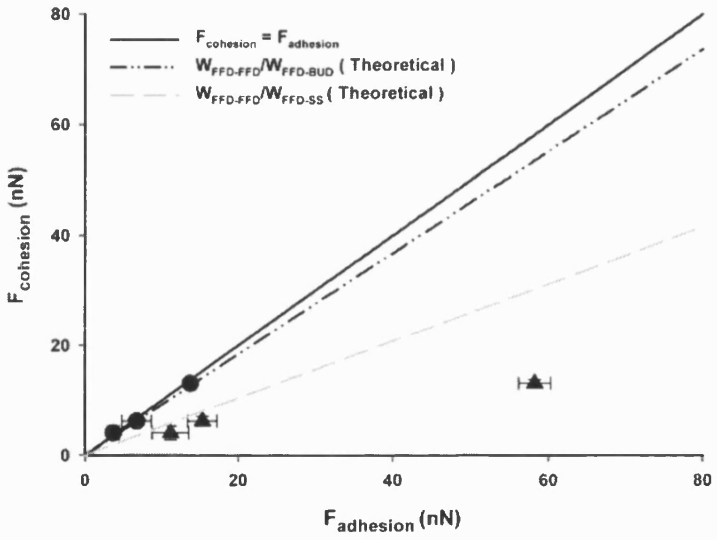

Figure 41 CAB plot. Relationship between AFM cohesion and adhesion measurements for formoterol probes (FFD, n=3). Solid line indicates line of cohesion/adhesion equilibrium ($F_{adhesion}$ = $F_{cohesion}$). Dotted lines are theoretical ratios calculated from surface component approach with polar and dispersive contributions. ▲= salbutamol (SS) substrate; ● = budesonide (BUD) substrate

Analysis of the salbutamol CAB graph in Figure 39 (together with measurements of the relative slopes of the different probes), suggested salbutamol to have a stronger cohesive rather than adhesive nature. In basic term, when comparing salbutamol cohesion forces to salbutamol adhesion forces on either budesonide or formoterol, (maintaining equivalent contact area) the cohesion forces were always greater.

Similar analysis of CAB data for the budesonide drug probes (Figure 40) suggests that budesonide is more adhesive with salbutamol than cohesive with itself. The theoretical approach is in agreement with this tendency for an adhesive interaction. Similar agreement between theory and experiment is found for the budesonide-formoterol interactions.

The CAB and theoretical analysis of formoterol interactions (Figure 41) suggests that formoterol is biased towards adhesion. This again confirmed experimental and theoretical findings.

A linear regression analysis of the balance of the cohesive and adhesive forces as measured by AFM was performed to calculate the cohesive/adhesive force ratio. The coefficient of determination (R^2) for all probes confirmed uniformity in contact area between crystal surfaces and the relationship between the adhesion and cohesion for the interactive probes. These ratios are summarised in Table 30, together with the theoretical ratio of the work of cohesion to the work of adhesion.

	Experimental ratio $F_{cohesion}/F_{adhesion}$	R^2 $F_{cohesion}/F_{adhesion}$	Theoretical ratio $W_{cohesion}/W_{adhesion}$
Salbutamol-Budesonide	2.41	0.9880	1.30
Salbutamol-Formoterol	1.29	0.9875	1.20
Budesonide-Salbutamol	0.11	0.9958	0.62
Budesonide-Formoterol	1.24	0.9832	1.04
Formoterol-Salbutamol	0.21	0.9005	0.52
Formoterol-Budesonide	0.94	0.9960	0.92

Table 30 Experimental, R^2 and theoretical ratio of the force and work of cohesion/adhesion

In general, there is a good correlation between the experimental and theoretical ratios, although absolute values are not well correlated, albeit of the same order of magnitude. The two approaches suggest the same bias towards either adhesive or cohesive interactions.

The discrepancy between experimental and theoretical measurements, which is of greatest significance for interactions involving salbutamol, may relate to a slight polarity of the model liquid propellant that has not been taken into account in the equation. This for instance is known to affect liquid-liquid surface tension predictions (AstraZeneca R&D, private communication). Other possible reasons could be related to the AFM measurements being conducted on the dominant face of each drug crystal, while the surface energy values were calculated from contact angles measurements derived from compacts of micronised drug. Thus, it is reasonable to assume that the less dominant faces will contribute to the interactions. The relationship between face specific surface free energy and work of adhesion should be considered for future investigation.

6.4 GENERAL DISCUSSION

Direct measurements of the interaction forces (via AFM measurements) responsible for the stability of colloid particles in binary pMDI formulations indicate a fine balance between adhesive and cohesive tendencies. A relationship between the theoretical interfacial thermodynamics, derived from the surface component approach, and experimental force measurements was demonstrated. The most relevant model to correlate experiment with theory is one that must include polar as well as dispersive components of surface energetics. This is an unexpected finding for interactions in a non-polar liquid such as mHFA. Furthermore, surface component parameters derived from contact angle measurements are preferred over IGC derived values.

Again, as with the investigations into drug canister adhesion (Chapter 5) such observations suggest the need to include polar acid/base interactions in the evaluation of suspension stability of colloid particles in non-aqueous media. The model developed in this work, and its correlation with direct AFM force measurement provides the basis for a powerful pMDI preformulation tool when selecting candidate drugs for inhalation.

CHAPTER 7: THE USE OF AFM MEASUREMENTS TO INVESTIGATE DRUG POLYMER INTERACTIONS

7.1 INTRODUCTION

As previously discussed, the transition from CFC to HFA propellants has been the motivation for further evaluation of the technology and performance of pMDIs. It has been established that the new alternative propellants are delivered in a manner that does not imitate CFCs. This may be attributed to the physico-chemical characteristics of the propellant (Vaervaet and Byron, 1999). In such a system, suspension based pMDIs are generally considered the most popular since the process of solubilisation in a relatively non-polar solvent is eluded. Conversely, suspension systems raise distinctive formulation challenges. While these new HFA liquid environments have comparable boiling points and vapour pressures to their CFC counterparts, their increased polarity make "controlled flocculation" an unresolved issue for many formulations (Blondino and Byron, 1998). Subsequently the use of secondary excipients such as surfactants and or stabilisers is of paramount importance to the final delivery and stabilisation of a suspension formulation. It is known that suspension stability can be facilitated via steric repulsive forces (arising from colliding particles with adsorbed layers) and/or electrostatic repulsive forces (that originates when the electrostatic double layer of interacting particles overlap) (Pugh et al., 1983). Previous reports have investigated the role of excipients in suspension pMDIs (Vearveat and Byron, 1999); however, to date, few papers have been published that quantitatively deal with the nature and range of interactions existing between drug - drug particulates and excipients in suspension (Clarke et al., 1993; Michael et al., 2000; Young et al., 2003). In addition, many of the investigations have been of empirical approach, subsequently leaving the subject relatively poorly understood.

7.1.1 Stabilisation of suspension based pMDIs

The stabilisation of pharmaceutical suspensions, against flocculation and or coalescence, necessitates the presence of an energy barrier between the particles that prevent their close approach where the van der Waals attraction is large.

In general, two mechanisms of stabilisation can be applied: electrostatic and steric stabilisation.

Electrostatic stabilisation is based on charge separation and controlling the relative balance of charge in solution with respect to the particle electrical double layers (Wyatt and Vincent, 1989). Briefly, the electrostatic double layer is characterised by a surface charge that is compensated by unequal distribution of counter ions. The magnitude of repulsion depends on the surface (or zeta) potential, the electrolyte concentration. This forms the basis of the theory of the DLVO colloid stability developed independently by Derjaguin and Landau (1941) and Verwey and Overbeek (1948) respectively. However, previous work (Pugh et al., 1983) has shown that, electrostatic stabilisation was ineffective in non-aqueous suspensions of carbon black until the zeta-potential was greater than 100 mV. Such a zeta -potential is far greater than reported for salbutamol (Clarke et al., 1993). Such observations are further substantiated via Kitahara Theory (1974), which stated unless particles in suspension are large and posses a substantial zeta -potential, the electrostatic mechanism of stabilization in a low dielectric constant is ineffective. Moreover, Osmond and Waite (1975) described such objections quantitatively with the DLVO theory concluding that 50-100mV potential was insufficient to stabilise their system. Consequently, for this study, the electrostatic double layer interactions can be considered of negligible importance.

The second mechanism is steric stabilisation or hindrance. This system is based on the use of surface active polymers which adsorb very strongly to the surfaces of particles (Heller and Pugh, 1960). In order to achieve such goals, the polymers, like other surface active substances, must be able to interact with both the particles and the medium in a way that they are adsorbed on the particle substrate and yet remain freely soluble in the medium. Such a combination of properties is generally obtained with steric stabilisers. Steric stabilisers are usually a block of copolymer molecules with a lypophobic "head", which attaches strongly to the particles surfaces, and a lyophilic "tail", which moves freely in the dispersive medium. The lyophilic tail extends from the surface giving a layer thickness (d) that is several nanometers in thickness. When two particles approach to a distance of separation l (l, distance between the particles) that is smaller than 2d, the polymeric chains may undergo overlap and/or become compressed preventing their relative approach to a distance where the net van der Waals energy of interaction will prevent them escaping by thermal motion. When these chains are in good solvent conditions, such overlap is unfavourable and this leads to strong repulsion that increases very sharply with decrease of separation distance. Poly ethylene glycol (PEG) is usually the hydrophilic polymer chosen to provide such a hydrated steric barrier in pMDI systems.

Stabilisers are generally macro molecular (M.W > 1000, i.e. Poly vinyl pyrrolidone - PVP), non-ionizing compounds with a relative number of hydrophilic groups. Poly vinyl pyrrolidone is a commonly used water-soluble and physiologically inert polyamide homopolymer. With respect to high molecular weight PEGs, these rigid macromolecules interact with the disperse phase (i.e. by adsorption and bridging) and lie flat on the surface of the "protected" particles, reducing the "effective" van der Waals energy of interaction between colliding colloidal particles (Eliassaf et al., 1960), hence altering the settling behaviour of the dispersed phase.

In summary, for pharmaceutical systems manufactured in non aqueous media, the latter mode of steric stabilisation has evidently a number of advantages over the electrostatic model: further of being equally effective in aqueous and non-aqueous media. They are effective even for suspensions with high solid content and reversible, since a true thermodynamic equilibrium is obtained. Hence the interaction forces can be reversed by changes in the physical state of the system.

It is well established that the success of flocculation by the use of polymers depends on various factors related to the surface chemistry of the particles as well as on the ionic nature, molecular weight, charge density and bulk properties of the flocculants in solution. However, it may be considered that the most important influence affecting the extent and mechanism of flocculation is dependent on the nature and conformation of polymer adsorption. It is also interesting to note, both theoretical calculations and previous experimental reports have suggested flocculation does not require high or complete coverage of the particle surface by the polymer (Kerkar and Feke, 1991; Heller and Pugh, 1960)

The aim of this work was to investigate the force of cohesion of salbutamol and its interactions with three different molecular weight non-ionic homo-polymers used in pMDIs pharmaceutical formulations in a model propellant with a low dielectric constant with or without stabilizer.

Salbutamol was chosen as a model drug since it was the most common generic drug used in respiratory therapy. The use of budesonide and formoterol in this part of the investigation were not considered since the matrix of experiments would have become too large.

7.2 MATERIALS AND METHODS

Poly ethylene glycol (M.W. 200, 400 and 600, polymers of industrial grade suitable for pharmaceutical applications) and Poly vinyl pyrrolidone (Povidone K25, M.W. 30-70, non-ionic polymer) were used as supplied. As previously stated only salbutamol drug-drug interactions in the presence of these polymers were investigated.

7.2.1 Preparation and characterisation of drug crystals

As previously discussed single crystals of salbutamol were nucleated and grown on a glass substrate using a sitting drop technique as described in Chapter 4. This process produced planar crystals with large areas of sub-nanometre smooth surfaces. Using mesoscopically smooth and pristine crystals, problems related with the heterogeneity of surface materials and the inadequate knowledge of the contact area is eliminated. To avoid problems related to potential contamination (due to polymers residues in the AFM *in situ* cell, between experiments, freshly nucleated crystals were used for each set of experiments (12 crystals in total). The surface topography of the drug crystal surfaces was investigated using the AFM in a conventional *ex situ* imaging mode prior to force measurement.

7.2.2 Preparation of polymeric solutions

Increasing concentration of PEGs in mHFA, ranging from 0.05, 0.1, 0.25 and 0.5% v/w, were prepared for PEG 200, 400 and 600. In addition, samples of PEG 400 and PVP in mHFA were prepared in a similar manner, where the concentration of PEG 400 ranged from 0.05, 0.1, 0.25 and 0.5% v/w, while concentration of PVP was kept constant at 0.001% w/w for all samples. All solutions were stored in tightly sealed containers under ambient conditions prior to use. For the solubility of PEGs in chlorine-free liquefied gas propellants the authors refer to previously published data by Blondino and Byron (1998).

7.2.3 *In situ* AFM colloid probe measurements of salbutamol drug probe and salbutamol crystal substrate with three different molecular weight non-ionic polymers

Measurements between each salbutamol drug probe and salbutamol crystal substrate were conducted using the methodology described previously in Chapter 4, section 4.1.4. Force separation measurements were collected using force-volume mode to produce multiple force distance curves (n = 512) between each drug probe and crystal surface over a 5 μm x 5 μm area with the following settings: approach-retraction cycle 0.5 μm, cycle rate 4.07 Hz and a loading force of 20 nN. A disadvantage in the use of the colloid probe technique in cohesion studies is the fact that the actual size and geometry of the AFM probe is unknown and, therefore cannot be normalised. Consequently, variability in probe contact radius geometry was expected. Accordingly, each study was performed in triplicate (n = 3 salbutamol probes for each set of PEG or PEG+PVP studies), with a new drug particle attached on the AFM cantilever and a new crystal substrate used for each set of experiments so as to minimise the effects of cross contamination and that of the environment on the particle and substrate. Furthermore, a great deal of care was taken to maintain the integrity of the colloid probe throughout each study to a avoid inter-intra probe variation. Twenty minutes were allowed to elapse after the addition in the *in situ* cell of each different concentration of the drug saturated polymeric solution to allow for system stabilisation.

7.3 RESULTS AND DISCUSSION

As previously discussed, the aim of the present study was to investigate the physical interactions between salbutamol in the presence of PEG stabilising polymers. Atomic force microscopy was used for the assessment of the cohesion of salbutamol with salbutamol crystals in a mHFA in the presence of different concentrations of these excipients. In addition, the influence of PVP on the force of interaction of the drug was evaluated.

7.3.1 Analysis of crystal substrates

Prior to AFM cohesion measurements, the surface roughness on the dominant crystal face of each drug substrate was investigated, avoiding problems related with face-specific crystal chemistry (Munster and Prestidge, 2002). Roughness analysis (n = 25, ± standard deviation, 5 x 5 μm area) of the surface topography for each drug crystal are presented in the following Table 31.

Analysis of the roughness data suggested extremely smooth surface morphologies for all salbutamol drug crystal face used in the investigation. In general, all crystals exhibited a root-mean-squared (R_{rsm}) below 5 nm over a 5 x 5 μm area. It is important to note, that significant differences in roughness between crystals were observed (ANOVA $p<0.05$). However, each PEG concentration study was conducted with a single specific crystal thus allowing comparison. Furthermore, in all cases, the salbutamol crystalline substrates possessed an absence of micrometre scale roughness (Buckton, 1995), thus making them highly suitable for quantitative colloidal probe AFM analysis.

Salbutamol crystals	R_{RMS} (nm)
1	0.96 ± 0.04
2	1.20 ± 0.01
3	1.68 ± 0.01
4	0.80 ± 0.03
5	0.41 ± 0.04
6	1.72 ± 0.05
7	2.93 ± 0.01
8	1.87 ± 0.02
9	1.08 ± 0.03
10	1.66 ± 0.06
11	1.95 ± 0.03
12	1.82 ± 0.05

Table 31 R_{RMS} analysis (n = 25, 5 x 5 µm area) of the surface topography for each salbutamol drug crystal dominant face (111)

7.3.2 *In situ* AFM force of cohesion measurement: the stabilising effect of surfactants and stabilisers and its variation with concentrations

As previously stated, the *in situ* AFM probe technique allowed direct measurement of the cohesion between single salbutamol drug particulates and salbutamol crystal surfaces in the presence of surfactants and/or stabilisers. As with the adhesion cohesion studies conducted on atomically smooth crystals, analysis of the adhesion data suggested normal Gaussian distributions of the measured forces. Thus, data were processed to produce mean cohesion values and standard deviations. Adhesion data for each drug probe in mHFA, in the presence of different PEG polymer concentrations are given in Figure 42.

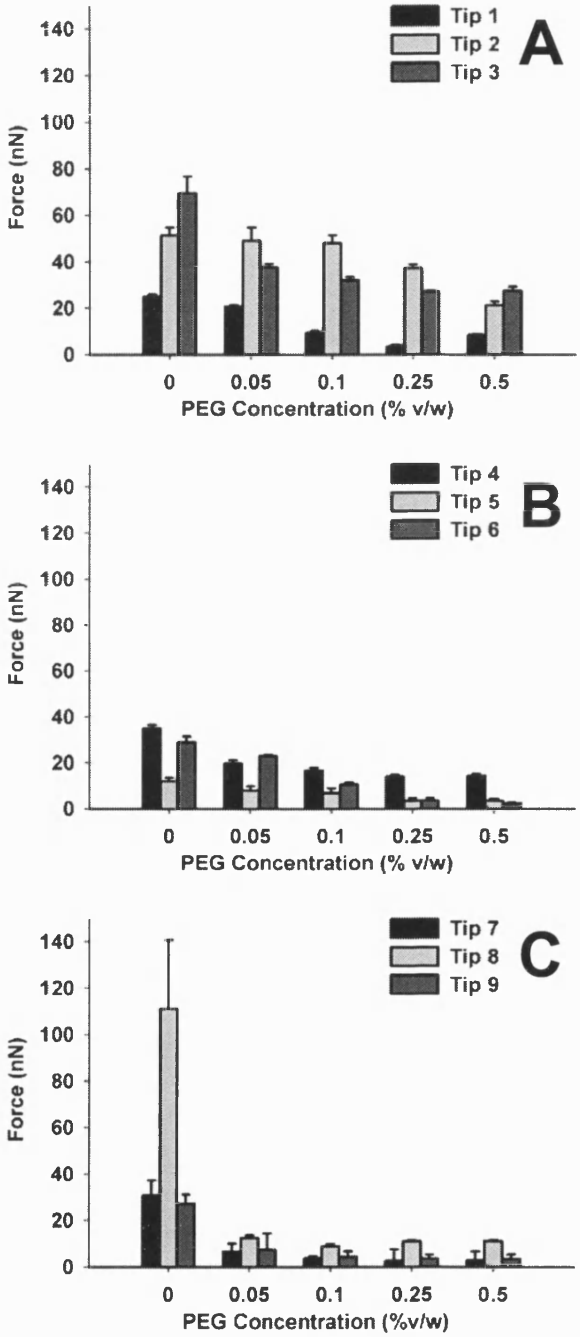

Figure 42 Force of cohesion between salbutamol drug probes on salbutamol crystals in mHFA with varied concentrations of (A) PEG 200, (B) PEG 400 and (C) PEG 600

As previously discussed, three AFM probes were utilised for each molecular weight polymer study (where probe 1-3 were used for PEG 200, probe 4-6 for PEG 400 and probe 7-9 for PEG 600). New probes and substrates were utilised for each set of measurements to avoid polymer contamination issues. Furthermore, each study was conducted using sequentially increased concentrated PEG solutions (i.e. lowest concentration first).

Analysis of the results suggested that strong attractive forces were present in the systems in the absence of any stabilising agents. In general, cohesion forces ranged from 11.84 nN ± 1.62 nN to 111.07 nN ± 29.79 nN in pure mHFA alone (n =12 probes). As previously discussed, the attractive forces observed in the pure mHFA most probably have their origin via the London dispersive component (van der Waals interactions) and surface polar components. It is unlikely that neither the salbutamol micronised drug particle nor drug crystal substrate are likely to form thick diffuse layers in a non-aqueous environment and will unlikely be influenced by electric double layer forces (Wyatt and Vincent, 1989; Romo, 1963).

A sequential increase in concentration of each of the chain length PEG solutions, up to a concentration of 0.5% v/w, resulted in a statistically significant decrease in cohesion (ANOVA $p<0.05$). In general, the decrease in cohesion was particularly evident at very low concentrations of PEG (0.05 - 0.1% v/w). In comparison, relatively high concentrations of PEG (0.25-0.5 % v/w) resulted in little cohesion decrease. Interestingly, such data correlated well with previous reports (Kerkar and Feke, 1991). In their work it has been reported that the adsorption of polymers onto solid surfaces showed adsorption isotherms with a rapid adsorption rate at low concentrations followed by a plateau (Kerkar and Feke, 1991). For pharmaceutical applications the ideal maximum absorbed layer thickness should be achieved at a lower surfactant concentration to avoid adverse effects on propellant evaporation and product performance.

Further data analysis (Fishers Pairwise $p<0.05$) suggested that variation in cohesion was dependent on concentration and PEG molecular weight. For example, analysis of the higher molecular weight PEG 600 data, suggested that no variation in cohesion was observed above concentrations of 0.25% w/w. In comparison, data for the PEG 200 suggested variation across the entire concentration range. It is envisaged that such observations may be due to increased steric hindrance with the higher molecular weight polymers.

In order to compare the relative decrease in cohesion with respect to polymer concentration and molecular weight, the mean values for each drug probe were normalised to the cohesion values obtained in mHFA only. The mean ± StDev for the normalised mean data values are shown in Figure 43.

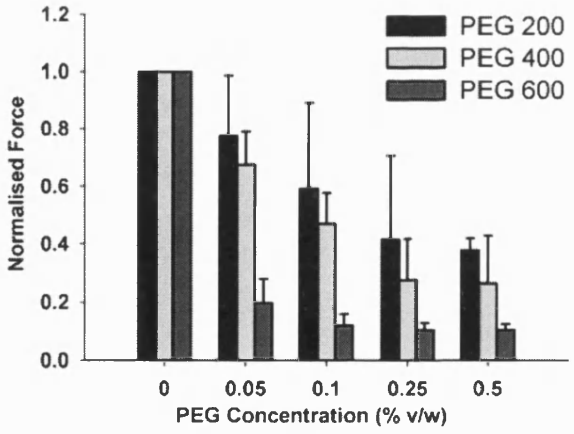

Figure 43 Normalised force of cohesion between salbutamol drug probes on salbutamol crystals in mHFA with varied concentrations of PEG 200, 400 and 600. Data represents mean ± STDev of the mean for 3 probes with each PEG

In general, analysis of the salbutamol cohesion force curves in the presence of PEG solutions suggest a rank decrease in nominal mean separation force of the order: PEG 200 > PEG 400 > PEG 600 (n = 3 probes for each polymer analysed). Equally, variability of the results decreases from PEG 600 < PEG 400 < PEG 200. Such observations may be due to both an increase in particulate surface coverage and increased polymer protrusion into the mHFA media with increase in molecular weight. As previously discussed it has been reported that the degree of the steric stabilisation is dependent, in part, on the adsorbed layer thickness (Kerkak and Feke, 1991), and accordingly would expect PEG 600 to be more effective at reducing cohesion due to a higher molecular weight and consequently longer polymeric chain.

In comparison, a different cohesion profile was observed with the addition of 0.001% w/w PVP to different concentrations of PEG 400. In the presence of only PVP and mHFA, a large statistical decrease (approximately 70%) in force of cohesion was observed when compared to mHFA only (ANOVA, Fishers Pairwise $p<0.05$). Interestingly, any further addition of different concentrations of PEG 400 (0.05, 0.1, 0.25 and 0.5% w/v) to the mHFA-PVP system did not result in any significant reduction of the force of cohesion (ANOVA, Fishers Pairwise $p<0.05$). As with the PEG studies the data was normalised to allow comparison of PVP systems to PEG. Data are presented graphically in Figure 44.

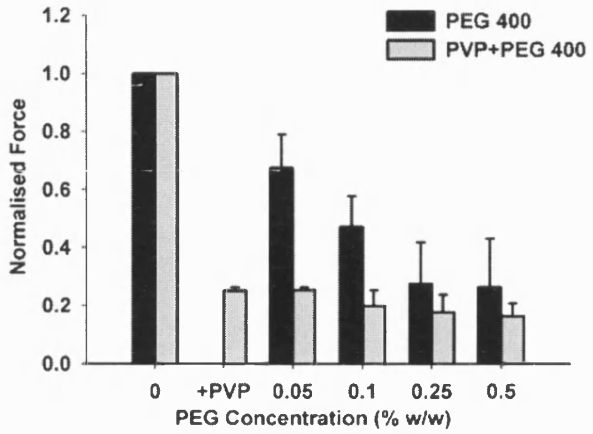

Figure 44 Normalised force of cohesion between salbutamol drug probes on salbutamol crystals in mHFA with PEG 400 with and without 0.001% w/w PVP. Data represents mean ± STDev of the mean for 3 probes with each PEG

In general such observations are in good agreement with the proposed mechanism of PVP adsorption. It is proposed that once PVP is added to the mHFA its large planar rigid molecules spread across the surface of the drug particles, achieving a greater surface coverage, preventing any further stabilizing effect due to the added concentration of PEG.

7.4 GENERAL DISCUSSION

The concept of steric stabilisation has been tested through direct particle adhesion measurements in a model propellant system. Results are believed to be quantitative and representative for this kind of model suspension system, where drug particulates have been proven to have a certain degree of instability in the presence and/or absence of polymers. It was found that an increase in chain length, of low molecular weight polymers, added to drug particulate suspensions in a low polarity media like mHFA, led to a decrease in inter-particulate cohesion. In addition, the use of stabilisers like PVP had a positive effect in decreasing particle-particle interactions.

There is no clear evidence of direct PVP-PEG binding: the changes in suspension stability are due to change in the thermodynamics of the system. The presence of PVP in a suspension system will dominate the suspension stability and further addition of a second polymer does not destabilise the suspension. (Griffiths et al., 2004)

With regards to the applicability of the AFM to investigate pMDI suspensions, it can be concluded that such techniques can allow a better insight into the interactions of such a complex system and it could prove invaluable during the early phases of formulation product development. Clearly, an understanding of the conformation of polymer molecules at interfaces is of vital importance when controlling the stability/flocculation behaviour of sterically stabilized suspensions.

CHAPTER 8: *IN VITRO* MEASUREMENT OF THE MICRONISED DRUG AEROSOLISATION PERFORMANCES

8.1 INTRODUCTION

Using a combination of surface energy and AFM measurements and the use of theoretical models to predict particulate interactions in non-aqueous solutions (Chapter 3 and 6), it has become apparent, that particulate adhesion and cohesion properties will play an important role in suspension behaviour in pressurised metered dose inhaler formulations. Nonetheless, there is a further requirement to correlate these measurements with aerosolisation processes within model pMDI systems.

Few studies to date have investigated these kinds of system, with the specific aim of relating the physical chemical properties of particles to *in vitro* performance (Williams et al., 1999, Martini et al., 1991). For this reason, *in vitro* studies were undertaken to assess the possibility of correlating both theoretical and empirical measurements of adhesion/cohesion behaviour with *in situ* particle interaction and aerosolisation performance of pMDIs.

.

Therefore, for comparison to the main component of Chapter 3 and 4, 6, a series of *in vitro* aerosolisation measurements were conducted on pMDI formulations, to assess the aerosolisation efficiency of pMDIs containing single or combination drugs.

Aerosolisation efficiency of the pMDI formulations was measured using an Andersen Cascade Impactor (ACI). The eight stage impactor separates the drug by effective mass median aerodynamic diameters (MMAD) (where an MMAD of 5.8 μm is separated between stage 2 and filter at a flow rate of 28.3 $L.min^{-1}$, equivalent to the fine particle fraction). Drug recovered from each stage of the ACI and inhaler components was determined by high performance liquid chromatography (HPLC).

8.2 QUANTIFICATION OF DRUG CONTENT BY HPLC

The drug concentrations collected from the various ACI stages and pMDI actuator during the *in vitro* studies were analysed by reverse phase HPLC.

8.2.1 Material and methods

HPLC operates by separating organic compounds by their relative affinity for the solid phase. Analyses were performed using a reverse phase HPLC and solvents used for the HPLC analysis are given in Table 32.

Material	Manufacturer
Acetonitrile (HiPerSolv Far UV grade for HPLC)	Fisher Scientific, Leicestershire, UK
Heptane Sulphonic Acid Sodium Salt	Fisher Scientific, Leicestershire, UK
Glacial Acetic Acid	Fisher Scientific, Leicestershire, UK
Water (purified through Millipore RiO5 and MilliQplus – at 18.5)	Millipore, Watford, UK

Table 32 Materials used for the in vitro study and HPLC analysis

The HPLC used throughout the investigation was produced by Jasco (Jasco Corporation, Tokyo, Japan) and comprised of a UV-970/975 Intelligent UV/VIS Detector, AS-950 Intelligent Auto-Sampler and PU-90 Intelligent HPLC Pump. Data were recorded and integrated using AZUR-OSIRIS Chromatography Software V 3.0. (Theix, France). Details of the experimental set-up for each of the drugs is summarised in Table 33.

Mobile phase used throughout the investigation was prepared by weighing 1.10 g of heptane sulphonic acid sodium salt into a 1 litre volumetric flask which was diluted to volume with purified water and mixed well. The solution was adjusted to pH 3.0 using glacial acetic acid, using a calibrated pH meter and de-gassed prior to use.

Dilution solvent, used throughout the study to recover drug deposits from the impactor and to dilute samples and standards was a 50:50 % $_{v/v}$ CH_3CN:H_2O.

Drug Substance	Salbutamol	Budesonide	Formoterol
HPLC Column	Hypersil, 5μm packing, 100 cm x 4.6 mm id	Hypersil, 5μm packing, 100 cm x 4.6 mm id	Hypersil, 5μm packing, 100 cm x 4.6 mm id
Column oven temperature (°C)	30° C	30° C	30° C
Column flow rate (mil.min^{-1})	1.75 ml.min^{-1}	1.75 ml.min^{-1}	1.75 ml.min^{-1}
Sample tray temperature (°C)	Ambient	Ambient	Ambient
Injection volume (μl)	100 μl	100 μl	100 μl
Detector wavelength (nm)	278 nm	278 nm	278 nm
Run time (minutes)	2.42 minutes	2.82 minutes	4.68 minutes

*Thermo Electron Corporation, Runcon, Cheshire, UK

Table 33 HPLC experimental set-up and instrument settings for the micronised drug substances

Standards for the combination of the three micronised drugs were prepared from duplicate stock standard solutions. Initial stock solutions were prepared by accurately weighing approximately 50 mg aliquots of each material into 100 ml volumetric flasks and dissolving to volume with dilution solvent. Each stock solution was ultrasonicated for no more than 10 minutes to ensure dissolution, left to cool at room temperature and made up to the mark with dilution solvent.

Working standard solutions were prepared by serial dilution of the stock standard solution using calibrated (class A) laboratory pipettes and same dilution solution. A series of working standard with concentrations between 0.1 $\mu g.ml^{-1}$ and 10 $\mu g.ml^{-1}$ were prepared for each of three drug substances.

Duplicate injections of each working standard were analysed by HPLC with a blank, containing dilution solution, being sampled before the first injection and after the higher standard.

8.2.2 Results and Discussion

Sample chromatographs for the combination of the three drugs (low and high concentration) are given in Figure 45.

Salbutamol exhibited a peak at an approximate retention time of ~ 2.42 mins. Budesonide exhibited a peak at an approximate retention time of ~ 2.81 mins. Formoterol exhibited a peak at an approximate retention time of ~ 4.68 mins.

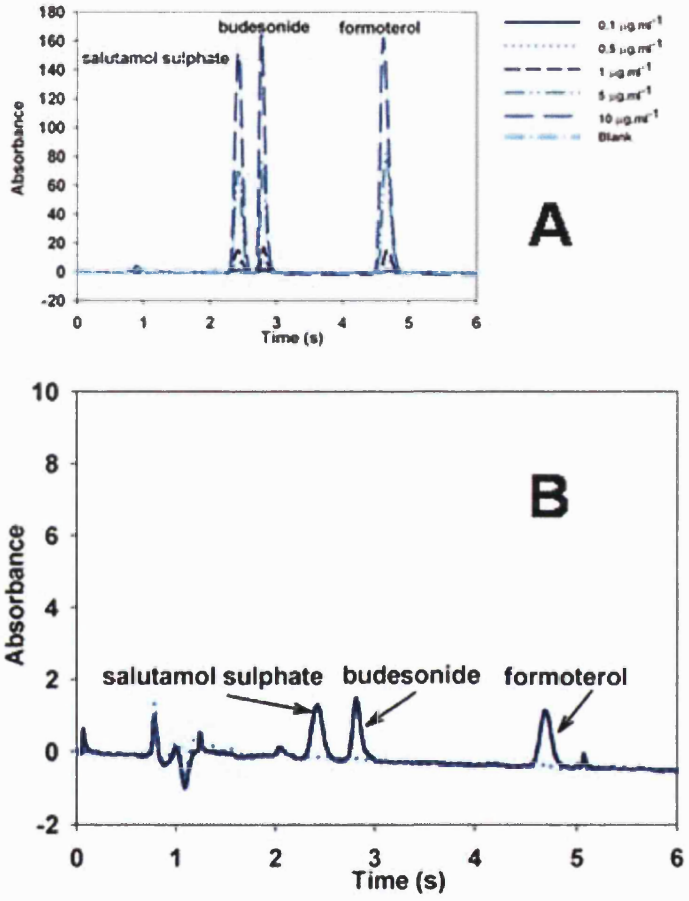

Figure 45 (A) Chromatograph of salbutamol, budesonide and formoterol mixed standards across 0.1-10 $\mu g.ml^{-1}$ concentration range, (B) Chromatograph of salbutamol, budesonide and formoterol mixed standards across at low 0.1 $\mu g.ml^{-1}$ concentration range with blank injection

The relationship between concentration and absorbance for each of the drugs is shown in Figure 46. Linear regression analysis for all three drugs indicated R^2 values of 1.000 for salbutamol, 0.9940 for budesonide and 0.9997 for formoterol, respectively, inferring a direct linear response between peak area and concentration over the range 0.1 $\mu g\ ml^{-1}$ to 10 $\mu g\ ml^{-1}$. Relative standard deviation for all duplicate injections of all three drugs were less than 5% and, in addition, no interfering peaks were observed in any of the initial blanks, and no sample carry over was observed in blanks injected after the higher standards.

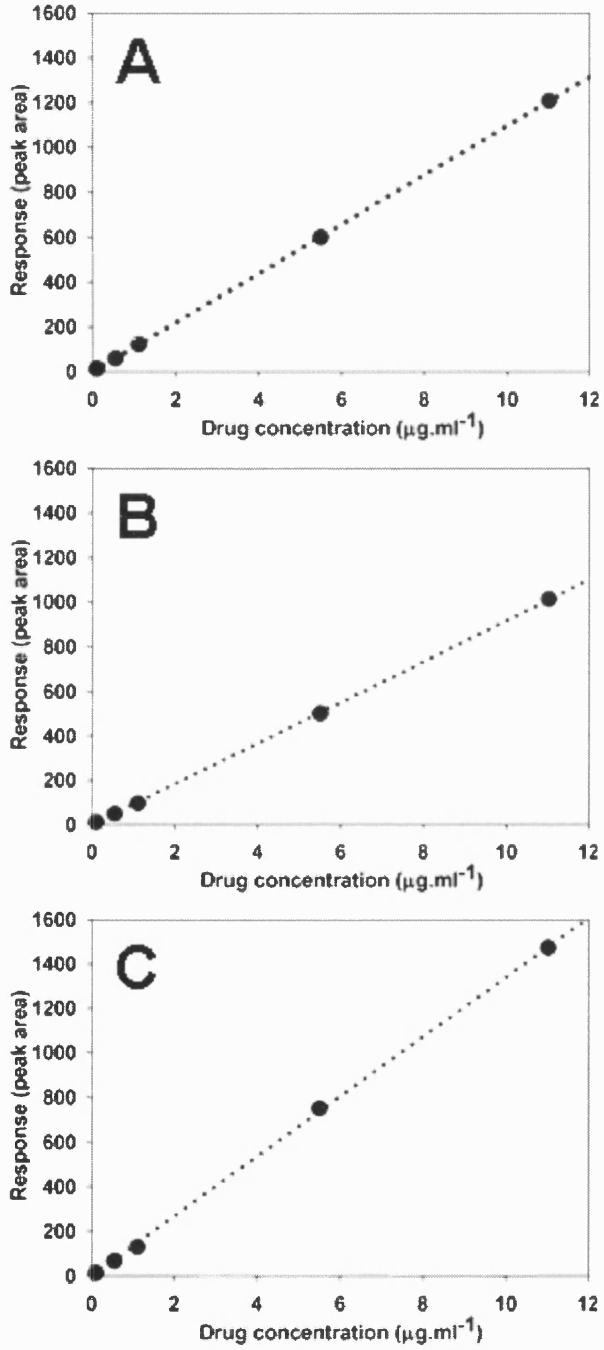

Figure 46 Peak area vs. concentration HPLC calibration plots for (A) salbutamol, (B) budesonide and (C), formoterol

As previously stated, two stock standard solutions were prepared from separate weightings, and were subsequently diluted to give standard concentrations either side of the expected sample concentrations. Both standard and sample concentrations were prepared and diluted to fit within validate linearity region. Comparison between each standard solution prepared from each stock solution indicated a coefficient of variance less than 1%, for all drugs in all cases.

During sample analysis, samples (SAMP) and standards (STD) were analysed using a bracketed method, using the entire standard range, i.e.

BLANK, STD1, STD2, STD3, STD4, STD5, SAMP1 to SAMP11, STD5, BLANK.

Each sample and standard was run twice and the mean peak area calculated.

8.3 PREPARATION AND ANALYSIS OF SUSPENSION FORMULATIONS

8.3.1 Materials and methods

8.3.1a Preparation of formulations

Approximately 25 mg of micronised drug materials was accurately weighted into aluminium canisters. For single drug formulations 25 mg of drug was weighed directly, while for combination formulations 12.5 mg of each drug was weighed. Each canister was fitted with a 50 μL metering valve and crimped. Approximately 10 g of HFA134a was then pressure filled into each canister. All cans were sonicated for 20 minutes and left to stabilise for 24 hours at ambient temperature prior to testing.

In addition, to visually assess the sedimentation of the combination products, glass containers containing 25 mg of micronised drug material (salbutamol, budesonide, formoterol) or containing the relative combination of micronised drugs (salbutamol-budesonide, salbutamol-formoterol and budesonide formoterol) (12.5:12.5 mg) were prepared. For such studies, containers were crimped with continuous valves and as with the standard formulations, filled with 10 g if HFA 134a. Again the glass container formulations were sonicated for 20 minutes and left to stand for at least 24 hours prior to analysis.

8.3.1b Investigation of the sedimentation of combination products

To evaluate the suspension properties, the filled glass aerosol containers were inspected visually over a time period of at least 24 h after preparation. Digital photographs were taken with a CCD 3 mega pixel digital camera (Pentax, Slough, UK) to document any tendency of the suspension to cream, sediment or to detect adhesion/cohesion characteristics.

8.3.1c In vitro testing using the Andersen Cascade Impactor

The influence of adhesion/cohesion on the aerosolisation of the pMDI formulations was investigated using Pharmacopoeia apparatus D (see Figure 47, the Andersen cascade impactor) (Copley Scientific, Nottingham, UK).

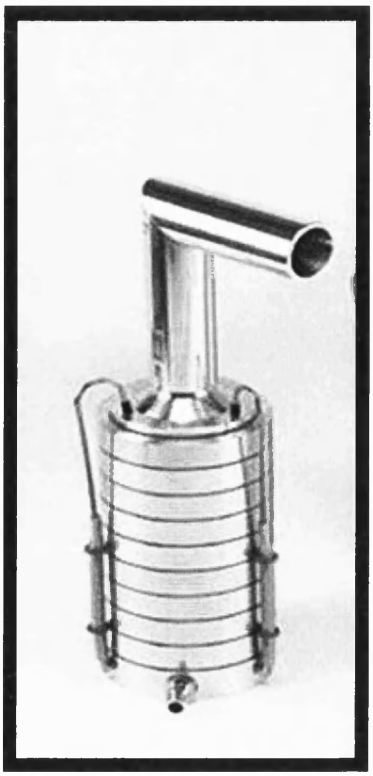

Figure 47 Adapted Image of the Andersen Cascade Impactor (adapted from Copley Scientific home page http://www.copleyscientific.co.uk)

All experiments were conducted at ambient temperature and humidity (25°C, 45 % RH). In general, the ACI is an eight stage cascade impactor that measures the fine particle dose and size of the aerosol cloud generated by a pMDI. The impactor is designed such that as the aerosol passes through each stage in an air stream, particles having a large enough inertia will impact upon a particular stage plate, whilst smaller particles will pass to the next impaction stage. Upon impaction, the aerosol may be divided into seven size categories according to its aerodynamic diameter. The aerodynamic particle size cut-off diameters for the ACI impactor at a flow rate of 28.3 $L.min^{-1}$ are presented in Table 34.

Stage number	**Nominal cut-off point (μm) at 28.3 $L.min^{-1}$**
0	9.0 - 10.0
1	5.8 - 9.0
2	4.7 - 5.8
3	3.3 - 4.7
4	2.1 - 3.3
5	1.1 - 2.1
6	0.7 - 1.1
7	0.4 - 0.7
Filter	< 0.4

Table 34 Mass median aerodynamic particle size cut-off points for the Andersen cascade impactor at a 28.3 $L.min^{-1}$ flow rate

After assembly of the impactor, the filter stage was covered with a 53 mm diameter GF/A filter (Whatmann Int. Ltd., Maidstone, UK). A pump (Model 1423-101Q-Q626X, GAST, Buckinghamshire, UK) generated a flow rate through the ACI of 28.3 $L.min^{-1}$ (± 2 $L.min^{-1}$), which was calibrated using a micromanometer (model FC012, Furness controls, Bexhill, UK) by adjustment of a needle valve flow regulator.

Prior to each analysis, the pMDI was shaken vigorously for 5 s. In addition 5 shots were actuated to waste, prior to experimental procedure, to ensure the valve stem was seated correctly and no blockage occurred. During analysis, the manufactured pMDIs were inserted into a specially constructed mouthpiece holder and actuated in a fixed position into the throat of the cascade impactor for ten seconds using a solenoid valve timer. A three second delay in activating the timer, after the pump was engaged, was invigilated to allow equilibrium of the pump. Ten consecutive doses (vigorous shaking in between) were released into the impinger for each single drug formulation (twenty for combination drug).

After testing of each formulation, the pMDI actuator, mouthpiece adaptor, throat assembly, stage zero to seven and filter stage were thoroughly rinsed into suitable volumetric flask with dilution solvent and made up to the mark, prior to analysis. Between analyses of each formulation, the actuator and ACI components were rinsed with distilled water followed by methanol, and dried at 40°C in an oven. The ACI components were left to cool, reassembled and re-used. No apparent degradation in component parts or actuator integrity was observed by conducting this procedure. All ACI investigations, for each formulation, were carried out in triplicate. As previously stated, all samples were analysed by HPLC.

8.3.2 Results and discussion

8.3.2a Visual analysis of combination based pMDI formulations

Information about the physical stability and the adhesive/cohesive characteristics of the suspension pMDI formulations may be obtained by observing the sedimentation characteristic of the drug particulates after a specific settling time. Figure 48 shows the settling characteristics of the individual drug pMDI formulations at time zero and after 24h.

In addition, the sedimentation behaviour of the combination formulations at time zero and after 24h is shown in Figure 49.

Analysis of the sedimentation data suggests the cohesive and adhesive characteristics of the three micronised drugs are reflected moreover in the respective combination products. When salbutamol is present (in combination with budesonide or formoterol) the system suggested a lower sedimentation volume when compared to budesonide-formoterol combinations. One possible explanation for such observations may be related to the higher affinity of budesonide and formoterol towards salbutamol, as suggested by the *in situ* AFM measurements

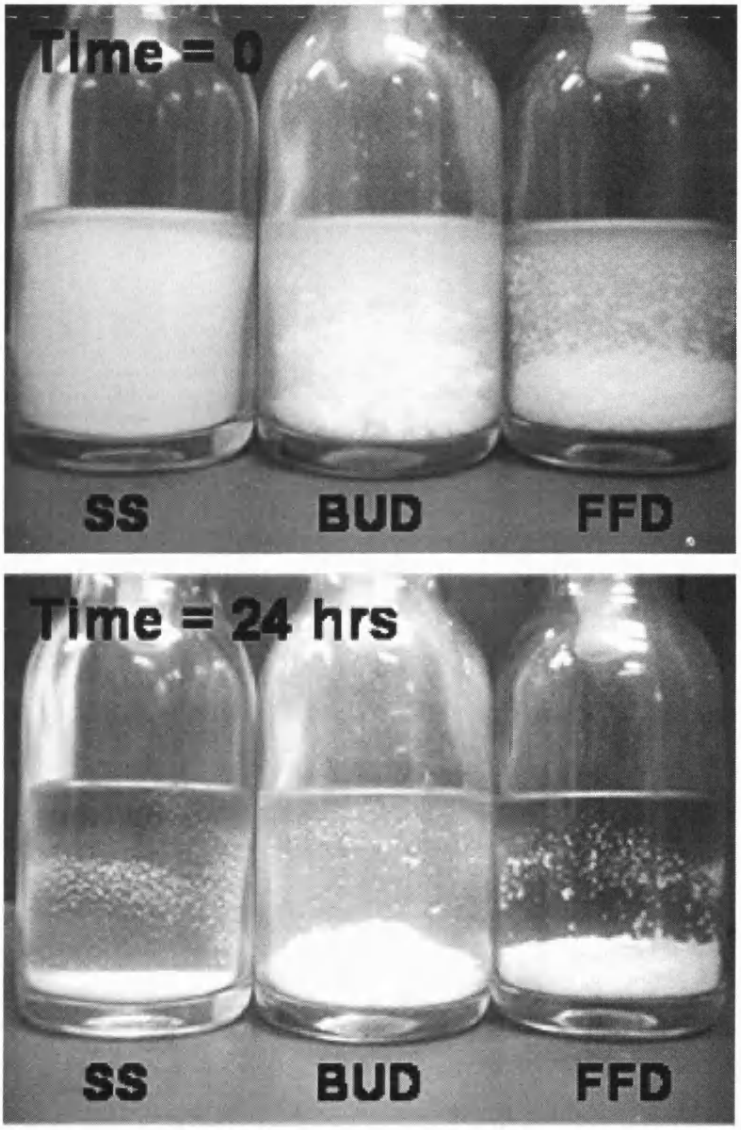

Figure 48 Sedimentation of single drug suspensions. At T =0, just after shaking, and after 24 hours

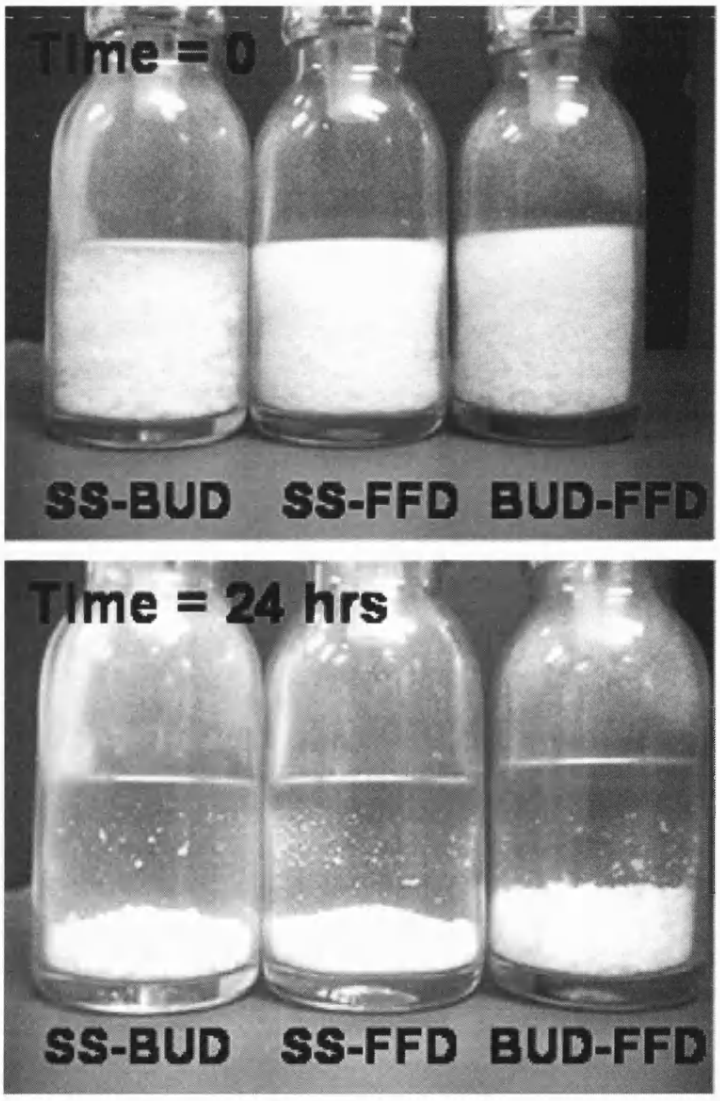

Figure 49 Sedimentation of combination drug suspensions. At T =0, just after shaking, and after 24 hours

It was interesting to note that, average floc size of budesonide aggregates were larger than that of salbutamol. This may be partially due to budesonide having a lower density (1.24 g/m^3) compared with salbutamol (1.31 g/m^3) and therefore occupying a larger phase volume at the same w/w concentration. However, the nature of the drugs may also influence aggregation behaviour in suspensions (Michael et al., 2001).

From the investigation in Chapter 6, it was suggested that formoterol and budesonide had more adhesive characteristics when related to salbutamol. Likewise salbutamol had and high cohesive tendency. Thus, the relative sedimentation volume of salbutamol-budesonide or salbutamol-formoterol decrease (or remain the same) with respect to budesonide or formoterol and increased with respect to salbutamol. This is most likely related to a rearrangement of the interparticulate forces within the combination based formulations.

In comparison, budesonie-formoterol formulations would form loose interparticulate bonds due to their adhesive bias, inducing higher sediment characteristics. Again, such observations are in good correlation when comparing fundamental surface energy and adhesion/cohesion measurement as discussed in Chapter 6.

8.3.2b In vitro analysis of combination formulations

The particle size distribution of the cumulative particle undersize for various aerodynamic cut-off stages (from stage 1 (<9 μm) to stage 4 (< 3.3 μm)) of salbutamol, budesonide and formoterol delivered from the single drug pMDIs, were compared with particle size distributions of the combination formulation inhalers (salbutamol-budesonide, salbutamol-formoterol and budesonide-formoterol) for the same stages.

Graphical representation for deposition of single drugs is presented in Figure 50.

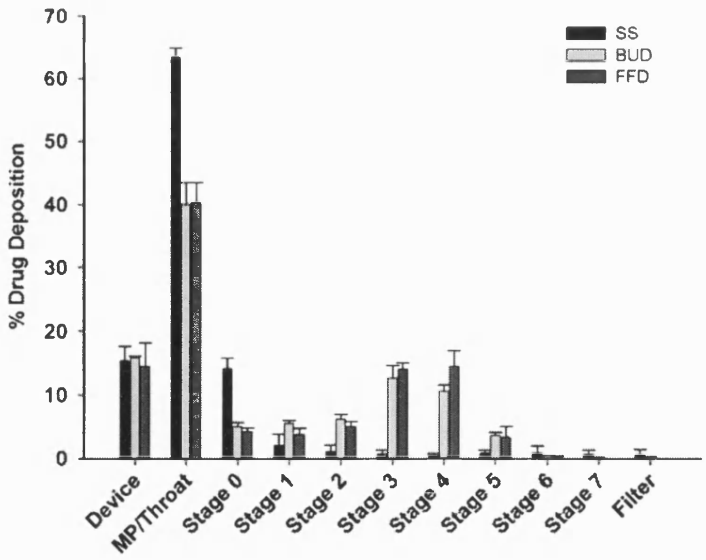

Figure 50 Graphical representation of percentage ACI deposition for salbutamol, budesonide and formoterol in single drug formulations

The mean percentile deposition and the range of mass on each stage (n=3), with respect to the effective cut-off diameter of each stage, for single drug formulations are shown in Table 35.

	% Deposition		
Size range (μm)	Salbutamol	Budesonide	Formoterol
< 9	7.58 ± 1.18	39.18 ± 3.51	41.03 ± 3.50
< 5.8	5.06 ± 1.53	33.63 ± 3.84	37.27 ± 4.14
< 4.7	3.22 ± 1.56	27.48 ± 3.25	32.20 ± 3.77
< 3.3	2.07 ± 1.15	14.86 ± 1.39	18.20 ± 3.42

Table 35 Particle size distribution of salbutamol, budesonide and formoterol delivered from a 125 μg single product (n = 10 actuations). Values given are mean n = 3 ± Standard deviation

Similarly, the mean percentile deposition and the range of mass on each stage, with respect to the effective cut-off diameter of each stage, for the combination drug formulations are shown in Table 36.

	% Deposition					
Combination product	**Salbutamol-Budesonide**		**Salbutamol- Formoterol**		**Budesonide- Formoterol**	
Size range (μm)	**SS**	**BUD**	**SS**	**FFD**	**BUD**	**FFD**
< 9	13.17 ± 1.65	33.06 ± 3.21	16.04 ± 3.14	44.20 ± 6.80	36.02 ± 2.72	40.64 ± 3.31
< 5.8	6.92 ± 0.60	28.43 ± 2.83	8.38 ± 2.27	41.84 ± 7.05	29.85 ± 1.58	35.97 ± 2.40
< 4.7	3.74 ± 1.05	24.26 ± 2.68	4.60 ± 1.10	38.99 ± 6.45	22.30 ± 1.91	28.67 ± 2.81
< 3.3	1.91 ± 0.90	15.11 ± 2.09	2.55 ± 0.67	28.49 ± 4.83	10.13 ± 3.05	12.86 ± 4.45

Table 36 Particle size distribution of salbutamol – budesonide, salbutamol – formoterol and budesonide -formoterol delivered from a 125 μg combination products (n = 20 actuations). Values given are mean n = 3, ± Standard deviation

To further analyse the behaviour of combination formulations in comparison to the respective drug only systems, the emitted drug deposition was presented as percentage of the theoretical dose formulated as both single drugs and combination products (Table 37).

Graphical representations of the emitted drug deposition of single drug formulations are shown in Figure 51, while combination formulation data for salbutamol-budesonide, salbutamol-formoterol and budesonide-formoterol are shown in Figure 52, Figure 53 and Figure 54, respectively.

In general, when delivered as a single entity, salbutamol presented very poor emitted dose performance, (% emitted dose /theoretical dose 37.78 % ± 11.08). In comparison, it was evident that emitted dose of salbutamol increased up to three times when delivered in a combination product (ANOVA, $p<0.05$). Such observations were observed with both budesonide (91.24 % ± 5.26) and formoterol (78.75 % ± 23.93) (Table 37). Such findings can be seen graphically in Figure 52 and Figure 53, for salbutamol-busedonide and salbutamol-formoterol drug-combination formulations, respectively.

The rationale behind such observation lies in the cohesive physical characteristic of salbutamol. As seen in Chapter 6, salbutamol particles, being predominantly cohesive, when delivered as homogeneous system, may have the tendency to aggregate due to the omnipresent van der Waals attractive forces. Consequently, the homogeneous flocs formed by random collisions would be difficult to break during inhalation (aerosolisation). Since breakage involves the expenditure of work during actuation, rupture of such aggregates will only take place if sufficient 'locally available' kinetic energy is available to overcome the 'energy barrier' associated with binding. Accordingly, cohesive drugs like salbutamol will not be proficiently delivered to the target site but impact in the upper stages of the ACI, giving poor drug delivery performances.

From a formulation perspective, the cohesive characteristic of salbutamol gathered from theoretical and experimental analysis performed in Chapter 6 correlated with observations obtained from the *in vitro* study. In general, the salbutamol formulation exhibited poor delivery efficiency unless a significant amount of shear energy was introduced to overcome the strong cohesive bonds. Moreover, unless formulated in combination with adhesive drugs, the salbutamol suspension formulation would probably be subjected to caking over time due to the very strong cohesive bonds.

% Emitted dose / Theoretical dose								
Single drug			Combination drugs					
SS	**BUD**	**FFD**	**SS-BUD**		**SS-FFD**		**BUD-FFD**	
37.78 ± 11.08	79.42 ± 7.44	88.81 ± 3.45	91.24 ± 5.56	69.83 ± 8.28	78.75 ± 23.93	63.69 ± 23.87	104.76 ± 15.51	90.13 ± 14.68

Table 37 Calculated emitted dose as function of the theoretical dose (125 μm dose) of salbutamol (SS) , budesonide (BUD) and formoterol (FFD) as single and combination products. Values given are mean n = 3, ± Standard deviation

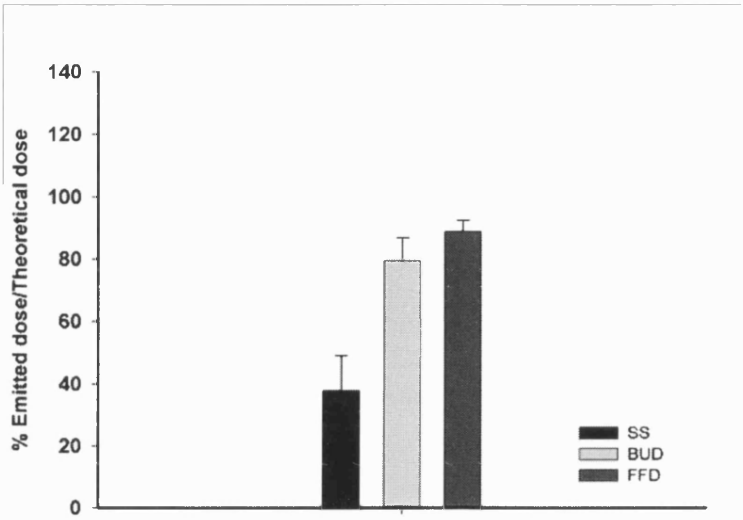

Figure 51 Graphical representation of ACI percentile of emitted dose against theoretical dose of salbutamol, budesonide and formoterol in single formulation format

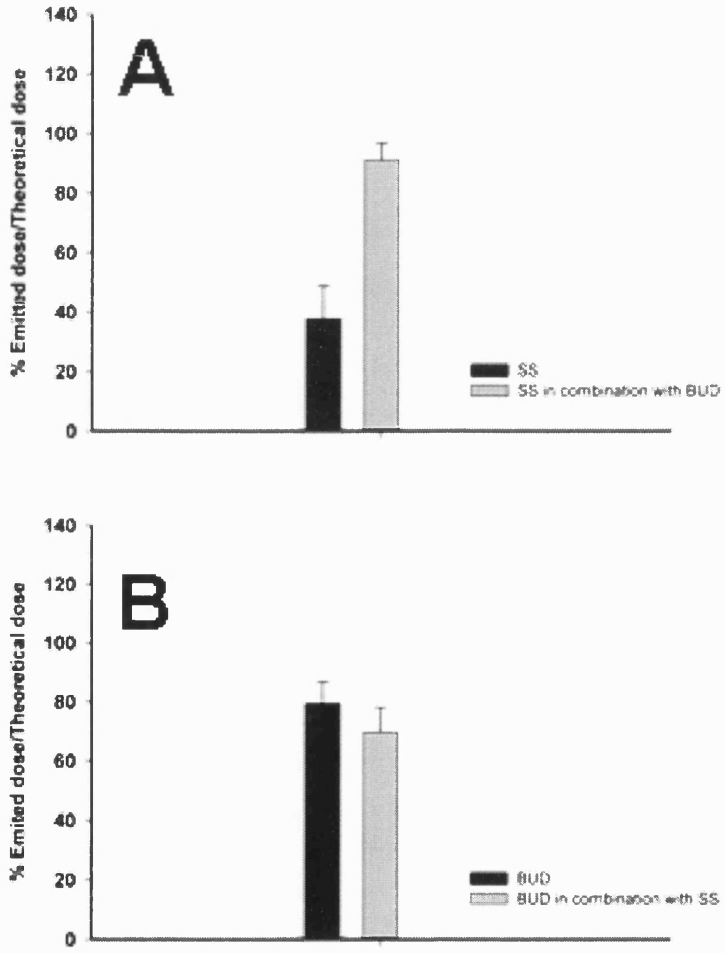

Figure 52 Graphical representation of ACI percentile of emitted dose against theoretical dose of (A) salbutamol and (B) budesonide in single and in mutual combination formulation

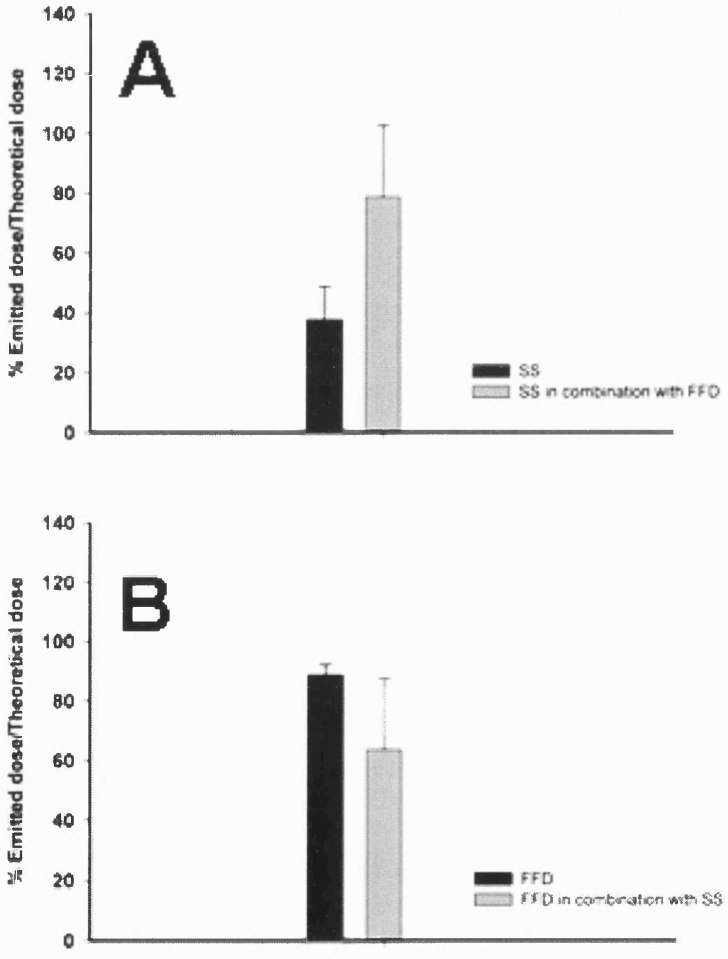

Figure 53 Graphical representation of ACI percentile of emitted dose against theoretical dose of (A) salbutamol and (B) formoterol in single and in mutual combination formulation

When combined with adhesive drugs like budesonide and formoterol, salbutamol will tend to flocculate and become loosely bound, therefore resulting in improved aerosolisation behaviour. Analysis of the *in vitro* data presented here along with corroborating data presented in Chapter 3 and 6 suggest such a system may exist in the salbutamol formulations.

In comparison, fundamental surface energy and adhesion measurements presented in 3 and 6 suggest budesonide and formoterol particle cohesion to be less than that of salbutamol. Furthermore, measurement of interparticulate adhesion between the two drugs indicated similar forces of interaction. Combining both fundamental values, along with the SCA and CAB data it would be logical to conclude little change in force would be required to re-disperse budesonide, formoterol or budesonide-formoterol combination formulation.

Analysis of both the visualisation study and the aerosolisation performance analysis of budesonide and formoterol as single entities or as a combination formulation further support these observations.

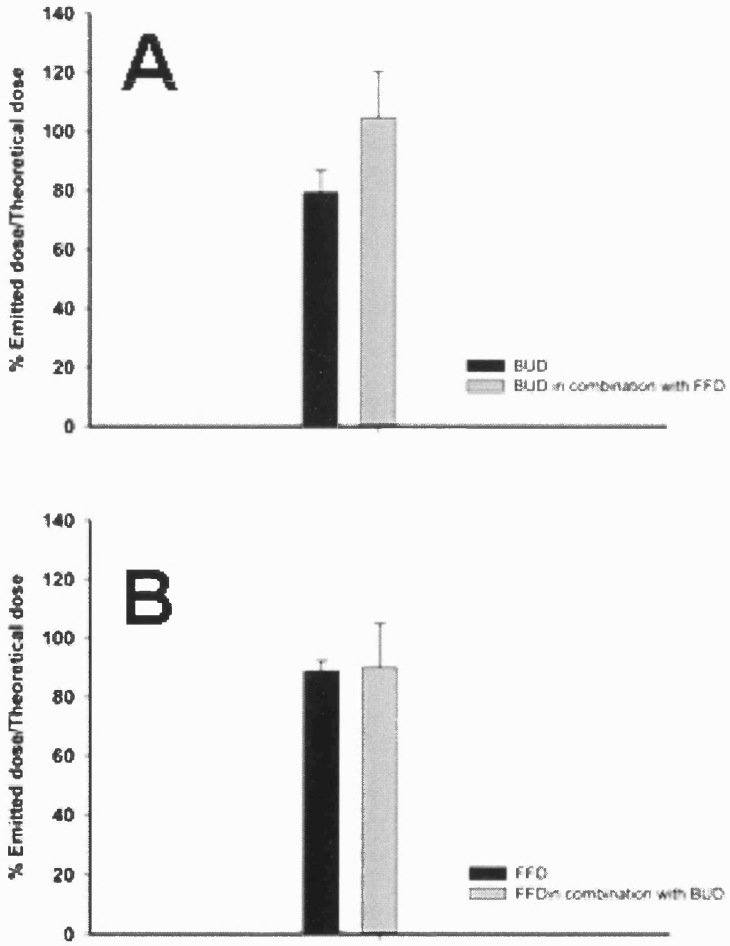

Figure 54 Graphical representation of ACI percentile of emitted dose against theoretical dose of (A) budesonide and (B) formoterol in single and in mutual combination formulation

8.4 GENERAL DISCUSSION

An *in vitro* investigation of the three drug systems was undertaken to determine if the relationship between adhesive/cohesive forces, measured by AFM and SCA, could be correlated with *in vitro* performance.

The *in vitro* investigation suggested that the three micronised drug materials had significantly different aerosolisation profiles when manufactured as single or combination formulations. The relationship between aerosolisation performances of the micronised drugs can be attributed to the modification in the balance of forces acting between the particulates within the respective formulations.

In general, the greatest significant differences were observed between salbutamol single drug and combination systems. Analysis of the *in vitro* performance for the salbutamol-only formulation suggested that the cohesive nature of salbutamol (as predicted by the SCA and observed with AFM) led to tightly bound flocs that did not fully de-aggregate upon aerosolisation. In comparison, the improved aerosolisation efficiency of salbutamol in combination with budesonide or formoterol showed the positive effect of the adhesive characteristics of the latter two drug particulates (also predicted by the SCA and observed with AFM).

In summary, when compared to fundamental theoretical calculations and direct measurement of the adhesion/cohesion forces (Chapter 3 and Chapter 6), the relationship between inter-particulate interactions and aerosol performance indicated a good correlation.

CHAPTER 9: CONCLUSIONS AND FURTHER WORK

9.1 GENERAL CONCLUSIONS

The extent to which particle-particle interactions dominate within colloidal based pharmaceutical systems will be dependent on direct assessment of all the possible interactions within a particular formulation preparation.

When considering pMDI systems (which target delivery of <5 mm particulates to the respiratory tract), the magnitude of the adhesion or cohesion phenomena on aerosolisation performance may form the basis for the necessary particle engineering optimisation requirements for the system.

Of particular interest was the nature and interactions of the various fundamental forces involved in non-aqueous based pharmaceutical suspensions. Such interactions will be critical during the aerosolisation process. Three micronised drugs (salbutamol, budesonide and formoterol), were chosen as models for investigation as they were directly applicable to inhalation therapy.

The primary aim of the study was to correlate AFM measurements of interparticulate forces with theoretical measurements of the interfacial free energy of particle interactions via surface free energy data. This approach was taken with a view to gain a greater understanding of the thermodynamic and surface physico-chemical properties which directly influence particle-particle interactions in suspension based pMDI systems.

Atomic force microscopy studies, surface energy investigations and theoretical measurements of the interfacial free energy of the three micronised drugs indicated significant differences in the adhesive/cohesive properties, when investigating both drug-drug and drug-canister interactions.

In general, when investigating drug-drug interactions, results indicated that the measured forces of interaction between particles in model propellant could not be accounted for by theoretical treatment of the dispersive surface free energy via CA and IGC. Furthermore, a correlation between theoretical work of adhesion/cohesion and AFM measurements was observed upon the introduction of the polar interfacial interactions within the SCA model. In addition, the force of interaction between the micronised drugs and pMDI canister sample surfaces indicated similar findings (however, it is interesting to note, although only small, significant variances in R^2 relationship were observed.)

In addition to drug-drug and drug-canister interactions the influence of polymer excipients were also investigated. This was mainly due to their common use as stabilising agents in current pMDI formulations (Adjei et al., 1995; Duan et al., 1994a, b; Israelachvili, 1992; Mistry and Gibson, 1992; Moris et al., 1992; Johnson, 1992; Johnson, 1994; Purewal and Greenleaf, 1989, Schultz and Quessy, 1991a, b; Somani and Booles, 1992; Steele et al., 1992). The influence of various concentrations of PEG and PVP on salbutamol interparticulate adhesion (measured by AFM) was investigated. Clear variation in particle adhesion was observed with both PEG polymer concentrations and/or upon the addition of low PVP concentrations. Such observations were related to a series of steric influences.

Finally, to fully investigate drug-drug interactions in combination formulations, a series of cascade impactor *in vitro* studies were conducted with single/combination based pMDI formulations. In general, the aerosolisation performance of salbutamol was shown to improve when formulated in a combination format, while budesonide and formoterol studies did not indicate significant differences when compared to single component formulations. Again, such findings indicated direct correlation with observations reported using surface energy, theoretical and AFM measurements.

Variations in the adhesive/cohesive properties of micronised drugs may be attributed to the balance of interparticulate forces of interaction that exist within the respective systems. Such a balance will be dependent upon a multitude of factors including, chemistry, surface free energy, crystal structure and surface morphology.

For pressurised metered dose inhalation systems the balance of such force of interactions are of essential importance in providing a quantitative relationship between the particle probes and the determinations of factors such as surface energy. Drug particulates of micron size must be aerosolised and delivered to the respiratory tract. Subsequently, the understanding and measurement of such interactions is of great interest.

Undoubtedly, combining the fundamental knowledge gained from AFM measurements with surface energy techniques provides a novel means of predicting suspension stability of pMDI formulations.

9.2 FURTHER WORK

Although the techniques used within this study have proven valuable in predicting the aerosolisation behaviour of micronised drug particulates, and the innovative approaches utilised in this study may provide a novel means of predicting suspension stability of pMDI formulations, many analogous investigations could be the subject of further work.

It has been demonstrated that a relationship between the theoretical interfacial thermodynamics, derived from the surface component approach, and experimental AFM based force measurements is present, which may have a dominant effect on the behaviour of pMDIs suspension systems.

The natural progression of this methodology would be able to apply the fundamental principles relating to experimental force measurements with the development of a high pressure AFM system for volatile HFA propellants. For this purpose, the initial design and manufacture of a pressurised atomic force microscope *in situ* cell was undertaken as part of the study (see Figure 55 below):

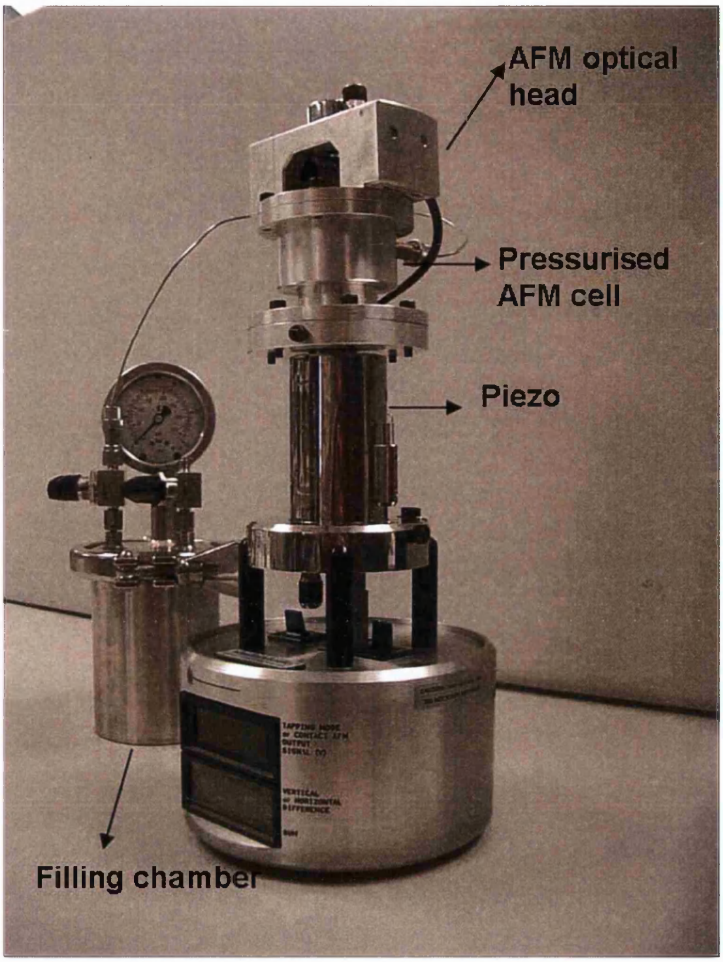

Figure 55 Schematic of the pressurised pMDI cell

While its development is still in its infancy, further development of the pressurised system would be beneficial for understanding the nature of the force involved and the behaviour of commercial pMDI systems.

Furthermore, although using the recently developed cohesive-adhesive balance analysis procedure eliminates the requirement for determining the true area of contact between drug probes, a complete understanding of the drug probe geometry and surface chemistry would prove invaluable when modelling adhesive/cohesive interaction forces.

This could be achieved by controlled crystallisation of the drug probes, or the application of novel characterisation techniques to existing micronised drug probes.

Finally it would be interesting to further develop surface energy techniques so that limitations that at the moment preclude the use of the surface component approach in determining the polar free energy of interaction via IGC and organic DVS measurements could be overcome, and could provide invaluable information that may predict the performance and stability of pMDI systems.

REFERENCES

Adjei, A. L., Gupta, P. K., and Fu Lu, M. Y. Aerosol formulations for use with non-CFC propellants. Patent Number: WO 95/15151. 1995.

Ahfat, N. M., Buckton, G., Burrows, R., and Ticehurst, M. D.: Predicting mixing performance using surface energy measurements. International Journal of Pharmaceutics **156:** 89-95, 1997.

Ahfat, N. M., Buckton, G., Burrows, R., and Ticehurst, M. D.: An exploration of inter-relationships between contact angle, inverse phase gas chromatography and triboelectric charging data. European Journal of Pharmaceutical Sciences **9:** 271-276, 2000.

Albertsson, J., Oskarsson, A., and Svensson, C.: X-ray study of budesonide: molecular structure and solid solution of the (22S) and (22R) epimers of 11B,21-dihydroxy-16alfa,17 alfa-propylmethylenedioxy-1,4-pregnadiene-3,20-dione. Acta Crystallographyca **B34:** 3027-3036, 1978.

Ashayer, R., Luckham, P. F., Manimaaran, S., and Rogueda, P.: Investigation of the molecular interactions in a pMDI formulation by atomic force microscopy. European Journal of Pharmaceutical Sciences **21:** 533-543, 2003.

Ashurst, I. C., Herman, C. S., Li. L. and Riebe, M. T. Metered dose inhaler for salmeterol. Patent Number: 6,143,277. 1996.

Atkins, D. T., and Pashley, R. M.: Surface forces between ZnS and Mica in aqueous electrolyte. Langmuir **9:** 2232-2236, 1993.

Barton, A. F. M.: Solubility Parameters. Chemical Reviews **75:** 731-753, 1974.

Barton, A. F. M.: Handbook of solubility parameters and other cohesion parameters, Boca Raton, FL., U.S.A, 1983.

Begat, P., Morton, D. A. V., Staniforth, J. N., and Price, R.: The cohesive-adhesive balances in dry powder inhaler formulations I: direct quantification by atomic force microscopy. Pharmaceutical Research **21:** 1826-1833, 2004.

Binnig, G., and Quate, C. F.: Atomic force microscope. Physical Review Letters **56:** 930-933, 1986.

Blondino, F. E., and Byron, P. R.: Surfactant dissolution and water solubilisation in chlorine-free liquefied gas propellants. Drug Development in Industrial Pharmacy **24:** 935-945, 1998.

Booth, S. W., and Newton, J. M.: Experimental investigation of adhesion between powders and surfaces. Journal of Pharmacy and Pharmacology **39:** 679-684, 1987.

Booth, J., and Williams, D. R.: The dispersive and non-dispersive components of the surface tension for various organic solvents, Surface Measurements Systems application note 17, 1998.

Brambilla, G., Ganderton, D., Garzia, R., Lewis, D., Meakin, B., and Ventura, P.: Modulation of aerosol clouds produced by pressurised inhalation aerosols. International journal of pharmaceutics **186:** 53-61, 1999.

British Standard: International Standard ISO 13320-1: Particle size analysis - Laser Diffraction - Part 1: General Principles, 1999.

British Thoracic Society, T. N. A. C., The Royal College of Physicians of London in association with the General Practitioner in Asthma Group, the British Association of Accident and Emergency Medicine, and the British Paediatric Respiratory Society and the Royal College of Paediatrics and Child Health.: The British Guidelines on Asthma Management Review and Position Statement. Thorax **52** (Supplement 1)**:** S1-S20, 1997.

Brunauer, S., Emmet, P. H., and Teller, E.: Adsorption of gases in multimolecular layers. Journal of the American Chemical Society **60:** 309-319, 1938.

Buckton, G., and Newton, J. M.: Assessment of the wettability of powders by use of compressed powder discs. Powder Technology **46:** 201-208, 1986.

Buckton, G.: Assessment of the wettability of pharmaceutical powders. *In* Contact angle, wettability and adhesion, pp. 437-451, K.L.Mittal, 1993.

Buckton, G.: Interfacial phenomena in drug delivery and targeting, Harwood Academic Publishers, Chur, Switzerland, 1995.

Buckton, G., and Darcy, P.: The use of gravimetric studies to assess the degree of crystallinity of predominantly crystalline powders. International Journal of Pharmaceutics **123:** 265-271, 1995.

Charsley, E. L., and Warrington, S. B.: Thermal analysis - techniques and applications, Cambridge, UK, 1992.

Chawa, A., Taylor, G. K. M., Newton, J. M., and Johnson, M. C. R.: Production of spray dried salbutamol sulphate for use in dry powder aerosol formulation. International Journal of Pharmaceutics **108:** 233-240, 1994.

Chibowski, E., Bolivar, M., and Gonzalez Caballero, F.: Studies on the surface free energy components of nitrofurantoin. Journal of Colloid and Interface Science **154:** 400-410, 1992.

Clarke, A. R.: How the industry makes inhalers. Journal of Pharmacy and Pharmacology **54** (Supplement 290)**:** S-10, 2002.

Clarke, J. G., Wicks, S. R., and Farr, S. J.: Surfactant mediated effects in pressurized metered dose inhalers formulated as suspension. I. Drug/surfactant interactions in a model propellant system. International Journal of Pharmaceutics **93:** 221-231, 1993.

Clarke, M. J., Peart, J., Cagnani, S., and Byron, P. R.: Adhesion of powders for inhalation: an evaluation of drug detachment from surfaces following deposition from aerosol streams. . Pharmaceutical Research **19:** 322-329, 2002.

Columbano, A., Buckton, G., and Wikeley, P.: A study of the crystallisation of amorphous salbutamol sulphate using water vapour sorption and near infrared spectroscopy. International Journal of Pharmaceutics **237:** 171-178, 2002.

Connors, K. A.: The Karl Fisher titration of water. Drug Development in Industrial Pharmacy **14:** 1891-1903, 1988.

Dalby, R. N., Byron, P. R., Shepherd, H. R., and Papadoupoulos, E.: CFC propellant substitution: P-134a as a potential replacement for P-12 in MDIs. Pharmaceutical Technology **14:** 26-33, 1990.

Dalby, R. N., Phillips, E. M., and Byron, P. R.: Determination of Drug Solubility in Aerosol Propellants. Pharmaceutical Research **8:** 1206-1209, 1991.

Dalton, C. R., and Hancock, B. C.: Processing and storage effects on water vapour sorption by some model pharmaceutical solid dosage formulations. International Journal of Pharmaceutics **156:** 143-151, 1997.

Debye, P.: Die van der Waals kohaesionskraefte. Physik Z. **21:** 178, 1920.

Derjaguin, B. V., and Landau, L. D.: Theory of the stability of strongly charged lyophobic sols and of the adhesion of strongly charged particles in solutions of electrolytes. Acta Physicochimica U.S.S.R. **14:** 663, 1941.

Derjaguin, B. V., Müller, V. M., and Toporov, Y. P.: Effect of contact deformations on the adhesion of particles. Journal of Colloid and Interface Science **53:** 314-326, 1975.

Desai, T. R., Li, D., Finlay, W. H., and Wong, J. P.: Determination of surface free energy of interactive dry powder liposome formulations using capillary penetration technique. Colloids and Surfaces B: Biointerfaces **22:** 107-12, 2001.

Dickinson, P. A., Seville, P. C., McHale, H., Perkins, N. C., and Taylor, G.: An investigation of the solubility of various compounds in the hydrofluoroalkane propellants and possible model liquid propellants. Journal of Aerosol Medicine **13:** 179-186, 2000.

Diggins, D., Fokkink, L. G. J., and Ralston, J.: The wetting of angular quartz particles: capillary pressure and contact angles. Colloids and Surfaces **44:** 299-313, 1990.

Dove, J. W., Buckton, G., and Doherty, C.: A comparison of two contact angle measurements methods and inverse gas chromatography to assess the surface energies of theophylline and caffeine. International Journal of Pharmaceutics **138:** 199-206, 1996.

Duan, D. C., Stefely, J. S., Schultz, D. W. and Leach, C. L. Aerosol formulation containing diol-diacid derived dispersing aid. Patent Number: WO 94/21228. 1994a.

Duan, D. C., Stefely, J. S., Schultz, D. W., and Leach, C. L. Aerosol formulation containing an ester-amide or mercaptoester derived dispersing aid. Patent Number: WO 94/21229. 1994b.

Ducker, W. A., Senden, T. J., and Pashley, R. M.: Direct measurement of colloidal forces using an atomic force microscope. Nature **353:** 239-241, 1991.

Ducker, W. A., Senden, T. J., and Pashley, R. M.: Measurement of Forces in Liquids Using a Force Microscope. Langmuir **8:** 1831-1836, 1992.

Dunbar, C. A., Watkins, A. P., and Miller, J. F.: An experimental investigation of the spray issued from a pMDI using laser diagnostic techniques. Journal of Aerosol Medicine **10:** 351-368, 1997.

Eklund, E. A., Wayman, W. H., Brillson, L. J., and Hays, D. A. *In* IS&T tenth International congress on advances in non-impact printing technologies, pp. 142, New Orleans, U.S.A, 1994.

Eliassaf, J., Eriksson, F., and Eirich, F. R.: The interaction of Poly(vinyl Pyrrolidone) with cosolutes. Journal of Polymer Science XLVII: 193-202, 1960.

Ertan, A., Stensland, B., and Ymen, I.: Crystal and molecular structure of formoterol fumarate dihydrate, Astra Production Chemicals AB, 1997.

Eve, J. K., Patel, N., Luk, S. Y., Ebbens, S. J., and Roberts, C. J.: A study of single drug particle adhesion interactions using atomic force microscopy. International Journal of Pharmaceutics **238:** 17-27, 2002.
Feeley, J. C., York, P., Sumby, B. S., and Dicks, H.: Determination of surface properties and flow characteristics of salbutamol sulphate before and after micronisation. International Journal of Pharmaceutics **172:** 89-96, 1998.

Florey, K.: Analytical profiles of drug substances, Academic Press, London, UK, 1972.

Fowkes, F. M.: Determination of interfacial tension, contact angles and dispersion forces in surface by assuming additivity of intermolecular interactions in surfaces. Journal of Physical Chemistry **66:** 382, 1962.

Fowkes, F. M.: Additivity of intermolecular forces at interfaces. I. Determination of the contribution to surface and interfacial tension of dispersion forces in various liquids. Journal of Physical Chemistry **67:** 2538-2541, 1963.

Franco, F., Perez-Maqueda, L. A., and Perez-Rodriguez, J. L.: The effect of ultrasound on the particle size and structural disorder of a well-ordered kaolinite. Journal of Colloid and Interface Science **274:** 107-117, 2004.

Fu, D., and Riman, R. E.: Evaluation of Dispersion Stability. Journal of Colloid and Interface Science **157:** 394-398, 1993.

Ganderton, D., and Jones, T.: Drug Delivery to the Respiratory Tract, Academic Press, London, UK, 1987.

Giles, H. C., MacEwan, T. H., Nakhwa, S. N., and Smith, D.: Studies in Adsorption. Part XI. A system of classification of solution adsorption isotherms, and its use in diagnosis of adsorption mechanisms in the measurements of specific surface areas of solids. Journal of Chemical Society **9:** 3973-3993, 1960.

Glover, W., and Chan, H. K.: Electrostatic charge characterization of pharmaceutical aerosols using electrical low-pressure impaction (ELPI). Journal of Aerosol Science **35:** 755-764, 2004.

Goebel, A., and Lunkenheimer, K.: Interfacial tension of the water/n-alkane interface. Langmuir **13:** 369-372, 1997.

Good, R. J., and Girifalco, L. A.: A theory for estimation of surface and interfacial energies. III. Estimation of surface energies of solids from contact angle data. Journal of Physical Chemistry **64:** 561-565, 1960.

Good, R. J., and Stromberg, R. R.: Surface and Colloid Science, Plenum Press, New York, U.S.A., 1979.

Good, R. J.: Contact-Angle, Wetting, and Adhesion - a Critical-Review. Journal of Adhesion Science and Technology **6:** 1269-1302, 1992.

Griffiths, P., Paul, A., and Rogueda, P.: Using polymers to control the stability of non-aqueous suspensions. *In* Advance in non-aqueous colloids meeting, Royal Society of Chemistry, London, UK, 2004.

Grundke, K., Bogumil, T., Gietzelt, T., Jacobasch, H. J., Kwok, D. Y., and Neumann, A. W.: Wetting measurements on smooth, rough and porous solid surfaces. Progress in Colloid and Polymer Science **101:** 58-68, 1996.

Guinier, A.: X-ray powder diffraction: In crystals, imperfect crystals and amorphous bodies, Dover Publications, New York, USA, 1994.

Gupta, P. K., and Hickey, A. J.: Contemporary approaches in aerosolized drug delivery to the lung. Journal of Controlled Release **17:** 127-147, 1991.

Hamaker, H. C.: The London - van der Waals attraction between spherical particles. Physica **4:** 1058-1072, 1937.

Heller, W., and Pugh, T. L.: "Steric" stabilisation of colloidal solutions by adsorption of flexible macromolecules. Journal of Polymer Science XLVII: (203-217), 1960.

Hertz, H.: On the contact of elastic solids. J. Reine Angew. Math. **92:** 156-171, 1882.

Hickey, A. J., and Martonen, T. B.: Behaviour of Hygroscopic Pharmaceutical Aerosols and the Influence of Hydrophobic Additives. Pharmaceutical Research **10:** 1-7, 1993.

Hinds, W. C.: Aerosol technology, John Wiley & Sons., New York, USA, 1999.

Hooton, J. C., German, C. S., Allen, S., Davies, M. C., Roberts, C. J., Tendler, S. J. B., and Williams, P. M.: An Atomic force microscopy study of the effect of nanoscale contact geometry and surface chemistry on the adhesion of pharmaceutical particles. Pharmaceutical Research **21:** 953-961, 2004.

Höper, R., Gesang, T., Possart, W., Hennemann, O. D., and Boseck, S.: Imaging elastic sample properties with an atomic force microscope operating in the tapping mode. Ultramicroscopy **60:** 17-24, 1995.

Ibrahim, T. H., Burk, T. R., Etzler, F. M., and Neuman, R. D.: Direct adhesion measurements of pharmaceutical particles to gelatine capsule surfaces. Journal of Adhesion Science and Technology **14:** 1225-1242, 2000.

I.P.A.C.: International Pharmaceutical Aerosol Consortium, Website-www.ipacmdi.com, 1997.

Israelachvili, J. N.: Intermolecular and surface forces, Academic Press, New York, U.S.A, 1992.

James, K. C.: Solubility and Related Proprieties, Marcel Dekker, New York, U.S.A., 1986.

Johnson, K. A., Kendall, K. L., and Roberts, A. D.: Surface energy and the contact of elastic solids. Proceedings of the Royal Society London. A. **324:** 301-313, 1971.

Johnson, K. A. Aerosol drug formulations. Patent Number: WO 92/00107. 1992.

Johnson, K. A. Methods for stabilising aerosol formulations. Patent Number: GB 2,268,507. 1994.

Johnson, K.A., Interfacial phenomena and phase behaviour in metered-dose inhaler formulations in: Hickey A.J. (Ed.), Inhalation Aerosols, Vol. 94, pp. 385-415, Marcel Dekker, New York, U.S.A.,1996.

Keesom, W. H.: On the second virial coefficient for di-atomic gasses. Suppl. Com. Physic. Lab. Univ. Leiden **25:** 3-19, 1912.

Kerkak, A. V., and Feke, D. L.: Induced flocculation in sterically stabilized ceramic powder dispersions. Colloids and Surfaces **53:** 363-381, 1991.

Kiesvaara, J., and Yliruusi, J.: The use of the washburn method in determining the contact angles of lactose powder. International Journal of Pharmaceutics **92:** 81-88, 1993.

Kiesvaara, J., Yliruusi, J., and Ahomaki, E.: Contact angles and surface free energies of theophylline and salicylic acid powders determined by the Washburn method. International Journal of Pharmaceutics **97:** 101-109, 1993.

Kitahara, A.: Zeta potential in non-aqueous media and its effect on dispersion stability. Progress in Organic Coatings **2:** 81-98, 1974.

Kulvanich, P., and Stewart, P. J.: Influence of relative humidity on the adhesive properties of a model interactive system. Journal of Pharmacy and Pharmacology **40:** 453-458, 1988.

Larhrib, H., Martin, P. G., Marriott, C., and Prime, C.: The influence of carrier and drug morphology on drug delivery from dry powder formulations. International Journal of Pharmaceutics **257:** 283–296, 2003.

Lavielle, L., and Schultz, J.: Surface properties of carbon fibres determined by inverse gas chromatography: role of pre-treatment. Langmuir **7:** 978-981, 1991.

Leger, P. J. M., Goursolle, M., and Gadret, M.: Structure Cristalline du sulphate de salbutamol [ter-Butylamino-2-(Hydroxy-4hydroxymethyl-3 phenyl)-1 Ethanol.1/2 H2SO4]. Acta Crystallographyca **B34:** 1203-1208, 1978.

Levoguer, C. L., and Williams, D. R.: Measurement of the surface energies of pharmaceutical powders using a novel vapour adsorption method, Surface Measurements Systems application note 17, 1999.

Li, Y. Q., Tao, N. J., Pan, J., Garcia, A. A., and Linsday, S. M.: Direct measurements of interaction forces between colloidal particles using the scanning force microscope. Langmuir **9:** 637-641, 1993.

Lifshitz, E. M.: The theory of molecular attractive forces between solids. Sov. Phys.JETP **2:** 73-83, 1956.

London, F.: Zur theorie und systematik de molekularkraefte. Phisik. Z. **63:** 245, 1930.

Louey, M. D., Mulvaney, P., and Stewart, P. J.: Characterisation of adhesional properties of lactose carriers using atomic force microscopy. Journal of Pharmaceutical and Biomedical Analysis **25:** 559-567, 2001.

Louey, M. D., Razia, S., and Stewart, P. J.: Influence of physico-chemical carrier properties on the in vitro aerosol deposition from interactive mixtures. International Journal of Pharmaceutics **252:** 87-98, 2003.

Martin, T. M., Bandi, N., Shulz, R., Roberts, C. B., and Kompella, U. B.: Preparation of Budesonide and Budesonide-PLA Microparticles Using Supercritical Fluid Precipitation Technology. AAPS PharmSciTech **3** (3 Article 18): 1-11, 2002.

Martini, A., Torricelli, C., and De Ponti, R.: Physico-pharmaceutical characteristics of steroid/crosslinked polyvinylpyrrolidone coground system. International Journal of Pharmaceutics **75:** 141-146, 1991.

Mc Donald, K., and Martin, G. P.: Transition to CFC-free metered dose inhalers- into the new millennium. International Journal of Pharmaceutics **201:** 89-107, 2000.

Michael, Y., Chowdhry, B. Z., Ashurst, I. C., Snowden, M. J., Davies-Cutting, C. J., and Gray, S.: The physico-chemical properties of salmeterol and fluticasone proprionate in different solvent environments. International Journal of Pharmaceutics **200:** 279-288, 2000.

Michael, Y., Snowden, M. J., Chowdhry, B. Z., Ashurst, I. C., Davies-Cutting, C. J., and Ripley, T.: Characterisation of the aggregation behaviour in a salmeterol and fluticasone propionate inhalation aerosol system. International Journal of Pharmaceutics **221:** 165-174, 2001.

Mistry, S. N., and Gibson, M. Pressurised aerosol composition. Patent Number: EP 534731. 1992.

Molina, M. J., and Rowland, F. S.: Stratospheric sink for chlorofluoromethane: chlorine atom catalysed destruction of ozone. Nature **274:** 810-812, 1974.

Moris, R. A., Schultz, D. W., Schultz, R. K. and Thiel, C.G. The use of soluble fluosurfactants for the preparation of metered dose aerosol formulations. Patent Number: WO 92/00062. 1992.

Muster, T. H., and Prestidge, C. A.: Face specific surface properties of pharmaceutical crystals. Journal of Pharmaceutical Sciences **91:** 1432-1444, 2002.

Neumann, A. W., Renzow, D. R., Reumuth, H., and Richter, J. E.: Fortschr. Kolloide Polymere **55:** 49-54, 1971.

Osmond, D. W. J., and Waite, F. A.: Dispersion polymerisation in organic media, ed. by K. E. Barret, pp. 19, Wiley Interscience, Hoboken, NJ, U.S.A., 1975.

Overbeek, J. T. G.: Colloid Science, Elsevier, Amsterdam, Holland, 1952.

Papirer, E., Brendle, E., Ozil, F., and Balard, H.: Comparison of the surface properties of graphite, carbon black and fullerene samples, measured by inverse gas chromatography. Carbon **37:** 1265-1274, 1999.

Parson, G. E., Buckton, G., and Chatham, S. M.: The use of surface energy and polarity determinations to predict physical stability of non-polar, non aqueous suspension. International Journal of Pharmaceutics **83:** 163-170, 1992.

Patton, J. S.: Mechanisms of macromolecule absorption by the lungs. Advanced Drug Delivery Reviews **19:** 3-36, 1996.

Planinsek, O., Trojak, A., and Srcic, S.: The dispersive component of the surface fee energy of powders assessed using inverse gas chromatography and contact angle measurements. International Journal of Adhesion and Adhesives **221:** 211-217, 2001.

Planinsek, O., and Buckton, G.: Inverse gas chromatography: considerations about appropriate use for amorphous and crystalline powders. Journal of Pharmaceutical Sciences **92:** 1286-1294, 2003.

Podczeck, F., Newton, J. M., and James, M. B.: The adhesion force of micronised Salmeterol Xinafoate particles to pharmaceutically relevant surface materials. Journal of Physic D: Applied Physic **29:** 1878-1884, 1996.

Polli, G. P., Grim, W. M., Bacher, F. A., and Yunker, M. H.: Influence of Formulation on Aerosol Particle Size. Journal of Pharmaceutical Science **54:** 484-486, 1969.

Prestidge, C. A., and Tsatouhas, G.: Wettability studies of morphine sulphate powders. International Journal of Pharmaceutics **198:** 201-212, 2000.

Preuss, M., and Butt, H. J.: Measuring the contact angle of individual colloidal particles. Journal of Colloid and Interface Science **208:** 468-477, 1998.

Price, R., Young, P. M., Edge, S., and Staniforth, J. N.: The influence of relative humidity on particulate interactions in carrier-based dry powder inhaler formulations. International Journal of Pharmaceutics **246:** 47-59, 2002.

Price, R., and Young, P. M.: Visualisation Of The Crystallisation Of Lactose From The Amorphous State. Journal of Pharmaceutical Sciences **93:** 155-164, 2004.

Pritchard, J. N.: The Influence of Lung Deposition on Clinical Response. Journal of Aerosol Medicine **14** (Supplement 1)**:** S-19-S-26, 2001.

Pugh, R. J., Matsunaga, T., and Fowkes, F. M.: The dispersability and stability of carbon black in media of low dielectric constant. I: Electrostatic and steric contributions to colloidal stability. Colloids and Surfaces **7:** 183-207, 1983.

Purewal, T. S., and Greenleaf, D. J. Medicinal aerosol formulations. Patent Number: EP 0372777. 1989.

Ranucci, J. A., Dixit, S., Bray, R. N. J., and Goldman, D.: Controlled flocculation in meterd-dose aerosol suspensions. Pharmacetical Technology: 68-73, 1990.

Rhodes, G.: Crystallography- Made crystal clear, Academic Press, New York, USA, 1993.

Riddle, F. L., and Fowkes, F. M.: Spectral Shifts in Acid-Base Chemistry .1. Van der Waals Contributions to Acceptor Numbers. Journal of the American Chemical Society **112** (9)**:** 3259-3264, 1990.

Rogueda, P. G. A.: HPFP, a model propellant for pMDIs. Drug Development and Industrial Pharmacy **29:** 39-49, 2003.

Romo, L. A.: Stability of non-aqueous dispersions. Journal of Physical Chemistry **67:** 386-389, 1963.

Ross, D. L., and Gabrio, B. J.: Advances in metered dose inhaler technology with the development of a chlorofluorocarbon free drug delivery system. Journal of Aerosol Medicine **12:** 151-160, 1999.

Roulison, C.: Wettability studies for porous solids including powders and fibrous material. Application Note 302, Kruss, GmbH, 1996.

Ruckenstein, E.: On the stability of concentrates. Non-aqueous dispersions. Colloids and Surfaces **69:** 271-275, 1993.

Ruoff, R. S., Tse, D. S., Malhotra, R., and Lorents, D. C.: Solubility of C_{60} in a Variety of Solvents. Journal of Physical Chemistry **97:** 3379-3383, 1993.
Sarid, D.: Scanning force microscopy, Oxford University Press, New York, USA, 1994.

Schaefer, D. M., Carpenter, M., Reifenberger, R., Demejo, L. P., and Rimai, D. S.: Surface forces interactions between micrometer-size polystyrene sphere and silicon substrates using atomic forces techniques. Journal of Adhesion Science and Technology **8:** 197-210, 1994.

Schaefer, D. M., Carpenter, M., Gady, B., Reifenberger, R., Demejo, L. P., and Rimai, D. S.: Surface roughness and its influence on particle adhesion using atomic force techniques. Journal of Adhesion Science and Technology **9:** 1049-1062, 1995.

Schultz, J., and Quessy.S.N. Use of soluble surfactant for the preparation of metered dose aerosol formulations. Patent Number: WO91/14422, 1991a.

Schultz, R. K., and Quessy.S.N. Use of soluble fluorosurfactants for the preparation of metered dose aerosol formulations. Patent Number: US 5,118,494.1991b.

Shekunov, B. Y., and York, P.: Crystallization processes in pharmaceutical technology and drug delivery design. Journal of Crystal Growth **211:** 122-136, 2000.

Sindel, U., and Zimmermann, I.: Measurement of interaction forces between individual powder particles using an atomic force microscope. Powder Technology **117:** 247-254, 2001.

Smyth, H. D. C.: The influence of formulation variables on the performances of alternative propellant-driven metered dose inhalers. Advance Drug Delivery Reviews **55:** 807-828, 2003.

Somani, A., and Booles, C. Pressurised aerosol compositions. Patent Number: WO 92/00061. 1992.

Staniforth, J.: Ordered mixing of drugs with particulate excipients. University of Aston, Birmingham, UK, 1980.

Steckel, H., and Brandes, H. G.: A novel spray-drying technique to produce low density particles for pulmonary delivery. International Journal of Pharmaceutics **278:** 187-195, 2004.

Steckel, H., Pichert, L., and Müller, B. W.: Influence of process parameters in the ASES process on particle properties of budesonide for pulmonary delivery. European Journal of Pharmaceutics and Biopharmaceutics **57:** 507–512, 2004.

Steele, G., Somani, A., and Lim, J. G. P.: Propellant compositions. Patent Number: WO 91/11173. 1992.

Sunkersetta, M. R., Grimsey, I. M., Doughtya, S. W., Osborna, J. C., York, P., and Rowe, R. C.: The changes in surface energetics with relative humidity of carbamazepine and paracetamol as measured by inverse gas chromatography. European Journal of Pharmaceutical Sciences **13:** 219-225, 2001.

Tang, P., Chan, H. K., and Raper, J. A.: Prediction of aerodynamic diameter of particles with rough surfaces. Powder Technology **147:** 64-78, 2004.

Ticehurst, M. D., Rowe, R. C., and York, P.: Determination of the surface properties of two batches of salbutamol sulphate by inverse gas chromatography. International Journal of Pharmaceutics **111:** 241-249, 1994.

Timsina, M. P., Martin, G. P., Marriott, C., Ganderton, D., and Yianneskis, M.: Drug delivery to the respiratory tract using dry powder inhalers. International Journal of Pharmaceutics **101:** 1-13, 1994.

Tiwari, D., Goldman, D., Malick, W. A., and Madan, P. L.: Formulation and evaluation of albuterol metered dose inhalers containing tetrafluoroethane (P134a), a non-CFC propellant. Pharmaceutical Development and Technology **3** (2)**:** 163-174, 1998.

United Nation Environment Programme, U. N.: U.N., Handbook for international treaties for the protection of the ozone layer, United Nation Environment Programme, Kenya, 1996.

van der Waals, J. D.: Die kontinuitaer der gasfoermigen und fluessigen zustaende, Peters, Leipzig, Germany, 1899.

van Oss, C. J., Good, R.J., Chaudhury, M.K: Additive and Nonadditive Surface Tension Components and the Interpretation of Contact Angles. Langmuir **4:** 884-891, 1988a.

van Oss, C. J., Chaudhury, M. K., and Good.R.J: Interfacial Lifshltz-van der Waals and polar interactions in macroscopic systems. Chemical Reviews **88:** 927-941, 1988b.

van Oss, C. J.: Interfacial forces in aqueous media, Marcel Dekker, New York, U.S.A., 1994.

Vervaet, C., and Byron, P. R.: Drug surfactant propellant interactions in HFA formulations. International Journal of Pharmaceutics **186:** 13-30, 1999.

Verwey, E. J. W., and Overbeek, J. T. G.: Theory of the stability of lyophobic colloids, Elsevier, Amsterdam, Holland, 1948.

Ward, G. H., and Schultz, R. K.: Process-induced crystallinity changes in albuterol sulphate and its effect on powder physical stability. Pharmaceutical Research **12:** 773-779, 1995.

Washburn, E. W.: The dynamics of capillary flow. Physical review **17:** 273-283, 1921.

Webb, P. A., and Orr, C.: Analytical methods in fine particle technology, Micrometrics Instrument Corp., Norcross, GA. U.S.A., 1997.

Weisenhorn, A. L., Maivald, P., Butt, H. J., and Hansma, P. K.: Measuring adhesion, attraction, and repulsion between surfaces in liquids with an atomic force microscope. Physical review B **45** (19)**:** 11226-11232, 1992.

Williams III, R. O., Barron, M. K., Alonso, J. M., and Remunan-Lopez, C.: Investigation of a pMDI system containing chitosan microspheres and P134a. International Journal of Pharmaceutics **174:** 209-222, 1998.

Williams III, R. O., Repka, M. A., and Barron, M. K.: Application of co-grinding to formulate a model pMDI suspension. European Journal of Pharmaceutics and Biopharmaceutics **48:** 131-140, 1999.

Wyatt, D. A., and Vincent, B.: Electrical effects in non-aqueous systems. Journal of Biopharmaceutical Science **3:** 27-31, 1989.

York, P.: Strategies for particle design using supercritical fluid technologies. Pharmaceutical Science & Technology Today **2:** 430-440, 1999.

Young, P. M.: Characterisation pf particle-particle interactions using the atomic force microscope. University of Bath, Bath, UK, 2002.

Young, P., Price, R., Lewis, D., Edge, S., and Traini, D.: Under pressure: predicting pressurized metered dose inhaler interactions using the atomic force microscope. Journal of Colloid and Interface Science (262)**:** *298-302*, 2003.

Young, P. M., Price, R., Tobyn, M. J., Buttrum, M., and Dey, F.: The influence of relative humidity on the cohesion properties of micronised drugs used in inhalation therapy. Journal of Pharmaceutical Science **93:** 753-761, 2004.

Young, S. A., and Buckton, G.: Particle growth in aqueous suspensions: the influence of surface energy and polarity. International Journal of Pharmaceutics **60:** 235-241, 1990.

Zhou, H., Götzinger, M., and Peukert, W.: The influence of particle charge and roughness on particle–substrate adhesion. Powder Technology **135-136:** 82-91, 2003.

Zisman, W. A.: Influence of constitution on adhesion. Industrial and Engineering Chemistry **55:** 10-38, 1963.

APPENDIX FOR CHAPTER 5

A1. REPRESENTATIVE FORCE-DISPLACEMENT CURVES

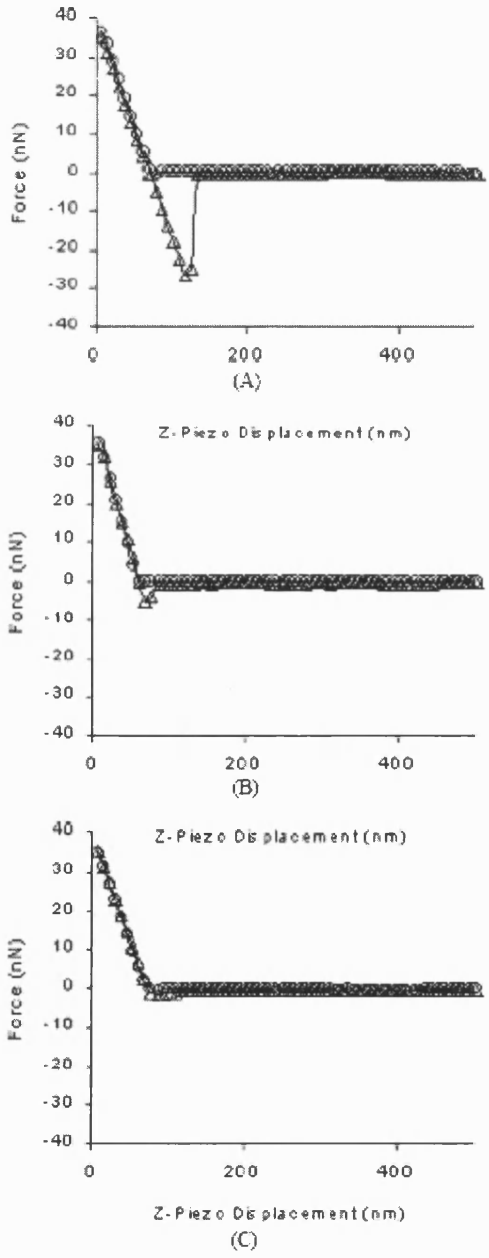

Appendix 1 Representative force–displacement curves for salbutamol sulphate drug probe interactions with (A) anodised aluminum, (B) PTFE canister, and (C) FEP-PES-coated canister. O = approach data; Δ = retraction data.

A2. REPRESENTATIVE SEPARATION ENERGY HISTOGRAM

To enable quantitative analysis, separation energy values obtained from drug probe–substrate interactions over 5 × 5 μm areas were compiled as cumulative frequencies and plotted as a function of probability. Linear regression analysis for the separation energies between the drug probe and substrates indicated a log-normal distribution for drug–aluminum/polymer coated canister under investigation. Such variations in separation energy distribution may be attributed to surface morphology. For example, recent investigations have indicated that roughness influences separation energy distribution (Price et al., 2002; Young et al., 2004). The interactions between a drug particle and an atomically flat drug substratehave been shown to produce a normal distribution (Price et al., 2002), in comparison to a log-normal distribution for irregular drug compacts (Price et al., 2002).

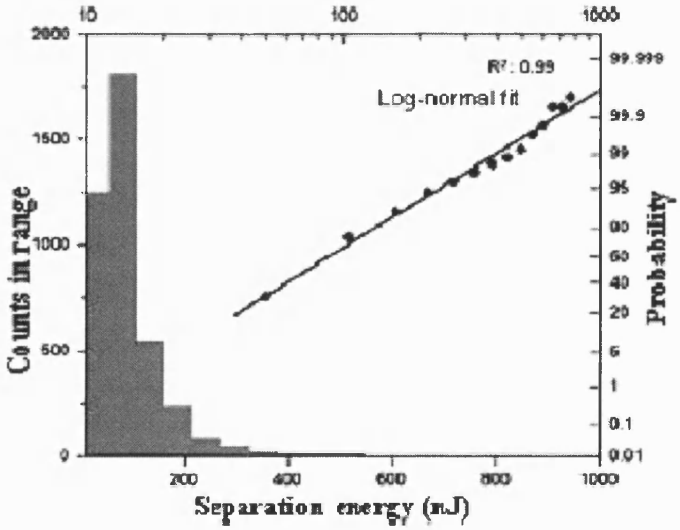

Appendix 2 Representative separation energy histogram for salbutamol sulphate drug probe interaction with aluminium canister material.

PUBLICATIONS

ACADEMIC PRESS

Available online at www.sciencedirect.com
SCIENCE DIRECT®

Journal of Colloid and Interface Science 262 (2003) 298–302

JOURNAL OF Colloid and Interface Science

www.elsevier.com/locate/jcis

Letter to the Editor

Under pressure: predicting pressurized metered dose inhaler interactions using the atomic force microscope

Paul M. Young,* Robert Price, David Lewis, Stephen Edge, and Daniela Traini

Pharmaceutical Technology Research Group, Department of Pharmacy and Pharmacology, University of Bath, Bath BA2 7AY, UK

Received 18 March 2002; accepted 3 January 2003

Abstract

Drug particulate interactions in pressurized metered dose inhalers (pMDI) may lead to a decrease in aerosolization efficiency and subsequent efficacy in patient treatment. The interactions between salbutamol sulfate (commonly used in Ventolin pMDIs) and a series of pMDI canister materials were investigated using the atomic force microscope (AFM) colloid probe technique. Approximately 4000 individual force–distance curves were determined for a drug probe and three surfaces (10 × 10 μm areas) in situ, in a model propellant. The area under each force–distance curve was integrated to obtain separation energy values. Median separation energy values followed the rank order borosilicate glass > aluminum > PTFE, suggesting PTFE to be the most suitable canister coating.

Keywords: pMDI; Suspensions; Separation energy; AFM; Force volume

1. Introduction

Pressurized metered dose inhalers (pMDI) have become ubiquitous for the treatment of asthma and other bronchial diseases. In simple terms, a pMDI is a colloidal system consisting of a drug suspended in propellant, with or without stabilizing and/or taste masking agents. The pressurized propellant drug system is metered in aliquots by a volumetric chamber located in the metering stem. During patient use, depression of the stem mechanism isolates the metering chamber from the reservoir, while exposing it to atmospheric pressure. Consequently, the metered propellant rapidly expands through the metering stem and is vaporized through a pMDI device orifice to deliver micrometer-sized drug particulates.

This pMDI technology has been successfully developed to produce devices with satisfactory performance. However, the advent of the 1999 Montreal Protocol has forced the industry to develop pMDI devices that do not contain chlorofluorocarbons (CFC) as a propellant. Subsequently, pMDIs have had to be reformulated with the more environmentally friendly hydrofluorocarbons (HFA). Although this was initially considered a simple task of switching one propellant for another, it quickly became clear that existing formulations were not compatible with the new propellants. This resulted in a surge of pMDI-based research and related patents [1].

Formulation stability, both chemical and physical, in pMDI systems is paramount in ensuring that a product meets the standards of the relevant pharmaceutical governing bodies. Particle–particle and particle–component interactions in a pMDI may lead to formulation caking, creaming, "wall loss," or chemical degradation. This results in nonconformity to dosing regulations. It is, therefore, important to have a fundamental understanding of such interactions in a propellant system in order to determine the most appropriate formulation.

In simple terms, the interactions present in a pMDI system will be dependent on both the van der Waals dispersive and electric double-layer forces. The degree to which such forces dominate the formulation will be dependent on many factors, including material chemistry and component morphology. For example, the ubiquitous van der Waals dispersive force (acting between all molecules over short separation distances, < 100 nm) will be directly influenced by the surface roughness of the two contiguous surfaces. Thus, a material with a roughness consisting of many nanoscopic asperities, in contact with an atomically flat substrate, would result in a decreased contact area and subsequent adhesion

* Corresponding author.
E-mail address: prspmy@bath.ac.uk (P.M. Young).

0021-9797/03/$ – see front matter
doi:10.1016/S0021-9797(03)00032-8

(when compared to the adhesion between two planar surfaces).

Furthermore, the physicochemical properties of the materials should be considered. Both the van der Waals force and electric double-layer interactions will be dependent on the chemical and macroscopic (e.g., crystal and/or amorphous structure) properties of a material. For example, the presence of polar groups on specific faces of a crystal may lead to an increased van der Waals force (due to a change in Hamaker constant and thus surface free energy) or variation in electric double-layer interaction (via promotion of charge accumulation at the solid–liquid interface).

The atomic force microscope (AFM) [2] has been extensively used to measure fundamental interactive forces between surfaces. In addition, the immobilization of colloidal particulates onto AFM cantilevers, as pioneered by Ducker et al. [3], allows the measurement of particulate surface interactions, which can be applied to such diverse areas as biology [4], polymer science [5], and xerography [6].

Here we describe the use of the AFM colloid probe technique as a tool for determining drug particulate–surface interactions in model propellant systems. A current HFA formulation [7] consisting of a micronized drug suspended in HFA-134a (HFA type) was chosen as an experimental model. The internal canister walls of the formulation contain a polytetrafluoroethylene (PTFE) coating, claimed to limit drug particulate–wall adhesion and subsequent dose irreproducibility. Canister wall materials and coatings were chosen for preliminary investigation, as the degree of drug–substrate contact will be relatively high. Such interactions become particularly important for higher potency, low-dose formulations, as the total drug surface area will be less than that of the canister wall.

In order to investigate the possible interactions between a formulation and canister coatings, AFM separation measurements were conducted between a colloidal drug probe and three surfaces in a model propellant.

2. Experimental

A commercially available AFM (Nanoscope III, DI, Cambridge, UK) was utilized for drug particulate–surface interactions. A salbutamol sulfate drug probe was prepared by mounting an individual drug particle (approximate diameter 5 μm) on a V-shaped tipless cantilever (spring constant 0.58 $N\,m^{-1}$, DNP-020, DI, Cambridge, UK) using a quick-setting epoxy resin. The micromanipulation technique is described in more detail elsewhere [8].

Three material substrates, borosilicate glass (Schott, Mainz, Germany), aluminum (Presspart, Lancashire, UK), and PTFE-coated aluminum (A64411, 3M, Berkshire, UK), were prepared from commercially available pMDI canisters. Each substrate was mounted on an AFM sample stub with epoxy resin, washed with isopropyl alcohol (commonly used to clean surfaces in the pharmaceutical industry), and dried with nitrogen prior to analysis.

Salbutamol sulfate drug probe interactions were determined for each of the substrates in a sealed, in situ liquid cell (DI, Cambridge, UK) containing the model hydrofluorocarbon (mHFA) 2H, 3H-decafluoropentane (Apollo Scientific, Derbyshire, UK). Force–distance measurements were collected using force–volume mode to produce 4096 individual force curves over a 10 × 10-μm area on each substrate surface. Settings were as follows; approach–retraction cycle 500 nm, cycle rate 8.14 Hz, constant compliance region 60 nm. The area under each of the force–distance curves was integrated using a custom-built program to produce separation energy values.

In addition, detailed topographical information on the three material substrates was investigated using AFM. Imaging was conducted in air, using Tapping Mode with a high-aspect-ratio silicon probe (OTESP, Digital Instruments, UK), at a scan rate of 0.7 Hz.

3. Results and discussion

Representative AFM topographical images of the borosilicate glass, aluminum, and PTFE substrates are shown in Figs. 1A, 1B, and 1C, respectively. The images of the surface of borosilicate glass suggest the presence of a uniform flat surface with low root-mean-square roughness (0.94 ± 0.08 nm, $n = 3$, 10 × 10-μm areas). Representative AFM images of the aluminum (Fig. 1B) and PTFE-coated material (Fig. 1C) suggested irregular surface morphologies with higher root-mean-square roughness (32.22 ± 1.81 nm and 27.87 ± 0.84 nm for aluminum and PTFE, respectively; $n = 3$, 10 × 10-μm areas).

Furthermore, apparent linear striations were observed on both the aluminum and PTFE-coated substrates. This is most likely due to the canister manufacture process, which involves drawing the canisters out from a single sheet of aluminum.

Drug probe integrity was investigated by imaging the tip with a high-magnification 500× long-working-distance reflective microscope. The drug probe appeared to have a columnar morphology approximately 5 μm in length and was clearly proud of the cantilever surface. Comparison of the drug probe at the start and end of the experimental procedures indicated no macroscopic change in drug probe morphology.

Representative force–displacement curves for the interaction between a salbutamol drug probe on borosilicate glass, aluminum, and PTFE samples are shown in Figs. 2A, 2B, and 2C, respectively. Analysis of the force–distance curves suggest a rank decrease in both force and separation energy of the order glass > aluminum > PTFE.

To enable quantitative analysis, separation energy values obtained from drug probe–substrate interactions over 10 × 10-μm areas were compiled as cumulative frequencies

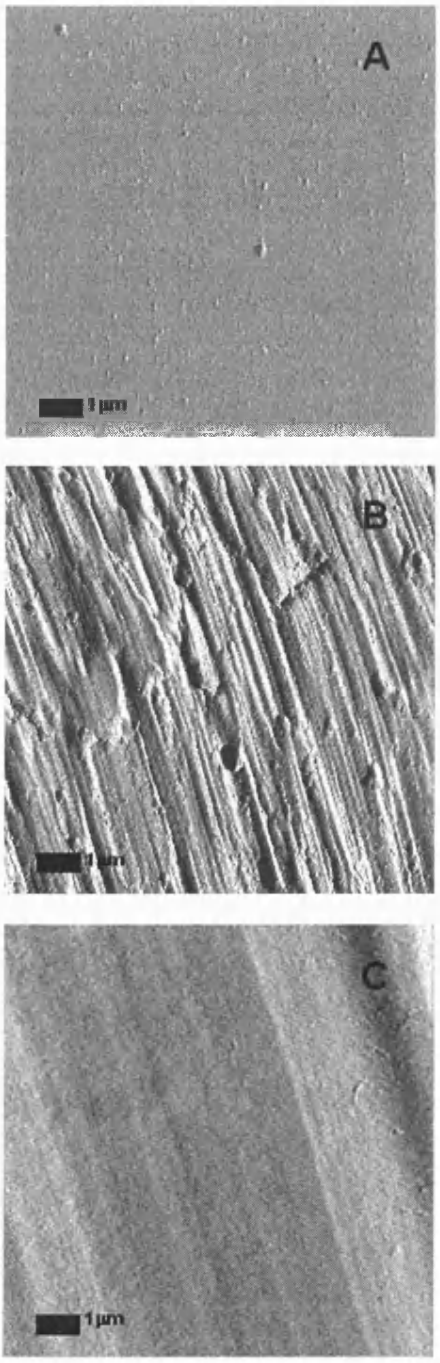

Fig. 1. Representative topographical AFM images of (A) borosilicate glass, (B) aluminum canister sample, and (C) PTFE-coated aluminum canister sample.

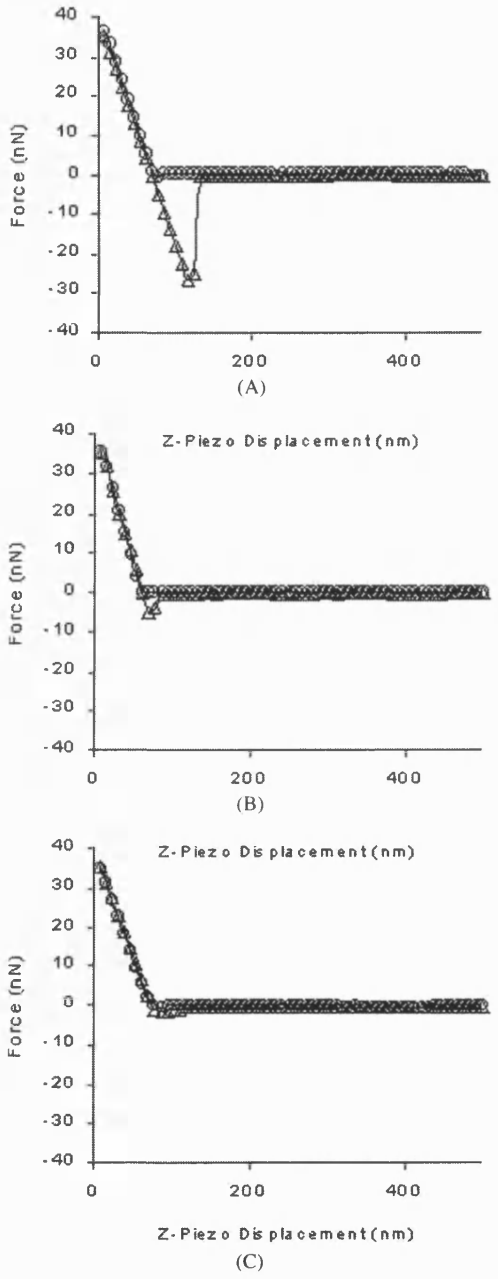

Fig. 2. Representative force–displacement curves for salbutamol sulfate drug probe interactions with (A) borosilicate glass canister, (B) aluminum canister, and (C) PTFE-coated aluminum canister. ○ = approach data; △ = retraction data.

and plotted as a function of probability. Linear regression analysis for the separation energies between the drug probe and substrates indicated a normal distribution for drug–glass interactions (Fig. 3A) and log-normal distribution for both drug–aluminum (Fig. 3B) and drug–PTFE interactions (where $r^2 \geqslant 0.99$). Such variations in separation energy distribution may be attributed to surface morphology. For example, recent investigations have indicated that roughness influences separation energy distribution [8,9]. The interactions between a drug particle and an atomically flat drug substrate have been shown to produce a normal distribution [9], in comparison to a log-normal distribution for irregular drug compacts [9].

Median separation energy values ($e_{0.5}$) were calculated from the specific distributions and are shown in Fig. 3C with 95% confidence intervals. Median $e_{0.5}$ values for drug probe interactions with borosilicate glass were 824, 68, and 3.7 nJ, respectively, suggesting that the adhesion of

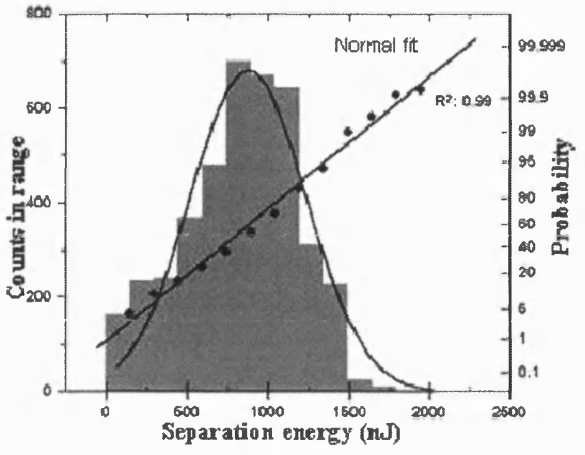

(A)

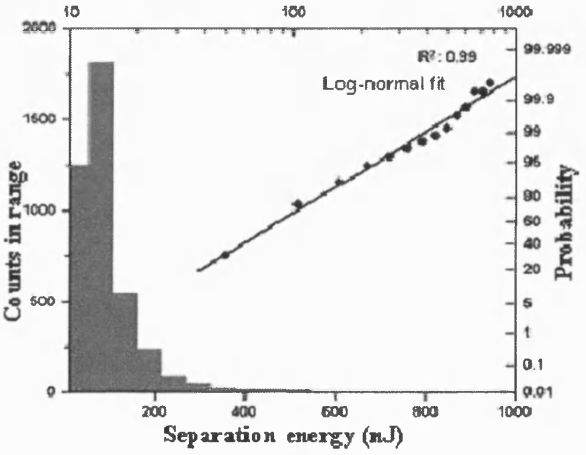

(B)

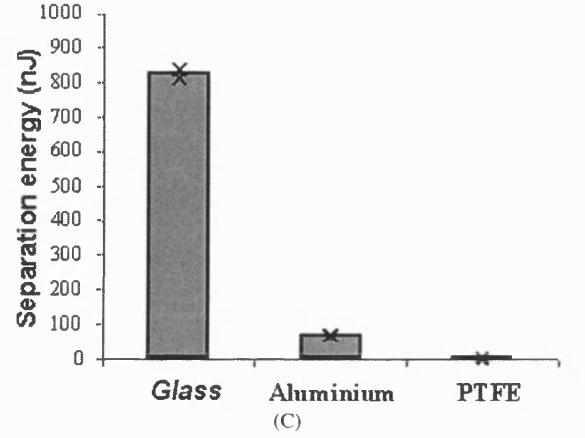

(C)

Fig. 3. Representative separation energy histograms for salbutamol sulfate drug probe interactions with (A) borosilicate glass and (B) aluminum canister materials. (C) Median separation energies for salbutamol drug probe interactions with glass, aluminum, and PTFE-coated pMDI canisters under model propellant ($n = 4096$); error bars indicate 95% confidence intervals.

salbutamol in a propellant system would be in the rank order glass > aluminum > PTFE. Again, the reason for this rank order may be a combination of factors including material morphology and surface free energies.

For example, the micronized salbutamol sulfate particles used for the investigation were approximately 5 μm in diameter and suggested a columnar morphology. When the interaction of such particulates with a planar surface (such as glass) is considered, the contact area and thus adhesion will be relatively high. However, small variations in the substrate morphology (as observed with the aluminum and PTFE substrates) could result in a significant decrease in contact area (and thus adhesion). No long-range attractive or repulsive forces were observed in the AFM force–distance curves, for any of the substrates, suggesting that electric double-layer forces did not play a dominating role (in this case).

In addition, it is important to consider the surface energy of the materials. Such factors could explain, for example, the low $e_{0.5}$ for PTFE–drug interactions when compared to aluminum (which have similar surface roughness parameters but contrasting surface energy values). It is clear that such particle–substrate interactions are complex and require further investigation. The influences of roughness and intrinsic surface energies on particulate–substrate interactions need to be investigated further.

In a pMDI system, other components should be considered for future investigation. These include valve stems, metering chambers, actuator orifices, and addition of cosolvents and/or surfactants. In addition, the study of particle–particle interactions may supply fundamental information relating to drug cohesion, flocculation, and caking mechanisms.

Furthermore, the selection of an mHFA is an important factor. In this case, 2H, 3H-decafluoropentane was chosen as a mHFA due to its chemical and physical similarities to HFA-134a, used in the example product [10]. Whilst these investigations were conducted in situ, particle adhesion may occur at the liquid–gas interface (in a real propellant system). This should also be considered for future investigation.

4. Summary

The use of the AFM colloid probe technique as a method for investigating interactions in model propellant systems opens the possibility of rapidly and safely screening materials during preformulation. The use of force–volume imaging to determine separation energy values allows quantitative analysis of particulate–substrate interactions as a function of surface topography.

A rank decrease in salbutamol–substrate median separation energies in the order borosilicate glass > aluminum > PTFE was observed. This correlated well with the route adopted in the example product [7], where the use of low-surface-energy material coatings (e.g., PTFE), in place of aluminum canisters, has the potential for decreasing particle wall adhesion and thus improving the formulation efficiency. In simple terms, the AFM presents itself as a possible preformulation tool for rapid characterization of particle interactions, allowing the collection of fundamental data that may facilitate the development of pMDIs.

References

[1] D. Greenleaf, P.A. Bowman, Int. J. Pharm. 186 (1999) 91.
[2] G. Binnig, C.F. Quate, C. Gerber, Phys. Rev. Lett. 56 (1986) 930.
[3] W.A. Ducker, T.J. Senden, R.M. Pashley, Nature 253 (1991) 239.
[4] W.R. Bowen, R.W. Lovitt, C.J. Wright, Colloids Surf. A 173 (2000) 205.
[5] S. Biggs, G. Spinks, J. Adhesion Sci. 12 (1998) 461.
[6] H. Mizes, M. Ott, E. Eklund, D. Hays, Colloids Surf. A 165 (2000) 11.
[7] I.C. Ashurst, C.S. Herman, L. Li, M.T. Riebe, Patent WO96320999, 1996.
[8] P.M. Young, R. Price, M.J. Tobyn, M. Buttrum, F. Dey, J. Pharm. Sci., in press.
[9] R. Price, P.M. Young, S. Edge, J.N. Staniforth, Int. J. Pharm. 246 (2002) 47.
[10] P. Rogueda, in: Proceedings from Respiratory Drug Delivery VIII, May 2002, Tucson, AZ, USA, Vol. 1, Davis Horwood International Publishing, Surrey, UK, 2002.

Pharmaceutical Research, Vol. 22, No. 5, May 2005 (© 2005)
DOI: 10.1007/s11095-005-2599-2

Research Paper

Surface Energy and Interparticle Force Correlation in Model pMDI Formulations

Daniela Traini,[1] Philippe Rogueda,[2] Paul Young,[1] and Robert Price[1,3]

Received November 1, 2004; accepted February 9, 2005

Purpose. To compare experimental measurements of particle cohesion and adhesion forces in a model propellant with theoretical measurements of the interfacial free energy of particulate interactions; with the aim of characterizing suspension stability of pressurized metered dose inhalers (pMDIs).
Methods. Interparticulate forces of salbutamol sulfate, budesonide, and formoterol fumarate dihydrate were investigated by *in situ* atomic force microscopy (AFM) in a model propellant 2H,3H perfluoropentane. The surface thermodynamic properties were determined by contact angle (CA) and inverse gas chromatography (IGC). Experimental data were compared with theoretical work of adhesion/cohesion using a surface component approach (SCA), taking into account both dispersive and polar contributions of the surface free energy.
Results. Results indicated that the measured forces of interaction between particles in model propellant could not be accounted for by theoretical treatment of the dispersive surface free energies via CA and IGC. A correlation between theoretical work of adhesion/cohesion and AFM measurements was observed upon the introduction of the polar interfacial interactions within the SCA model.
Conclusions. It is suggested that the polar contributions of the surface free energy measurements of particles may play a crucial role in particle interaction within propellant-based systems. Together with the application of a SCA model, this approach may be capable of predicting suspension stability of pMDI formulations.

KEY WORDS: AFM; pMDI; surface energy; suspension.

INTRODUCTION

The delivery of drug particulates to the respiratory tract has become an essential and effective means of treating a variety of pulmonary disorders, including asthma, chronic obstructive pulmonary disease, bronchitis, and cystic fibrosis (1,2). Such popularity can be related to the relative small dose required for effective and often rapid onset of the therapeutic effect while reducing systemic exposure and minimizing drug-related side effects. The pressurized metered dose inhaler (pMDI) remains the most commonly prescribed device for therapeutic aerosol delivery (3). Currently, this dosage form may contain hydrofluoroalkane (HFA) propellants alongside the drug substance, surfactant, and cosolvents. The formulation of a pMDI can generally be subdivided into two categories: solution- and suspension-based systems. Suspension-based pMDIs are generally the most popular because drugs are generally insoluble in the propellant system and thus solubilization in a nonpolar solvent and/or the potential for chemical degradation are obviated (4).

Non-aqueous suspensions raise particular formulation challenges. Their preparation requires careful consideration of the interaction between drug particulates in liquefied propellant, and various components of the pMDI device (3,4). Previous approaches have investigated the behavior of pMDI system mainly through empirical measurements of the flocculation behavior of particulates, and analytical measurement of the loss of drug within the device (4,5). Techniques such as zetametry, sedimentation, and particle size analysis (6), microscopy and spectroscopy (7,8) are routinely used to measure pMDI formulation stability. However, indirect and direct measurement of the various interactions, which govern their behavior, have seldom been performed. The use of surface energetic measurements, via contact angle (CA) and inverse gas chromatography (IGC) measurements, together with the use of particle interactions theories have enabled indirect evaluation of the particulate interactions (9–12). Moreover, the advent of the atomic force microscope colloid probe approach (13) provides an approach to directly quantify interactions between drug particles and formulation components in model pMDI systems (14,15).

The primary aim of the study was to correlate atomic force microscopy (AFM) measurements of interparticulate forces with theoretical measurements of the interfacial free energy of particle interactions via surface free energy data and to gain a greater understanding of the thermodynamic and surface physicochemical properties that directly influence particle-particle interactions in suspension-based pMDI systems. The quantitative study of adhesion/cohesion interac-

[1] Pharmaceutical Technology Research Group, Department of Pharmacy, University of Bath, Bath, United Kingdom.
[2] AstraZeneca R&D Charnwood, Loughborough, United Kingdom.
[3] To whom correspondence should be addressed. (e-mail: r.price@bath.ac.uk)

tions in a model pMDI was carried out by *in situ* colloid probe AFM. The surface thermodynamic properties of the active ingredients were measured using contact angle (CA) and inverse gas chromatography (IGC). The relationship between AFM measurements and the interfacial behavior of the colloid particles was modeled using a surface component approach (SCA) derived from Fowkes, Good-Girifalco, and van Oss models (9,16,17).

Particle Interaction Theory

Interactions between colloidal particles are usually described by the Derjaguin-Landau-Verwey-Overbeek (DLVO) theory (18,19). The DLVO theory considers two types of interactions: a dispersive attractive interaction of the Lifshitz van der Waals (LW) type and a predominately repulsive electrostatic interaction due to the interpenetration of electrical double layers. The application of the DLVO theory for the stabilization of drug suspensions in non-aqueous pMDI media has not been fully validated (20). The possible limitation of the approach, which has been successfully used to describe the behavior of aqueous suspensions, is the absence of an ionic double layer (21,22). A quick theoretical calculation of the repulsive electrostatic energy of interaction between 1-μm solid particles as a function of interparticulate distances in liquefied propellants with varying dielectric constants (reciprocal thickness of the diffuse double layer set at 2×10^6 cm^{-1}) show that the electrostatic repulsive forces acting between particles are small. This may be attributed to the overlap of very diffusive electrical double layers due to a combination of low dielectric constants and low ionic strengths (23). Thus, the attractive LW forces are thought to predominate at all separation distances. As a result, theoretical descriptions of non-aqueous drug suspensions via a DLVO approach are very limited, as they fail to adequately predict the stability of these formulations (4,20).

An alternative approach to the DLVO theory has been proposed by van Oss (9,24,25). The approach decomposes the surface energetics (i.e., surface tension or contact angle values) into independent contributions and in particular introduces a polar acid-base (AB) (electron donor/electron acceptor) component (9). The corresponding polar free energy of interaction (AB), which can be repulsive or attractive (depending on the chemical structure, suspending medium properties and surface potential) can control the total energy of interaction at small separation distances. According to this surface contribution approach (SCA), the total surface free energy of a solid is determined by the LW dispersive component (γ^{LW}) and the polar AB component (γ^{AB}) as given in Eq. (1):

$$\gamma^{TOT} = \gamma^{LW} + \gamma^{AB} \tag{1}$$

The total free energy of interaction between two surfaces in a liquid medium is subsequently defined as the sum of LW dispersive interactions, the polar component (AB), and electrostatic double layer (EL) interactions [Eq. (2)]:

$$\Delta G^{TOT} = \{\Delta G^{LW} + \Delta G^{AB}\} + \Delta G^{EL} \tag{2}$$

In the absence of an electrostatic influence, the interaction energy between solid surfaces (S) immersed in a liquid (L) can be expressed by the interfacial free energy (ΔG_{SLS}), see Eq. (3). This in turn can be related to the solid-liquid interfacial tension via:

$$\Delta G_{SLS} = \Delta G^{LW} + \Delta G^{AB} = -2\gamma_{SLS} = -2(\gamma_{SLS}^{LW} + \gamma_{SLS}^{AB}) \tag{3}$$

The interfacial energy parameters for the LW and AB contributions between similar solids (1) in a liquid (3) can be obtained from the surface free energy and surface tensions of the solid and liquid by using the Good-Girifalco-Fowkes approach (16,17) [Eq. (4)]:

$$\Delta G_{131} = -2\left[\left(\sqrt{\gamma_1^{LW}} - \sqrt{\gamma_3^{LW}}\right)^2 + 2\left(\sqrt{\gamma_1^+\gamma_1^-} + \sqrt{\gamma_3^+\gamma_3^-} - \sqrt{\gamma_1^+\gamma_3^-} - \sqrt{\gamma_1^-\gamma_3^+}\right)\right] \tag{4}$$

For liquids with very low polarity ($\gamma_3^+ = \gamma_3^- \sim 0$ mJ/m^{-2}), the free energy of interaction can be simplified to [Eq. (5)]:

$$\Delta G_{131} = -2\left(\sqrt{\gamma_1^{LW}} - \sqrt{\gamma_3^{LW}}\right)^2 - 4\sqrt{\gamma_1^+\gamma_1^-} \tag{5}$$

Hence, knowledge of the surface energy of the solid (γ_1^{LW}, γ_1^+, and γ_1^-) and the surface tension of the liquid (γ_3^{LW}, γ_3^+ and γ_3^-) enables the determination of interaction energy between particles within the media.

Similarly, the energy of interaction between dissimilar solid surfaces (1 and 2) in a liquid (3) can be calculated using the following expression (6):

$$\Delta G_{132} = 2\left[\sqrt{\gamma_1^{LW}\gamma_3^{LW}} + \sqrt{\gamma_2^{LW}\gamma_3^{LW}} - \sqrt{\gamma_1^{LW}\gamma_2^{LW}} - \gamma_3^{LW} + \sqrt{\gamma_3^+}\left(\sqrt{\gamma_1^-} + \sqrt{\gamma_2^-} - \sqrt{\gamma_3^-}\right) + \sqrt{\gamma_3^-}\left(\sqrt{\gamma_1^+} + \sqrt{\gamma_2^+} - \sqrt{\gamma_3^+}\right) - \sqrt{\gamma_1^+\gamma_2^-} - \sqrt{\gamma_1^+\gamma_2^+}\right] \tag{6}$$

In an apolar medium (γ_3^+ and $\gamma_3^- \sim 0$ $mJ\ m^{-2}$), the energy of interaction can be used in the simplified form (7):

$$\Delta G_{132} = 2\left[\sqrt{\gamma_1^{LW}\gamma_3^{LW}} + \sqrt{\gamma_2^{LW}\gamma_3^{LW}} - \sqrt{\gamma_1^{LW}\gamma_2^{LW}} - \gamma_3^{LW} - \sqrt{\gamma_1^+\gamma_2^-} - \sqrt{\gamma_1^+\gamma_2^+}\right] \tag{7}$$

The influence of the van der Waals interactions on the force of adhesion can be related to the thermodynamic work of adhesion ($W_{ad} = -\Delta G_{SLS} = -\Delta G_{132}$) through the Hertz approximation for elastic bodies (26), which takes into account the separation distance and the contact geometry of interacting surfaces. Two models can be used for this purpose, the Johnson, Kendall, and Roberts (JKR) and the Derjaguin, Müller, and Toporov (DMT) models (27,28). Their validity have been found to depend on the interacting materials and their geometries. The DMT theory is typically valid for small particles, low surface energies and high elastic moduli, whilst the converse is true for the JKR model.

The general form of the relationship of the force of adhesion with the energy (derived for LW interactions between two spherical particles) can be expressed as in Eq. (8) (27):

$$F_{ad} = n\pi R^* W_{ad} \tag{8}$$

where R^* is the harmonic mean of the particle radii (also called contact radius) and n is a predetermined constant depending on the selected model (n = 3/2 for JKR and n = 2 for the DMT model).

MATERIALS AND METHODS

Materials

Micronized salbutamol sulfate, budesonide, and formoterol fumarate dihydrate were supplied by AstraZeneca (Loughborough, Leicestershire, UK) and were used as received. The model propellant HPFP (2H, 3H perfluoropentane) was supplied by Apollo Scientific (Stockport, Derbyshire, UK). The purity of HPFP was in excess of 99.9%, with a moisture content less than 9 ppm. Further purification of the HPFP was achieved by filtering and purifying with chromatographic grade acidic and basic alumina (Fluka, Gillingham, UK). This treatment was necessary to remove impurities in the organic liquid that may otherwise directly influence particle adhesion measurements. All organic solvents (diiodomethane and ethylene glycol) used in the study were supplied by BDH (Poole, Dorset, UK) and were of analytical grade. Purified water was prepared by reverse osmosis (MilliQ, Molsheim, France).

Scanning Electron Microscopy

Scanning electron microscopy (SEM) was used to characterize the morphology of the micronized drugs. Powder samples were deposited on adhesive carbon black tabs, which were premounted on aluminum stubs. Particles were coated with a thin gold film using a sputter coater (model S150B, Edwards High Vacuum, Sussex, UK). Samples were imaged using a JEOL 6310 SEM (Jeol, Tokyo, Japan) at 10KeV.

Particle Sizing

Particle sizing of the micronized drug samples were performed using a Mastersizer X (Malvern Instruments Ltd, Malvern, UK). The instrument was equipped with a small volume cell (with a capacity of approximately 20 ml) and a 100 mm lens, allowing particle detection in the size range of 0.5–120 μm. Approximately 1 mg of drug material was suspended in a 0.1% w/v lecithin/cyclohexane solution and sonicated for 10 min at 25°C prior to analysis. The particle size distribution was characterized by the 10th, 50th, and 90th percentile of the cumulative particle undersize frequency distribution. All samples were run as triplicates.

Preparation and Characterization of Drug Crystals

One of the limitations of the colloidal probe AFM approach to date has been associated with dramatic inter- and intra-variations in cohesion and adhesion measurements related to slight differences in contact geometry between interacting surfaces. In this study, direct comparisons of the force of interaction between specific colloid probes and an array of substrate materials was made possible by crystallizing molecularly smooth crystals from solution. Single crystals of salbutamol, budesonide, and formoterol were heterogeneously nucleated and grown on a borosilicate glass substrate using a sitting drop technique, described elsewhere (29). This process produced planar crystals with large areas of sub-nanometre smooth surfaces.

AFM Topographical Measurements

The surface topography of the drug crystal surfaces was investigated using the AFM in its conventional imaging mode. Imaging was conducted in Tapping Mode operation with a high-aspect-ratio silicon probe (OTESP, Digital Instruments, UK), at a scan rate of 0.7 Hz. All AFM studies were performed using a commercially available Multi Mode AFM with a Nanoscope III controller [Digital Instruments (DI), Cambridge, UK]. The root mean squared surface roughness (R_{rms}) of the deviations from the average height was calculated from the AFM height data over a 5 μm × 5 μm area via:

$$R_{rms} = \sqrt{\frac{1}{n}\sum_{i=1}^{n} y_i^2} \quad (9)$$

where n is the number of points in topography profile and y_i is the heights of the surface asperities (i).

Model Drugs Compact Preparation

Contact angle measurements were obtained using the sessile drop method on model compacts of the micronized drug. Compacts were prepared by direct compression using a servo hydraulic press (model 25010, Specac Ltd., Kent, UK). Approximately 250 mg of the micronized material was weighed into a 10-mm stainless steel die, spread evenly in the die, and compacted with a compression force of 10 kN. Compacts were stored in sealed containers in a controlled environment (25°C, 44% RH) for at least 24 h prior to use.

AFM Colloid Probe Measurements

Colloid probes were prepared by mounting an individual micronized drug particle (approximate diameter 5 μm) onto a V-shaped tipless cantilever (spring constant k = 0.32 N/m, DNP-020, DI, Cambridge, UK) using a quick-setting epoxy resin (30). Extreme care was taken during drug probe preparation to limit the amount of drug-glue contact. The micromanipulation technique is described in detail elsewhere (31). The measurement of the forces of adhesion and cohesion between individual particles and their respective crystal surfaces were carried out in HPFP with an *in situ* liquid AFM cell (7,8). It is important to note that conventional AFM systems are currently limited to studies in air and/or low vapor pressure liquid environments. Thus, HPFP was chosen for its similarities to the physicochemical properties of HFA227, used in pMDIs (32). The use of HPFP as a model system for studying the behavior of pMDIs, when characterization methods cannot be adapted to the pressure regime, has been extensively studied by Rogueda (32).

Force-distance profiles were recorded by measuring the deflection of the cantilever as the substrate surface was ramped into and out of contact with the cantilever in a stepwise fashion (30,33,34). By applying Hooke's law, $F = kx$ (where x is the deflection of the cantilever and k the spring constant), a quantitative measurement of the force of adhesion can be obtained. Multiple force distance curves (n = 512) were determined between each drug probe and crystal surface over a 5 μm × 5 μm area with the following settings: approach-retraction cycle 0.5 μm, cycle rate 4.07 Hz, and a loading force of 20 nN. Each study was performed with three probes of each drug. To avoid significant variations in contact

area between an individual probe and the respective substrate surfaces, a great deal of care and attention were taken to maintain the integrity of the colloid probe throughout the study.

To further overcome the limitation of not knowing the true area of contact between drug probes, the cohesive and adhesive forces ratios were analyzed and compared using the recently developed cohesive-adhesive balance (CAB) analysis procedure (35). This approach provides a quantitative measurement of the adhesive and cohesive balance of the interactive forces within a formulation. The CAB analysis procedure allows AFM measurements of inter-particulate forces to be directly correlated to the thermodynamic work of cohesion and adhesion of interacting surfaces via surface energy measurements. For a particulate interacting with two surfaces (one alike and one different) the cohesive-adhesive balance between the two materials can be expressed by:

$$\frac{F_{coh}}{F_{adh}} = \frac{R^*_{cohesion}\, n\pi W_{coh}}{R^*_{adhesion}\, n\pi W_{adh}} \tag{10}$$

where F_{coh} and F_{adh} are the cohesive and adhesive forces measured by AFM, and W_{coh} and W_{adh} are the thermodynamic work of cohesion and adhesion, respectively. Assuming the contact mechanics of the cohesive and adhesive interaction follow the same theoretical model, the ratio of the van der Waals forces for a series of colloidal probes should be constant and directly proportional to the thermodynamic ratio of the work of cohesion and adhesion of the interfacial interactions calculated via the surface free energy measurements of the interacting particles. Furthermore, determining the balance of van der Waals forces for a series of colloidal probes via AFM measurements overcomes the need to determine variations in the spring constant (k) of each individual AFM cantilever.

Contact Angle Measurements

The contact angle of the powder compact surfaces were measured using the sessile drop method (10,16,36–38) with a NRL goniometer (Ramé-Hart, Inc., Mountain Lakes, NJ, USA) equipped with a 2.3× objective lens, and a 10× Ramsden type eyepiece. A liquid drop was introduced onto the substrate surface via a microsyringe. Advancing contact angles were measured for three different liquids (water, diiodomethane, and ethylene glycol) at room temperature (20°C). A summary of the surface tension components of the liquids used in the direct contact angle determination (9) are presented in Table I. The surface energy parameters of the compact surfaces were determined using the Young-Duprè equation, which requires the contact angle (θ) measurements for a minimum of three liquids (one apolar and two polar) via the following relationship:

$$\gamma_L(1+\cos\theta) = 2\left(\sqrt{\gamma_S^{LW}\gamma_L^{LW}} + \sqrt{\gamma_S^{+}\gamma_L^{-}} - \sqrt{\gamma_S^{-}\gamma_L^{+}}\right) \tag{11}$$

where γ_S and γ_L are the surface free energies of the solid and the liquid, respectively.

Table I. Surface Tension Components and Parameters of Liquids Used in CA Measurements at 20°C (van Oss, 1994) (14)

	Surface tension components and parameters (mJ · m^{-2})			
	γ^{LW}	γ^{+}	γ^{-}	γ^{AB}
Diiodomethane	50.8	~0	0	0
Water	21.8	25.5	25.5	51.0
Ethylene glycol	29.0	1.92	47.0	19.0

Inverse Gas Chromatography

Inverse gas chromatography (IGC) provides a means of determining both the dispersive and polar components of surface free energy for micronized drugs (11,12), without potential modification of the surface properties of the particles upon compaction (39). The surface free energy characteristics of the micronized powders were determined using a commercially available IGC (IGC 2000, Surface Measurement Systems Ltd, London, UK). The dispersive component of the solid surface free energy (γ_s^d) can be calculated by measuring the retention time (volume) of a series of alkanes of known γ_l^d injected at an infinite dilution using the following relationship (40):

$$RT \ln V_N = 2N\sqrt{\gamma_s^d}\, a \sqrt{\gamma_l^d} + C \tag{12}$$

where R is the gas constant, T the temperature, N is Avogadro's number, a is the projected surface area of the sample probe, γ_l^d the dispersive component of the probe, and V_N the net volume of carrier gas required to elute the probe molecules from the column (corrected for column dead time and compression factors). This procedure is based on the determination of a linear relationship between the retention volume ($RT\ln V_N$) of the nonpolar probe against $a(\gamma_l^d)^{0.5}$. The dispersive component of the surface free energy of the solid can be calculated from the slope.

The electron donor and electron acceptor properties of the micronized powders were determined by IGC using polar liquids in the vapor phase. The specific (polar) interactions ΔG_{sp} can be related to the acidic or electron accepting parameter (K_a) and the basic or electron donor parameter (K_b) by the following equation:

$$\frac{\Delta G_{sp}}{AN^*} = \left(\frac{DN}{AN^*}\right)K_a + K_b \tag{13}$$

where DN is an electron donor or base number characterized according to Gutmann (41) and AN^* is an electron acceptor or acid number (42). The values of K_a and K_b of the powder samples were determined from the gradient and the intercept of the line obtained plotting $\Delta G_{sp}/AN^*$ vs. DN/AN^*.

Approximately 1.0 g of the micronized powder was weighed into standard glass IGC columns and plugged with glass wool. Each column was tapped for 5 min, using the minimum setting on a jolting voltameter (Surface Measurement Systems Ltd, London, UK) to a produce "homogeneous" powder bed. Each column was purged in the IGC at 0% RH, at 318.05 K with dry nitrogen for 3 h prior to analysis to remove surface moisture. The retention time of a series of n-alkanes (hexane to decane) and polar (ethanol, chloroform, dioxane, ethyl acetate, and acetone) probes were detected at infinite dilution with a flame emission detector. Column settings and run times for all three drugs were optimized at 318.05 K. Each column was analyzed twice.

Statistical Analysis

The statistical analysis of forces of interaction between individual colloid probes and respective substrates were compared using one-way ANOVA. The results were found to be significantly different based upon 95% probability values ($p < 0.05$).

RESULTS AND DISCUSSION

Physical Characterization

The morphology and size of the micronized drugs were fully characterized by SEM and laser light diffraction.

Scanning Electron Microscopy

Representative scanning electron micrographs of the micronized drugs are shown in Fig. 1. In general, all three drugs exhibited irregular crystal morphology with clear variations in crystal size, which correlated well with particle size measurements.

Particle Size

Micronized budesonide was found to have a median equivalent volume diameter of 3.24 μm, with over 82% of particles below 5 μm. By comparison, formoterol was found to have a median equivalent volume diameter of 2.69 μm, with 93% of particles below 5 μm. Salbutamol was found to have the largest median equivalent volume diameter of 6.61 μm, with 46% of particles below 5 μm. In general, the particle sizing data agreed well with SEM observations, with drug samples falling within the required size range for pulmonary delivery.

Determination of Contact Angle and Relative Surface Energy Values for Powder Compacts

The surface energy components obtained by CA (9,10) and IGC measurements are presented in Table II. Both CA and IGC values follow a similar trend. The highest dispersive (LW) values were measured for budesonide by both techniques, followed by formoterol and then salbutamol. These observations are in general agreement with related studies of the ranking of the dispersive parameters of pharmaceutical powders (43,44). A direct comparison of the data between the two techniques is rather difficult due to the variations in the experimental and theoretical approaches (11). The acidic and basic components of the powder samples from IGC measurements are not consistent with the results obtained from CA measurements. A quantitative determination of the polar components from IGC would require specific knowledge of the surface contact area of the polar component of the solvent probes with the solid. This limitation currently precludes the use of the surface component approach in determining the polar free energy of interaction via IGC measurements.

Determination of the Theoretical Work of Adhesion/ Cohesion

The dispersive and polar components of the work of cohesion and adhesion of the drug particles were calculated from the surface energy measurements derived from the CA studies and the surface tension value of HPFP. The dispersive LW work of cohesion and adhesion was obtained using the Good-Girifalco-Fowkes combining rule from the IGC measurements [Eq. (4)]. The thermodynamic work of adhesion and cohesion were calculated for the various particle-particle combinations in HPFP, and are shown in Table III.

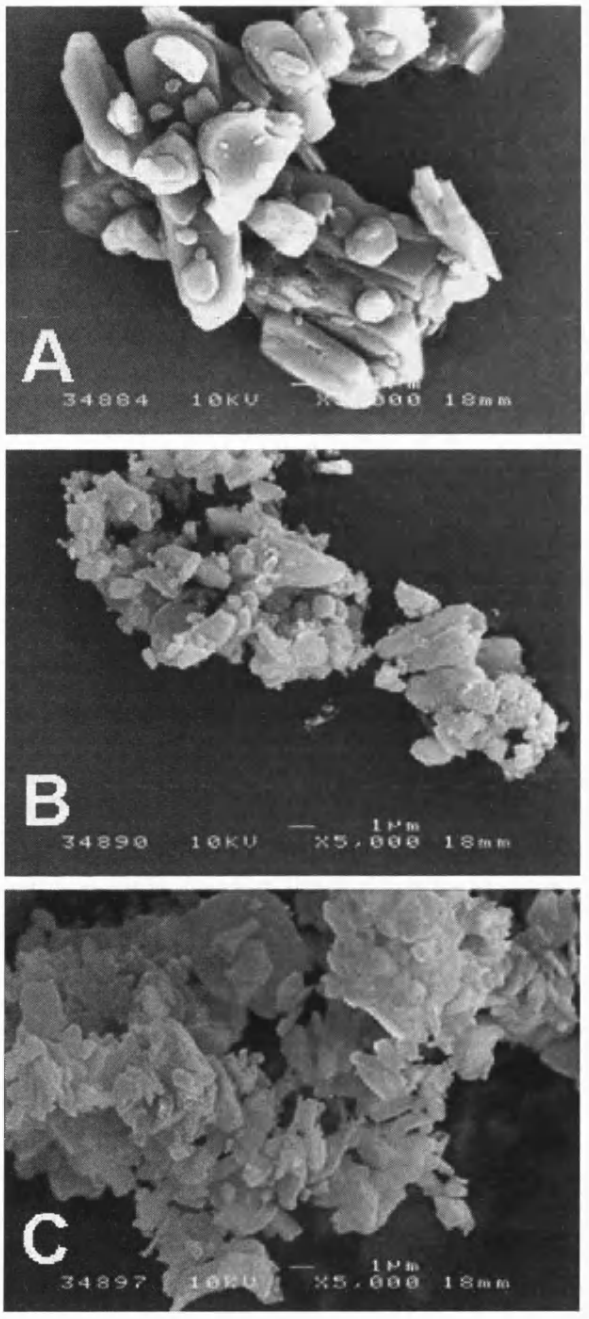

Fig. 1. Scanning electron micrographs of micronized salbutamol sulfate (A), budesonide (B), and formoterol fumarate dihydrate (C).

Comparison of the LW and AB work of cohesion/ adhesion for salbutamol suggests that both the cohesive and adhesive interactions are dominated by polar interactions. The dispersive part of the interactions is greatest for the salbutamol-budesonide combination and smallest for salbuta-

Table II. Surface Free Energy Components Obtained via CA and IGC Measurements

	Surface energy components from CA (mJ · m^{-2})				Surface energy components from IGC (mJ · m^{-2})		
	γ^{LW}	γ^{+}	γ^{-}	γ^{AB}	γ^{LW}	K_a	K_b
Salbutamol sulphate	46.5 ± 0.7	8.3 ± 1.5	18.5 ± 1.2	24.6 ± 2.5	39.1 ± 1.3	0.085 ± 0.002	0.029 ± 0.001
Budesonide	49.1 ± 0.4	0.3 ± 0.4	22.5 ± 3.8	4.6 ± 2.9	62.9 ± 1.7	0.113 ± 0.002	0.013 ± 0.001
Formoterol	48.5 ± 0.4	0.1 ± 0.2	35.0 ± 3.0	3.2 ± 3.0	51.2 ± 0.7	0.93 ± 0.002	0.026 ± 0.001

Values are mean ± SD, n = 3.

mol-salbutamol. This is true for both CA and IGC measurements. The total energy, that is, when both LW and AB components are taken into consideration, is greater for the cohesive salbutamol interactions, followed by the adhesion energies of salbutamol-formoterol and salbutamol-budesonide.

For budesonide, the LW components dominate the AB interactions for cohesive and adhesive (budesonide-formoterol) energies. However, the polar contributions are higher for the budesonide-salbutamol adhesive energy. Interestingly, the total theoretical work of interaction is greater for budesonide-salbutamol, with a strong polar component.

For formoterol, the dispersive energy component is greater for the budesonide-formoterol adhesion. The polar energy component is greater for the formoterol-salbutamol adhesion, and the total energy is greatest for this system. Thus, further highlighting the importance of polar energetic components in particle interactions.

This brief theoretical treatment of particle interactions derived from surface energetic components highlights the possibility of significant variations between interfacial interactions depending on whether they are calculated from dispersive components or a combination of polar and dispersive contributions. The fact that polar components of the solids should be taken into account in non-polar liquids is counter-intuitive and cannot be overlooked.

In an attempt to quantify these theoretical predictions, the thermodynamic work of adhesion and cohesion was compared with adhesive and cohesive force measurements via AFM experiments.

Atomic Force Microscopy Analysis

Measurement of pull-off forces between individual particles and substrate surfaces by AFM and the influence of complex interactive forces on particle adhesion have been reported previously (15,31,45). However, wider application of the AFM technique for preformulation development has been limited by the dramatic influence of the contact area between contiguous surfaces on quantitative force measurements. Although attempts to quantify the contact radii of the asperities of the colloid probes have been made (45), normalization and direct comparison of cohesive and adhesive forces in multicomponent systems remains onerous, due to the limited knowledge of the true contact area between probe and a substrate of varying surface roughness. Furthermore, efforts to predict adhesive interactions using theoretical approaches and surface energy measurements have, to date, proved unsatisfactory (46). Theoretical estimates are often several orders of magnitude greater than experimental measurements (47,48). The most plausible explanation for this discrepancy is the variation in the mesoscopic contact area between contiguous surfaces from the expected macroscopic dimensions. These difficulties can, however, be overcome by the use of the novel cohesive-adhesive balance (CAB) analysis procedure developed by Begat *et al.* (35).

Table III. Theoretical Values of the Thermodynamic Work of Adhesion and Cohesion for Particulate Interactions in HPFP, Calculated via Equation VII

	W^{LW} IGC	W^{LW} CA	W^{AB} CA	W^{TOT} CA
		Cohesive energies		
Salbutamol-Salbutamol	13.15	19.62	49.40	69.00
Formoterol-Formoterol	24.08	21.50	7.74	29.24
Budesonide-Budesonide	36.04	22.04	11.12	33.14
		Adhesive energies		
Salbutamol-Formoterol	17.79	20.54	36.82	57.34
Salbutamol-Budesonide	21.77	20.80	32.26	53.06
Budesonide-Formoterol	29.46	21.76	10.04	31.8

All values are in mJ · m^{-2}.

Analysis of Substrates Surfaces

Prior to adhesion studies, the surface roughness on the dominant crystal face of each drug substrate was investigated. Roughness analysis (n = 25, 5 × 5 μm area) of the surface topography for each drug crystal indicated R_{RMS} values of:

Salbutamol, 1.33 nm (±0.04)
Budesonide, 0.68 nm (±0.01)
Formoterol, 1.52 nm (±0.01)

The data suggested extremely smooth surface morphologies, with surfaces exhibiting a root-mean-squared roughness well below 2 nm over a 25 μm^2 area. Although different degrees of roughness did exist between drugs (most likely related to differing crystal growth processes and kinetics during crystallization), the uniform and smooth topography made them highly suitable for maintaining reproducible contact geometry between an individual colloid probe and the substrate surfaces under investigation.

Measurement of Forces of Cohesion and Adhesion

The *in situ* AFM probe technique allowed direct measurements of the cohesion and adhesion between single drug particulates and the dominant crystal faces of each drug material. The integrity of all drug probes was investigated prior to and post measurement using a high-magnification 500× long-working distance optical microscope. In all cases, the drug probes appeared proud of the cantilever surface, with no visible differences between the start and end of the experimental procedure (indicating no macro/microscopic change in drug-probe morphology). The number distribution of each

data set indicated a normal distribution with low variability, suggesting the interaction with a highly smooth substrate surfaces providing a uniform contact geometry for the interacting probe. The specific mean values and standard deviations for the interaction for each drug probe and substrate are provided in Table IV. As expected, comparisons between probes of the same drug (probes 1–3) indicate large variations in adhesion force. This may be explained by the difference in particle size and variations in contact geometry due to the irregular shape of the probes. Without prior knowledge of the true contact area of each probe, inter-probe variations cannot be quantified. However, trends can be discerned for each drug probe and their forces of interactions measured ranked.

Hence, the cohesive salbutamol-salbutamol force of interaction was shown to be stronger than the adhesion salbutamol-formoterol, which in turn was higher than salbutamol-budesonide interactions. The AFM data suggested that the salbutamol-formoterol interaction was approximately twice that of the salbutamol-budesonide adhesion.

For the budesonide probes, the order was budesonide-salbutamol, budesonide-budesonide and budesonide-formoterol. The quantitative AFM data suggested that the adhesive (budesonide-salbutamol) interaction was nine times greater than the cohesive one.

Finally, for formoterol, the rank order was formoterol-salbutamol, formoterol-formoterol, and formoterol-budesonide. AFM data suggested that the formoterol-salbutamol interaction was approximately five times greater than the force of cohesion.

Comparisons Between Thermodynamic Work of Adhesion and AFM Measurements

As previously discussed, the thermodynamic work of adhesion is directly proportional to the force of adhesion. To highlight this relationship and the specific role of the dispersive (LW) and total (LW + AB) interactions, representative plots of the theoretical work of adhesion of the LW (W_{ad}^{LW}) interactions and the influence of acid-base interactions ($W_{ad}^{Tot} = W_{ad}^{LW} + W_{ad}^{AB}$) vs. the force measurements are shown in Fig. 2 (for the case of salbutamol drug probe). It is anticipated that the work of adhesion/cohesion should increase with an increasing force of adhesion/cohesion.

The plots suggest no direct relationship between the separation force measurements and the dispersive component of the work of adhesion (W_{ad}^{LW}) calculated from either IGC or CA measurements (Fig. 2, IGC and CA). However, a positive relationship was observed between the force measurements and the total work of adhesion (W_{ad}^{Tot}) when taking into accounts both the non-polar and polar contributions.

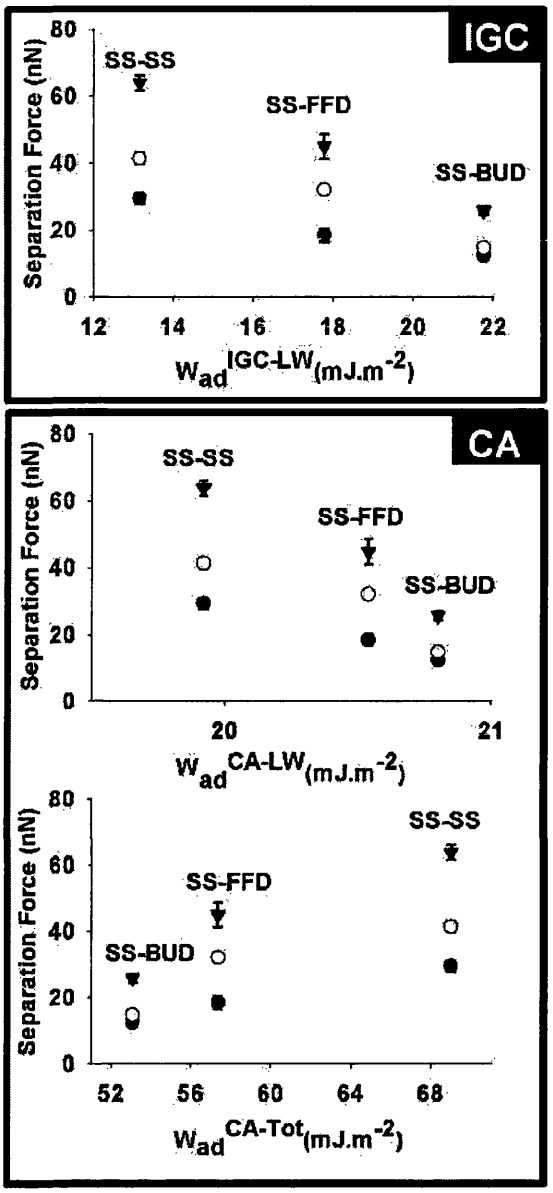

Fig. 2. Plot of the theoretical thermodynamic work of adhesion *vs.* AFM force measurements for salbutamol sulfate drug probes (n = 3 probes, ● = 1; ○ = 2; ▼ = 3). Energies were calculated from IGC and CA measurements. The upper two plots take into account the dispersive contribution only. The lower plot includes the polar as well as dispersive contributions. Key to the abbreviations: salbutamol (SS), formoterol (FFD), and budesonide (BUD).

Table IV. AFM Separation Force Measurements for Micronised Salbutamol Sulphate, Budesonide and Formoterol Fumarate Dihydrate

	Probe								
	Salbutamol			Budesonide			Formoterol		
Substrate	Tip 1	Tip 2	Tip 3	Tip 1	Tip 2	Tip 3	Tip 1	Tip 2	Tip 3
Salbutamol	29.5 ± 1.5	41.5 ± 1.7	63.9 ± 2.3	10.9 ± 1.1	48.2 ± 2.9	71.9 ± 2.2	58.2 ± 2.1	15.3 ± 1.9	11.2 ± 2.4
Budesonide	12.5 ± 0.9	14.8 ± 1.0	25.8 ± 1.3	0.9 ± 0.2	5.0 ± 2.2	7.9 ± 4.0	13.7 ± 0.3	6.7 ± 1.9	3.7 ± 0.2
Formoterol	18.4 ± 1.9	32.1 ± 0.8	45.0 ± 3.7	1.2 ± 1.1	3.7 ± 0.7	6.7 ± 1.4	13.1 ± 0.7	6.2 ± 0.9	4.1 ± 1.3

Values are ± SD, n = 3 probes. All forces are in nN.

Similarly, analysis of the budesonide and formoterol interactions indicated no correlation between the LW work of adhesion (from IGC and CA) and AFM measurements, while the total theoretical work correlated well with experimental AFM data. Such observations suggest that polar interactions between contiguous surfaces play a significant role in particle adhesion/cohesion in non-aqueous media and should not be neglected in predictive theoretical approaches.

Relationship Between CAB Plots and Theoretical Cohesion/Adhesion Ratios

An estimation of the separation force from theoretical treatment of the interfacial interactions via surface energy measurements would require knowledge of the effective contact area of each probe, as indicated by Eq. (8). This limitation precludes direct correlation of individual AFM force measurements for each probe with theoretical measurements of the work of adhesion/cohesion. However, the determination of the force balance for a series of colloid probes using the CAB analysis procedure does allow quantification of the relationship between the theoretical work of cohesion and adhesion and corresponding AFM measurements.

From theory, the cohesion between material 1 and adhesion between material 1 and 2 in a liquid media (3) can be expressed as:

$$\frac{F_{131}}{F_{132}} = \frac{n\pi R^*_{131} W_{131}}{n\pi R^*_{132} W_{132}} \tag{14}$$

where F_{131} and F_{132} are the cohesive and adhesive forces, respectively. Assuming that the tailoring of the substrate surfaces enables equivalence of the contact radii R^*_{131} and R^*_{132}, the relationship between theory and experimental measurements can be discerned. From Eq. (14), the slope of a plot of the force of cohesion *vs.* the force of adhesion for a series of probes would yield the ratio of the thermodynamic work of cohesion to the work of adhesion.

The AFM data and the theoretical estimation of the cohesive-adhesive balance from the thermodynamic surface free energy measurements for salbutamol, budesonide, and formoterol probes are shown in Figs. 3, 4, and 5, respectively. The bisecting (dotted) line in each figure corresponds to the balance between of cohesion and adhesion ($F_{coh} = F_{adh}$, or $W_{adh} = W_{coh}$). The relative position of the AFM data points with respect to the bisector is a direct indication of the cohesive and adhesive tendencies of the drug particles considered. Data below the bisector indicate an affinity for the probe material to develop adhesive interactions ($F_{adh} > F_{coh}$). Conversely, data above the bisector denote dominant cohesive properties.

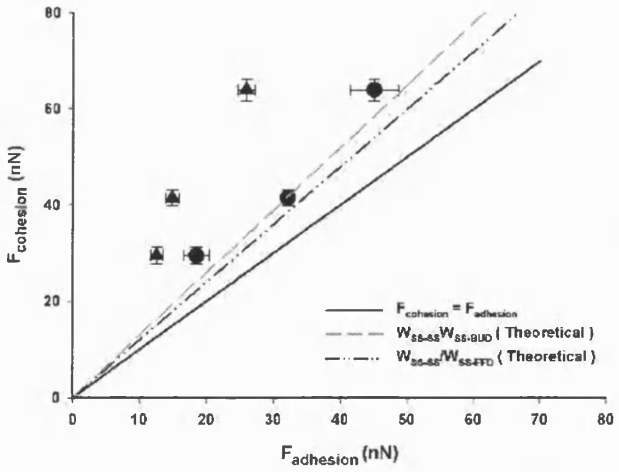

Fig. 3. Relationship between AFM cohesion and adhesion measurements for salbutamol sulfate probes (SS, n = 3) illustrated as a CAB plot. The bisecting (solid) line is the equilibration of the cohesion and adhesion. Dotted lines are theoretical ratios calculated from surface component approach with polar and dispersive contributions. ▲, budesonide (BUD) substrate; ●, formoterol (FFD) substrate.

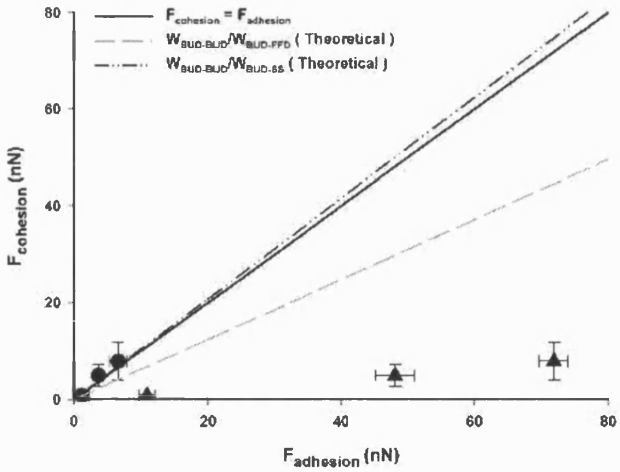

Fig. 4. Relationship between AFM cohesion and adhesion measurements for budesonide probes (BUD, n = 3) illustrated as a CAB plot. The bisecting (solid) line is the equilibration of the cohesion and adhesion. Dotted lines are theoretical ratios calculated from surface component approach with polar and dispersive contributions of the surface free energy measurements. ▲, formoterol (FFD) substrate; ●, salbutamol (SS) substrate.

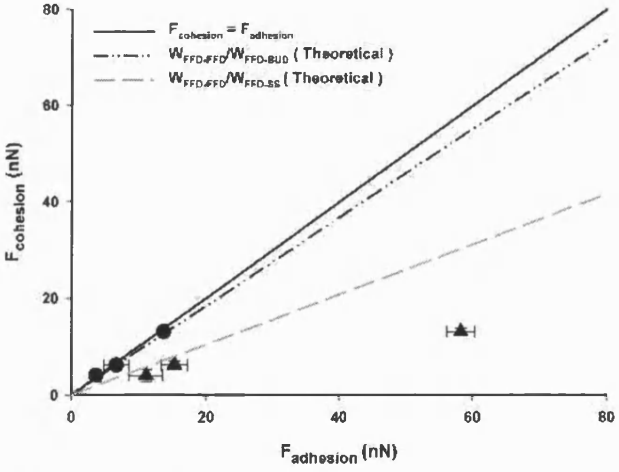

Fig. 5 Relationship between AFM cohesion and adhesion measurements for formoterol fumarate dihydrate probes (FFD, n = 3) illustrated as a CAB plot. The bisecting (solid) line is the equilibration of the cohesion and adhesion. Dotted lines are theoretical ratios calculated from surface component approach with polar and dispersive contributions. ▲ = salbutamol (SS) substrate; ● = budesonide (BUD) substrate.

Table V. Linear Regression Analysis and Measurements of Cohesive/Adhesive Ratios via AFM Measurements Together With the Theoretical Ratios of the Cohesive/Adhesive Interactions

	Experimental ratio $F_{cohesion}/F_{adhesion}$	R^2 $F_{cohesion}/F_{adhesion}$	Theoretical ratio $W_{cohesion}/W_{adhesion}$
Salbutamol-Budesonide	2.41	0.9880	1.30
Salbutamol-Formoterol	1.29	0.9875	1.20
Budesonide-Salbutamol	0.11	0.9958	0.62
Budesonide-Formoterol	1.24	0.9832	1.04
Formoterol-Salbutamol	0.21	0.9005	0.52
Formoterol-Budesonide	0.94	0.9960	0.92

Analysis of Fig. 3 suggested salbutamol to be more cohesive than adhesive, when interacting with formoterol and budesonide. This is in accordance with the theoretical predictions of the total work of adhesion/cohesion shown in Table III.

Similar analysis of CAB data for the budesonide drug probes (Fig. 4) suggested that budesonide was more adhesive with salbutamol than cohesive with itself. The theoretical approach was in agreement with this tendency for an adhesive interaction. Similar agreement between theory and experiment was found for the budesonide-formoterol interactions.

The CAB and theoretical analysis of formoterol interactions (Fig. 5) suggested that formoterol was biased toward adhesion. This again confirmed the experimental and theoretical findings.

A linear regression analysis of the balance of the cohesive and adhesive forces as measured by AFM was performed to calculate the cohesive/adhesive force ratio. These ratios are summarized in Table V, together with the theoretical ratio of the work of cohesion to the work of adhesion. There is a good correlation between the experimental and theoretical ratios, although absolute values are not well correlated, albeit of the same order of magnitude. The two approaches suggest the same bias toward either adhesive or cohesive interactions. The discrepancy between experimental and theoretical measurements, which is of greatest significance for interactions involving salbutamol, may relate to a slight polarity of the model liquid propellant that has not been taken into account. This for instance is known to affect liquid-liquid surface tension predictions. Other possible reasons could be related to the AFM measurements being conducted on the dominant face of each drug crystal, while the surface energy values were calculated from contact angles measurements derived from compacts of micronized drug. Thus, it is reasonable to assume that the less dominant faces may influence the measurements. The relationship between face specific surface free energy and work of adhesion is a subject of ongoing investigations.

The theoretical model developed in this work and its correlation with direct AFM force measurement may provide the basis for a powerful pMDI preformulation tool. This understanding of the influence of the physicochemical properties of colloid particles on particulate interactions may provide the formulation scientist with a guide to improving the stability of pMDI suspensions and the behavior of the system under development.

CONCLUSIONS

Direct measurements of the interaction forces (via AFM measurements) responsible for the stability of colloid particles in pMDI formulations indicate a fine balance between adhesive and cohesive tendencies. A relationship between the theoretical interfacial thermodynamics, derived from the surface component approach, and experimental force measurements were demonstrated. Correlation of the experimental measurements with theory required the introduction of the polar as well as dispersive components of surface energies of the interacting solids. This combined approach may provide a novel means of predicting suspension stability of pMDI formulations.

REFERENCES

1. D. Ganderton and T. Jones. *Drug Delivery to the Respiratory Tract*, Academic Press, London, 1987.
2. J. S. Patton. Mechanisms of macromolecule absorption by the lungs. *Adv. Drug Deliv. Rev.* **19**:3–36 (1996).
3. D. L. Ross and B. J. Gabrio. Advances in metered dose inhaler technology with the development of a chlorofluorocarbon free drug delivery system. *J. Aerosol Med.* **12**:151–160 (1999).
4. H. D. C. Smyth. The influence of formulation variables on the performances of alternative propellant-driven metered dose inhalers. *Adv. Drug Deliv. Rev.* **55**:807–828 (2003).
5. D. Ganderton. Patients, devices and formulations. *J. Aerosol Med.* **23**:441–444 (2003).
6. J. A. Ranucci, S. Dixit, R. N. J. Bray, and D. Goldman. Controlled flocculation in meterd-dose aerosol suspensions. *Pharmacetical Technology* **0**:68–73 (1990).
7. Y. Michael, M. J. Snowden, B. Z. Chowdhry, I. C. Ashurst, C. J. Davies-Cutting, and T. Ripley. Characterisation of the aggregation behaviour in a salmeterol and fluticasone propionate inhalation aerosol system. *Int. J. Pharm.* **221**:165–174 (2001).
8. E. M. Phillips, P. R. Byron, and R. N. Dalby. Axial-ratio measurements for early detection of crystal-growth in suspension-type metered dose inhalers. *Pharm. Res.* **10**:454–456 (1993).
9. C. J. van Oss. *Interfacial Forces in Aqueous Media*, Marcel Dekker, New York, 1994.
10. R. J. Good. Contact-angle, wetting, and adhesion—a critical-review. *J. Adhes. Sci. Technol.* **6**:1269–1302 (1992).
11. M. D. Ticehurst, R. C. Rowe, and P. York. Determination of the surface properties of two batches of ss by inverse gas chromatography. *Int. J. Pharm.* **111**:241–249 (1994).
12. O. Planinsek and G. Buckton. Inverse gas chromatography: considerations about appropriate use for amorphous and crystalline powders. *J. Pharm. Sci.* **92**:1286–1294 (2003).
13. G. Binnig and C. F. Quate. Atomic force microscope. *Phys. Rev. Lett.* **56**:930–933 (1986).
14. R. Ashayer, P. F. Luckham, S. Manimaaran, and P. Rogueda. Investigation of the molecular interactions in a pMDI formulation by atomic force microscopy. *Eur. J. Pharm. Sci.* **21**:533–543 (2004).
15. P. Young, R. Price, D. Lewis, S. Edge, and D. Traini. Under pressure: predicting pressurized metered dose inhaler interactions using the atomic force microscope. *J. Colloid Interface Sci.* **262**:298–302 (2003).
16. F. M. Fowkes. Additivity of intermolecular forces at interfaces. I. Determination of the contribution to surface and interfacial ten-

sion of dispersion forces in various liquids. *J. Phys. Chem.* **67**: 2538–2541 (1963).
17. R. J. Good and L. A. Girifalco. A theory for estimation of surface and interfacial energies. III. Estimation of surface energies of solids from contact angle data. *J. Phys. Chem.* **64**:561–565 (1960).
18. B. V. Derjaguin and L. D. Landau. Theory of the stability of strongly charged lyophobic sols and of the adhesion of strongly charged particles in solutions of electrolytes. *Acta Physicochimica. U.S.S.R.* **14**:663 (1941).
19. E. J. W. Verwey and J. T. G. Overbeek. *Theory of the Stability of Lyophobic Colloids*, Elsevier, Amsterdam, 1948.
20. C. Vervaet and P. R. Byron. Drug surfactant propellant interactions in HFA formulations. *Int. J. Pharm.* **186**:13–30 (1999).
21. R. J. Pugh, T. Matsunaga, and F. M. Fowkes. The dispersability and stability of carbon black in media of low dielectric constant. I: Electrostatic and steric contributions to colloidal stability. *Colloids Surf.* **7**:183–207 (1983).
22. A. Kitahara. Zeta potential in non-aqueous media and its effect on dispersion stability. *Prog. Organic Coatings* **2**:81–98 (1974).
23. D. A. Wyatt and B. Vincent. Electrical effects in non-aqueous systems. *J. Biopharm. Sci.* **3**:27–31 (1989).
24. J. A. Brant and A. E. Childress. Assessing short-range membrane-colloid interactions using surface energetics. *J. Membr. Sci.* **203**:257–273 (2002).
25. J. A. Brant and A. E. Childress. Colloidal adhesion to hydrophilic membrane surfaces. *J. Membr. Sci.* **241**:235–248 (2004).
26. H. Hertz. On the contact of elastic solids. *J. Reine Angew. Math.* **92**:156–171 (1882).
27. K. Johnson, K. L. Kendall, and A. D. Roberts. Surface energy and the contact of elastic solids. *Proc. R. Soc. Lond. A* **324**:301–313 (1971).
28. B. V. Derjaguin, V. M. Müller, and Y. P. Toporov. Effect of contact deformations on the adhesion of particles. *J. Colloid Interface Sci.* **53**:314–326 (1975).
29. G. Rhodes. *Crystallography—Made Crystal Clear*, Academic Press, New York, USA, 1993.
30. W. A. Ducker, T. J. Senden, and R. M. Pashley. Direct measurement of colloidal forces using an atomic force microscope. *Nature* **353**:239–241 (1991).
31. P. M. Young, R. Price, M. J. Tobyn, M. Buttrum, and F. Dey. The influence of relative humidity on the cohesion properties of micronised drugs used in inhalation therapy. *J. Pharm. Sci.* **93**:753–761 (2004).
32. P. G. A. Rogueda. HPFP, a model propellant for pMDIs. *Drug Dev. Ind. Pharm.* **29**:39–49 (2003).
33. H. Mizes, M. Ott, E. Eklund, and D. Hays. Small particle adhesion: measurement and control. *Colloids and Surfaces A* **165**:11–23 (2000).
34. R. Price, P. M. Young, S. Edge, and J. N. Staniforth. The influence of relative humidity on particulate interactions in carrier-based dry powder inhaler formulations. *Int. J. Pharm.* **246**:47–59 (2002).
35. P. Begat, D. A. V. Morton, J. N. Staniforth, and R. Price. The cohesive-adhesive balances in dry powder inhaler formulations I: direct quantification by atomic force microscopy. *Pharm. Res.* **21**:1591–1597 (2004).
36. C. J. Van Oss, R. J. Good, and M. K. Chaudhury. Additive and non-additive surface tension components and the interpretation of contact angles. *Langmuir* **4**:884–891 (1988).
37. R. J. Good and R. R. Stromberg. *Surface and Colloid Science*, Plenum Press, New York, 1979.
38. G. Buckton. *Interfacial Phenomena in Drug Delivery and Targeting*, Harwood Academic Publishers, Chur, Switzerland, 1995.
39. G. Buckton, P. Darcy, and D. McCarthy. The extent of errors associated with contact angles 3. The influence of surface roughness effects on angles measured using a Wilhelmy plate technique for powders. *Colloids and Surfaces A* **95**:27–35 (1995).
40. J. Schultz, L. Lavielle, and C. Martin. The role of the interface in carbon fibre-epoxy composites. *J. Adhes. Sci. Technol.* **23**:45–60 (1987).
41. V. Gutmann. *The Donor-Acceptor Approach to Molecular Interactions*, Plenum Publishing Corporation, New York, 1978.
42. F. L. Riddle and F. M. Fowkes. Spectral shifts in acid-base chemistry.1. Van der Waals contributions to acceptor numbers. *J. Am. Chem. Soc.* **112**:3259–3264 (1990).
43. N. M. Ahfat, G. Buckton, R. Burrows, and M. D. Ticehurst. Predicting mixing performance using surface energy measurements. *Int. J. Pharm.* **156**:89–95 (1997).
44. O. Planinsek, A. Trojak, and S. Srcic. The dispersive component of the surfac fee energy of powders assessed using inverse gas chromatography and contact angle measurements. *Int. J. Adhesion Adhesives* **221**:211–217 (2001).
45. J. C. Hooton, C. S. German, S. Allen, M. C. Davies, C. J. Roberts, S. J. B. Tendler, and P. M. Williams. An atomic force microscopy study of the effect of nanoscale contact geometry and surface chemistry on the adhesion of pharmaceutical particles. *Pharm. Res.* **21**:953–961 (2004).
46. J. L. Parker, D. L. Cho, and P. M. Claesson. Plasma modification of mica: forces between fluorocarbon surfaces in water and nonpolar liquid. *J. Phys. Chem.* **93**:6121–6125 (1989).
47. H. Yotsumoto and R.-H. Yoon. Application of extended DLVO theory. *J. Colloid Interface Sci.* **157**:426–433 (1993).
48. P. M. Claesson and H. K. Christenson. Very long range attractive forces between uncharged hydrocarbon and fluorocarbon surfaces in water. *J. Phys. Chem.* **92**:1650–1655 (1988).

Available online at www.sciencedirect.com
SCIENCE DIRECT®
International Journal of Pharmaceutics 296 (2005) 26–33
international journal of pharmaceutics
www.elsevier.com/locate/ijpharm

The influence of dose on the performance of dry powder inhalation systems

Paul M. Young*, Stephen Edge, Daniela Traini, Matthew D. Jones, Robert Price, Dina El-Sabawi, Claire Urry, Charlotte Smith

Pharmaceutical Technology Research Group, Department of Pharmacy, University of Bath, Bath BA2 7AY, UK

Received 23 September 2004; received in revised form 7 February 2005; accepted 9 February 2005
Available online 7 April 2005

Abstract

The relationship between drug/lactose ratio and aerosolisation performance of conventional carrier based formulations was investigated using the twin stage impinger. A dose range of ~10–450 μg of drug in a 50 mg lactose carrier formulation was studied. Statistical differences in both the fine particle dose and fine particle fraction were observed across the dosage range (ANOVA, $p < 0.05$). In general, no statistically significant difference (Fishers Pairwise, $p < 0.05$) in fine particle dose was observed between drug levels of approximately 10 μg and 135 μg, whereas a linear decrease in fine particle fraction was observed across the same drug level range ($R^2 = 0.977$). Increasing the dose from ~135 μg to 450 μg resulted in a statistically significant increase in both fine particle dose and fraction (ANOVA $p < 0.05$). Such observations may be attributed to the occupation of 'active' carrier sites by drug particles at low drug concentration, since the quantity of drug particles liberated from the carrier during aerosolisation remains constant at the lower dosing regimes.

Keywords: Dry powder inhaler; Low dose; Active sites; Pulmonary delivery

1. Introduction

Dry powder inhalers (DPI) are routinely used in the treatment of respiratory diseases such as asthma. In general, the therapeutic agents employed in such systems are typically processed/milled to produce 'micron-sized' particulates that are of a size range suitable for respiratory deposition (0.5–8 μm, Ganderton and Kassem, 1992). Micron-sized particles have a relatively high surface area to mass ratio and consequently exhibit greater cohesiveness and adhesiveness compared to larger, unprocessed particles. For low dose drugs, this high adhesivity and cohesivity can result in product development hindrance in regard to issues such as content uniformity, stability and drug metering.

* Corresponding author. Tel.: +61 2 9036 7035; fax: +61 2 9351 4391.
E-mail address: py@pharm.usyd.edu.au (P.M. Young).

0378-5173/$ – see front matter © 2005 Elsevier B.V. All rights reserved.
doi:10.1016/j.ijpharm.2005.02.004

A common approach used in order to combat these ever present formulation challenges, is to blend the micron-sized drug particles with a larger inert carrier material, such as lactose, to form an 'ordered mix' (Hersey, 1975). This approach results in improvement of handling and processing properties, accurate dosing by dilution of drug to mass ratio and an increase in device drug emptying.

In addition to the advantages that ordered mixes can offer, upon inhalation, the drug particles must be liberated from the formulation so as to penetrate the lower respiratory airways. This is achieved by the forces generated from the patient's inspiration and can be aided by device characteristics, for example, increased pressure drops or turbulent air flows.

The forces required to successfully remove drug particles from the surfaces of the carrier will be dependent on the physico-chemical properties of the drug and carrier, and the environmental conditions under which they are formulated, stored and used. Many studies have been conducted to investigate the influence of such factors on the performance of DPI based systems (Ganderton and Kassem, 1992). These include the study of carrier morphology/crystallinity (Kawashima et al., 1998; Zeng et al., 2000; Young et al., 2002; Larhib et al., 2003; Flament et al., 2004), the influence of carrier material, grade and size (Steckel and Muller, 1997; Larhrib et al., 1999; Louey et al., 2003; Steckel and Bolzen, 2004), the influence of carrier fines (Lucas et al., 1998; Zeng et al., 1998, 1999; Louey et al., 2003) and the addition of ternary force control agents (Young et al., 2002).

In general, the morphology and roughness of carrier particles are not uniform. This is in part due to the fact that carriers, such as lactose, are produced on a relatively large scale from natural sources. The processing and production of such organic materials will invariably lead to particles containing regions which exhibit different roughness parameters (peaks and troughs). Furthermore, since DPI carrier based systems are based on organic crystalline materials there may also be specific crystal faces with different surface free energies present (Muster and Prestidge, 2002). In addition, production and processing methods may also result in the presence of surface macroscopic and/or microscopic amorphous regions.

Clearly, these possible inter–intra batch variations in physico-chemical properties in the surface of a carrier material may lead to differences in apparent adhesion properties of drug particles. Furthermore, during the dynamic process of mixing, the adherence of drug particles to the more adhesive areas of the carrier surface is likely to occur. Indeed, Hersey (1975) proposed that the surfaces of larger particles consisted of distinct regions containing so-called 'active sites'. It was further suggested that when the number fine carrier particles in the mixture is below the saturation limit of the large particles' adhesive potential, the fine particles will preferentially bind to these active sites. When these active sites have been completely occupied with fine particles a binary carrier system would then exist, i.e., carrier with strongly bound fine particles, and free or weakly bound fine particles.

This presence of active sites has obvious implications for DPI drug delivery, since retention of drug particles on these relatively high-energy sites during processing and aerosolisation would result in a decrease in apparent respirable drug fraction as suggested by Staniforth (1996). The possible detrimental effect of active sites may not be an issue for the majority of marketed DPIs since they are designed to deliver relatively high drug doses (e.g. Ventolin Accuhaler™, Ventodisks™, Pulvinal™, and Cyclohaler™ $\geq 200\,\mu g$) More recently, the development of DPIs which can deliver lower doses of drugs has received attention. In this case, the drug has a higher potency and consequently requires a lower dose (e.g. formoterol fumarate 6–12 μg). This may lead to variations in drug delivery as a consequence of drug retention in high-energy sites resulting in severe deviations from target doses and label claims.

Current methods for overcoming such issues include 'filling' the potential active sited by increasing the fine particle content present on the carrier surface (Zeng et al., 1999) or pacifying the effects of active sites by the addition of so-called 'force control agents' such as magnesium stearate (Young et al., 2002). However, this approach does not answer questions concerning the role of active sites in DPI science.

As part of an ongoing study, the influence of drug dose (carrier/drug ratios 100:1–5000:1) on the aerosolisation performance of a model DPI system has been investigated. The use of such a system may give a valuable incite into the role of active sites in the performance of lactose based DPI systems.

2. Materials and methods

2.1. Materials

Micronised salbutamol sulphate was supplied by Aventis Pharma (Holmes Chapel, UK). α-Lactose monohydrate was supplied by Borculo Domo (Netherlands) and was sieved to produce a 63–90 μm size fraction. Water used was purified by reverse osmosis (MilliQ, Millipore, France). All solvents used throughout the study were supplied by BDH (Poole, Dorset, UK) and were of at least analytical grade.

2.2. Particle size analysis

The particle size distribution of the sieve fractioned lactose and micronised salbutamol sulphate was determined by laser light scattering (Malvern Mastersizer X, Malvern, Worcs, UK). Approximately 100 mg of sample was suspended in a 0.1% (w/v) lecithin–cyclohexane solution and ultra-sonicated at 25 °C prior to analysis (experimentally determined sufficient for de-agglomeration). A small volume, circulating cell was used equipped either with a 100 mm (salbutamol sulphate) or 300 mm lens (lactose).

2.3. Scanning electron microscopy

Morphology of the lactose blends was examined by scanning electron microscopy (SEM) (Jeol 6310, Jeol, Japan) at 10 keV. Samples were gold-coated prior to analysis (Edwards Sputter Coater, UK).

2.4. Drug content determination

Quantification of salbutamol sulphate content uniformity and in vitro deposition was by high performance liquid chromatography (HPLC). The HPLC system consisted of an AS950 intelligent sampler, PU-980 intelligent HPLC pump, 975 UV/VIS detector (all Jasco, Japan) and Spherisorb 15 cm, 5 μm ODS1 column.

The mobile phase used throughout the investigation was methanol/water (60:40) and acetic acid 0.1% (v/v). Settings were as follows: detection wavelength 276 nm; flow rate 1.25 ml min^{-1}; pressure approximately 400 kg m^2; injection volume 100 μl; analysis time 4 min; approximate retention time 2 min.

Linearity was confirmed between 0.1 μg ml^{-1} and 10 μg ml^{-1} ($R^2 = 0.99$). Lactose did not interfere with the salbutamol sulphate response. Sample injections were performed in duplicate using a bracket standard method containing standards prepared from separate stock solutions.

2.5. Preparation of blends

Powder formulations containing different levels of salbutamol sulphate were prepared by varying the ratio of lactose carrier to salbutamol sulphate. Eight blends with ratios ranging from approximately 100:1 to 5000:1 were prepared. Each formulation was designed so that 50 mg of the powder blend would contain the desired dose. The volume of the powder in the mixing cell was kept constant to reduce the effect of friction.

Salbutamol sulphate was blended with the lactose geometrically. Briefly, an amount of lactose, equivalent to about twice the total mass of salbutamol sulphate was used to 'sandwich' the drug in the blend. This was mixed for 1 min using a Whirlimixer (Fisons, UK). Lactose was then added in geometric quantities, mixing with a Whirlimixer for 1 min after each addition. The final blend was mixed in a Turbula (Bachofen, Basel, Switzerand) at 46 rev min^{-1} for 30 min.

The doses formulated were approximately 10 μg, 30 μg, 40 μg, 90 μg, 135 μg, 190 μg, 350 μg and 450 μg of drug.

Content uniformity (50 mg samples) across each blend indicated a coefficient of variation less than 5% ($n = 10$).

Each blend was stored in tightly sealed containers with a saturated solution of potassium carbonate (44% RH) for a minimum of 48 hours prior to analysis.

2.6. In vitro analysis

The influence of drug–lactose ratio on the aerosolisation performance was investigated using the twin stage impinger (TSI) (Copley Scientific, Nottingham, UK). Methodology followed that of the British Pharmacopoeia. Briefly the TSI contained 7 ml of mobile phase in stage one and 30 ml mobile phase in stage two, which at 60 l min^{-1} produces a cut off mass median aerodynamic diameter of 6.4 μm between the two stages. The flow through the TSI apparatus was controlled using a GAST rotary vein pump and solenoid

valve timer (Copley Scientific, Nottingham, UK). Flow rate was tested prior to operation using a calibrated flow meter.

A filled (49.90 ± 0.20 mg) size 3 gelatine capsule was placed into the dosage chamber of the Cyclohaler®. The mouthpiece was attached to the TSI apparatus and the Cyclohaler® inserted until the end met the inner edge of the rubber mouthpiece. The pump was turned on and allowed to stabilise for 10 s before starting the valve-timer for a 5 s period. The device was removed carefully, the empty capsule placed into a beaker, and the device was primed and tested with a second capsule. This procedure was repeated until five actuations had been conducted.

The TSI apparatus was then dismantled and each stage was washed with mobile phase into volumetric flasks. In addition, the device and capsules were washed into a separate volumetric flask. Appropriate sample dilutions were made prior to testing by HPLC. All values were divided by five to approximate a single dose.

The TSI aerosolisation studies were conducted in triplicate for each formulation and were randomised for dose.

3. Results

3.1. Particle size analysis

The particle size distributions for both lactose and salbutamol sulphate are shown in Fig. 1A and B, respectively. The size distribution for the lactose sample (volume median diameter) indicated the majority of particles to be between 60 μm and 200 μm in diameter. It is interesting to note that the upper size was higher than the sieve fraction value (90 μm) and was most likely due to the tomahawk geometry of the lactose particles. Furthermore, approximately 6% of the particles exhibited diameters of less than 20 μm with 2% less than 5 μm. These can be related to the presence of fine lactose particles attached to the large carrier particles which were clearly visible using SEM. This demonstrates that simple sieving does not provide sufficient energy to remove adhered lactose fines from larger carrier particles and that lactose fractions produced by sieving consist of a pseudo-ordered mix which has obvious formulation implications. Analysis of the particle size distribution of the micronised

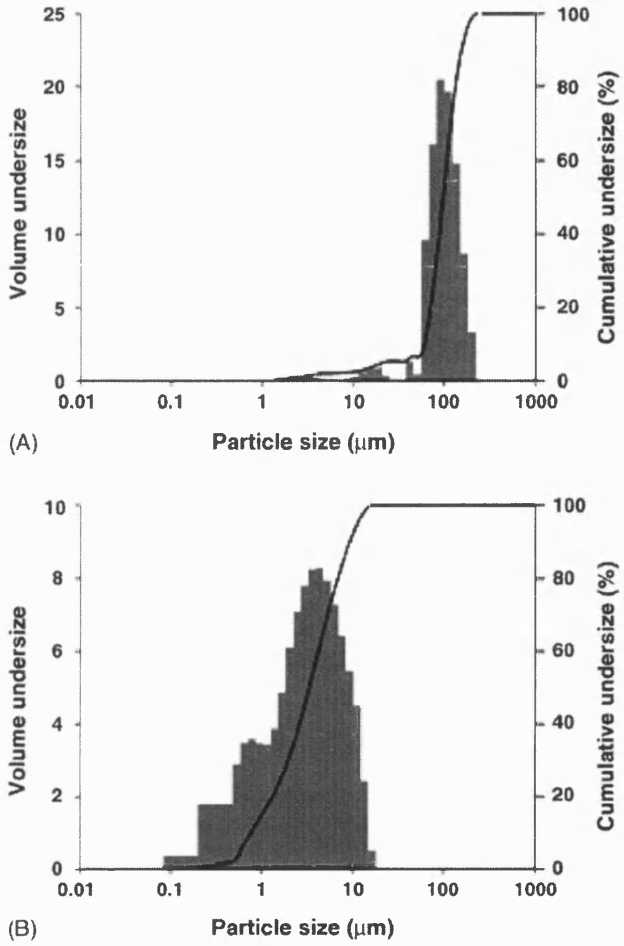

Fig. 1. Particle size distribution of 63–90 μm sieve fractioned lactose (A) and the micronised salbutamol sulphate (B).

salbutamol sulphate suggested 90% of the particulates exhibited a diameter less than 9.4 μm and 50% less than 3.4 μm.

3.2. Scanning electron microscopy

Representative SEM images of 12 μg, 135 μg and 450 μg dose blends are shown in Fig. 2A–C, respectively. Clear variation in the degree of fine particulates (<5 μm) was observed when comparing the blends. In general, a rank-order in particulate number matched that of the blend dose.

Unformulated lactose SEM images showed large carrier particles with some smaller adhering lactose particles which is in agreement with the previously described particle size data.

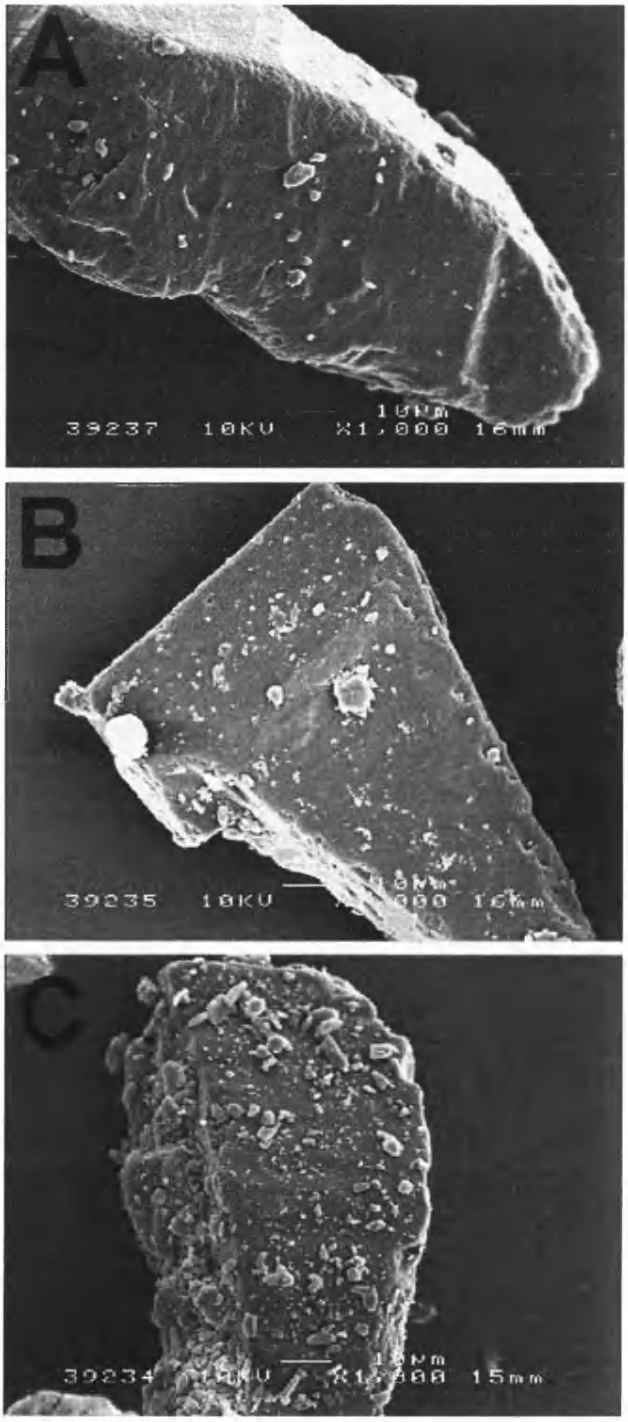

Fig. 2. Scanning electron microscope images of (A) 12 μg, (B) 135 μg and (C) 450 μg blends.

3.3. In vitro analysis

The aerosolisation efficiency of salbutamol sulphate from lactose carriers was investigated using the TSI. Specifically, the influence of dose on the fine particle aerosolisation was investigated since this is a good indicator of respiratory delivery. Data were processed and represented as follows: loaded dose (total recovered from all stages and device/capsules); emitted dose (total recovered from TSI stages); fine particle fraction (dose recovered in stage 2/loaded dose × 100); fine particle dose (dose recovered in stage 2).

The relationship between the emitted dose and loaded dose is shown in Fig. 3 which suggests a linear response ($R^2 = 0.998$) with a device removal efficiency of 89 ± 4% across all doses. Since the percentage drug loss in the device was apparently independent of dose, it is reasonable to assume that such losses are due to drug adhered to retained lactose, since the formulation mass remained constant.

The relationship between fine particle fraction and loaded dose is shown in Fig. 4. It can be seen from Fig. 4 that the loaded dose has a significant effect on performance (ANOVA $p < 0.05$). In general, a linear decrease ($R^2 = 0.977$) in aerosolisation (i.e., fine particle fraction) was observed on increasing the dose from 11 μg to 135 μg followed by an increase when the dose was increased from 135 μg to 450 μg.

In comparison, the relationship between fine particle dose and loaded dose, shown in Fig. 5, suggested that the dose level only had a statistically significant effect over the range 135–450 μg (ANOVA, Fishers pairwise,

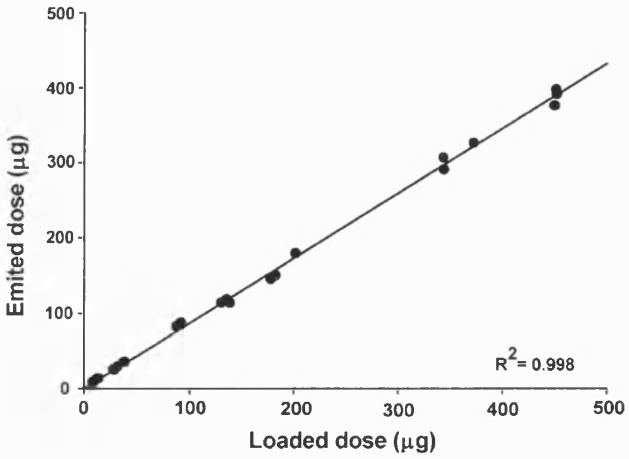

Fig. 3. Influence of loaded dose on the emitted dose.

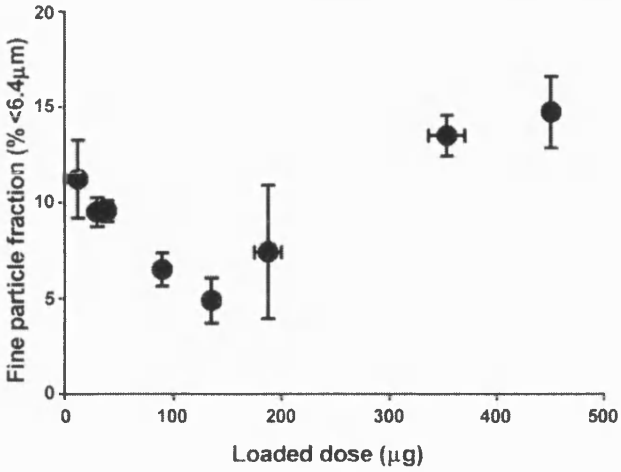

Fig. 4. Influence of loaded dose on the fine particle fraction.

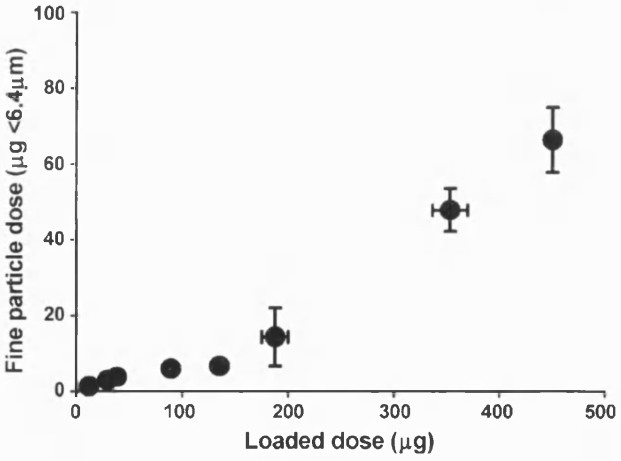

Fig. 5. Influence of loaded dose on the fine particle dose.

$p < 0.05$). No significant increase in fine particle dose was observed between 10 μg and 135 μg dose.

4. Discussion

The term active site may refer to variations in morphology and surface free energy (which will directly influence the thermodynamic work of adhesion). In terms of morphological effects, there are many possible topographical features that a drug particle may encounter on a lactose surface as represented in Fig. 6A. It is envisaged that sites with 'high energy' (area 1 in Fig. 6A) in the carrier surface would be preferentially occupied compared to sites with low energy (area 2 in Fig. 6A) as

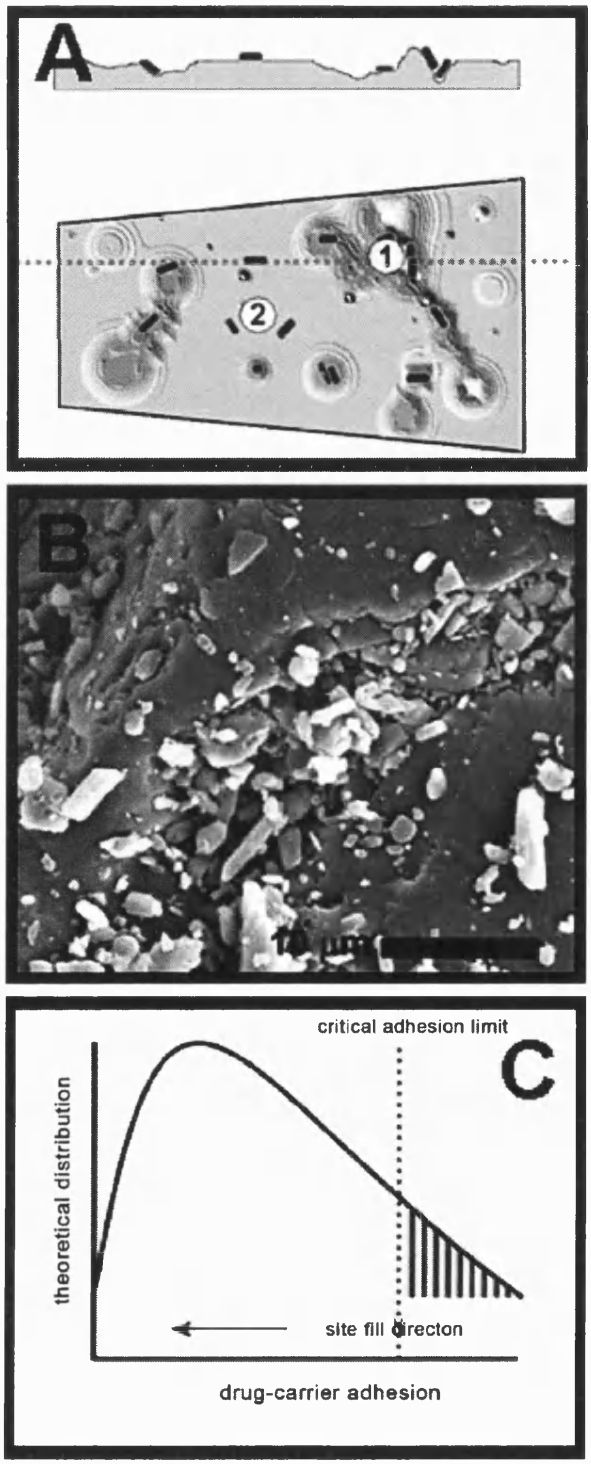

Fig. 6. (A) Schematic of regions on a carrier surface containing potential (1) high energy and (2) low energy 'active' sites. (B) SEM of a crevice on a lactose carrier surface containing many micron-sized particulates. (C) Theoretical distribution and process of active site filling.

a consequence of a combination of increased contact area, high surface free energy and simple geometric constraints.

A possible example of this is shown in Fig. 6B, where micron sized particulates have accumulated in a recess in the surface of a large lactose carrier particle.

Furthermore, it is suggested that the active sites present on the surface of the carrier will have a specific energy distribution (Fig. 6C) with a critical, average adhesion point below which particles, drug or lactose, could be removed. This concept correlates with previous studies, which have suggested that surface roughness and carrier material directly influence aerosolisation of drug from lactose carriers.

Analysis of variation in FPD with loaded dose (shown in Fig. 5) indicates that such a critical point exists, since no statistical variation in FPD was observed across the dose range 10–135 μg. As expected, a concurrent linear decrease in fine particle fraction was observed, since the FPD remained constant as total dose was increased linearly. Increase in dose from 135 μg to 450 μg resulted in an increase in both FPD and FPF, suggesting that the critical adhesion limit had been overcome. However, the relationship between loaded dose and FPF across the dose range 135–450 μg was not linear. This is to be expected, however, since such a system would still contain a certain distribution of active sites below the critical adhesion limit and therefore would result in a non-uniform performance response (i.e., the probability of drug–particle removal will dependent on the filling of differing energy sites). Furthermore, the inherent particle size distribution of the micronised drug would set an upper fine particle fraction limit.

Another point to consider is the potential for formation of drug or drug–lactose fines agglomerates. Previous studies have reported the presence of fines to increase the fine particle fraction through the formation of agglomerates or multiplets (Lucas et al., 1998). However, recent studies have suggested that the agglomeration or individual drug–carrier formation of a blend will be related to the balance of adhesion and cohesion in the system (Begat et al., 2004). It was suggested that for a salbutamol sulphate–lactose system, adhesion would dominate, thus reducing the potential for agglomeration (Begat et al., 2004). Such observations correlate well with the SEM images of the blends in this study, which suggested many of the micronised particulates in the salbutamol lactose system to be distributed as discrete entities. However, it is important to remember that the formulation mechanism will be dependent on the drug and carrier properties.

Indeed, recent studies by Louey et al. (2003) suggest that increased lactose fines result in an agglomerate based system. This is likely, since the potential free carrier space would be reduced. Furthermore, it is envisaged that the fine particle fraction would eventually plateau and decrease due to multilayer or aggregate formation and formulation segregation.

However, observations across the dose range 10–450 μg suggested the aerosolisation performance to be dominated by the active site theory. Clearly many variables would influence this relationship and are worth considering for future investigation. These include quantifying the influence of inherent fines and directly relating the influence of modified carrier surfaces to fine particle adhesion.

5. Conclusions

Clear variations in the FPF and FPD were observed as a function of dose or drug/lactose ratio (~10–450 μg in 50 mg formulation). Furthermore, the relationship between drug/lactose ratio and aerosolisation performance was related to the possibility of active sites present on the lactose carrier surface.

Although the investigation here suggests the presence of such regions, a fundamental understanding of the mechanisms and mechanics of such a dynamic process is required further to circumvent the empirical formulation approaches used today. However, it is important to note, this study was conducted using one device, lactose and flow rate. In future, it would be interesting to study the influence of different carrier morphologies, devices (with different sheer and de-agglomeration mechanisms) and varied flow rates.

References

Begat, P., Morton, D.A.V., Staniforth, J.N., Price, R., 2004. The cohesive–adhesive balances in dry powder inhaler formulations II: Influence on fine particle delivery characteristics. Pharm. Res. 21 (10), 1826–1833.

Flament, M.P., Leterme, P., Gayot, A., 2004. The influence of carrier roughness on adhesion, content uniformity and the in vitro

deposition of terbutaline sulphate from dry powder inhalers. Int. J. Pharm. 275, 201–209.

Ganderton, D., Kassem, N.M., 1992. Advances in Pharmaceutical Sciences. Academic Press, London, UK.

Hersey, J.A., 1975. Ordered mixing: a new concept in powder mixing practice. Powder Technol. 11, 41–44.

Kawashima, Y., Serigano, T., Hino, T., Yamamoto, H., Takeuchi, H., 1998. Effect of surface morphology of carrier lactose on dry powder inhalation property of pranlukast hydrate. Int. J. Pharm. 172, 179–188.

Larhrib, H., Zeng, X.M., Martin, G.P., Marriott, C., Prichard, J., 1999. The use of different grades of lactose as a carrier for aerosolised salbutamol sulphate. Int. J. Pharm. 191, 1–14.

Larhib, H., Martin, G.P., Marriott, C., Prime, D., 2003. The influence of morphology on drug delivery from dry powder formulations. Int. J. Pharm. 247, 283–296.

Louey, M.D., Razia, S., Stewart, P.J., 2003. The influence of physico-chemical carrier properties on the in vitro aerosol deposition from interactive mixtures. Int. J. Pharm. 252, 87–98.

Lucas, P., Anderson, K., Staniforth, J.N., 1998. Protein deposition from dry powder inhalers: fine particle multiplets as performance modifiers. Pharm. Res. 15, 562–569.

Muster, T.H., Prestidge, C.A., 2002. Face specific surface properties of pharmaceutical crystals. J. Pharm. Sci. 91, 1432–1444.

Staniforth, J.N., 1996. Pre-formulation aspects of dry powder aerosols. In: Proceedings from Respiratory Drug Delivery V, Phoenix, AZ, pp. 65–74.

Steckel, H., Muller, B.S., 1997. In vitro evaluation of dry powder inhalers II: influence of carrier particle size and concentration on in vitro deposition. Int. J. Pharm. 154, 31–37.

Steckel, H., Bolzen, N., 2004. Alternative sugars as potential carriers for dry powder inhalations. Int. J. Pharm. 270, 297–306.

Young, P.M., Cocconi, D., Colombo, P., Bettini, R., Price, R., Steele, D.F., Tobyn, M.J., 2002. Characterisation of a surface modified dry powder inhalation carrier prepared by "particle smoothing". J. Pharm. Pharmacol. 54, 1339–1344.

Zeng, X.M., Martin, G.P., Tee, S.-K., Marriott, C., 1998. The role of fine particle lactose on the dispersion and deaggregation of salbutamol sulphate in an air stream in vitro. Int. J. Pharm. 176, 99–110.

Zeng, X.M., Martin, G.P., Tee, S.-K., Ghoush, A.A., Marriott, C., 1999. Effects of particle size and adding sequence of fine lactose on the deposition of salbutamol sulphate from a dry powder formulation. Int. J. Pharm. 182, 133–144.

Zeng, X.M., Martin, G.P., Marriott, C., Prichard, J., 2000. The influence of carrier morphology on drug delivery by dry powder inhalers. Int. J. Pharm. 200, 92–106.